

Gianluca □□□□ Greco

Production of engineered biomass-derived carbons through pressurized slow pyrolysis under N₂ and CO₂ atmosphere

Director/es

Manyá Cervelló, Joan José

<http://zaguan.unizar.es/collection/Tesis>

© Universidad de Zaragoza
Servicio de Publicaciones

ISSN 2254-7606

Tesis Doctoral

PRODUCTION OF ENGINEERED BIOMASS-
DERIVED CARBONS THROUGH PRESSURIZED
SLOW PYROLYSIS UNDER N₂ AND CO₂
ATMOSPHERE

Autor

Gianluca □□□□ Greco

Director/es

Manyá Cervelló, Joan José

UNIVERSIDAD DE ZARAGOZA
Escuela de Doctorado

Programa de Doctorado en Ingeniería Química y del Medio Ambiente

2022



Department of Chemical Engineering and Environmental Technologies

Production of engineered biomass-derived carbons through pressurized slow pyrolysis under N₂ and CO₂ atmosphere

The present thesis is submitted to the Department of Chemical Engineering and Environmental Technologies of the University of Zaragoza, in compliance with the requirements for the degree of Doctor

Gianluca Greco

Huesca, 2022



Escuela Politécnica
Superior - Huesca
Universidad Zaragoza



Departamento de Ingeniería
Química y Tecnología
del Medio Ambiente
Universidad Zaragoza



Instituto Universitario de Investigación
de Ingeniería de Aragón
Universidad Zaragoza



Dr. Joan J. Manyà, Professor at the University of Zaragoza in the Department of Chemical Engineering and Environmental Technologies and member of the Thermochemical Research Group, informs that:

The PhD thesis entitled:

“Production of engineered biomass-derived carbons through pressurized slow pyrolysis under N₂ and CO₂ atmosphere”

has been written by the PhD student Gianluca Greco under my supervision in the Department of Chemical Engineering and Environmental Technologies and has not been submitted in support of an application for another degree at this or any other university and I authorize and approve the presentation of this dissertation.

Joan J. Manyà

A handwritten signature in black ink, appearing to read 'Joan J. Manyà', written in a cursive style.

The present PhD thesis entitled “Production of engineered biomass-derived carbons through pressurized slow pyrolysis under N₂ and CO₂ atmosphere” is presented by compendium of the following publications:

Article 1: Evolution of the mass-loss rate during atmospheric and pressurized slow pyrolysis of wheat straw in a bench-scale reactor, G. Greco, M. Videgain, C. Di Stasi, B. González, J. J. Manyà, *Journal of Analytical and Applied Pyrolysis*, 2018, 136: 18–26.
Impact Factor: 3,470; Q1: 30/138 (Engineering, Chemical). Source: JCR 2018.

Article 2: Effects of slow-pyrolysis conditions on the products yields and properties and on exergy efficiency: A comprehensive assessment for wheat straw, G. Greco, C. Di Stasi, F. Rego, B. González, J. J. Manyà, *Applied Energy*, 2020, 279: 115842.
Impact Factor: 9,746; Q1: 6/143 (Engineering, Chemical). Source: JCR 2020.

Article 3: Importance of pyrolysis temperature and pressure in the concentration of polycyclic aromatic hydrocarbons in wood waste-derived biochars, G. Greco, M. Videgain, C. Di Stasi, E. Pires, J. J. Manyà, *Journal of Analytical and Applied Pyrolysis*, 2021, 159: 105337.
Impact Factor: 5,541; Q1: 26/143 (Engineering, Chemical). Source: JCR 2020.

Article 4: Biomass-derived carbons physically activated in one or two steps for CH₄/CO₂ separation, G. Greco, R. L. S. Canevesi, C. Di Stasi, A. Celzard, V. Fierro, J. J. Manyà, *Renewable Energy*, 2022, 191:122–133.
Impact Factor: 8,001; Q1: 16/114 (Energy & Fuels). Source: JCR 2020.

A Elena e Romana

I. Acknowledgements

First of all, I would like to thank Prof. Joan Manyà for his impeccable supervision during these years. Besides your constant support and your remarkable suggestions at any time, I would like to express my deepest gratitude to you for introducing me in the biochar world and for teaching me so many things which would be impossible to list all of them here. Now, I know that I can make the difference, and it is thanks to you.

A special thanks to Dr. Elisabet Pires, for dedicating me your precious time and your guidance during the trickiest experimental activity of this thesis. I am really grateful to have had the possibility to work with you.

Thanks to Prof. Vanessa Fierro and Rafael Canevesi for your collaboration, your support and your kindness.

Muchísimas gracias a José Antonio, este trabajo no habría sido posible sin tu infinita paciencia y constante ayuda. Cualquier frase que yo pueda escribir no podrá jamás expresar plenamente lo que ha significado para mí tus recomendaciones y tu disponibilidad a cualquier hora. Mil gracias a Begoña, amiga antes de ser compañera de trabajo.

Infinitas gracias a María, por estar presente siempre, dentro y fuera de la universidad. Nunca me olvidaré de cómo me acogiste desde el primer momento, de tu soporte y de tu paciencia.

Il mio ringraziamento più profondo va a Christian di Stasi, no, Cristian Di stasi, no, Christian di stassi.. non scriverò bene il tuo nome completo neanche qui, quindi un grazie di cuore a Christian, che mi ha accompagnato, aiutato, infastidito durante ogni secondo speso per questo lavoro di tesi. Non dimenticherò mai questi anni trascorsi a lavorare insieme, così come te che mai potrai ricordare cosa avevi scritto in quelle famose note sul vetro del laboratorio cancellate da una mia "involontaria" strusciata di spalla.

Gracias a May, Fer, Miguel, Antonio, Darío por haberme alegrado los días en la universidad con comidas inolvidables. Un gracias especial a Dani, por su infinita paciencia conmigo, sobretodo a primera hora de la mañana.

Ai miei migliori amici Marco, Luca, Dani, Leo. Nonostante la distanza, a volte basta una sola parola.

Ai miei genitori Giuseppe e Fiorella, per l'eterno sostegno da parte vostra, per i vostri sacrifici e per la vostra comprensione. Ve ne sarò grato per sempre.

A mio fratello Marco, alla sua costante presenza nella mia vita. Sei la mia Stella Polare.

Mil gracias a Francisco, Carmina y Guillermo, por todo el apoyo y el cariño recibido por vuestra parte durante estos años. Aquí queda constancia de que hay algo que celebrar.

L'ultimo, enorme ringraziamento va a Carlota, che mi ha sostenuto sin dal primo momento con la sua grinta, la sua determinazione ed il suo immenso affetto. Mi hai insegnato molto in questi anni e continuerai a farlo: se oggi sono una persona migliore è grazie soprattutto a te.

II. Summary / Resumen

The serious concerns about the climate change, energy crisis, environmental pollution and food productivity have generated in the last years a growing interest in biochar, a term referring to a renewable and sustainable carbon-rich, fine-grained, porous substance, produced by thermal decomposition of biomass under oxygen-limited conditions and at relatively low temperatures. It is strongly believed that using biochar could mitigate the current environmental situation by achieving three complementary goals:

- Soil improvement, from both pollution and productivity point of view.
- Energy production, if energy is captured during the biochar production process.
- Waste valorization, if waste biomass is used for this purpose.

Among the available thermochemical routes, it should be mentioned slow pyrolysis as one of the most important processes for the biomass conversion into biochar, since its operating conditions could be optimized in order to produce tailored biochars and derived materials with proper characteristics for their final application.

The present PhD project was conducted within the framework of a European Training Network: the GreenCarbon project¹, which main purpose was to develop advanced biomass-derived carbons to drive new technologies for biomass/biowaste upcycling. In this context, the main objective of this PhD Thesis was the research of the most appropriate pyrolysis conditions in order to improve the biochar properties for its employment as a carbon sequestration agent. In addition, further uses of the produced biochars (i.e., as soil amendment and as an adsorbent in gas phase) have been explored. Depending on the severity of the operating conditions, biochar properties, and also the energy efficiency of pyrolysis process, might result considerably different at the end of the process; therefore, an optimization step is required in order to make the produced biochars suitable for their final application. In conclusion, the present thesis provides scientific evidence on the effect of pressure, peak temperature and vapor residence time on the main physicochemical properties of the biochar obtained from two types of feedstock (wheat straw pellets and wood waste), under both inert N₂ and CO₂ atmospheres.

¹ This project has received funding from the European Union's Horizon 2020 research and innovation program under the Marie Skłodowska-Curie grant agreement No 721991.



After the *Introduction*, *State of the Art* and *Methodology* sections, the document is structured into four blocks, which correspond to the main research studies conducted in the framework of this PhD Thesis:

1. A study on the mass-loss rate evolution during atmospheric and pressurized slow pyrolysis of wheat straw.
2. Analysis on the influence of slow-pyrolysis conditions on the products yields and properties and on exergy efficiency.
3. Polycyclic aromatic hydrocarbons (PAHs) and potential phytotoxicity assessment on wood waste-derived biochars produced through pressurized slow pyrolysis.
4. An assessment of the performance as adsorbents of physically activated biochar (through one- and two-step processes) for biogas upgrading purposes.

Following the presented four blocks, the *Results* section summarizes the outcomes obtained along the experimental campaigns. Finally, the *Conclusions* section points out the most important findings achieved during this work, whereas a discussion on the most significant research to be developed in the next future is given in the *Future Perspectives* section.

La preocupación por el cambio climático, la crisis energética, la contaminación ambiental y los problemas de productividad alimentaria han generado un creciente interés en el biochar. El biochar es un compuesto rico en carbono, renovable, sostenible, de granulado fino y relativamente poroso. Se puede producir mediante descomposición térmica de biomasa bajo condiciones limitantes de oxígeno y a temperaturas relativamente bajas (350–700 °C). Existe la creencia que el uso de biochar puede mitigar ciertos problemas ambientales relacionados con las emisiones de carbono y el calentamiento global. En concreto, el biochar es interesante para:

- Mejorar las propiedades del suelo en términos de contaminación y de productividad.
- Producir energía renovable, si se captura la energía residual durante el proceso de producción de biochar.
- Valorizar residuos lignocelulósicos de bajo valor añadido.

Entre los procesos termoquímicos disponibles, cabe mencionar la pirólisis lenta como uno entre los más importantes para la conversión de la biomasa en biochar, debido a la posibilidad de optimizar sus condiciones operativas para producir biochars a medida y materiales derivados de los mismos con características específicas para su aplicación final.

La presente Tesis Doctoral se ha desarrollado dentro del marco del proyecto europeo GreenCarbon², cuyo principal objetivo ha sido desarrollar carbonos avanzados derivados de biomasa para su aplicación en nuevas tecnologías en un contexto de economía circular. En el marco de la red establecida en el proyecto GreenCarbon, el principal objetivo de esta Tesis Doctoral ha sido la investigación de las condiciones de pirólisis más apropiadas para optimizar las propiedades del biochar producido, con la vista puesta en su posterior utilización en procesos de secuestro de carbono. Además, se han explorado usos adicionales para los biochars producidos: como enmienda de suelos agrícolas y como adsorbentes en procesos de purificación en fase gas. Dependiendo del grado de severidad de las condiciones operativas, tanto las variar sensiblemente; por este motivo, es necesario establecer las condiciones de operación óptimas para el biochar producido resulte adecuados para su uso final. En conclusión, la presente Tesis Doctoral proporciona evidencias científicas sobre los efectos que la presión, temperatura máxima y tiempo de residencia de la fase gas ejercen sobre las

² Este proyecto ha recibido fondos por parte del programa de investigación e innovación European Union's Horizon 2020 bajo acuerdo de subvención Marie Skłodowska-Curie No 721991.



principales propiedades físicoquímicas del biochar, que en el presente trabajo, se ha obtenido a partir de dos tipos de biomásas (pellets de paja de trigo y residuos de madera) y bajo dos atmósferas distintas (N_2 y CO_2).

Tras las secciones de *Introducción*, *Estado del Arte* y *Metodología*, el presente documento se estructura en cuatro bloques, que corresponden a los principales temas de investigación desarrollados en el marco de la Tesis Doctoral:

1. El estudio sobre el comportamiento dinámico del proceso de pirólisis lenta de paja de trigo a distintos niveles de presión.
2. El análisis de la influencia de las condiciones del proceso de pirólisis lenta sobre la distribución de productos y las propiedades de los mismos, así como sobre la eficiencia exergética.
3. El análisis del contenido de hidrocarburos policíclicos aromáticos (PAHs) y la fitotoxicidad potencial de biochars producidos a través de pirolisis lenta presurizada de residuos de madera no tratados.
4. El estudio del rendimiento como adsorbente de biochar activado físicamente (en una o dos etapas) para el enriquecimiento de biogás mediante adsorción de CO_2 .

A continuación, la sección de *Resultados* resume los resultados obtenidos en los cuatro frentes, donde cada uno de ellos ha derivado en una publicación. Finalmente, la sección *Conclusiones* remarca los aspectos más importantes obtenidos en el presente trabajo, y se presenta en la sección *Perspectivas Futuras* una discusión sobre la investigación mas significativa a desarrollar en el futuro.

III. List of abbreviations and acronyms

<i>1S</i>	One-Step Activation
<i>2S</i>	Two-Step Activation
AAEMS	Alkali and Alkaline Earth Metals
ANA	Acenaphthene
ANT	Anthracene
ANY	Acenaphthylene
<i>BaA</i>	Benzo[a]anthracene
<i>BaP</i>	Benzo[a]pyrene
<i>BbF</i>	Benzo[b]fluoranthene
<i>BkF</i>	Benzo[k]fluoranthene
<i>BPE</i>	Benzo[ghi]perylene
CEC	Cation Exchange Capacity
<i>CHR</i>	Chrysene
COD	Chemical Oxygen Demand
CVC	Constant-Volume Carbonization
<i>DBA</i>	Dibenz[a,h]anthracene
DoE	Design of Experiments
$e_{out,i}$	Exergy of the Product i (MJ kg^{-1})
<i>FLT</i>	Fluoranthene
<i>FLU</i>	Fluorene
<i>G</i>	Germination Percentage
GCMC	Grand Canonical Monte Carlo
GHG	GreenHouse Gas
GHSV	Gas Hourly Space Velocity (h^{-1})
<i>GI</i>	Germination index (%)
HHV	High Heating Value (MJ kg^{-1})
h_{in}	Input Specific Enthalpy (MJ kg^{-1})
h_{out}	Output Specific Enthalpy (MJ kg^{-1})
IAST	Ideal Adsorbed Solution Theory

IBI	International Biochar Initiative
ICC	Intra-Class Correlation Coefficient
IPY	Indeno[1,2,3,-cd]pyrene
<i>L</i>	Average Root Length (mm)
<i>m_{biochar}</i>	Mass of Biochar
<i>m_{biomass}</i>	Mass of Biomass
<i>m_f</i>	Final Mass of the Sample
MOFs	Metal Organic Frameworks
<i>MSe</i>	Mean Square of the Error term
<i>MSt</i>	Mean Square of the Treatment term
NAP	Naphthalene
<i>P</i>	Absolute Pressure during Pyrolysis (MPa)
PAH	Polycyclic Aromatic Hydrocarbons
PHE	Phenanthrene
PID	Proportional Integral Derivative
ppm	Part Per Million
PSD	Pore Size Distribution
PYR	Pyrene
<i>Q_{process}</i>	Enthalpy Required for the Process that should be Supplied Externally (MJ kg ⁻¹)
<i>S_{BET}</i>	Brunauer–Emmet–Teller specific surface area (m ² g ⁻¹)
<i>S_{CO2/CH4}</i>	CO ₂ selectivity over CH ₄
SOM	Soil Organic Matter
<i>S_{2D-NLDFT}</i>	Surface Area (calculated by two-dimensional non-local density functional theory model for heterogenous surfaces)
<i>T</i>	Pyrolysis Peak Temperature (°C)
TC#	temperatures measured by the thermocouples placed within the reactor (°C)
TGA	Thermogravimetric Analysis
TTEC	Total Toxic Equivalent Concentrations (µg kg ⁻¹ biochar, Dry Basis)
<i>V_{meso}</i>	Mesopore Volume
<i>V_{micro}</i>	Micropore Volume

VOCs	Volatile Organic Compounds
V_{tot}	Total Pore Volume
V_{ultra}	Ultra-Micropore Volume ($\text{cm}^3 \text{g}^{-1}$)
WS	Wheat Straw
WW	Wood Waste
x_{FC}	Mass Fraction of Fixed-Carbon in the Biochar in a Dry and Ash-Free Basis (%)
X_i	Burn-Off
XRF	X-Ray Fluorescence Spectroscopy
y_{char}	Mass Yield of Biochar in a Dry and Ash-Free Basis (-)
y_{FC}	Fixed-Carbon Yield in a Dry and Ash-Free Basis (-)
y_{gas}	Mass Yield of Produced Gas in a Dry and Ash-Free Basis (-)
y_{org}	Mass Yield of Condensable Organics in a Dry and Ash-Free Basis (-)
y_{water}	Mass Yield of Produced Water in a Dry and Ash-Free Basis (-)
Ψ_{char}	Exergy Efficiency of the Biochar (-)
Ψ_{gas}	Exergy Efficiency of the Gas Product (-)
$\Psi_{process}$	Exergy Efficiency of the Overall Process (-)
Σe_{in}	Sum of the Input Exergies (MJ kg^{-1})
Σe_{out}	Sum of the Output Exergies (MJ kg^{-1})
τ	Gas Residence Time
$\mu\text{-GC}$	Micro Gas Chromatograph

Contents

I. Acknowledgements	I
II. Summary / Resumen	IV
III. List of abbreviations and acronyms	IX
1. Introduction	1
1.1 Context	1
1.1.1 <i>Global warming</i>	1
1.1.2 <i>Agriculture decline</i>	3
1.2 The potential of biomass	4
1.3 The concept of biochar	6
1.4 Production of biochar	7
1.4.1 <i>Pyrolysis</i>	7
1.4.1.1 <i>Slow pyrolysis</i>	8
1.4.1.2 <i>Intermediate pyrolysis</i>	8
1.4.1.3 <i>Fast pyrolysis</i>	9
1.4.2 <i>Hydropyrolysis</i>	9
1.4.3 <i>Gasification</i>	10
1.4.4 <i>Flash carbonization</i>	10
1.5 Potential applications of biochar	11
1.5.1 <i>Soil carbon sequestration</i>	12
1.5.2 <i>Agricultural growing media</i>	12
1.5.3 <i>Recovery of contaminated soils</i>	13
1.5.4 <i>Biochar activation</i>	14
1.5.5 <i>Adsorption processes</i>	14
1.5.6 <i>Catalysis</i>	18
1.5.7 <i>Energy storage</i>	18
2. State of the art	19
2.1 Influence of pyrolysis conditions	19
2.1.1 <i>Peak temperature</i>	19

2.1.2 Absolute pressure.....	20
2.1.3 Vapor residence time	22
2.1.4 Pyrolysis environment.....	23
2.1.5 Additional factors.....	24
2.2 Energy and exergy efficiencies of slow pyrolysis process	25
2.3 Key properties of biochar	26
2.3.1 Contents of PAHs in biochar	26
2.3.2 Physically activated biochar as CO ₂ adsorbent.....	27
3. The GreenCarbon project.....	29
4. Objectives.....	31
5. Methodology	33
5.1 Biomass sources.....	33
5.2 Pyrolysis device and experimental procedure	36
5.3 Characterization of pyrolysis products.....	37
5.4 Design of experiments.....	38
5.5 Assessment of repeatability	39
5.6 Energy and exergy assessment.....	39
5.7 PAHs content quantification	41
5.8 Germination assays.....	42
5.9 Physical activation with CO₂.....	43
5.9.1 One-step activation	43
5.9.2 Two-step activation.....	43
5.10 Characterization of resulting activated carbons	44
5.10.1 Adsorption isotherms	44
5.10.2 Adsorption equilibrium	45
5.10.3 Adsorption kinetics.....	46
5.10.4 Breakthrough Simulations.....	47
6. Results	48

6.1. Theme I: assessment of the effects of slow pyrolysis process conditions on products yields and properties of resulting biochars.....	48
6.2. Theme II: study on the energy/exergy efficiency of the pyrolysis process	50
6.3. Theme III: assessment of the potential toxicity of biochar for soli application purposes.....	53
6.4. Theme IV: physically activated biomass-derived carbons for CH₄/CO₂ separation purposes	55
7. Conclusions / Conclusiones	58
8. Future Perspectives.....	62
9. References.....	64

Tables and Figures

Table 1	Operating conditions of different carbonization processes.
Table 2	Peat/biochar mixtures reported in literature.
Table 3	CO ₂ uptakes for different porous carbon materials reported in literature.
Table 4	Consortium (beneficiaries) of the GreenCarbon Project.
Table 5	Lignocellulosic composition, proximate, ultimate and XRF analyses of wheat straw and wood waste biomasses
Table 6	Monitored ion profiles and toxic equivalent factor (TEF) for each PAH compound
Figure 1	Chemical structures of a) cellulose monomer, b) a fraction of hemicellulose, and c) a fraction of lignin.
Figure 2	GreenCarbon Project objectives
Figure 3	Layout of the main tasks of the PhD project.
Figure 4	Biomass feedstock employed in this work
Figure 5	Schematic layout of the pyrolysis plant
Figure 6	Control volume considered for energy and exergy assessment

1. Introduction

1.1 Context

1.1.1 Global warming

The great concerns on the relentlessly increase of global energy demand, due to the growing population, are forcing the most part of the governments in the world to find alternatives to fossil fuels, the current main source of energy (Yaashikaa *et al.*, 2020). The fossil fuel resources available in our planet are the result of geologic and biological processes, which occurred over hundreds of millions of years ago and currently in progress. With amounts estimated between 4000 and 6000 gigatons, the carbon sequestered in these resources was originally a constituent of the atmosphere of a younger Earth, possessing approximately 1500 parts per million (ppm) of CO₂ (Rackley, 2010). With the dawn of the industrial age, about 280 gigatons equivalent in carbon have been combusted and released back into the atmosphere. In the same period, an additional 150 gigatons of CO₂ was released to the atmosphere from soil carbon pools, as a result of changes in land use. Overall, it is estimated that the CO₂ concentration in the atmosphere has increased from 280 ppm to 368 ppm in 2000, with a slight decrease to 338 ppm in 2010, whereas values around 412 ppm have been reported during 2020 (“NOAA Climate.gov,” 2021). It is expected that such dramatic increase in CO₂ concentration in air can worsen the already compromised balance of incoming and outgoing energy in the Earth-atmosphere system. For this reason, CO₂ is considered the principal anthropogenic GreenHouse Gas (GHG) (IPCC, 2000; Rackley, 2010). The first efforts in demonstrating the influence of CO₂ on global warming can be attributed to (Tyndall, 1859) and (Arrhenius, 1896). Nowadays, the world of industry is compromised in an active struggle to reduce their intrinsic CO₂ emissions. It is widely known that around 40% of global anthropogenic CO₂ emissions are originated from industrial processes (Fennell, 2015). Within this percentage, approximately 26% comes from the cement manufacture (Dean *et al.*, 2011), producing CaO and CO₂ from CaCO₃, whereas the iron and steel manufacture generates a 30% of CO₂. The release of CO₂ is inevitable without a radical redesign of such processes and many others like them (Fennell, 2015).

The Intergovernmental Panel on Climate Change (IPCC) (Rackley, 2010) published the Fourth Assessment Report in 2007, declaring that the average global surface temperature had increased by 0.74 ± 0.18 °C over the 20th century, pointing at the increasing anthropogenic GHG concentrations as the most responsible for the observed increase in global average

temperatures (Rackley, 2010). Furthermore, the anthropogenic-related changes have also reduced the effectiveness of certain climate feedback mechanisms; for instance, changes in land use and land-management practices have reduced the ability of soils to build soil carbon inventory in response to higher atmospheric CO₂ concentration, while the ocean acidification has reduced their capacity to take up additional CO₂ from the atmosphere (Rackley, 2010). In the absence of CO₂ mitigation, the resulting emissions will lead to further increase in atmospheric CO₂ concentration, causing an enhancing warming and inducing many changes in the global climate. Even if the CO₂ concentration is stabilized before 2100, the warming and other climate effects are expected to continue for centuries, due to the long-time scales associated with climate processes. The climate predictions suggest warming over a multicentury time scale in the range from 2 °C to 9 °C (Rackley, 2010). Hence, it is necessary to urgently find a solution to reduce the CO₂ emissions and, consequently, to minimize the long-term climate change.

In light of the worrying context above described, several international agreements have been implemented. Among the most important ones, the Kyoto Protocol is an international agreement linked to the United Nations Framework Convention on Climate Change (UNFCCC, 1992). Its purpose was to struggle the global warming by reducing the GHG concentrations in the atmosphere to "a level that would prevent dangerous anthropogenic interference with the climate system" (Art. 2) ("United Nations, Framework Convention on Climate Change," 2008). Accordingly, the measures for the climate change mitigation can be grouped as following:

- Reduce energy use;
- Improve energy efficiency technologies;
- Technology implementation for the climate change mitigation (e.g., Carbon Capture and Storage, CCS).

The Kyoto Protocol has been followed, over the decades, by many other climatic summits dealing with the same topic (see, e.g., the recent COP-21 Conference of Paris, in 2015).

A reduction in world energy use is likely to be difficult to achieve, due to the increasing global population and to the progressive improvements in the quality of life. One quarter of the world's population is thought to have no access to electricity and therefore, if this fraction decreases, the energy use will have to increase (Cotton, 2013). The second option for improving the energy efficiency requires new technology and implementation of renewable energy sources. However, both of them are expensive whereas, across the most part of the world, fossil

fuels, in particular coal, are cheaper and more abundant than renewable energy sources (Cotton, 2013). The third option (technology implementation for carbon sinks) in order to achieve a CO₂ emissions mitigation is considered the most achievable one at the moment (short/medium term).

1.1.2 Agriculture decline

Another worldwide critical issue is to ensure the food supply for an increasing world population. For this purpose, an intensification of agricultural production on a global scale is required. In many tropical environments, soils lack nutrient contents, meaning that the sustainable agriculture is constrained in these areas. The low nutrient contents typically accelerate the mineralization of soil organic matter (SOM) (Tiessen *et al.*, 1994; Zech *et al.*, 1997), leading to a gradual decrease in the cation exchange capacity (CEC) of soils. Under such circumstances, the applied mineral fertilizers lose their relatively high efficiency (Cahn *et al.*, 1993; Melgar *et al.*, 1992). Besides, many farmers cannot afford the costs of regular applications of inorganic fertilizers (Glaser *et al.*, 2002).

Slash-and-burn techniques are currently the most common route to improve cultivations in the tropics. Indeed, when the biomass burns, the nutrients are rapidly released into the soil. The main drawback of this technique is that the positive effects on soil properties are limited to the short term (Cochrane and Sanchez, 1980; Kauffman *et al.*, 1995; Kleinman *et al.*, 1995). In addition, burning biomass always releases certain amounts of GHGs as CH₄ and N₂O, which contribute to worsen the level of global warming (Fearnside *et al.*, 1999).

Organic matters such as manures, mulches and composts have frequently been applied to increase soil fertility (Glaser *et al.*, 2002). Nevertheless, the mineralization of organic matter is typically very quick under tropical conditions (Tiessen *et al.*, 1994); only a small portion of it will be stabilized in the soil in the long term, and then released into the atmosphere as CO₂ (Fearnside, 2000).

As alternative option for soil amendment, the idea of employing more stable compounds like carbonized materials is gaining attention. These materials embrace a wide variety, from charred material (e.g., biochar) to graphite and soot particles (Schmidt and Noak, 2000). Several investigations (Glaser *et al.*, 2001, 2000) have already been conducted on the topic, finding out that carbonized materials obtained by the incomplete combustion of organic material are responsible for keeping high levels of SOM and available nutrients in anthropogenic soils of

the Amazonia. These soils, called *Terra Preta*, are characterized by a large amount of black C, indicating a high and prolonged input of carbon organic matter.

1.2 The potential of biomass

A possible sustainable solution to mitigate the critical scenarios mentioned above is biomass. Among renewable energy resources available in the current scenario, biomass is one of the most plentiful and well-utilized sources in the world (Demirbaş *et al.*, 2010). It is defined as the plant biocomponent derived from the reaction between CO₂ present in the air, water and sunlight by photosynthesis process, resulting into the synthesis of carbohydrates, the building blocks of biomass (Aysu and Küçük, 2014). There exist numerous resources of biomass across the world, including woody, herbaceous and aquatic plants as well as animal manures and processing residues (McKendry, 2002). Lignocellulosic biomass is defined as non-edible dry plant matter, being among the most abundant and low-cost source of renewable energy (Dhyani and Bhaskar, 2017). Its structure is typically composed of three main building blocks: cellulose, hemicelluloses and lignin. Cellulose (see Figure 1a) is the most abundant organic polymer (Dhyani and Bhaskar, 2017), present in the cell wall of the plant cells. It is a natural polymer of repeating D-glucose unit, a six-carbon ring. Cellulose shows unique properties in terms of mechanical strength and chemical stability, due to its crystalline structure, originated from the three hydroxyl groups in the six-carbon ring, which can react among themselves, which allows to form intra- and intermolecular hydrogen bonds. Hemicelluloses (see Figure 1b) represent the interconnection between cellulose and lignin (Dhyani and Bhaskar, 2017) surrounding the cellulose fibers. While cellulose is characterized by a homogeneous structure, a complex system of heterogeneous groups of branched polysaccharides coexist in hemicelluloses. The structural elements are monomers like glucose, galactose, mannose, and xylose, having amorphous structures with low physical strength. Lignin (see Figure 1c), mostly present in the outer layer of the fibers, is responsible for the structural rigidity and acting as a bridge among the fibers of polysaccharides. It is an aromatic, three-dimensional and cross-linked phenolic polymer consisting of a random assortment “hydroxyl-“ and “methoxy-“ substituted phenylpropane units, whose monomers can be categorized as syringyl, p-hydroxylphenyl and guaiacyl units (Carrier *et al.*, 2011; Mohan *et al.*, 2006). There exist different types of lignin structures, depending on the type of biomass; for instance, hardwood lignin has a high methoxyl content, due to the presence of both guaiacyl and syringyl units, whereas softwood lignin is only composed of guaiacyl units (Liu *et al.*, 2008). Biomass also contains further components in smaller quantities: extractives, such as alkaloids, essential oils, fats, gums, and

proteins, acting as intermediates in metabolism, as energy reserves, and as plant defenses against microbial and insect attack (Mohan *et al.*, 2006). The last fraction included in biomass to be mentioned is the inorganic one, whose percentage ranges from less than 2% to as much as 15% in mass basis (Dhyani and Bhaskar, 2017). It mainly consists of compounds based on potassium, calcium, silicon, sodium, chlorines and phosphorus (Dhyani and Bhaskar, 2017).

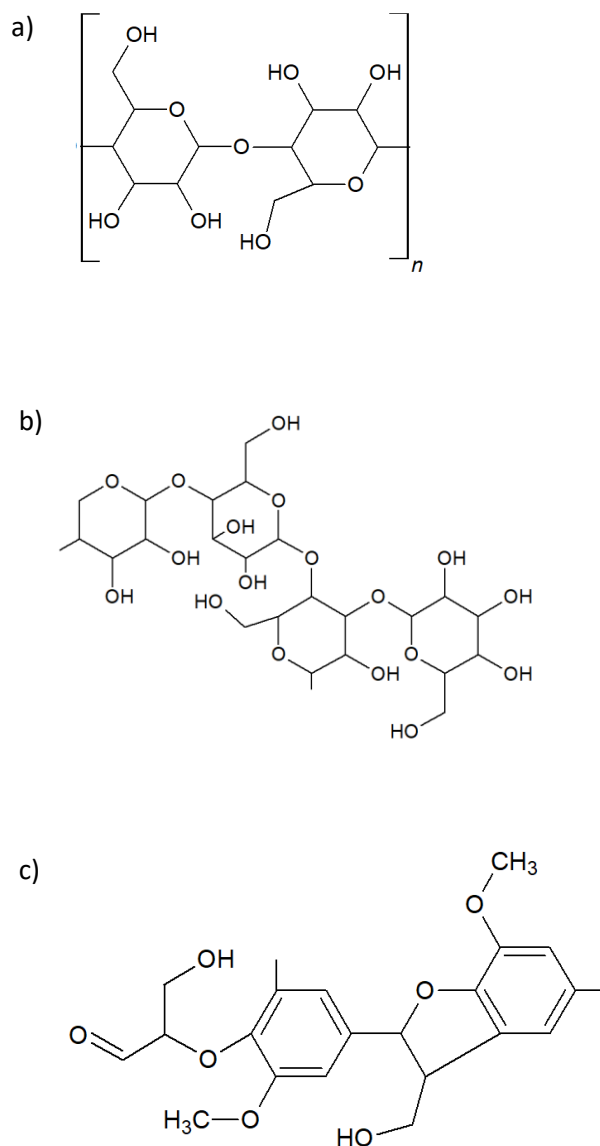


Figure 1. Chemical structures of a) cellulose monomer, b) a fraction of hemicellulose, and c) a fraction of lignin.

1.3 The concept of biochar

Concerns about climate change and food productivity have recently generated interest in biochar (Manyà, 2012), a form of charred organic matter, which is applied to soil in a deliberate manner as a means of potentially improving soil productivity and carbon sequestration (Lehmann and Joseph, 2009). A relevant number of studies are focused on the benefits of using biochar for mitigating global warming and as a solution to manage soil health and productivity (Fowles, 2007; Gaunt and Lehmann, 2008; Glaser *et al.*, 2002; Laird, 2008; Lehmann, 2007). However, these studies were often geographically limited and constrained by limited experimental data, due to the complexity of the research tasks (Manyà, 2012).

The term *biochar* refers to a carbon-rich, fine-grained, porous substance, produced by thermal decomposition of biomass under oxygen-limited conditions and at relatively low temperatures (i.e., indicatively below 700 °C) (Lehmann and Joseph, 2009; Sohi *et al.*, 2009). There exists a common misconception about the word “biochar”, which is often used to refer to “charcoal” or “char”. However, its definition stated by the International Biochar Initiative (IBI) clarifies the need for purposeful application of this material to soil for both agricultural and environmental gains (Sohi *et al.*, 2009). For the sake of clarity, in this work the word *biochar* will be used to address the solid product of the thermal degradation of biomass material, without considering its final application.

The commercial exploitation of biochar as a soil amendment is still in its infancy (Brassard *et al.*, 2019; Sohi *et al.*, 2009), since the relationship between its properties and its applicability into soil is still unclear (Manyà, 2012). For this reason, a synergic collaboration between different fields of research is needed: production and characterization of biochar on one side, and investigation of the biochar behavior in the agricultural soils on the other side, measuring both environmental and agronomical benefits.

One of the most interesting properties of biochar is its porous structure, which is believed to be responsible for improved water retention and increased soil surface area (Sohi *et al.*, 2009). Furthermore, an increase in the nutrient use efficiency has been observed when the biochar was added to the soil. This is due to the nutrients contained in biochar as well as the extent of physicochemical processes, which allow a better utilization of soil-inherent or fertilizer-derived nutrients. In addition, a key property of biochar is its biological and chemical stability (Nguyen *et al.*, 2009; Swift, 2001), allowing it to act as a carbon sink (Sohi *et al.*, 2009). Therefore, the conversion of biomass to more stable carbon species may result in a long-term

carbon sink, as the biomass removes atmospheric carbon dioxide through photosynthesis (McHenry, 2009), leading to a net removal of carbon from the atmosphere.

1.4 Production of biochar

Depending on the final use of biochar, a wide range of properties may be required. Therefore, different processes are adopted to synthesize the wide variety needed of biochars. This section describes several carbonization processes (see Table 1 for a summary) to produce biochar from biomass feedstocks.

1.4.1 Pyrolysis

The conversion of biomass into energy is mainly based on biochemical and thermochemical processes. Among all the thermochemical processes, it should be mentioned pyrolysis, during which the thermal decomposition of organic matter occurs within an environment under limited oxygen concentrations. The heating of biomass in an inert atmosphere results in the production of permanent gases (e.g., CO₂, CO, CH₄, H₂ and light hydrocarbons), and an organic volatile fraction from the cellulose, hemicelluloses and lignin polymers. These vapors can be condensed, giving an organic liquid known as pyrolysis oil or bio-oil. The bio-oil composition mainly depends on the lignocellulosic composition of the biomass (Mythili *et al.*, 2013). The non-condensable gases leave the reaction system and can be employed to provide heat for self-sustain the pyrolysis process. The remaining solid carbon-rich product is what we call biochar.

In the last decades, the reactions mechanism involved in pyrolysis process have deeply been studied. The most common classification reported in literature recognizes two type of pyrolysis reactions: primary and secondary. With reference to primary reactions, Collard and Blin (2014) applied a further classification, dividing them into three categories. The reactions belonging to the first class are responsible of the biochar formation, also known as primary biochar, characterized by high thermal stability and solid reticulation degree. The second category of reactions includes the depolymerization of the bio-polymers constituents, leading to the formation of condensable monomers, which result to be the main components of the liquid fraction (Mullen and Boateng, 2011; Scheirs *et al.*, 2001). Finally, the third group of reactions involves the production of permanent gases, when the monomer units interact among each other, creating new covalent bonds and releasing smaller molecules (Lu *et al.*, 2011). On the other hand, all the reactions of pyrolysis process involving further decomposition or recombination of by-products (i.e., volatile species) are known as secondary reactions. Their resulting products might condense on the biochar structure, leading to the formation of

secondary biochar, a carbon material thermally more stable than the primary one. Broadly speaking, the decomposition of hemicelluloses occurs at 220–315 °C, whereas the cellulose decomposes at 315–400 °C (Yang *et al.*, 2007). Differently from the cellulose and hemicelluloses, the highest fraction of produced biochar during pyrolysis derives from lignin; its temperature decomposition varies with its organic composition, and typically ranges from 160 °C to 900 °C.

The operating conditions of the pyrolysis process deeply affect distribution and yields of products (Varma and Mondal, 2017). Therefore, the process conditions can be adjusted as a function of the desired product. Depending on the operating conditions selected, pyrolysis can be categorized in three main types: slow, intermediate and fast.

1.4.1.1 Slow pyrolysis

Slow pyrolysis is indicated as one of the most appealing ways to obtain elevated biochar yields. Typical operating temperatures are around 400 °C (Antal and Gronli, 2003; Basu, 2013), even if wider ranges up to 700 °C are reported in the literature in some case (Sadaka and Negi, 2009). The process is characterized by slow heating rates (generally lower than 10 °C min⁻¹) as well as relatively long solid and vapor residence times (Sadaka and Negi, 2009), from minutes up to hours or even days. Overall, slow pyrolysis is aimed at producing large amounts of biochar, despite the resulting quantities of produced bio-oil, which cannot be considered negligible (Yang *et al.*, 2013). The available literature also refers to slow pyrolysis as “conventional pyrolysis”, since it is considered as the oldest type of pyrolysis, having been used for thousands of years for biochar production (Basu, 2013).

It is important to note that slow pyrolysis is often confused with torrefaction, which is carried out at lower temperatures, generally comprised between 200 °C and 350 °C (Arias *et al.*, 2008; Basu, 2013; Kolokolova *et al.*, 2013; Sadaka and Negi, 2009), in order to partly decompose the feedstock. The lower level of temperatures employed allows to obtain higher solid yield (around 80%) than that of slow pyrolysis (30%–35%) (Arias *et al.*, 2008; Sadaka and Negi, 2009).

1.4.1.2 Intermediate pyrolysis

Intermediate pyrolysis has recently gained particular attention, due to a significant technologic development. It is a technique adopted to improve the co-production of both biochar and bio-oil. It is characterized by aspects of both slow and fast pyrolysis, with moderate heating rates (indicatively around 100 °C min⁻¹), reaction temperatures from 400 up to 550 °C and short

residence times (10–30 s). This set of operating conditions permits an adequate control of the reaction environment, leading to a more even distribution among the resulting products (Yang *et al.*, 2014). An interesting feature of this process is that the produced liquid is often seen to readily split up into an aqueous and organic phase. A possible explanation is given by the contact with the by-product biochar, which acts as a catalyst (Bridgwater, 2012).

1.4.1.3 Fast pyrolysis

Fast pyrolysis exploits high heating rates (above 200 °C min⁻¹ and up to 1000 °C min⁻¹) and short vapor residence time (around 2 s) at temperatures indicatively of 500–550 °C (Manyà, 2012) in order to maximize the formation of liquid products (bio-oil) at the expense of minor yields of biochar (Zhang *et al.*, 2010). Resulting fractions of 60%–75% (in weight basis) for bio-oil are generally achievable by fast pyrolysis, whereas the final fractions of biochar and non-condensable gases are comprised between 15%–25% and 10%–20%, respectively, depending on the feedstock used.

From a chemical point of view, employing high heating rates leads to the production of biochars with a higher oxygen content (Yanik *et al.*, 2007) and a lower calorific value (Duman *et al.*, 2011), compared to the biochar derived from slow pyrolysis. This is explained by the shorter residence time of the vapor fraction, which inhibits the extent of secondary charring reactions. However, the biochar obtained through fast pyrolysis may exhibit larger specific surface area for the relatively small size of the feedstock usually required for such process (Manyà, 2012), as well as for the faster devolatilization, which causes the formation of more fragmented particles (Scala *et al.*, 2006) and a certain development of large micropores and mesopores at the expense of narrow micropores (which are dominant in slow pyrolysis-derived biochars).

1.4.2 Hydrolysis

Hydrolysis is considered as an alternative pyrolysis process, conducted at 300–550 °C in a reductive hydrogen environment instead of an inert one (Dayton *et al.*, 2016). The reducing H₂ gas generates hydrogen radicals, which react with the volatiles released from the biomass, leading to the production of H₂O, CO and CO₂, and hydrocarbons (Resende, 2016). Reacting with the hydrogen radicals, the reactive volatiles released by the process are prevented by any type of polymerization reactions (Melligan *et al.*, 2013; Thangalazhy-Gopakumar *et al.*, 2012). This leads to the formation of hydrocarbons with higher selectivity, if compared to that of the fast catalytic pyrolysis (Krishna *et al.*, 2016; Singh *et al.*, 2016). Energetically speaking, one

of the most important advantages of hydrolysis is its global exothermicity, which sustains in part the energetic costs related to the process. However, a continuous supply of H₂ and an operating pressure of 3.0 MPa are required along the process. Further studies are needed to assess the viability of this technology from both technical and economic points of view.

1.4.3 Gasification

The term gasification refers to the thermal conversion of biomass into a gas fuel by increasing the temperature over 700–800 °C in presence of a gasification medium such as air (Guizani *et al.*, 2015), oxygen or steam (Barisano *et al.*, 2016). The main products coming from this process are CO, CO₂, CH₄, H₂ and H₂O. Due to the severe conditions of temperature, gasification is not indicated as the best thermal process to obtain high biochar yields. However, biochars produced from gasification show higher carbon and ash content than those obtained by pyrolysis or torrefaction (Brewer *et al.*, 2009), likely due to the high process temperature, which enhances cracking reactions along with a simultaneous reduction of volatiles and an increment of fixed carbon.

1.4.4 Flash carbonization

Flash carbonization is a novel technology developed at the University of Hawaii at Manoa which allows the biomass to convert into biochar in a more efficient way than conventional slow pyrolysis, at temperatures comprised between 400 and 1000 °C (Antal *et al.*, 2003; Nunoura *et al.*, 2006; Wade *et al.*, 2006). The experimental apparatus consists of a pressurized vessel, which contains a canister with a fixed bed of a given biomass. Air is used to pressurize the vessel to an initial pressure of 1.0–2.0 MPa, and a flash fire is ignited at the bottom of the packed bed. Air is delivered to the top of the packed bed after a short time and the biomass is converted into biochar. The reaction lasts less than 30 min and the temperature profile is affected by several factors, such as the type of biomass, the air flow delivered, the heating time and the moisture content of the feedstock (Antal *et al.*, 2003). Antal *et al.* (2003) carried out a study on the flash carbonization behavior of some woods and agricultural byproducts, achieving biochar mass yields ranging between 29.5% and 40%, fixed carbon yields from 27.7% to 30.9%, and biomass energy conversion efficiencies into biochar from 55.1% to 66.3%.

The flash carbonization process seems to be a promising alternative route to produce biochar for the very short reaction times compared to those of the slow pyrolysis process (in batch operating mode), and for the possibility of retaining a larger amount of fixed carbon from the feedstock (Antal *et al.*, 2003).

Table 1. Operating conditions of different carbonization processes.

	Temperature	Pressure	Vapor residence time	Medium	Heating rate
Slow pyrolysis	≈ 400 °C	0.1–2.0 MPa	From minutes to days	Oxygen-free	<10 °C min ⁻¹
Torrefaction	<300 °C	Atmospheric	From minutes to days	Oxygen-free	<10 °C min ⁻¹
Intermediate pyrolysis	400–550 °C	Atmospheric	10–30 s	Oxygen-free	100 °C min ⁻¹
Fast pyrolysis	500–550 °C	Atmospheric	2 s	Oxygen-free	200–1000 °C min ⁻¹
Hydropyrolysis	300–550 °C	3.0 MPa	From seconds to minutes	H ₂ reductive atmosphere	> 10 °C min ⁻¹
Gasification	700–800 °C	Atmospheric	Few seconds	Oxygen-free or limited	> 10 °C min ⁻¹
Flash carbonization	400–1000 °C	1.0–2.0 MPa	Few seconds	Oxygen-free	Hundreds of °C min ⁻¹

1.5 Potential applications of biochar

It is widely known that biochar could be employed in several applications (Qian *et al.*, 2015) thanks to its unique properties —which strictly depends on the initial biomass composition— and to its current well-balanced commercial cost of 0.8–2.4 €/kg (Maroušek, 2014; Vochozka *et al.*, 2016). Today, the main use of biochar is addressed to the soil health improvement (Maroušek *et al.*, 2019) and as solid fuel (Abdullah and Wu, 2009). Limiting the employment of biochar to only these two applications would not allow to exploit its intrinsic potential, owed to its easy tuneability by simply adjusting the production process parameters (Al-Wabel *et al.*, 2013). In this section, a comprehensive overview on the possible multiple uses of biochar is reported.

1.5.1 Soil carbon sequestration

Traditionally, biochar has always been employed in agriculture, with the aim to increase the crop production, thanks to its favorable characteristics, which improve the physical, chemical and biological properties of soil. Many examples have been reported in the available literature during decades. For instance, it has been demonstrated that many biochars deriving from biowaste may enhance the soil water holding and capacity, and even improve the structural stability of soil (Méndez *et al.*, 2012) as well as nutrient content and cation exchange capacity (Paz-Ferreiro *et al.*, 2012). Furthermore, the biochar application in soils may really help decreasing the CO₂ emissions as well as other GHGs, like CH₄ or NO_x. With this purpose, the biochar storage in soils have been suggested as a potential technology for struggling the climate change, estimating that it can contribute in abating the CO₂ emissions up to 130 Pg over the course of a century (Woolf *et al.*, 2010). The carbon stability of biochar is a direct indicator of its potential carbon sequestration in soil, and strictly depends on both raw biomass feedstock and pyrolysis conditions, especially pyrolysis temperature. The operating conditions significantly affect the final biochar properties, such as the fixed carbon content, volatile matter, organic compounds and recalcitrance. In particular, the higher the pyrolysis temperature, the lower the biochar labile fraction. According to this, Bruun *et al.* (2011) observed a visible reduction in the cumulative CO₂ emissions (from 11% to 3%) originated from soil when the employed wheat-straw derived biochar produced at 475 °C was replaced with another one prepared at 575 °C.

1.5.2 Agricultural growing media

Recently, biochar has been proposed as growing media to reduce the current pressure on peatlands, which represent one of the most important type of soil carbon sink for CO₂ and CH₄ (Strack, 2008). Unfortunately, they are resources not considered as renewable at the human timescale; for this reason, great concerns on the peatland protection and their overexploitation have been emerged today. Being characterized by chemical and hydrophysical properties under the required level of other typical growing media components (e.g., vermiculite, perlite, clays), biochar is not indicated for its individual use as a growing media. However, its addition in proper rates as component in peat mixtures might result in benefic effects. In this sense, different biochars were tested, showing remarkable effects when mixed with peat, reaching yield increases over 100% (Méndez *et al.*, 2015; Nieto *et al.*, 2016). Other relevant results reported in literature are visible in Table 2.

Table 2. Peat/biochar mixtures reported in literature. Table adapted from Manyà and Gascó (2021).

Feedstock	Temperature (°C)	Feedstock	Component (% v/v)	Yield (%)	References
Organic fraction urban waste	270	Ryegrass	Peat	100	(Gascó <i>et al.</i> , 2018)
			Biochar	175	
			Peat + Biochar (50/50)	274	
Pruning waste	500	Lettuce	Peat	100	(Nieto <i>et al.</i> , 2016)
			Peat + Biochar (50/50)	200	
Deinking sludge	300	Lettuce	Peat	100	(Méndez <i>et al.</i> , 2015)
			Biochar	2	
			Peat + Biochar (50/50)	165	
Crushed wooden boxes	600	Sunflower	Biochar	100	(Steiner and Hartung, 2014)
			Peat	137	
			Biochar + Peat (25/75)	115	
			Biochar + Peat (50/50)	112	
			Biochar + Peat (75/25)	125	
Urban green waste	550	Wheat	Scoria (20% coir) + Biochar (70/30)	121	(Cao <i>et al.</i> , 2014)
			Scoria (20% coir) + Biochar (60/40)	111	
			Scoria + Biochar (60/40)	111	
Green waste	160–220	Calathea	Biochar	100	(Tian <i>et al.</i> , 2012)
			Biochar + Peat (50/50)	163	
			Peat	133	

1.5.3 Recovery of contaminated soils

Biochar has recently gained attention as means for soils recovery from organic and inorganic contaminants (Méndez *et al.*, 2009; Sopena *et al.*, 2012). Biochar properties such as surface area, surface functional groups, pH, high content of $\text{Ca}^{2+}/\text{Mg}^{2+}$ and CEC play a key role in the immobilization of heavy metals in soils, preventing their mobility and bioavailability (Méndez *et al.*, 2009; Paz-Ferreiro *et al.*, 2014) through processes of adsorption, precipitation or redox

reactions. The synergistic effect between the contaminants immobilization and the truly improvement of soils characteristics —water holding capacity, nutrient and organic contents, biological properties— resulting from the biochar addition made it one of the most promising candidates for soil amendment from an economic as well as sustainable point of view.

1.5.4 Biochar activation

Biochar usually has a relatively high surface area and developed porosity, but generally not sufficient to guarantee satisfactory performance in catalytic and adsorption applications (Shen *et al.*, 2014). In this kind of processes, such properties are highly recommended to facilitate high mass transfer fluxes and active loading (Titirici *et al.*, 2012). Therefore, an activation step with the objective to improve the original textural properties is needed. The activation process is defined physical when raw biochar is partly gasified with CO₂, steam or H₂ in the temperature range of 800–1000 °C, usually resulting in carbons with a well-developed microporosity (Liu *et al.*, 2015). The biochar activation can also occur chemically, by impregnating or mixing it with alkali species, such as KOH or K₂CO₃ at temperatures of 600–800 °C. Depending on the ratio between the alkali chemical and biochar, it is possible to tune the final porosity; in particular, lower ratios promote the development of micropores and ultra-micropores (Wei *et al.*, 2012), while higher ratios lead to pore widening high surface areas and high total pore volumes (Li *et al.*, 2014).

1.5.5 Adsorption processes

Nowadays, environmental pollution is gaining worrying magnitudes, due to recognized factors as the growing urbanization and the heavy industrialization. It is crucial to find new and more efficient routes to facilitate clean water, air and environments, preserving the human health and safety. In this scenario, biochar is a very appealing candidate as sustainable, precursor material able to remove both inorganic and organic pollutants through processes of adsorption or degradation (Bartoli *et al.*, 2020). For instance, Huggins *et al.* (2016) analyzed the possibility of its employment in the detoxification of watery sources, clearly demonstrating that biochar-based filtering materials adopted in their study reduced both the total chemical oxygen demand (COD) and ion concentrations (e.g., Cd²⁺, Pb²⁺, Cu²⁺, Zn²⁺, As³⁺) with outstanding efficiency. Biochar has also been employed for Cr(VI) removal, which is particularly toxic, instead of using more expensive adsorptive systems (Huggins *et al.*, 2016; Rengaraj *et al.*, 2001). Banerjee *et al.* (2018) claimed a very high Cr(VI) removal efficiency (94% wt.) when a zirconium-caged steam-activated biochar was employed as adsorbent in a contaminated water

flux. Regarding the removal of organic pollutants, the great variety of interactions that occur between biochar and organic molecules ranges from very weak (e.g., hydrophobic) to very strong (e.g. hydrogen bond). In several cases, the simultaneous presence of these interactions is the reason behind the remarkable performance of biochar as adsorbent of many compounds (Peiris *et al.*, 2017; Premarathna *et al.*, 2019; Tong *et al.*, 2019). In the available literature, biochar has been employed as means for removing persistent small organic molecules, such as aromatics. For instance, Jayawardhana *et al.* (2019) reported an efficiency of 850 and 550 $\mu\text{g g}^{-1}$ for toluene and m-xylene, respectively, when municipal solid waste-derived biochar was used for alkylated benzenes removal. Similarly, biochar-derived materials were employed in other studies to remove nitroaromatics (Lingamdinne *et al.*, 2015) and crude oil spills from synthetic seawater (AlAmeri *et al.*, 2019). Biochar is also used for dyes adsorption, which represents a great concern for water purification, due to their toxicity and persistency (Robinson *et al.*, 2001). Zazycki *et al.* (2018) assessed the feasibility of pecan nutshell biochar as low-cost adsorbent for Reactive Red 141 removal from aqueous solutions, reporting uptakes up to 130 mg g^{-1} , a result totally comparable with typical uptake capacities related to metal hydroxides (Netpradit *et al.*, 2003). On the other hand, Hou *et al.* (2019) used hydrochars produced at 800 °C from bamboo shoot shells for rhodamine B adsorption, achieving high uptakes (up to 86 mg g^{-1}).

Biochar can also be employed as precursor material in gas adsorption applications, presenting many advantages such as low cost, relatively easy regeneration (since a weak bonding between CO_2 and the adsorbent surface are typically involved in the process, differently from other adsorbent materials like zeolites or Metal Organic Frameworks, also known as MOFs) and hydrophobicity, a very useful feature to ensure appropriate performance in wet conditions (González *et al.*, 2013). In this context, one of the most common applications of carbon materials is CO_2 capture in post-combustion. Adsorbent carbons suitable for this purpose must show specific characteristics, such as high CO_2 uptake at low CO_2 partial pressures (10–15 kPa), high CO_2 selectivity over N_2 , relatively low heat of adsorption and fast adsorption kinetic rate (Hao *et al.*, 2013; Yang *et al.*, 2017). Despite the CO_2 uptake capacity of the adsorbent at low CO_2 partial pressures is mainly affected by the ultra-micropores volume (<0.7 nm) (Hao *et al.*, 2013), a certain extent of mesoporosity may help enhancing gas diffusion and transport within the ultra-micropores, reducing the resistance to mass transfer (Nelson *et al.*, 2016). On the other side, the CO_2 selectivity over N_2 is controlled by kinetics and thermodynamics. The small difference existing between the kinetic diameters of CO_2 (0.33 nm) and N_2 (0.36 nm)

molecules within porous solids favors the former one in terms of diffusion rate, especially when the adsorbent is characterized by pores with size very close to the N₂ kinetic diameter (Zhao *et al.*, 2015). From a thermodynamic point of view, the higher quadrupole moment of CO₂ ($-13.7 \cdot 10^{-24}$ cm²) compared with that of N₂ ($-4.9 \cdot 10^{-26}$ cm) leads to more intense interactions with the electrical field gradients of the sorbent, promoting the selective CO₂ uptake. The literature available on this kind of application is very extended; Liu and Huang (2018) reported a CO₂ uptake of 119 mg g⁻¹ at 35 °C for carbon materials deriving from spent coffee grounds. Huang *et al.* (2019) obtained uptakes of up to 53 mg g⁻¹ for sewage sludge-derived biochars produced by microwave torrefaction. In addition, several pyrolysis post-treatments are often recommended in order to improve the CO₂ adsorption capacity (e.g., introduction of basic groups by ammonia functionalization processes) (Przepiórski *et al.*, 2004; Shafeeyan *et al.*, 2011; Shen and Fu, 2018). More results from available studies in literature are reported in Table 3.

Other meaningful applications where biochar is employed as precursor are biogas upgrading and hydrogen purification. Generally, undesired compounds such as H₂S, H₂O and CO₂ can be sequentially removed through processes of absorption, adsorption or membrane separation in order to upgrade biogas. Biochar chemical activation with NaOH, KOH or K₂CO₃ is particularly indicated for H₂S removal from raw biogas, even at relatively low concentrations (i.e., lower than 0.1 vol. %) (Castrillon *et al.*, 2016). In addition, biochar impregnation with Fe₂O₃ has emerged as an alternative way to improve the H₂S uptake (Bagreev *et al.*, 2001). A further option is physical activation; for instance, Hervy *et al.* (2018) observed outstanding H₂S uptakes (up to 67 mg g⁻¹) for wastes pyrolysis carbons physically activated with steam, obtained from wood pallets, food waste and coagulation-flocculation sludge.

In hydrogen purification processes, the removal of impurities such as CO, CO₂, CH₄ and H₂O can be achieved by pressure swing adsorption (PSA) in a multilayer bed of different adsorbents. The first layer is typically a silica or alumina gel bed for water vapor removal. Activated carbons are typically employed in the second layer for CO₂ adsorption, whereas CO and CH₄ are removed in a third layer of zeolite-based adsorbents (Manyà and Gascó, 2021).

Table 3. CO₂ uptakes at 25 °C and 0.015 MPa for different porous carbon materials reported in literature. Table adapted from Manyà and Gascó (2021).

Precursor	Preparation	CO ₂ uptake (mmol g ⁻¹)	Reference
HTC biochar from grass cuttings	Physical activation with CO ₂ at 800 °C	1.10	(Hao <i>et al.</i> , 2013)
Vine shoots biochar	Physical activation with CO ₂ at 800 °C	1.22	(Manyà <i>et al.</i> , 2018)
Rice husk biochar	Chemical activation with KOH	1.55	(Li <i>et al.</i> , 2015)
Coconut shell biochar	Chemical activation with KOH	1.45	(Yang <i>et al.</i> , 2017)
Coconut shell biochar	Precursor modification by urea and chemical activation with KOH	1.40	(Chen <i>et al.</i> , 2016)
Pine nut shell biochar	Chemical activation with KOH	2.00	(Deng <i>et al.</i> , 2014)
Almond shells	Single-step activation with CO ₂ at 800 °C	1.10	(González <i>et al.</i> , 2013)
Coconut shell biochar	Preoxidation with H ₂ O ₂ followed by ammoxidation. Then, chemical activation with KOH	1.35	(Guo <i>et al.</i> , 2016)
HTC biochar from empty fruit brunch	Chemical activation with KOH	1.20	(Parshetti <i>et al.</i> , 2015)
Pomegranate peels	Single-step activation with KOH	1.25	(Serafín <i>et al.</i> , 2017)
HTC biochar from Jujun grass	Chemical activation with KOH	1.50	(Coromina <i>et al.</i> , 2016)

1.5.6 Catalysis

Given the elevated tuneability in physical and chemical properties and their relatively low cost, the conception of biochar as catalyst or catalytic support has been gaining interest among the scientific community (Chatterjee *et al.*, 2018). Despite the most common use of biochar in catalysis is as support for metal or metal oxide active sites, the presence of oxygen-containing groups like carboxylic, furanic or phenolic, makes biochar suitable for its own catalytic activity too. However, the addition of further surface functionalities, such as acidic $-\text{SO}_3\text{H}$ groups or dispersed metal nanoparticles, is recommended for better catalytic performance of these materials. Moreover, it is important to mention also other properties such as surface area, porosity, hydrophobicity, mineral content and particle strength, playing a key role in catalysis. Biochar use has already been tested in many related fields of application, such as syngas cleaning and conversion, air pollution control (Church *et al.*, 2021), biodiesel production (Yan *et al.*, 2013), pyrolytic vapor (Di Stasi *et al.*, 2021) and oil upgrading (Dong *et al.*, 2018).

1.5.7 Energy storage

Among the wide class of carbon-based materials, biochar emerges as one of the most relevant for energy storage, showing important advantages as high stability, high sustainability, low cost and nontoxicity, when compared to other materials. Most applications in this field requires its previous activation and/or functionalization steps, leading to engineered carbons having appropriate textural, surface chemistry and structure features. Their relatively good heat and electric conductivity are high desirable features for heat storage and charged ions. While it is believed that biochar-based materials can offer several advantages in heat storage applications but no extensive literature is available on the topic, much more research has been carried out in storage of charged ions and electrons, especially in development of supercapacitors and batteries (Yu *et al.*, 2013).

2. State of the art

Biochar can be produced as a coproduct from several different processes, as explained in the previous sections. The properties of a given biochar strongly depend on the characteristics of each process and on the material to which the process is applied. In addition, selecting proper process operating conditions might be crucial not only on the resulting biochar features, but also on the energy and exergy efficiency of the process.

In this work, the most appropriate pyrolysis conditions were determined in order to improve the biochar properties for its employment as a carbon sequestration agent. Moreover, further uses of the produced biochars have been explored; they were tested in germination assays—to evaluate their possible phytotoxicity, assessing their employment in eventual soil amendment applications—and in adsorption applications for biogas upgrading. In this chapter, a comprehensive state of the art about the influence of slow pyrolysis operating conditions on the final biochar properties and on the energy/exergy efficiency of the process is reported. A special emphasis has been paid on the absolute pressure, of which potential, beneficial effects on biochar characteristics as well as on the energy demand required by the production process still remain unclear. In addition, an overview on the properties of biochar and derived materials that are closely related to the applications assessed in the present study (i.e., PAHs content assessment, phytotoxicity, and biochar physical activation for biogas upgrading) is also presented.

2.1 Influence of pyrolysis conditions

Given the high number of variables affecting the process and the wide range of available biomass sources, a large variability in the biochar properties should be expected (Manyà, 2012). Therefore, one of the main challenges nowadays is to optimize the process conditions of pyrolysis for a given biomass feedstock (Mašek *et al.*, 2013; Ronsse *et al.*, 2013) with the aim of obtaining an appropriate set of characteristics in line with those required for the biochar end-use.

2.1.1 Peak temperature

Peak temperature is generally defined as the highest temperature reached during the pyrolysis process (Antal and Gronli, 2003). The influence of peak temperature on the biochar yield and its potential stability has already been studied in a large number of works available in the literature. As a general trend, the biochar yield decreases as the peak temperature increases (Abdullah and Wu, 2009; Demirbaş, 2004; Di Blasi *et al.*, 1999; Duman *et al.*, 2011; Méndez

et al., 2013), whereas the resulting fixed-carbon content in biochar gradually increases with temperature (Antal, M. J. *et al.*, 2000; Antal and Gronli, 2003; Enders *et al.*, 2012; Manyà *et al.*, 2013; Zhao *et al.*, 2013). An increase in peak temperature usually contributes to an overall increment of the aromatic C fraction (McBeath *et al.*, 2011; Wu *et al.*, 2012; Zhao *et al.*, 2013) and to a decrease in both H:C and O:C atomic ratios (Enders *et al.*, 2012; Ghani *et al.*, 2013; Sun *et al.*, 2012). All these aspects suggest that higher peak temperatures lead to higher biochar chemical recalcitrance to abiotic and biotic degradation.

McBeath *et al.* (2015) conducted several hydrolysis experiments, producing biochar from common feedstocks at ten different temperatures between 300 and 900 °C, in order to assess their influence on carbon stability. They observed that higher temperatures resulted in lower biochar yields for each feedstock tested. During the process, the initial decline in biochar yield was visible in the range of 300–450 °C, depending on the feedstock type, as a consequence of the thermal decomposition of cellulose and hemicelluloses. For peak temperatures ranging from 300 to 600 °C, the biochar yield halved the value obtained at 300 °C. From 600 °C to 900 °C, the effect of peak temperature became relatively smaller if compared at lower temperatures. On the other hand, the positive effect of temperature on potential biochar stability must be mentioned. Manyà *et al.* (2014a) examined the combined effect of pressure and peak temperature on the potential stability of two-phase olive mill waste biochar obtained by slow pyrolysis in a laboratory-scale fixed-bed reactor, using the atomic H:C and O:C ratios, the fixed-carbon yield and the aromatic C fraction as rough indicators of the biochar stability. They observed a negative effect of temperature on biochar yield, but also a favorable effect on the fixed-carbon yield, improving the long-term C sequestration potential of biochar. The authors achieved high potential stability and adequate biochar yields at 600 °C and 1.1 MPa. In addition, the marked increase in the aromatic C fraction with peak temperature was accompanied by an increase in pH, probably due to the reduction of acid functional groups, which led to a visible drop in the cation exchange capacity of biochar in soils. The main conclusion was then the impossibility to achieve both the highest potential carbon stability and the most proper biochar properties —for soil improvement purposes— under the same pyrolysis conditions.

2.1.2 Absolute pressure

The role of absolute pressure in slow pyrolysis has not been properly demonstrated yet, given the inconsistency revealed in previous studies. Most of them reported an increase in biochar and gas yields, at the expense of the liquid yield, when both the pressure and vapor residence

time raised (Antal, M. J. *et al.*, 2000; Antal, *et al.*, 1996; Noumi *et al.*, 2015; Qian *et al.*, 2014; Recari *et al.*, 2014; Rousset *et al.*, 2011). Antal, *et al.* (1996) conducted experiments in order to identify the effects of operating pressure on biochar yields from macadamia nut shells. They accomplished a solid yield of 40.5% wt. with just 0.4 MPa. A further increase in pressure to 3.3 MPa resulted into a biochar yield of 51% wt. This increase was partly justified by the prevalence of interactions with the higher volatile matter content at higher pressures, meaning that the pressure effect on biochar yield was less strong than expected. For values above 1.0 MPa, the pressure lost its relevant influence, becoming its effect very slight on the biochar yield. On the other side, it is important to highlight that an improved heat transfer within the reactor was achieved at higher pressures, allowing the synthesis of a more uniform biochar in a shorter heating time required by the process. In line with these considerations, Qian *et al.* (2014) reported an increasing trend for the yields of biochar, water, and gas from 0.1 MPa to 1.0 MPa at a constant linear velocity of the gas flow (i.e., constant gas residence time) as well as a decreasing organic condensable products yield during the pyrolysis of rice husks. The reason behind these outcomes can be found in an enhancement of reactions involved in the pyrolysis process, such as polycondensation, dehydration and cracking of the volatiles, which result into a further formation of biochar, water and gas. Nevertheless, in the range of pressures comprised between 1.0 and 5.0 MPa, this effect became negligible. The same study (Qian *et al.*, 2014) was then carried out with same level of pressures and keeping constant the volumetric flow rate. In other words, this means that the higher the pressure, the higher the gas residence time in order to ensure the desired conditions of volumetric flow rate. While the yield trends for all the pyrolysis products as a function of pressure were similar to those observed at constant linear velocity of gas flow, the yields of biochar and gas resulting from atmospheric pyrolysis were similar to the previous ones. On the other hand, the yield of condensable organics increased, whereas the water yield decreased. To conclude, the obtained results suggested that the vapor residence time plays an important role under atmospheric pressure in promoting the dehydration of volatiles.

In contrast to the findings reported above, Manyà *et al.* (2014a) observed a significant decrease in biochar yield when the pressure was increased, keeping constant the gas residence time (i.e., constant velocity of the carrier gas) within the reactor. This could be attributed to the enhancement of the kinetics of the steam gasification reaction with pressure—and catalyzed by the alkaline metals inherently present in the biomass source—. Furthermore, the combined effects of pressure and temperature resulted into higher fixed-carbon contents and lower H:C

and O:C atomic ratios, leading to better long-term C sequestration potentials. Similarly, Azuara *et al.* (2017) observed a slight decrease in the yield of vine shoots-derived biochar when the pressure varied from 0.1 MPa to 1.1 MPa, as a consequence of the promotion of the steam gasification reaction together with a dilution effect of pyrolysis volatiles, caused by an increase in the mass flow rate of carrier gas to keep constant its residence time within the reactor. In this sense, the minor volatiles partial pressures due to the dilution effect could lead to a lower extent of secondary charring reactions. On the other hand, the fixed-carbon yield was practically unaffected by pressure, suggesting that other process parameters, such as peak temperature, could mainly explain the fixed-carbon content in the produced biochar. An important contribution was given by Legarra *et al.* (2018), whose study was focused on constant-volume carbonization (CVC) of spruce and birch wood employing a sealed reactor, which retained the pyrolytic products in the reaction zone in the absence of gas flow. In this way, it was possible to decouple the pressure effect from that related to the gas residence time, allowing the evaluation of the truly effect of pressure on carbonization processes. The resulting biochar showed a fixed-carbon yield that approached the highest value predicted by thermodynamics. Similarly, Mok *et al.* (1992) carried out carbonization experiments in sealed vessels, reporting an exothermic behavior of the process and high biochar yields (40% wt. from cellulose and 48% wt. from *Eucalyptus gummifera*). Furthermore, the concentration of the released volatiles, instead of the effect of absolute pressure, revealed to be the real main factor affecting the reported results. The addition of an external gas to increase the reactor pressure resulted to be negligible on biochar yield and reaction heats. In conclusion, it is believed that absolute pressure could affect (directly or indirectly, if its influence is coupled with other effects) the potential stability of biochar and, to a lesser extent, the biochar yield. The magnitude of its influence will depend on the nature of the feedstock (since a higher content in alkaline metals will further promote gasification) as well as the selected operating conditions in terms of vapor residence time, reactor configuration, and partial pressure of volatiles.

2.1.3 Vapor residence time

It is widely recognized that long vapor residence times associated with low temperatures usually leads to higher biochar yields (Encinar *et al.*, 1996). An increase in the gas residence time results in a prolonged contact between the solid and gas phases, leading to a further decomposition of the tarry vapors onto the solid carbonaceous matrix through secondary reactions as condensation, repolymerization and thermal cracking (Manyà, 2012). As a consequence, biochar yield increases at the expense of the condensable fraction of products

(Akhtar and Saidina Amin, 2012; Guedes *et al.*, 2018; Heo *et al.*, 2010). It is also known that differences in gas residence time not only influence the resulting biochar yield; the biochar quality and properties might be visibly affected by longer residence times, which favor well-developed micro- and macro-pores (Tsai *et al.*, 1997). However, evaluating the role of residence time upon biochar production could be very complex, since its effect is often overwhelmed by peak temperature, heating rate or other parameters (like pressure, as discussed in previous section). For instance, high temperatures combined with high residence times lead to a decrease in biochar yield. On the other hand, higher biochar yield is expected when prolonged residence times are applied at lower temperatures (Tripathi *et al.*, 2016).

2.1.4 Pyrolysis environment

The idea of employing the flue gas generated by combustion of pyrolysis gas as pyrolysis gas environment can lead to important cost savings (Mašek *et al.*, 2013), resulting in an improvement in the biochar production process in terms of thermal efficiency, environmental impact and economic feasibility. However, further investigations are needed in order to assess the effects of modifying the type of atmosphere on the pyrolysis products distribution as well as on the biochar properties. Currently, only few studies are available on analyzing the proper pyrolysis environment and its effect during pyrolysis. For instance, Biswas *et al.* (2018) investigated the pyrolysis behavior of rice straw under CO₂ atmosphere at temperatures comprised between 300 and 450 °C, using a fixed-bed reactor. They observed a marginal improvement of biochar and organic condensable compounds yields in the presence of CO₂ instead of N₂, whereas the gas yield was slightly reduced. The authors also suggested that CO₂ could promote some repolymerization reactions, resulting in a higher biochar yield. In line with this, using a CO₂-containing atmosphere resulted in higher degrees of carbonization (i.e., lower H:C and O:C atomic ratios), especially at relatively high pyrolysis peak temperature. In contrast to these results, no influence of the pyrolysis environment on the yield of vine shoots-derived biochar were observed in the study by Azuara *et al.* (2017). The main finding from this study was the fact that the switch from N₂ to CO₂ led to a significant decrease in the yield of produced CO₂, together with a proportional increase in the release of CO, due to the relatively high CO₂ partial pressures, which promoted the reverse Boudouard reaction. In addition, the extent of this reaction could explain the higher porosity development observed for biochars produced under CO₂.

During the production of red pepper stalk-based biochars under a CO₂ environment, Lee *et al.* (2017) observed that thermal degradation occurred faster than under a pure N₂ environment, meaning that CO₂ enhanced the thermal degradation of amorphous substances such as lignin. Pyrolysis under CO₂ also resulted in higher degrees of carbonization and a clearly enhancement of the thermal cracking of condensable volatiles. The authors also reported that the aromatic fraction contained in biochars produced under CO₂ was higher than those of the biochars produced under N₂. Bearing in mind that the aromatic carbon is more stable than aliphatic carbon under conditions of biotic and abiotic oxidation, it was possible to conclude that biochar produced under CO₂ could be more recalcitrant than that produced under an inert atmosphere.

2.1.5 Additional factors

Besides the effects of peak temperature, absolute pressure, gas residence time and pyrolysis environment explained in the previous sections, there are further factors to be mentioned which might have certain effects on the final biochar characteristics. For instance, biochar yield is certainly influenced by the feedstock composition (i.e., percentage of lignin, cellulose, hemicelluloses, extractives and inorganic matter). Indeed, biomasses possessing high lignin contents generally lead to higher yields of biochar (Antal and Gronli, 2003; Mok *et al.*, 1992). Similarly, higher yields of biochar were observed from pyrolysis of extractive-rich woods, such as chestnut (Di Blasi *et al.*, 2001). The moisture content can also play a relevant role; previous studies (Antal, *et al.*, 1996; Dai and Antal, 1999; Demirbaş, 2004; Varhegyi *et al.*, 1993) demonstrated a visible improvement in the biochar yield produced by pressurized pyrolysis of biomasses containing between 42% wt. and 62% wt. In addition, the presence of alkali and alkaline earth metals (AAEMs) is always associated with lower temperatures required for pyrolysis, higher yields of biochar and gas, and lower yields of condensable products (Di Blasi *et al.*, 2009; Raveendran *et al.*, 1995). Z. Wang *et al.* (2010) reported an increase in the yields of biochar and gas produced from pine wood through slow pyrolysis by adding K₂CO₃. In contrast to that, in another work (D. Wang *et al.*, 2010) the presence of CaO resulted to have a catalytic effect on the cracking of volatiles, promoting the decarboxylation of organic acids and leading to the formation of light hydrocarbons. After a study carried out on the effects of pressure combined with the addition of a rejected material from municipal waste composting on the pyrolysis behavior of two-phase olive mill waste, Manyà *et al.* (2016) observed that it was possible to accomplish a decrease in the biochar yield at any pressure by adding AAEMs-rich materials. This might be likely related to a higher catalytic role of AAEMs during the primary devolatilization as well as secondary reactions (e.g., cracking and steam and dry

reforming of volatiles). In other words, the secondary charring reactions were not sufficiently promoted by AAEMs.

Particle size is another factor reported in the literature as highly correlated with the final biochar yield. An increase in particle size leads to more pronounced gradients of temperature within the particles during the carbonization process, resulting in higher biochar yields as well as lower liquid and gas yields (Encinar and Gonzalez, 2000; Şensöz *et al.*, 2000; Şensöz and Kaynar, 2006). The greater the particle size, the lower the diffusion rate of volatiles within the biochar particles, leading to prolonged contact times between the solid and the gas phase; as a consequence, a further formation of biochar is favored by means of secondary reactions (Di Blasi *et al.*, 1999; Manyà *et al.*, 2007; Varhegyi *et al.*, 1998). The possibility of using large biomass particles also leads to important cost savings, such as the absence of energy-intensive milling processes and the improvement of the self-sustaining pyrolysis process, given the exothermic nature of the secondary reactions (Antal, *et al.*, 1996; Stenseng *et al.*, 2001).

2.2 Energy and exergy efficiencies of slow pyrolysis process

As already stated by Mok and Antal (1983), the pyrolysis process is very complex, since it comprises both endothermic (i.e., evaporation and tar formation) and exothermic (i.e., formation of char and gas) steps. Furthermore, the global amount of energy will depend on the operating conditions considered for the process. Hence, energy and exergy assessments are of great interest for scaling the process up to a commercial scale (Daugaard and Brown, 2003). It is important to note that the energy analysis provides the amount of energy required for pyrolysis, while the exergy analysis gives information about the energy quality, since exergy accounts for the irreversibility of the process and the maximum work that can be obtained (Dincer and Rosen, 2013). In other words, exergy shows a reverse relationship with energy sustainability: a decrease in energy quality loss corresponds to the incline of sustainability (Saidur *et al.*, 2012). For this reason, its assessment could result to be of great relevance in order to evaluate and improve the efficiency related to the thermochemical routes of different biomasses (Chaiwatanodom *et al.*, 2014).

Exergy analysis of processes like pyrolysis or torrefaction of biomass is not very common in the available literature, and the number of studies focused on the effects of temperature and pressure on the exergy efficiency is very limited and mainly restricted to gasification processes. Nonetheless, the positive effect of pressure on the exergy efficiency during pyrolysis was already observed by Srinivas *et al.* (2009), which promoted the conversion of the volatile organic compounds in further gas products and, hence, reducing the exergy losses at the end of

the process. The opposite trend was however observed by Prins and Ptasinski (2005) and Wang *et al.* (2016), who reported a negative effect of pressure on the exergy efficiency of the overall biomass gasification and combustion processes. This discrepancy could be justified by the different operating conditions and nature of the thermochemical processes analyzed.

2.3 Key properties of biochar

This section aims at describing the main biochar's properties related to the applications under study herein: (1) its addition to soil as a means of sequestering carbon, and (2) its subsequent activation to be used as selective CO₂ adsorbent in biogas upgrading processes. For the former final use, the PAHs contents in biochar and its potential phytotoxicity should be assessed. For adsorption purposes, assessing the textural properties (specific surface area and pore size distribution) of activated biochar is essential.

2.3.1 Contents of PAHs in biochar

Although biochar can be used in a wider range of applications (Antal and Gronli, 2003; Basu, 2013), a clear understanding of its employment as soil amendment still lacks. Regardless its potential agronomic benefits, the application of biochar into soil also embraces potential risks for the environment due to its content of polycyclic aromatic hydrocarbons (PAHs). Being the largest group of carcinogenic, mutagenic and teratogenic compounds, PAHs are nowadays classified as priority pollutants in the lists of the European Union and US Environmental Protection Agency (European Commission Regulation (ECR), 2006). In light of this, many international institutions established a range of allowed concentrations of PAHs in biochar for soil applications, which stands under 4 and 12 mg kg⁻¹ for premium and regular biochars, respectively, according to the (European Biochar Certificate (EBC), 2019), and within the range comprised between 6 and 20 mg kg⁻¹, as established by the International Biochar Initiative (International Biochar Initiative (IBI), 2015). Therefore, it is essential to produce biochars with low PAH concentrations in order to prevent adverse effects on the soil ecosystem and on human and animal health, in line with the environmental legislation.

PAHs are highly condensed aromatic structures produced during the pyrolysis process (Schmidt *et al.*, 2015). Their final concentrations in the produced biochar range from <0.1 to >10.000 mg kg⁻¹ (Wang *et al.*, 2017), strictly depending on the pyrolysis operating conditions adopted, the design of the pyrolysis unit and the raw biomass employed (Fabbri *et al.*, 2013). However, the influence of the pyrolysis factors analyzed in this work still remains unclear. The relationship between the pyrolysis peak temperature and the distribution of the produced PAHs

results to be inconsistent in the literature (Brown *et al.*, 2006; Buss *et al.*, 2016; Hale *et al.*, 2012; Rogovska *et al.*, 2012). It is known that dehydrogenation, dealkylation, cyclization and aromatization are the main reactions involved in the PAHs formation at relatively low pyrolysis conditions (Simoneit, 1998), whereas a further recombination of reactive radicals occurs when higher energy pyrolysis conditions are applied, leading to the formation of more condensed PAHs (De la Rosa *et al.*, 2008). It is believed that gas residence time might affect the final PAHs content. Generally, longer gas residence times could result in biochars with higher PAHs contents, since PAHs are predominantly synthesized in the gas phase (Lehmann and Joseph, 2009). Madej *et al.* (2016) observed that using relatively high carrier gas (N₂) flow rates during the pyrolysis of several biomass sources resulted into the synthesis of biochars with relatively low PAHs contents (less than 1.5 mg kg⁻¹), regardless of the peak temperature used. It is also believed that the absolute pressure plays a key role in the PAHs formation, even if its influence has been much less explored on the overall pyrolysis process (Azuara *et al.*, 2017; Bui *et al.*, 2016; Manyà *et al.*, 2013; Rousset *et al.*, 2011). Matamba *et al.* (2020) observed that higher pressures led to the selective production of higher molecular weight PAHs at the expense of two-ring structures, suggesting that an increase in both pyrolysis pressure and temperature promoted the ring growth mechanism. Such class of reaction could be enhanced by longer retention times of volatiles in the biochar matrix, as a consequence of a mass transfer inhibition due to the high pressures. A CO₂-based pyrolysis atmosphere could also influence the PAHs formation during the thermal process, as reported in earlier studies, which found out that the presence of CO₂ can promote the soot production under certain conditions. For instance, Abian *et al.* (2012a; 2012b) stated that an increase in the soot yield during ethylene pyrolysis was observed when the CO₂ concentrations was relatively low, whereas the soot formation was inhibited with much higher CO₂ concentrations. On the other hand, Chang *et al.* (2018) noticed that the sooting tendency during coal pyrolysis increased much more within a CO₂ atmosphere than in one consisting in pure N₂. However, the effect of CO₂-based atmosphere on PAH formation during biomass pyrolysis has not been studied yet.

2.3.2 Physically activated biochar as CO₂ adsorbent

Having a low environmental impact, biofuels represent a valuable alternative to fossil fuels: their widespread use might significantly contribute to reduce the emissions of CO₂, hydrocarbons and SO_x (Shuba and Kifle, 2018). Biogas is mainly produced by anaerobic digestion processes (Goula *et al.*, 2006) and can be certainly considered as a biofuel, due to its relatively high CH₄ content. Indeed, it generally contains CO₂ and CH₄ in different proportions

(30%–45% and 55%–70%, respectively, in vol. %) (Castrillon *et al.*, 2016) but also NH₃ and H₂S in smaller percentages, depending on the organic substrate. Prior to its application as biofuel, biogas needs to be refined by reducing the CO₂ content, in order to improve its heating value, raising it close to that of natural gas (Castrillon *et al.*, 2016), as well as to lower the risk of pipelines corrosion in presence of water (Durán *et al.*, 2018). Among all the available technologies for biogas upgrading, one of the most promising for its relatively low cost and high energy efficiency is CO₂ separation through adsorption processes (Grande, 2012). For this purpose, activated carbons (ACs) are denoted as appealing candidates, presenting many advantages such as high CO₂ adsorption capacity (even at environmental conditions), fast kinetics, thermal stability and low costs related to their production and regeneration (Durán *et al.*, 2018; Peredo-Mancilla *et al.*, 2019; Zheng *et al.*, 2019).







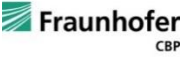

The sustainable production of ACs from biomass typically consists in two main steps: the first involves the thermal degradation of biomass via pyrolysis (or hydrothermal carbonization), obtaining biochar (hydrochar) as a precursor of such advanced carbon materials. Since the pristine biochar is usually characterized by a low specific surface area and is dominated by narrow micropore distributions (Manyà *et al.*, 2018), a second step of activation (either physical or chemical) is required for a further development of porosity (Molina-Sabio *et al.*, 1996; Plaza *et al.*, 2014).

In line with the observations made in the previous sections, a proper choice of pyrolysis operating conditions is necessary in order to obtain the most appropriate biochar for its subsequent activation towards porous carbon materials. From an environmental point of view, it is important to highlight that the employment of steam or CO₂ as activating agents makes physical activation more convenient than chemical activation. Another option for producing ACs is by a one-step activation pathway, adopting pyrolysis peak temperature over 650 °C and replacing the inert gas (typically N₂) with an activating agent (e.g., CO₂, H₂, H₂O). It is considered a very appealing solution in terms of energy recovery at large scale, allowing to directly produce activated carbons avoiding any intermediate pyrolysis step. The few previous studies available in the literature (González *et al.*, 2013; Linares-Solano *et al.*, 1980; Lua and Guo, 2000; Yang *et al.*, 2010) reported encouraging results concerning the one-step synthesis process, indicating that activated carbons obtained directly from biomass showed similar or even better properties than those produced via traditional two-step processes.

3. The GreenCarbon project

This work was carried out within the framework of a training-through-research network (GreenCarbon project), which was funded by the European Union’s Horizon 2020 research and innovation program under the Marie Skłodowska-Curie grant agreement No 721991 (2016–2021). The main goal of the research program was to develop advanced biomass-derived carbons to be employed in several energy and environmental applications to drive new technologies for biomass/biowaste upcycling. The GreenCarbon project consortium was constituted by eight beneficiaries and several partner organizations from both academic and industrial sectors. More details about the consortium are given in Table 4.

Table 4. Consortium (beneficiaries) of the GreenCarbon Project.

Beneficiary	Country	Person in charge	
University of Zaragoza (coordinator)	 Universidad Zaragoza	Spain	Joan J. Manyà
University of Ghent	 UNIVERSITEIT GENT	Belgium	Frederik Ronsse
Stockholm University	 Stockholm University	Sweden	Niklas Hedin
University of Hohenheim	 UNIVERSITY OF HOHENHEIM	Germany	Andrea Kruse
Aston University	 Aston University Birmingham	United Kingdom	Tony Bridgwater
Queen Mary University of London	 Queen Mary University of London	United Kingdom	Magdalena Titirici / Ana J. Sobrido
The Fraunhofer Center for Chemical-Biotechnological Processes	 Fraunhofer CBP	Germany	Christine Rossberg / Ireen Gebauer
The University of Edinburgh	 THE UNIVERSITY OF EDINBURGH	United Kingdom	Ondrej Masek

The specific objectives to be achieved by the project are listed below (see also Figure 2):

- The development and optimization of thermochemical processes (hydrothermal carbonization, slow and intermediate pyrolysis, as well as cascaded processes) to produce tailor-made biomass-derived carbons.
- The production of sustainable and low-cost biomass-derived adsorbents and heterogeneous catalysts and their employment in: CO₂ adsorption in postcombustion conditions, H₂S adsorption from biogas, catalytic pyrolysis vapors upgrading, catalytic methanation of CO₂, and catalytic hydrothermal processing of biomass toward platform chemicals (e.g., levulinic acid and 5-HMF).
- Assessing the suitability of biochars (as well as spent biochar-based materials) as soil enhancers and peat replacement in growing media for horticultural applications.

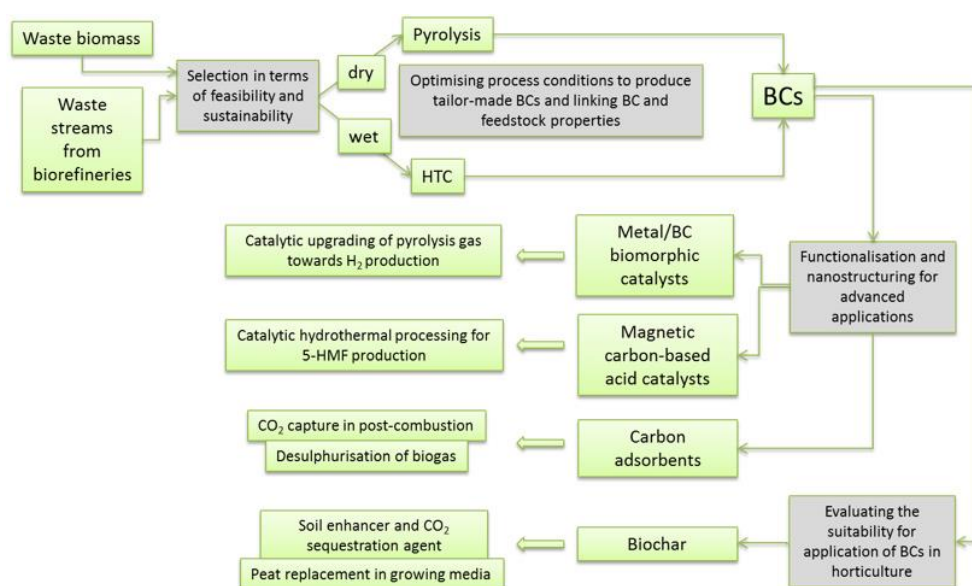


Figure 2. GreenCarbon Project objectives (reproduced under permission of the GreenCarbon project consortium).

The present PhD research project was included in the work package related to biochar production and was mainly focused on providing scientific evidence on the effect of absolute pressure, peak temperature and vapor residence time on the main biochar properties obtained by slow pyrolysis of two types of feedstock (wheat straw pellets and wood waste), under both inert N₂ and CO₂ atmospheres, and demonstrating its potential use in the above-mentioned kind of applications (as final product for soil enhancing purposes and as precursor material for adsorption and heterogeneous catalysis processes).

4. Objectives

Keeping in mind the current state of knowledge concerning the influence of pyrolysis operating conditions on the key biochar properties affecting its performance as soil amendment and adsorbent in biogas upgrading processes, the main objective of this PhD Thesis is to analyze the effects of several pyrolysis conditions (i.e., peak temperature, absolute pressure, gas residence time, and type of pyrolysis atmosphere) on the product yields and distributions as well as the physicochemical properties of produced biochars. A special attention has been paid on (i) the effect of the absolute pressure on the overall pyrolysis process (in terms of energy efficiency and products quality), and (ii) using a CO₂-containing gas carrier to replace the most common, but also more expensive pure N₂. From the results obtained and the continuous interactions with other researchers within the GreenCarbon network, the PhD project has continually been developed around four main *research themes*:

- I. An in-depth assessment of the effects of slow pyrolysis process conditions on products yields and properties of resulting biochars.
- II. A study on the energy/exergy efficiency of the pyrolysis process under different sets of operating conditions.
- III. An assessment of the biochar-related potential in using it as soil amendment with a special focus on its potential toxicity.
- IV. Producing biomass-derived activated carbons —through both one-step and two-step pathways— for biogas upgrading via CO₂ adsorption.

The knowledge and experience acquired during the course of the research in the two first themes have been crucial to direct further research on producing engineered carbons via the proper selection of the best operating conditions for a given purpose. A schematic resume of the main objectives is given in Figure 3.

The present PhD Thesis is presented as a compendium of four research articles, which have been published during the course of the PhD project as a result of the accomplishment of the four research studies mentioned above. The topics covered by the four published papers reflect the progress of the work over time, starting from the preliminary study of mass-loss evolution during pyrolysis process and ending with the optimization of the pyrolysis operating conditions in order to ensure the production of biochars with desired properties for their employment as soil amendment and precursors of CO₂ carbon-based adsorbents.

The experimental works related to *research themes III* and *IV* were carried out in collaboration with the research teams led by Dr. Elisabet Pires —[Group of Heterogeneous Catalysis for Organic Synthesis](#) at the University of Zaragoza (*Theme III*)— and by Prof. Vanessa Fierro —[Biosourced Materials Group](#) at the *Institut Jean Lamour* in France (*Theme IV*)—, respectively.

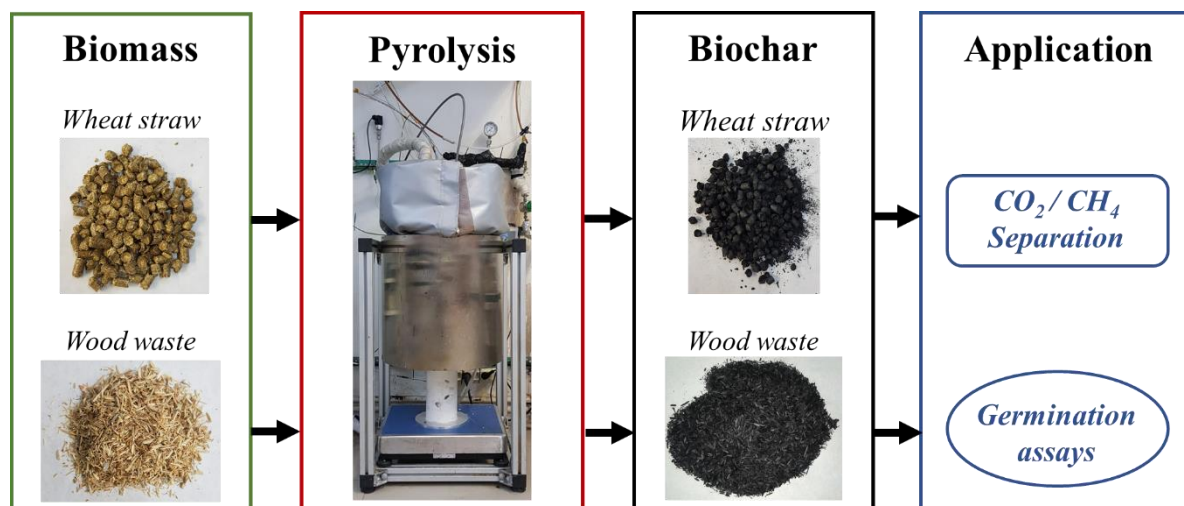


Figure 3. Layout of the main tasks of the PhD project.

5. Methodology

5.1 Biomass sources

The biomass feedstocks employed for biochar production were wheat straw (WS) pellets (see Figure 4a) an untreated wood waste (WW) (Figure 4b). WS pellets were provided by a Belgian company, while WW biomass was basically composed by a mixture of sawdust deriving from sawmills, wood, pallets and crates of a Belgian wood recycling company. Both the WS (7 mm OD and approximately 12 mm long) and WW (with a particle size in the range of 0.30–4.0 mm) biomasses were manufactured without using any binder.

The as-received biomasses were directly pyrolyzed without any preliminary milling step, since the carbonization efficiency may be improved for large particles as compared to smaller ones, leading to biochar with higher fixed-carbon contents (Manyà *et al.*, 2014b). Both feedstocks were characterized by proximate analysis (performed in quadruplicate according to ASTM standards D3173 for moisture, D3174 for ash, and D3175 for volatile matter) as well as ultimate analysis, which was carried out in triplicate using a combustion elemental analyzer Leco CHN628 (Leco Corporation, USA). Only for WS pellets, the high heating value (HHV) was estimated from the ultimate analysis using the Channiwala and Parikh correlation (Channiwala and Parikh, 2002), in order to fulfill with the above-explained objectives of the *Theme II*. In addition, X-Ray Fluorescence (XRF) spectroscopy analysis (ADVANT'XP+XRF spectrometer from Thermo ARL, Switzerland) was performed in order to determine the inorganic constituents of the biomass ash.



Figure 4. Biomass feedstock employed in this work: (a) wheat straw pellets and (b) untreated wood waste.

The main biomass constituents (i.e., hemicelluloses, cellulose, lignin and extractives) of the feedstocks were determined by leaching the WS and WW biomass samples in a benzene/ethanol mixture, followed by a boiling step firstly in a NaOH solution, then in a H₂SO₄ solution. The experimental procedure—reported in literature (Li *et al.*, 2004)—was conducted in duplicate and consisted of four main steps, performed in duplicate:

The dried biomass was weighted (G_0) and added in a benzene/ethanol solution (2:1 v/v). Then, the residue obtained (G_1) was dried until a constant weight was reached. The extractive content was calculated as:

$$W_1 \text{ (wt. \%)} = \frac{G_0 - G_1}{G_0} \cdot 100 \quad (1)$$

The residue G_1 from the extractive analysis was added in a NaOH solution and boiled for 3.5 hours. Then it was filtered and washed of all the Na⁺ ions left, and dried to a constant weight (G_2). The hemicelluloses content was then calculated as:

$$W_2 \text{ (wt. \%)} = \frac{G_1 - G_2}{G_0} \cdot 100 \quad (2)$$

1 g of the residue G_1 after the extractive analysis was dried to a constant weight (G_3). Then, it was poured in sulphuric acid solution and kept overnight. Afterwards, it was diluted with distilled water and boiled for 1 h. After cooling and filtration, the residue was washed of all the sulphate ions left, and dried to a constant weight (G_4). The lignin content was calculated as:

$$W_3 \text{ (wt. \%)} = \frac{G_4(1 - W_1)}{G_3} \cdot 100 \quad (3)$$

The cellulose was then determined by difference:

$$W_4 \text{ (wt. \%)} = 100 - (A_d + W_1 + W_2 + W_3) \quad (4)$$

The full characterization of the WS and WW biomasses is reported in Table 5.

Table 5. Lignocellulosic composition, proximate, ultimate and XRF analyses of wheat straw and wood waste biomasses

Component (wt. %)	Wheat straw	Wood Waste
Hemicelluloses	33.0 ± 0.61	18.0 ± 0.7
Cellulose	40.7 ± 0.50	52.3 ± 0.3
Lignin	18.4 ± 0.54	28.9 ± 0.2
Extractives	8.05 ± 0.28	0.80 ± 0.2
Proximate (wt. %)		
Ash	3.87 ± 0.07	0.36 ± 0.05
Moisture	7.27 ± 0.06	7.61 ± 0.02
Volatile matter	74.99 ± 0.33	80.2 ± 0.21
Fixed carbon	14.0 ± 0.29	11.9 ± 0.23
Ultimate (wt. % in daf basis)		
C	49.0 ± 0.52	45.9 ± 0.07
H	7.01 ± 0.04	6.36 ± 0.02
N	0.704 ± 0.01	0.36 ± 0.01
O	43.2 ¹	47.0
HHV (MJ kg ⁻¹)	18.01	–
Inorganic matter as equivalent oxides (wt. % of ash) ²		
K ₂ O	53.20	10.37
CaO	17.40	42.46
SiO ₂	16.90	8.65
TiO ₂	–	8.48
MnO ₂	–	4.80
P ₂ O ₅	4.46	–
Al ₂ O ₃	1.66	3.15
Cl (inorganic)	1.53	3.01
MgO	1.46	2.99
PbO	–	1.79
Pt	–	1.60
ZnO	–	1.12
SnO ₂	–	1.02
S (inorganic)	1.31	3.28
Fe ₂ O ₃	1.14	7.27

¹ Oxygen was calculated by difference.

² Only listed components with a composition higher than 1%.

5.2 Pyrolysis device and experimental procedure

Pyrolysis runs were conducted in a bench-scale fixed-bed reactor (see Figure 5 for the scheme of the experimental device). The reactor (140 mm ID and 465 mm long) was made of austenitic stainless steel (EN 1.4835³). A basket of 4 L, made of EN 1.4401⁴ stainless steel wire mesh, was used to allocate the biomass into the reactor. The initial sample weight was approximately 400 g, which represented more than 30% of the basket volume, depending on the feedstock apparent density. A weighing platform from Kern (model DS with a measuring range up to 100 kg and a reading precision of 0.5 g) was placed at the bottom of the reactor system. A ceramic tube (117 mm OD and 330 mm long) was positioned between the reactor vessel and the weighing platform for thermal insulation purposes. Flexible stainless-steel tubing from Swagelok (10 mm OD) were used for the reactor connections to minimize any force component.

Pyrolysis experiments were performed by varying the peak temperature between 400 and 550 °C, whereas the ranges of absolute pressure and gas residence time were 0.2–0.9 MPa and 100–200 s, respectively. Moreover, the composition of the carrier gas varied from pure N₂ to a binary mixture of 60:40 v/v of CO₂/N₂. A soaking time of 60 min (at the peak temperature) was maintained to ensure the thermal equilibrium. The temperature profiles inside the bed were measured by four thermocouples placed in two thermowells, located at the axis and at a radial distance of 35 mm from the axis, respectively. The thermocouples were placed two by two in the thermowells, at different heights from the bottom of the sample basket: 10 mm (TC₀ and TC₁) and 70 mm (TC₂ and TC₃).

The proper residence time of the gas phase within the reactor as well as the pyrolysis environment were guaranteed by adjusting the mass flow rates at STP conditions for both N₂ and CO₂. The real flow rate of the carrier gas within the reactor varied approximately between 1.60 and 3.30 L min⁻¹ for WS, and between 1.40 and 2.80 L min⁻¹ for WW, which corresponded in all cases to gas-hourly space velocity (GHSV) values ranged from 18 to 36 h⁻¹, assuming a void-volume fractions of 0.9 and 0.5 in the entire reactor for WS and WW, respectively. A back-pressure regulator was used to keep the pressure of the system steady at a desired value. The outlet gas stream passed through a heated line, at a constant temperature of around 375 °C, before being passed through a series of glass traps, which were immersed in ice-water baths.

³ Equivalent to AISI 253MA and UNS S3081.

⁴ Equivalent to AISI 316 and UNS S31600.

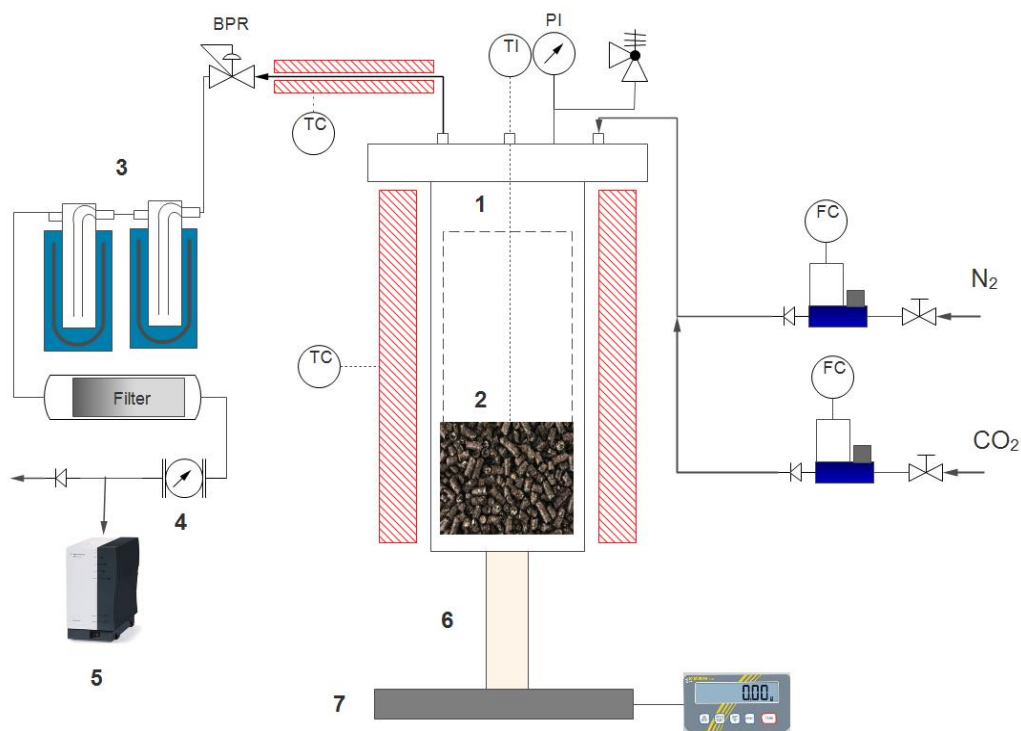


Figure 5. Schematic layout of the pyrolysis plant: (1) pyrolysis reactor, (2) biomass bed, (3) condensation system, (4) volumetric gas meter, (5) micro-GC, (6) ceramic tube, (7) weighing platform.

5.3 Characterization of pyrolysis products

After each experiment, the biochar produced was collected and weighted. The glass traps and their flexible connections were weighted before and after each experiment to calculate the total mass of liquid (organics + water). The pyrolysis liquid was recovered directly from the condensers without undergoing any washing step with solvents. The water content was evaluated by Karl Fischer titration, while the organic fraction was determined by difference from the total mass of liquid. The composition of the pyrolytic gases (i.e., CO_2 , CO , CH_4 and H_2) was measured using a micro gas chromatograph (μ -GC, Agilent 490) equipped with two analytical columns: a PolarPlot U (using He as carrier gas) and a Molsieve 5A (using Ar as carrier gas). The mass yield of biochar (y_{char}), produced gas (y_{gas}), organic condensable compounds (y_{org}) and produced water (y_{wat}) were calculated in a dry and ash-free (*daf*) basis. The produced biochar samples were characterized by proximate analysis and, additionally, ultimate analyses together with the liquid products, under the same procedure described for the biomass feedstock. The fixed-carbon yield (y_{FC}), firstly introduced by Antal and Gronli (2003), was adopted to evaluate the carbonization efficiency. It was defined as following:

$$y_{FC} = x_{FC} y_{char} \quad (5)$$

where x_{FC} is the fixed-carbon content in mass fraction (*daf* basis). The fixed-carbon yield corresponds to the fraction of organic matter initially present in the biomass feedstock, which was converted into fixed carbon.

The BET specific surface areas (S_{BET}) of the biochars were determined from the CO₂ adsorption isotherms at 0 °C, since biochars typically present a highly ultra-microporous structure (not reachable by N₂ at -196 °C). The adsorption isotherms were obtained using an ASAP 2020 gas sorption analyzer (Micromeritics, USA). The samples (approximately 120 mg) were firstly degassed under dynamic conditions at 150 °C until constant weight was reached. This relatively low outgassing temperature was selected to avoid any thermochemical conversion step. Ultra-micropore volume (V_{ultra} , i.e., pore size lower than 0.7 nm) of the samples was calculated adopting a Grand Canonical Monte Carlo method (GCMC) for carbon slit-shaped pores. All the calculations related to the adsorption isotherms were carried out using the MicroActive software (Micromeritics). In addition, Fourier transform infrared analyses (FT-IR) were performed using a Perkin Elmer FT-IR Spectrometer with PIKE Technologies GladiATR and Spectrum software in order to determine the functional groups on the surface of the produced chars. The FT-IR analyses were performed at least in triplicate under a range of wavenumber of 400 to 4000 cm⁻¹ with a resolution of 4 cm⁻¹, doing 16 scans for each point in order to accomplish a reliable level of accuracy.

5.4 Design of experiments

In the most part of the experiments performed in order to accomplish with the objectives pursued in this work, several unreplicated 2-level full factorial designs were adopted to evaluate the effects of the assessed pyrolysis process parameters on a certain number of response variables. The response variables selected in the overall experimental work were the pyrolysis products yields and properties, parameters related to the mass-loss evolution along the pyrolysis experiments, pyrolysis energy and exergy outputs, PAHs content, germination indexes and parameters related to the textural properties of biochar-based ACs. Three replicates at the center point of the design of experiments (DoE) were carried out to estimate the experimental error and the overall curvature effect (Montgomery, 2005). The structure of the regression model (using normalized values for factors in the range from -1 to 1) used during statistical analysis for the response variables was as follows:

$$\hat{y} = \beta_0 + \beta_1 T + \beta_2 P + \beta_3 \tau + \beta_4 CO_2 + \beta_{12} T \cdot P + \beta_{13} T \cdot \tau + \beta_{14} T \cdot CO_2 + \beta_{23} P \cdot \tau + \beta_{24} P \cdot CO_2 + \beta_{34} \tau \cdot CO_2 + \beta_{123} T \cdot P \cdot \tau + \beta_{124} T \cdot P \cdot CO_2 + \beta_{134} T \cdot \tau \cdot CO_2 + \beta_{234} P \cdot \tau \cdot CO_2 \quad (6)$$

where T , P , τ , and CO_2 refer to peak temperature, absolute pressure, gas residence time and pyrolysis environment; β_0 , β_i , β_{ij} , and β_{ijk} are the intercept, linear, 2-way interaction and 3-way interaction coefficients, respectively. The model structure was simplified whenever was possible. Statistical calculations were conducted using Minitab software (v17).

5.5 Assessment of repeatability

Three repeated measurements related to the center point were analyzed using a one-way ANOVA in order to ensure an appropriate level of repeatability for the mass-loss evolution during the experiments concerning the biochar production. Assuming normality and homogeneity of variances, the mean squares for the treatment and error terms (MS_t and MS_e , respectively) were computed. The intra-class correlation coefficient (ICC), which is commonly used as a measure of repeatability, was then estimated as follows (Nakagawa and Schielzeth, 2010):

$$ICC = \frac{MS_t - MS_e}{MS_t + (n_0 - 1)MS_e} 100 \quad (7)$$

where n_0 is the number of replicates (3).

5.6 Energy and exergy assessment

This section covers an important part of the methodology adopted in *Theme II* of this work. The enthalpy required for the pyrolysis process that should be supplied externally ($Q_{process}$) and the exergy efficiencies related to the biochar (Ψ_{char}), produced gas (Ψ_{gas}) as well as the global exergy efficiency of the process ($\Psi_{process}$) were partly calculated using the process simulation software Aspen Plus v10 (Aspentech, USA). The pyrolysis reactor was simulated as a yield reactor block, in which the WS pellets (nonconventional component) were converted into biochar, CO_2 , CO , CH_4 , H_2 , water, and condensable tars. The mass flow rate of each stream was defined on the basis of the experimental data generated in the pyrolysis device. A layout of the control volume considered for simulations is given in Figure 6, where T_0 , T_p and P are the reference temperature (25 °C), pyrolysis peak temperature (which was also considered as the process temperature) and process absolute pressure, respectively.

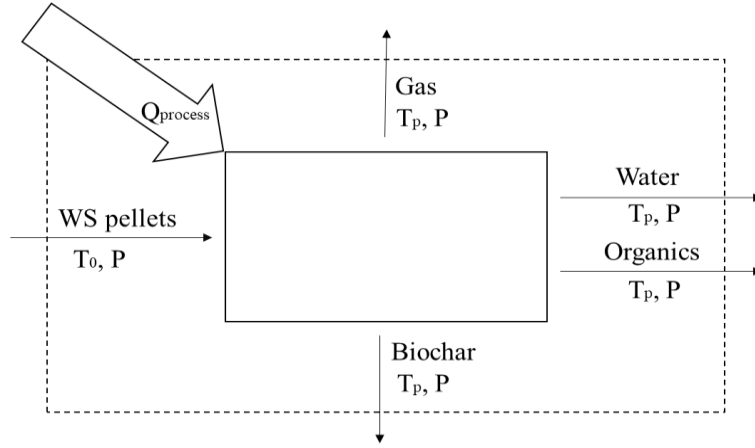


Figure. 6. Control volume considered for energy and exergy assessment.

The methodology followed to calculate the energy and exergy balances was based on a previous work carried out by Atienza-Martínez *et al.* (2018). Briefly, $Q_{process}$ was calculated according to Eq. 8, where h_{in} and h_{out} are the specific input and output enthalpies (in MJ kg⁻¹), respectively.

$$Q_{process} = h_{out} - h_{in} \quad (8)$$

On the other hand, the exergy efficiencies were calculated as following:

$$\Psi_i = 100 \frac{e_{out,i}}{\sum e_{in}} \quad (9)$$

where $e_{out,i}$ is the exergy of the product (biochar or gas), and $\sum e_{in}$ is the sum of the input exergies (both physical and chemical). The exergy associated to the heat required for the process was also taken into account in Eq. 9. Calculations were conducted assuming the following considerations:

- The standard reference was $T_0 = 25$ °C and $P_0 = 0.1$ MPa.
- Chemical exergies for all the involved species were obtained from the literature (Perry and Green, 1998).
- Process heat losses as well as kinetic and potential exergies of the streams were considered to be negligible (Szargut, 2005).
- The energy and exergy contents inherent to the carrier gas streams were considered in the respective balances.
- Exergies of condensable tar streams were not calculated (due to the impossibility to know their real chemical composition) and thus they were taken as exergy losses.

5.7 PAHs content quantification

This section deals with the methodology adopted in *Theme III* of the present work, where the main objective was to assess the PAHs concentration in biochar after its production. In line with the methodology described by De la Rosa *et al.* (2019), 2 g of dried biochar underwent a Soxhlet extraction using 200 mL of toluene throughout 24 h without any clean-up treatment. The obtained extracts were concentrated to 1–2 mL by means of a rotary vacuum evaporator (R-210, Buchi, Switzerland). Prior to concentration, the biochar samples were spiked with 10 μ L of toluene containing 400 ng of a PAH deuterated internal standard mix in order to detect any possible loss of analyte during sample preparation. The analysis of the 16 PAHs prioritized by the US EPA in the resulting extracts was performed using a 6890 GC coupled with a 5973i MS detector (Agilent, USA). The PAH deuterated internal standard mix used to detect any possible loss of analyte during sample preparation was PAH-Mix 31 (Dr. Ehrenstorfer, Germany), containing naphthalene-d8, acenaphthene-d10, phenanthrene-d10, chrysene-d12, and perylene-d12.

The extract (2 μ L) was injected in splitless mode in a ZB-5HT Inferno capillary column (30 m, 0.25 mm ID, 0.25 μ m film thickness), where the separation was carried out under a He constant flow rate of 1.2 mL min⁻¹. The oven temperature program was the following: 80 °C held for 1 min, then ramped at 6 °C min⁻¹ to 175 °C (held for 4 min), then heated again at 3 °C min⁻¹ to 270 °C (held for 1 min), and finally ramped at 1 °C min⁻¹ to 290 °C (held for 3 min).

The PAHs detection and quantification were conducted in single ion monitoring (SIM) mode, in order to enhance the selectivity and sensitivity of the method. The standard mixture PAH-Mix 63 (Dr. Ehrenstorfer, Germany) containing the 16 US EPA PAHs⁵ was used for the preparation of calibration curves, which were used for PAH quantification. Each calibration curve was built for eight concentration levels, and the quantification limit for the individual PAH was approximately 10 μ g kg⁻¹. The entire procedure was performed in duplicate for each biochar and the resulting PAHs contents were given by the average. Table 6 reports the monitored ion profiles and toxic equivalent factor (TEF) for each PAH compound. The total toxic equivalent concentrations (*TTEC*) related to the carcinogenic risk assessment for each

⁵ naphthalene (NAP), acenaphthylene (ANY), acenaphthene (ANA), fluorene (FLU), phenanthrene (PHE), anthracene (ANT), fluoranthene (FLT), pyrene (PYR), benzo[*a*]anthracene (BaA), chrysene (CHR), benzo[*b*]fluoranthene (BbF), benzo[*k*]fluoranthene (BkF), benzo[*a*]pyrene (BaP), indeno[1,2,3-*cd*]pyrene (IPY), dibenz[*a,h*]anthracene (DBA), and benzo[*ghi*]perylene (BPE).

biochar sample was then calculated according to the procedure described by (Dat and Chang, 2017).

Table 6. Monitored ion profiles and toxic equivalent factor (TEF) for each PAH compound

Compounds	Monitored ions	MS retention time (min)	TEF
Naphthalene-d ₈	136–108	6–8	–
Naphthalene	128–129	6–8	0.001
Acenaphthylene	152–153	12–14	0.001
Acenaphthylene-d ₁₀	164–162	13–14	–
Acenaphthene	154–153	14–15	0.001
Fluorene	166–165	15–17	0.001
Phenanthrene-d ₁₀	188–189	19–21	–
Phenanthrene	178–179	20–21	0.001
Anthracene	178–179	20–21	0.01
Fluoranthene	202–203	28–31	0.001
Pyrene	202–203	28–31	0.001
Benzo[a]anthracene	228–226	39–40	0.1
Chrysene-d ₁₂	240–236	39–40	–
Chrysene	228–226	39–40	0.01
Benzo[b]fluoranthene	252–253	46–48	0.1
Benzo[k]fluoranthene	252–253	46–48	0.1
Benzo[a]pyrene	252–253	48–50	1
Perylene-d ₁₂	264–260	49–50	–
Indeno[1,2,3-cd]pyrene	276–277	55–57	0.1
Dibenz[a,h]anthracene	278–279	55–57	1
Benzo[g,h,i]perylene	276–277	58–59	0.01

5.8 Germination assays

The methodology adopted in the second part of *Theme III* deals with germination assays, in order to evaluate the level of biochar phytotoxicity or phytostimulation (if any). The procedure consisted of the incubation of 10 seeds (of barley, watercress, and basil) in 5 mL of an aqueous solution containing 0.5 g of biochar poured in a Petri dish over a sterile filter paper. All the samples were then covered and stored in an oven at 25 °C for 72 h. The root length of germinated seeds was measured using a Vernier caliper and the average values were calculated for each sample. According to Liang *et al.* (2016), the germination index (*GI*) was calculated as follows:

$$GI = \frac{G}{G_0} \frac{L}{L_0} 100 \quad (10)$$

where G and L are the germination percentage and average root length, respectively. G_0 and L_0 refer to the control condition (i.e., Petri dish with 5 mL of deionized water).

5.9 Physical activation with CO₂

The present section describes in detail the methodology used in *Theme IV*, concerning the CO₂ physical activation of biochar, achieved by one- or two-step processes, with the aim of synthesizing highly porous biochar-based materials for biogas upgrading.

5.9.1 One-step activation

The one-step activation process was performed using the same bench-scale fixed-bed reactor described in *Section 5.2*. The following ranges of operating conditions were considered: maximum temperature between 650 and 750 °C, absolute pressure between 0.2 and 0.9 MPa, reactor environment varying between pure N₂ and a binary CO₂/N₂ mixture (75:25 v/v), and constant gas residence time of 100 s. In order to study the pyrolysis behavior in this range of process parameters, experiments using a pure N₂ atmosphere were included in the experimental design. The heating rate and the soaking time (at the maximum temperature) were 5 °C min⁻¹ and 1 h, respectively.

5.9.2 Two-step activation

The pyrolysis step was also performed using the bench-scale fixed-bed reactor described in *Section 5.2*. The maximum temperature, absolute pressure, and gas residence time varied in the range of 400–550 °C, 0.2–0.9 MPa, and 100–200 s, respectively. In addition, the pyrolysis atmosphere adopted for these experiments varied from pure N₂ to a CO₂/N₂ mixture (60:40 v/v). As before, the heating rate and the soaking time (at the maximum temperature) were 5 °C min⁻¹ and 1 h, respectively.

All biochars obtained after pyrolysis were then physically activated at 800 °C and atmospheric pressure under a pure CO₂ atmosphere. The device used for activation consisted of a tubular reactor (nickel-chromium alloy EN 2.4816⁶, 600 mm long and 28.1 mm ID), placed inside a vertical tubular furnace (model EVA 12/300 mm from Carbolite Gero, UK). A K-type thermocouple was placed along the longitudinal axis of the reactor to monitor the temperature inside the bed in real-time. Following the same procedure as in a previous work (Di Stasi *et*

⁶ Equivalent to UNS N06600.

al., 2019), the raw biochars were first ground and sieved to obtain particle sizes between 0.21 and 1.41 mm. Then, samples of 10 g were heated at 10 °C min⁻¹ under a constant flow of N₂. Once the activation temperature was reached (i.e., 800 °C), the gas feed was switched from N₂ to CO₂ and held isothermally for 1 h. Under these conditions, the gas-hourly space velocity (GHSV) was approximately 7000 h⁻¹.

5.10 Characterization of resulting activated carbons

The burn-off of the activated carbons (X_i) was estimated as follows:

$$X_i = (m_{biomass} - m_f) / m_{biomass} \cdot 100 \quad (11)$$

where i refers to the type of activation process: one-step (1S) or two-step (2S). $m_{biomass}$, $m_{biochar}$, and m_f are the masses of biomass, biochar and final sample, respectively.

The textural characterization of the carbon materials was performed by N₂ and H₂ adsorption at -196 °C using an ASAP 2020 automatic adsorption device from Micromeritics (USA). Samples were outgassed under secondary vacuum at 110 °C for at least 48 h and outgassing at the same temperature for at least 6 h was also carried out in the analysis port. Warm and cold volumes were determined after analysis to avoid He entrapment in ultramicropores. Processing of the adsorption isotherm data was performed using Microactive[®] and SAIEUS[®] software provided by Micromeritics. Pore size distributions (PSDs) and surface areas ($S_{2D-NLDFT}$) were calculated by applying the two-dimensional non-local density functional theory model for heterogenous surfaces (2D-NLDFT-HS) (Jagiello *et al.*, 2020) to N₂ and H₂ isotherms simultaneously. The total pore volume (V_{tot}), ultra-micropore volume (V_{ultra}), micropore volume (V_{micro}) and mesopore volume (V_{meso}) were obtained by integrating the PSDs in the corresponding pore size ranges.

Infrared spectra were performed in the wavenumbers range of 600–4000 cm⁻¹ using a Fourier-Transform Infrared (FTIR) spectrometer (Frontier Spotlight 400, Perkin-Elmer, Japan).

5.10.1 Adsorption isotherms

CO₂ and CH₄ adsorption isotherms were measured up to 3.5 MPa, at 25 and 50 °C, using a HPVA II high-pressure manometric device (from Micromeritics). The samples were firstly outgassed under secondary vacuum (5×10^{-7} Pa) at 110 °C for at least 48 h. Afterwards, the pressure was gradually increased from 0.005 to 3.5 MPa, and then decreased stepwise to 0.5 MPa. The amount of gas adsorbed was calculated as the difference between the amount of gas dosed and the amount of gas determined at each equilibrium pressure.

The transient pressure change prior to the first isotherm point was recorded to obtain the adsorption kinetics.

The experimental data obtained from the isotherms were described using the Sips model. The ideal adsorbed solution theory (IAST) was adopted to predict the adsorption behavior of CO₂/CH₄ binary mixtures at different volume concentrations (i.e., 10:90 v/v, 30:70 v/v, 50:50 v/v, and 70:30 v/v). The selectivity towards CO₂ over CH₄ (S) was then calculated as follows:

$$S = (x_{CO_2} y_{CH_4}) / (x_{CH_4} y_{CO_2}) \quad (12)$$

where x and y are the gas molar fractions in the adsorbed and gas phases, respectively.

5.10.2 Adsorption equilibrium

The Sips model, a combination of (Langmuir, 1916) and (Freundlich, 1907) isotherms, was used to describe the resulting experimental data. The model can be described by the following equation:

$$q_{eq} = \frac{q_s b_s P^{1/n_s}}{[1 + b_s P^{1/n_s}]} \quad (13)$$

where q is the adsorbed amount (mol kg⁻¹), P (bar) the equilibrium pressure, q_{eq} (mol kg⁻¹) is a constant reflecting the saturation adsorption capacity, b_s (bar⁻¹) is the Sips constant or affinity constant, and $1/n_s$ is the heterogeneity factor. All model parameters were fitted in Maplesoft using the sum of square error and the Dunhill simplex method (Nelder and Mead, 1964) as objective functions.

The Ideal Adsorption Solution Theory (IAST), initially proposed by Myers and Prausnitz (1965), is found to be a good tool to predict the adsorption of mixed gas using data from single-compound isotherms. This theory is based on an ideal relationship mathematically represented by:

$$P y_i = P_i^0 (\pi_i) x_i \quad (14)$$

where P and P_i^0 are the total pressure and the theoretical pressure giving the same spreading pressure as observed in the single gas adsorption study, y_i and x_i are the molar fractions at the gas and adsorbed phases, and π_i is the spreading pressure of component i in the mixture. The Gibbs adsorption isotherm is used to obtain π_i as follows:

$$z = \frac{\pi_i}{RT} = \int_0^{P_i^0} \frac{q_i^{pure}(P)}{P} dP \quad (15)$$

where R is the ideal gas constant, T (K) is the temperature and q_i^{pure} (mol kg⁻¹) is the molar concentration of compound i in the adsorbed phase from the single compound isotherm. Note that, under equilibrium conditions, the spreading pressure of each component must be the same:

$$\pi_1 = \pi_2 = \dots = \pi_n \quad (16)$$

The total adsorbed amount, q_T (mol kg⁻¹), is calculated as follows:

$$\frac{1}{q_T} = \sum_{i=1}^n \frac{x_i}{q_i^0} \quad (17)$$

where q_i^0 (mol kg⁻¹) is the adsorbed amount at the pressure giving the same spreading pressure as observed when studying the adsorption of a single gas.

5.10.3 Adsorption kinetics

The diffusion of the adsorbate on the adsorbent was estimated from the adsorption kinetics by means of mathematic modeling. The adopted kinetic model considers that the adsorbent particle was approximated by a sphere in order to describe the transport phenomena by the diffusion equation in spherical coordinates. In addition, further assumptions were made: (i) isothermal behavior, and (ii) linearity of the isotherm at the kinetic point condition. The resulting equation is as follows:

$$\frac{\partial q}{\partial t} = \frac{1}{r^2} \frac{\partial}{\partial r} \left(r^2 D_C \frac{\partial q}{\partial r} \right) \quad (18)$$

where D_c (m² s⁻¹) is the intraparticle diffusion coefficient and q (mol kg⁻¹) is the adsorbed phase concentration. When the bulk phase concentration is not constant and the boundary condition is time-dependent, the analytical solution of Eq. 18 is:

$$\frac{q}{q_{eq}} = 1 - 6 \sum_{n=1}^{\infty} \frac{\text{EXP}(-p_n^2 D_C / r_c^2 t)}{9 \frac{A}{1-A} + (1-A)p_n^2} \quad (19)$$

where q_{eq} (mol kg⁻¹) is the adsorbed amount at equilibrium, r_c (m) is the particle radius, A (dimensionless) is the fraction of sorbate ultimately adsorbed by the adsorbent ($A \equiv (P_0 - P_{\infty})/P_0$), and p_n (dimensionless) are the non-zero roots of the following equation:

$$\tan(p_n) = \frac{3p_n}{3 + \left(\frac{1}{A} - 1\right)p_n^2} \quad (20)$$

At least 40 different roots of Eq. 20 should be used in order to obtain meaningful results. The diffusion parameters were obtained by non-linear fits of the equations described above using the Dunhill simplex method in a calculation routine implemented in Python (Nelder and Mead, 1964).

5.10.4 Breakthrough Simulations

Simulations of adsorption breakthrough curves were carried out at 0.1, 0.3, 0.5, 0.7 and 1.0 MPa considering an initial temperature of 30 °C and a total feed flow rate of 0.75 NL min⁻¹, with a molar composition of 40% CO₂ and 60% CH₄. A simulated fixed-bed column with length and diameter of 60 cm and 2.8 cm, respectively, was considered to run the simulations using gPROMS ModelBuilder.

The samples tapped densities were obtained in an Autotap equipment of Quantachrome. The bed porosity was calculated using the bed and particle densities as follows:

$$\varepsilon_{bed} = 1 - \rho_{bed}/\rho_{par} \quad (21)$$

where ρ_{bed} and ρ_{par} are the bed and particle densities, respectively. The particle density and porosity were measured by mercury porosimetry (Autopore IV, Micromeritics). The average particle diameter was measured by laser diffraction using a Mastersizer Hydro 3000 analyzer (Malvern instruments Ltd.) equipped with a Hydro LV sampler and a measurement cell for liquid phase suspensions.

The mathematical model adopted for the simulation of breakthrough curves is based on the following assumptions:

- Ideal gas behavior.
- Heat, mass, and momentum transport are considered negligible in the radial directions.
- The momentum balance was described by the Ergun equation.
- The dual Linear Driving Force (LDF) model was used to simplify the macropore and micropore diffusion equations.
- The mass transfer resistance surrounding the pellets was taken into account.
- The void fraction, cross-sectional area and adsorbent properties were constant along the column.
- The heat transfer in different phases (gas, solid and wall) was described by different energy balances.

More details regarding the mentioned mathematical model are available in Appendix A of article 4 (*Theme IV*).

6. Results

6.1. *Theme I*: assessment of the effects of slow pyrolysis process conditions on products yields and properties of resulting biochars

The first research theme focuses on assessing the main effects of both absolute pressure and gas environment on the behavior of wheat straw pellets during their slow pyrolysis, as well as on the products' distribution and properties of produced biochars. In this study, the absolute pressure was in the range of 0.1–0.5 MPa, and two type of pyrolysis environment were adopted: pure N₂ or a mixture of CO₂/N₂, 60/40 v/v. Pyrolysis peak temperature and soaking time were kept constant at 500 °C and 1 h, respectively. A special attention was paid to monitor the real-time mass-loss data for the biomass sample, using a weighing platform placed on the bottom of the pyrolysis device. This research study was published in *Journal of Analytical and Applied Pyrolysis* (article 1).

Among the main results to be mentioned, an increase in pressure led to a higher extent of devolatilization, which was clearly visible on the resulting mass-loss profiles acquired during the course of the pyrolysis process. On the other hand, an increased pressure also resulted into higher yields of gas at the expense of those related to water and condensable organic compounds. An explanation of this finding might be the promotion by pressure of the exothermic secondary reactions involving intermediate volatile organic compounds in both liquid and vapor phases. When atmospheric pressures were applied, the switch from pure N₂ to the binary mixture of CO₂ and N₂ also led to a significant increase in the yield of produced gas at the expense of the total liquid, mainly due to the promotion of the thermal cracking of the volatile organic compounds at a high partial pressure of CO₂. This result was consistent with the measured higher yields of CH₄ and CO. In addition, the higher yield of CO can also be related to an enhanced reverse Boudouard reaction, which may also explain the much higher specific surface area (and ultra-micropore volume) measured for the biochar produced under these operating conditions. Another interesting point is the apparent absence of influence of pressure and pyrolysis atmosphere on the biochar yield for the range of operating conditions considered in this work. The biochar potential stability —measured as a function of the fixed-carbon yield as well as the atomic H:C and O:C ratios— was found to be similar, regardless of the operating parameters used.



Evolution of the mass-loss rate during atmospheric and pressurized slow pyrolysis of wheat straw in a bench-scale reactor



Gianluca Greco^a, María Videgain^a, Christian Di Stasi^a, Belén González^a, Joan J. Manyà^{a,b,*}

^a Technological College of Huesca, Spain

^b Aragón Institute of Engineering Research (I3A), University of Zaragoza, crta. Cuarte s/n, Huesca, E-22071, Spain

ARTICLE INFO

Keywords:

Wheat straw
Pyrolysis
Biochar
CO₂ atmosphere
Pressure
Devolatilization rate

ABSTRACT

In the present study, the effects of the absolute pressure (0.1 or 0.5 MPa) and the reactor atmosphere (pure N₂ or a mixture of CO₂/N₂) on the pyrolysis behavior of wheat straw pellets (at 500 °C) were investigated. The most interesting aspect of this work was the use of a weighing platform (with a maximum capacity of 100 kg and a resolution of 0.5 g) to monitor the real-time mass-loss data for the biomass sample (with an initial mass of 400 g). It was observed that an increased pressure considerably affects the mass-loss profiles during the pyrolysis process, leading to higher devolatilization rates in a shorter period of time. Regardless of the pyrolysis atmosphere, an increase in the absolute pressure led to higher yields of gas at the expense of produced water and condensable organic compounds. This finding could be due to the fact that an increased pressure favors the exothermic secondary reactions of the intermediate volatile organic compounds in both liquid and vapor phases. The switch from pure N₂ to a mixture of CO₂ and N₂ at 0.1 MPa also led to a remarkable increase in the yield of produced gas at the expense of the total liquid. This could be mainly due to the promotion of the thermal cracking of the volatile organic compounds at a high partial pressure of CO₂, which is also consistent with the measured higher yields of CH₄ and CO. The increased yield of CO can also be seen as a direct result of the enhanced reverse Boudouard reaction, which can also explain the much higher specific surface area (and ultra-micropore volume) measured for the biochar produced under the same operating conditions (0.1 MPa and a mixture CO₂/N₂ as pyrolysis medium).

1. Introduction

The energy crisis, environmental pollution and global warming are serious problems, which have recently generated a growing interest in developing new technologies focused on reducing the greenhouse gas emissions and increasing the carbon sinks [1]. A promising solution for such issues is biochar [2], a form of charred organic matter, which is possible to apply to soil in a deliberate manner as a means of potentially improving soil productivity and carbon sequestration [3]. In order to produce biochar, pyrolysis of agricultural wastes seems to be an interesting solution, due to its feasibility to manage biowaste and simultaneously generate environmental and agronomic benefits [4,5]. Among the wide range of pyrolysis processes, slow pyrolysis is a promising route to produce a relatively high yield of biochar, obtaining gas as co-product for cogeneration use. This process, which is carried out at low heating rates and long residence times of both the solid and vapor phases [6], is relatively simple and robust and can be feasible for small-scale and farm-based production of biochar [7]. Given the high number

of variables affecting the process (such as peak temperature, heating rate, gas residence time, and pressure) and the wide range of available biomass sources, (the nature of which largely affects the pyrolysis process) a large variability in the yield and properties of the produced biochar should be expected. Therefore, one of the main challenges nowadays is to optimize the process conditions of the pyrolysis process for a given biomass feedstock [8,9] with the aim to obtain an engineered biochar with the desired properties to be used for a given application. Regardless of the final use of the produced biochar (e.g., soil amendment, material precursor for activated carbons), the assessment of the stability of biochar's carbon appears to be essential in order to evaluate its potential as carbon sequestration agent.

Among all the process variables, the absolute pressure is probably one of the most interesting parameters to study in deep. Relatively few studies [4,10–16] have been focused on the effect of the absolute pressure on the biomass pyrolysis behavior. Most of these earlier studies reported an increase in the char and gas yields, while the yield of the condensable fraction decreased, when both the pressure and the

* Corresponding author at: Aragón Institute of Engineering Research (I3A), University of Zaragoza, crta. Cuarte s/n, Huesca E-22071, Spain.

E-mail address: joanjoma@unizar.es (J.J. Manyà).

<https://doi.org/10.1016/j.jaap.2018.11.007>

Received 31 August 2018; Received in revised form 30 October 2018; Accepted 4 November 2018

Available online 06 November 2018

0165-2370/ © 2018 Elsevier B.V. All rights reserved.

Nomenclature		
R_{50}	Harvey's recalcitrance index (–)	Y_{org} mass yield of condensable organics in a dry and ash-free basis (–)
S_{BET}	Brunauer–Emmet–Teller specific surface area ($m^2 g^{-1}$)	Y_{water} Mass yield of produced water in a dry and ash-free basis (–)
<i>stable-C</i>	Mass fraction of C remaining after H ₂ O ₂ oxidation (–)	
$TC\#$	Temperatures measured by the thermocouples placed within the reactor (°C)	Acronyms
T_{max}	Process temperature at which the highest devolatilization rate is attained (°C)	AAEMs Alkali and alkaline Earth metal species
V_{DR}	Limiting micropore volumes from the Dubinin–Radushkevich equation ($cm^3 g^{-1}$)	DTG Differential thermogravimetric analysis
V_{ultra}	Ultra-micropore volume ($cm^3 g^{-1}$)	daf Dry-ash-free
$x_{FC, bc}$	Mass fraction of fixed-carbon in the biochar (daf basis)	GCMC Grand Canonical Monte Carlo
y_{char}	Mass yield of biochar in a dry and ash-free basis (–)	GHSV Gas hourly space velocity (h^{-1})
y_{FC}	Fixed-carbon yield in a dry and ash-free basis (–)	PID Proportional integral derivative
y_{gas}	Mass yield of produced gas in a dry and ash-free basis (–)	WS Wheat straw
		XRF X-ray fluorescence spectroscopy
		μ -GC Micro gas chromatograph

residence time of the vapor phase were increased [13,15–19]. Nevertheless, some authors found a negligible [20] or even a negative [10,21] effect of the absolute pressure on the char yield. For instance, Manyà et al. [10], who analyzed the effect of the absolute pressure (in the range of 0.1–1.0 MPa) on the pyrolysis of two-phase olive mill waste in a laboratory-scale fixed-bed reactor (keeping constant the residence time of the vapor phase within the reactor by adjusting the mass flow rate of the inert gas), already observed a significant decrease in the char yield when the pressure was increased. This finding suggested that the real effect of pressure (i.e., without interaction of the residence time of the vapor phase) was really complex, since an increased pressure could lead to an enhancement of the kinetics of the steam gasification reaction, which might be further explained by the catalytic effect of the alkali and alkaline earth metal species (AAEMs) present in the biomass feedstock. Therefore, the effect of the absolute pressure on the pyrolysis behavior of any feedstock has not been properly demonstrated yet.

Another important parameter affecting the pyrolysis behavior is the type of carrier gas used to maintain oxygen-free conditions [5]. In terms of energy efficiency, the flue gas generated by combustion of pyrolysis gas can be used as pyrolysis gas environment. This approach, which can lead to important cost savings [22], may be suitable in small-scale and farm-based systems, resulting in an improvement in the biochar production process in terms of economic feasibility, environmental impact, and thermal efficiency. Nevertheless, further research is needed to analyze the effects of modifying the inert environment (i.e., from pure N₂ to a flue gas containing CO₂) on the pyrolysis products distribution as well as on the biochar properties.

As mentioned above, special attention should also be paid to those properties of biochar that are related to its carbon sequestration potential. For this purpose, the fixed-carbon content and the atomic H:C and O:C ratios appear as useful rough indicators of the long-term stability of biochar's carbon [9,23–26]. In fact, a recent publication [25] reported that the above-mentioned indicators exhibited a strong correlation with both the recalcitrance index (R_{50}) [27] and the *stable-C* [28], which are based on the relative thermal stability of a given biochar to that of graphite (R_{50}), and on oxidation of biochar using H₂O₂ to accelerate the oxidative loss of carbon (*stable C*).

The specific aim of this study is to analyze the effect of both the absolute pressure (0.1 or 0.5 MPa) and the type of pyrolysis atmosphere (pure N₂ or a binary mixture of CO₂ and N₂, 60:40 v/v), at a constant peak temperature of 500 °C, on the pyrolysis behavior of wheat straw pellets in a pressurized fixed-bed reactor. The pyrolysis device is equipped with a weighing platform, which was employed to monitor the real-time mass loss of the biomass along the pyrolysis process. To the best of our knowledge, this is one of the first studies using a bench-scale reactor coupled to a weighing platform. This approach can provide very useful insights to better understand the pyrolysis behavior at

a relatively large scale (compared to traditional TGA or even macro-TGA measurements), where the secondary reactions of primary volatiles play a key role. The simultaneous analysis of the real-time mass-loss data, gas composition, and temperature profiles can provide a unique way to assess the role played by the studied factors (pressure and pyrolysis atmosphere) on the pyrolysis process.

2. Experimental section

2.1. Biomass feedstock

The wheat straw (WS) pellets (7 mm OD and approximately 12 mm long) used in this work were supplied by a Belgian company. No binder was used in making the pellets. WS pellets were directly pyrolyzed without any preliminary milling step. The reason is that the efficiency of carbonization can be improved for large particles as compared with small ones, leading to charcoals with higher fixed-carbon contents [24,29].

Proximate analysis was performed in quadruplicate according to ASTM standards (D3173 for moisture, D3174 for ash, and D3175 for volatile matter), whereas ultimate analysis was carried out in triplicate using a combustion elemental analysis Leco CHN628 (Leco Corporation, USA). In addition, X-Ray Fluorescence (XRF) spectroscopy analysis (ADVANT'XP + XRF spectrometer from Thermo ARL, Switzerland) was performed in order to determine the inorganic constituents of the biomass ash.

A thermogravimetric analyzer (Netzsch 449 F1 Jupiter) was used to obtain the pyrolysis thermogravimetric curves (at a heating rate of 10 K min^{−1} and a final temperature of 800 °C) under an environment of pure N₂. The initial mass of sample was 10 mg. In order to roughly estimate the contents of the main biomass constituents, the experimental differential thermogravimetric (DTG) curve was deconvoluted into three peaks using the "Peak Analyzer" tool implemented in OriginPro version 9.0 (OriginLab, USA). These three peaks can be associated to the devolatilization of hemicelluloses plus extractives (peak 1), cellulose (peak 2), and lignin (peak 3) [25].

2.2. Pyrolysis device and experimental procedure

Pyrolysis runs were conducted in duplicate in a bench-scale fixed-bed reactor. Fig. 1 shows the scheme of the experimental device, the details of which are available in a previous study [5]. Briefly, the reactor (140 mm ID and 465 mm long) was made of Sandvik 253 MA stainless steel (EN 1.4835). A basket of 4 L, made of AISI 316 (EN 1.4401) stainless steel wire mesh, was used to allocate the biomass into the reactor. The initial sample weight was approximately 400 g, which represented around 30% of the basket volume. A weighing platform

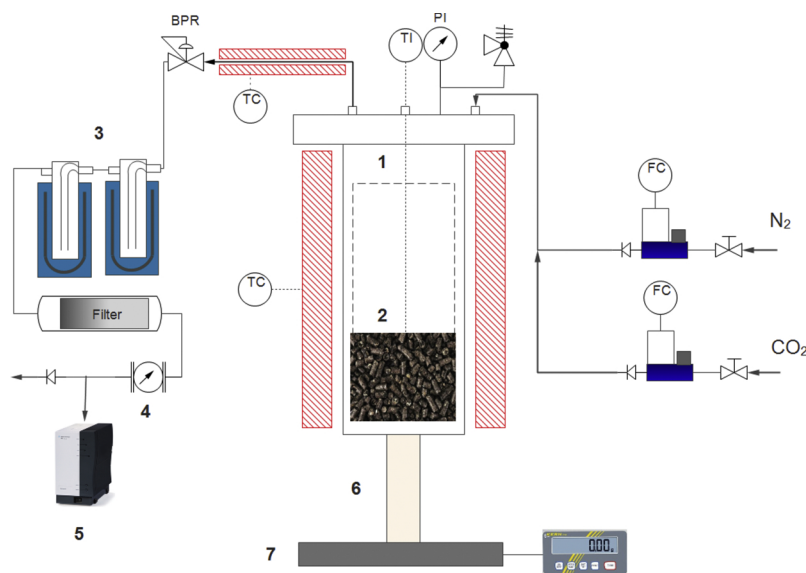


Fig. 1. Schematic layout of the pyrolysis device: (1) pyrolysis reactor, (2) biomass bed, (3) condensation system, (4) volumetric gas meter, (5) micro-GC, (6) ceramic tube, and (7) weighing platform.

from Kern (model DS with a measuring range up to 100 kg and a reading precision of 0.5 g) was placed at the bottom of the reactor system. A ceramic tube (117 mm OD and 330 mm long) was positioned between the reactor vessel and the weighing platform for thermal insulation purposes. Flexible stainless-steel tubing from Swagelok (10 mm OD) were used for the reactor connections to minimize any force component.

As widely reported in literature [7,8,10,30–34], higher pyrolysis temperatures usually led to lower biochar yields, hydrogen and oxygen contents, and aliphatic carbon fraction. In other words, increasing peak temperature results in more potentially stable biochars. However, it is interesting to find a compromise between yield and potential stability. In this sense, a previous study [35] showed that pyrolysis peak temperatures higher than 500 °C could be enough to obtain a biochar with an appropriate content of stable polycyclic aromatic carbon. Moreover, our previous experience with other biomass sources [25] indicated that higher temperatures (e.g., 600 °C) did not necessarily lead to a further improvement in the potential stability of biochar. Therefore, a peak temperature of 500 °C was selected as a reasonable trade-off between the biochar yield and its potential stability and was kept constant for all the pyrolysis runs.

In the present study, the experimental factors to consider were the absolute pressure (0.1 or 0.5 MPa) and the type of carrier gas (pure N₂ or a mixture of CO₂ and N₂, 60:40 v/v). The real flow rate of the carrier gas within the reactor at 500 °C was kept constant at 3.24 L min⁻¹, regardless of the pressure applied, by properly adjusting the mass flow rate. Assuming an entire reactor's void-volume fraction of 0.9, the above-mentioned flow rate corresponds to a gas-hourly space velocity (GHSV) of 36 h⁻¹. This approach is interesting in order to assess the effect of the absolute pressure instead of the combined effect of the absolute pressure plus the pressure-dependent gas residence time.

Temperature inside the bed was measured by four thermocouples located in a thermowell (placed at a radial distance of 35 mm from the axis) at different heights from the bottom of the sample basket: 10 mm (TC₀), 50 mm (TC₁), 200 mm (TC₂), and 300 mm (TC₃). During the course of the pyrolysis runs, the sample was heated at an average heating rate of 5 °C min⁻¹ to reach the peak temperature (500 °C). Due to the fact that a certain thermal gradient can exist along the packed bed, the average temperature of the two thermocouples placed at the bottom of the bed (TC₀ and TC₁) was chosen as the main process temperature. A soaking time of 60 min (at the peak temperature) was chosen to ensure the thermal equilibrium.

A back-pressure regulator was used to maintain the pressure of the system at a desired value. The outlet gas stream passed through a heated line, maintained at a temperature of around 375 °C, before being passed through a series of glass traps, which were immersed in ice-water baths. After each experiment, the biochar produced was collected and weighed. The glass traps were weighted before and after each pyrolysis run to estimate the total mass of liquid (water + organics). The pyrolysis liquid was recovered directly from the condensers without using any solvent as wash liquid. The water content of the pyrolysis liquid was then determined by Karl Fischer titration, while the yield of organic compounds was determined by difference from the total mass of liquid.

The composition of the major components of the pyrolysis gas (N₂, CO₂, CO, CH₄, C₂H_x and H₂) was determined using a micro gas chromatograph (μ-GC, Agilent 490) equipped with two analytical columns: a Molsieve 5A (using Ar as carrier gas) and a PolarPlot U (using He as carrier gas). The mass of produced gas was estimated from the N₂ mass balances.

In order to correct the buoyancy and other thermal expansion effects, blank tests (i.e., empty reactor) at 0.1 and 0.5 MPa were carried out employing the same heating program as for the experiments with biomass. The real-time mass loss for a given pyrolysis test was then obtained by subtracting the blank measurement from the raw signal.

2.3. Characterization of the pyrolysis products

The mass yield of biochar (y_{char}), volatile organic compounds (y_{org}), produced water (y_{water}) and produced gas (y_{gas}) were calculated on a dry and ash-free (daf) basis. Biochar samples were characterized by both proximate and ultimate analyses following the same procedures as described in Section 2.1. The carbonization efficiency was assessed by determining the fixed-carbon yield (y_{FC}), similarly to how it was done in previous studies [10]:

$$y_{FC} = x_{FC, bc} Y_{char} \quad (1)$$

where $x_{FC, bc}$ is the mass fraction of fixed-carbon in the biochar (calculated in a dry and ash-free basis). The value of y_{FC} corresponds to the fraction of organic matter initially present in the biomass feedstock that is converted into fixed carbon.

Due to the highly microporous structure of biochar, specific surface areas (S_{BET}) were determined from the CO₂ adsorption isotherms at 0 °C [36], which were obtained using an ASAP 2020 gas sorption analyzer

Table 1
Proximate, ultimate, and XRF analyses of the wheat straw pellets.

Proximate (wt. %)	
Ash	3.67 ± 0.13
Moisture	6.60 ± 0.20
Volatile matter	77.7 ± 0.31
Fixed carbon	12.0 ± 0.18
Ultimate (wt. % in daf basis)	
C	49.0 ± 0.52
H	7.01 ± 0.04
N	0.704 ± 0.01
O	43.2 ^a
Inorganic matter as equivalent oxides (wt. % of ash) ^a	
K ₂ O	53.2
CaO	17.4
SiO ₂	16.9
P ₂ O ₅	4.46
Al ₂ O ₃	1.66
Cl (inorganic)	1.53
MgO	1.46
S (inorganic)	1.31
Fe ₂ O ₃	1.14

^aOxygen was calculated by difference.

^bOnly listed components with a composition higher than 1%.

from Micromeritics (USA). Samples (around 120–200 mg) were previously degassed under dynamic vacuum conditions to constant weight at 150 °C. Pore size distributions (from 0.35 to 1.0 nm) and the ultramicropore volume (V_{ultra} , for pore sizes lower than 0.8 nm) of biochars were estimated using a Grand Canonical Monte Carlo (GCMC) method for carbon slit-shaped pores. All the calculations from CO₂ adsorption isotherms were performed using the MicroActive software supplied by Micromeritics.

3. Results and discussion

Table 1 shows the results pertaining to the characterization of the wheat straw pellets (proximate, ultimate, and XRF analysis). From the results concerning the inorganic constituents, it should be highlighted the high amount of K and Ca (AAEMs). Hence, a certain catalytic role of them should be expected in this study.

The mass-balance closures for the pyrolysis tests were estimated to be within 91%–99% (see Table S1 in the Supplementary Data). The mass yields of the different pyrolysis products (y_{char} , y_{water} , y_{org} and y_{gas}) were calculated attributing the error in the mass-balance closure to minor inaccuracies in determining the mass of produced gas. As each experimental run was conducted in duplicate, the mass yields of the pyrolysis products correspond to the average values.

With regard to the accuracy of the obtained mass-loss curves, we assessed the repeatability of three blank tests (two at 0.1 MPa and one at 0.5 MPa) as well as four pyrolysis runs (at 0.1 MPa and using a mixture of CO₂ and N₂ as carrier gas). The results from the three blank tests (see Fig. S1) indicated a reasonable degree of repeatability. Also according to Fig. S1, pressure had a negligible effect on the blank mass-loss curve. Therefore, we took the average from the three replicates as the blank signal to be subtracted from the raw mass-loss curves. For its part, Fig. S2 displays the results obtained from the four repeated pyrolysis runs. As can be seen from Fig. S2, a more than acceptable degree of repeatability was reached (see also explanatory notes for Fig. S2 in the Supplementary Data).

3.1. Pyrolysis behavior

Fig. 2 shows the mass-loss profiles obtained for the four pyrolysis runs: at 0.1 and 0.5 MPa under pure N₂ (0.1_N₂; 0.5_N₂) in Fig. 2a; and at 0.1 and 0.5 MPa under the mixture CO₂/N₂ (0.1_N₂&CO₂; 0.5_N₂&CO₂) in Fig. 2b. A certain level of noise can be seen in the mass loss plots. This noise is difficult to avoid in practice, since several factors

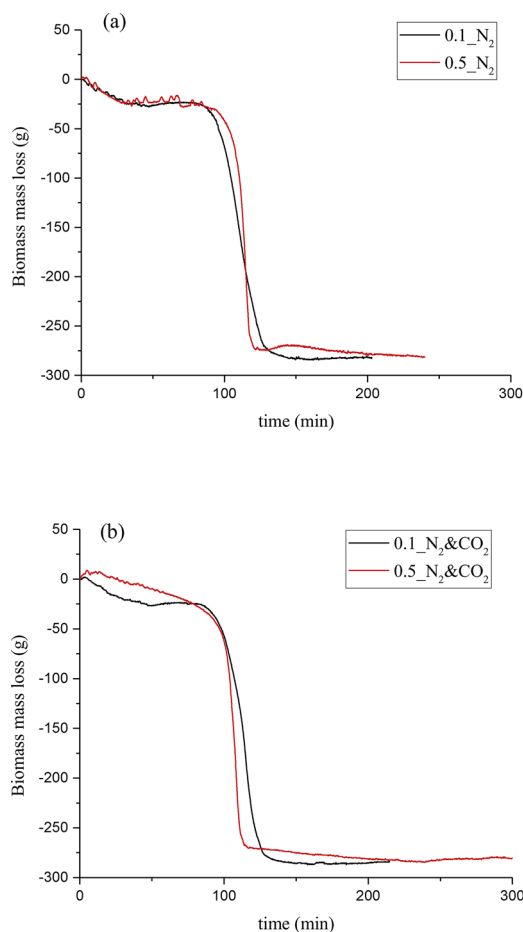


Fig. 2. A comparison between the mass-loss evolutions along the pyrolysis process at 0.1 MPa and 0.5 MPa, using (a) a N₂ atmosphere, and (b) a CO₂/N₂ environment.

such as the room temperature (small changes of which could slightly alter the weight measurement due to the extreme sensitivity of the scale), small changes in the heating program, and the exact position of the reactor inside the furnace could markedly affect the stability of the acquired signal over time. However, the plots displayed in Fig. 2 provide a very interesting information for the purpose of the present work. As expected, two mass-loss steps are clearly shown in Fig. 2. The first one corresponds to the evaporation of the moisture fraction of the feedstock, whereas the second one is the mass loss due to the devolatilization process at 180–500 °C.

To better visualize the effects of the studied factors on the pyrolysis behavior, Fig. 3 simultaneously displays the time derivative of the mass loss, the evolution of temperature within the bed (TC₀ and TC₁), and the molar flows of the main gaseous species released during the pyrolysis process (produced CO₂, CO, CH₄, and H₂). The detailed location of the four thermocouples and the obtained axial temperature profiles (for all thermocouples) are shown in Figs. S3 and S4, respectively. The plots in Fig. S4 clearly show severe axial temperature gradients throughout the reactor, especially for the thermocouples located outside the packed bed (TC₂ and TC₃). For pyrolysis runs performed at 0.5 MPa, the temperature gradients slightly decreased (i.e., higher values were recorded by thermocouples TC₂ and TC₃), probably as a consequence of the enhanced convective heat transfer related to the higher N₂ mass flow rate. Nevertheless, no large differences in the temperatures measured by TC₀ and TC₁ (both located within the bed) were found. This could confirm a relatively homogeneous heating throughout the bed length.

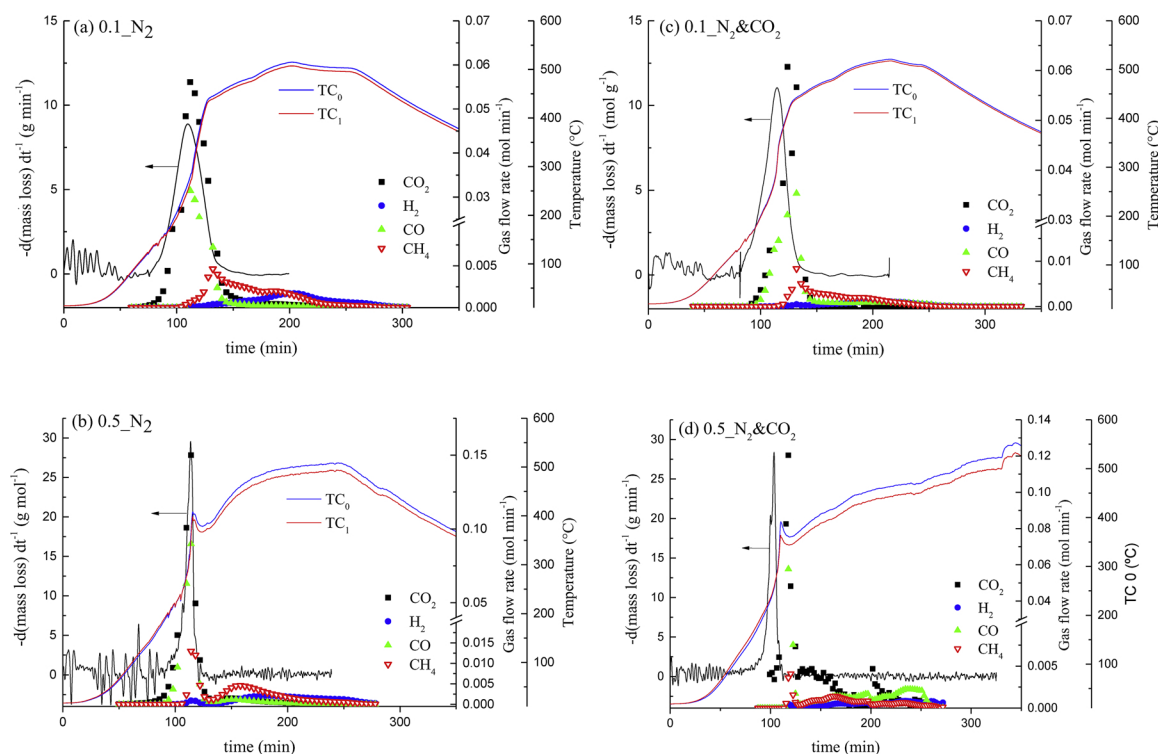


Fig. 3. Time derivative of the mass loss, evolution of temperatures within the bed (TC_0 and TC_1), and molar flows of the main gaseous species released during the pyrolysis process (produced CO_2 , CO , CH_4 , and H_2) for experiments conducted at 0.1 MPa under N_2 (a), 0.5 MPa under N_2 (b), 0.1 MPa using a mixture CO_2/N_2 (c), and at 0.5 MPa using a mixture CO_2/N_2 (d).

In light of the shape of the time derivatives of the mass loss shown in Fig. 3, it can be pointed out that the absolute pressure greatly affected the release of volatiles during the pyrolysis process. At 0.5 MPa, and regardless of the pyrolysis atmosphere, higher devolatilization rates in a narrower period of time, compared to the two experiments conducted at 0.1 MPa, were clearly observed. Regarding the position of the mass-loss peaks, the temperatures at which the highest devolatilization rate was attained (T_{max}) were: 263 °C (0.1 N_2), 339 °C (0.5 N_2), 300 °C (0.1 N_2 & CO_2), and 261 °C (0.5 N_2 & CO_2). Therefore, the values of T_{max} seem to depend on both the absolute pressure and the pyrolysis atmosphere. Unexpectedly, these temperature values were relatively similar and, in the most of cases, even lower than that deduced from the thermogravimetric analysis (around 325 °C, as can be deduced from the DTG curve shown in Fig. S5). Considering the heat transfer limitations existing in our fixed-bed reactor system, this unexpected result could be due to the presence of large radial temperature gradients. In other words, the temperatures registered by the thermocouples could correspond to the lowest (or almost lowest) temperature values in the bed at a given time. In the next subsections, further discussion is provided for each of the two different pyrolysis atmospheres.

3.1.1. Pure N_2 atmosphere

It is generally assumed that an increase in the absolute pressure could lead to a promotion of the secondary cross-linking reactions at relatively low temperatures (i.e., lower than T_{max}), as a consequence of the restricted release of volatiles [25,37]. This fact can explain the observed behaviors when the pyrolysis atmosphere was pure N_2 : an increase in T_{max} with pressure and, as shown in Fig. 4a, an increase in the yield of produced gas (y_{gas}) at the expense of both the produced water (y_{water}) and, to a lesser extent, the condensable organic compounds (y_{org}). The yield of biochar, however, was kept almost constant, regardless of the pressure applied. This can suggest that an increased pressure results in a double effect: (1) a higher pressure (probably

combined with the catalytic role of the AAEM species) can enhance the release of volatiles (once they reach the increased saturation temperature), leading to a higher devolatilization rate at higher temperatures; and (2), and as mentioned above, a higher pressure can also promote the secondary charring reactions (especially at intra-particle level and at relatively low temperatures) and simultaneously favor the thermal cracking and steam reforming of intermediate volatile organic compounds, leading to a decrease in the cumulative yield of the total liquid (mainly water) at the expense of produced gas and biochar.

The observed decrease in the yield of produced water with pressure, which was also reported by Ates et al. [38] for the pressurized pyrolysis of two biomass sources, seems to be contradictory with the higher extent of the secondary reactions of the primary volatile species, since both thermal cracking and dehydration processes can notably increase the production of water [19]. However, a higher consumption of water can also be promoted by pressure by means of an enhancement of several reactions: (1) steam reforming of volatile organic compounds and/or light hydrocarbons, (2) water-gas-shift reaction (reaction #1 in Table 2), and (3) steam gasification (reaction #5 in Table 2). Despite the fact that secondary reactions of primary volatiles could mainly explain the obtained product yields, a certain role of the theoretical reactions listed in Table 2 cannot be ignored, since the residence time of permanent gases within the reactor is quite long (around 100 s assuming a GHSV of 36 h^{-1}). In this sense and as already observed in previous studies [4,10], a low (but certain) extent of the steam gasification reaction cannot be discarded. In spite of the extremely low temperature and the related thermodynamic limitations, the AAEMs contained in the wheat straw pellets (especially K, with a relatively high content, as reported in Table 1) can enhance the kinetics of the reaction, especially at 0.5 MPa. This can also partly explain the almost constant yield of biochar regardless of the pressure applied. In other words, a certain consumption of carbon via steam gasification can compensate the additional char produced through secondary charring

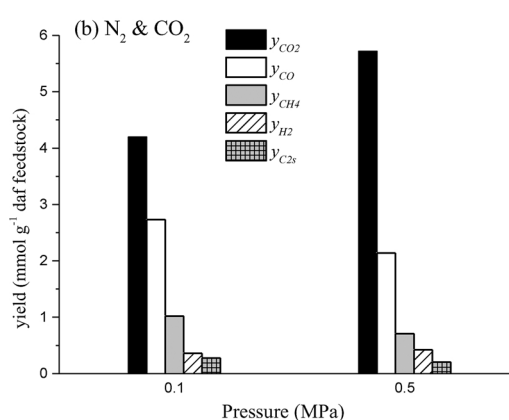
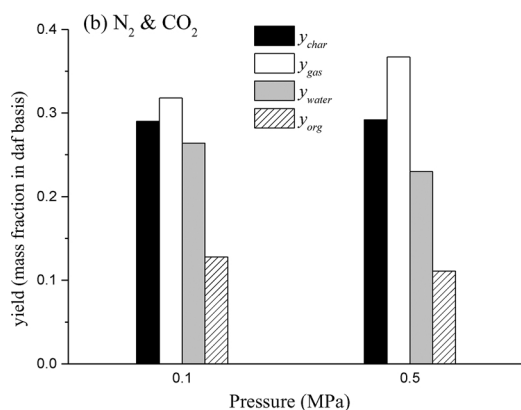
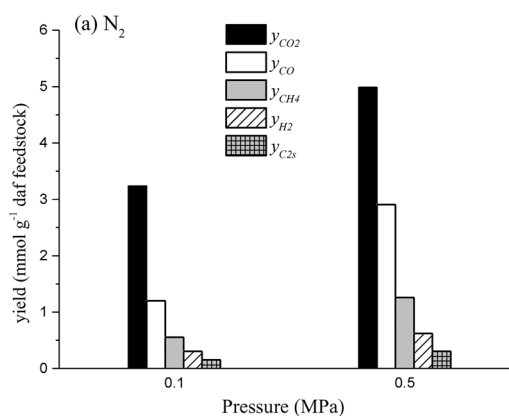
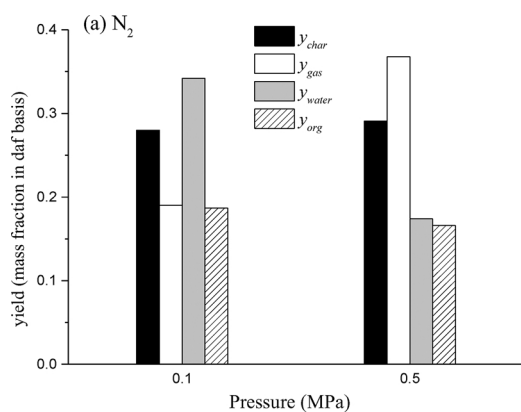


Fig. 4. Mass yields (in a daf basis) of biochar (y_{char}), produced water (y_{water}), organics (y_{org}), and gas (y_{gas}) as a function of the absolute pressure: (a) pyrolysis runs conducted under pure N_2 , (b) runs conducted within a CO_2/N_2 environment.

Table 2

Main reactions probably occurring during the release of the pyrolysis gas.

No.	Reaction	Extent of reaction (ξ) ^a (kmol h ⁻¹)	
		500 °C and 0.1 MPa	500 °C and 0.5 MPa
1	$H_2O + CO \rightleftharpoons CO_2 + H_2$	0.390	0.390
2	$2CO \rightleftharpoons CO_2 + C$	0.937	0.972
3	$3H_2 + CO \rightleftharpoons CH_4 + H_2O$	0.614	0.825
4	$C + 2H_2 \rightleftharpoons CH_4$	0.343	0.693
5	$C + H_2O \rightleftharpoons CO + H_2$	-0.714	-0.871
6	$2H_2 + 2CO \rightleftharpoons CO_2 + CH_4$	0.706	0.867

^aCalculated using Aspen Plus V8.8; NRTL package and a Gibbs Reactor module. Stoichiometric coefficients were taken as initial molar flow rates (in kmol h⁻¹) for all the species involved in the reaction.

reactions of the primary volatiles.

Fig. 3 also shows that the absolute pressure caused a certain effect on the evolution of the two temperatures inside the bed (TC_0 and TC_1). Both temperatures just increased up to approximately 500 °C (the selected peak temperature) at 0.1 MPa, showing the highest heating rate in correspondence with the highest devolatilization rate. However, when the pressure was set at 0.5 MPa, the two temperatures increased along the process, showing a heating rate (during the devolatilization step) faster than that observed at atmospheric pressure. This is consistent with the higher extent of the above-mentioned secondary reactions, which have an exothermic nature. The observed slight decrease in temperature (of about 30 °C, just after attaining the highest devolatilization rate) for pressurized experiments can be explained by a transient

Fig. 5. Cumulative yields of the main gaseous compounds (mmol g⁻¹ daf feedstock) as a function of the absolute pressure: (a) pyrolysis runs conducted under pure N_2 , (b) runs conducted within a CO_2/N_2 environment.

response of the PID controller (i.e., a lower power was supplied to the furnace during a relatively short period).

Concerning the gas release profiles (also shown in Fig. 3), it can be seen that CO_2 and CO were the first gases to be released in all the cases, showing a peak at approximately the value of T_{max} (263 °C and 339 °C at 0.1 and 0.5 MPa, respectively; see Fig. 3a), followed by the generation of CH_4 and H_2 at considerably higher temperatures. The production of CO_2 and CO at relatively low temperatures was mainly due to the thermal decomposition of hemicelluloses and extractives, in particular to their decarboxylation and decarbonylation reactions. Fig. S6 shows that the percentage of area corresponding to the first peak (attributed to the decomposition of hemicelluloses and extractives) was 52.5%. Further release of CO_2 and CO at higher temperatures can be attributed to the decomposition of cellulose (with a related second peak representing 27.8% of the total area). For its part, the release of CH_4 (which is partly due to the decomposition of lignin) occurred at temperatures in the range of 375 – 450 °C. As can be seen in Figs. 4a – b, two different peaks in the release of CH_4 can be distinguished: the first one (at lower temperature) could correspond to the decomposition of lignin, whereas the second one (more pronounced at 0.5 MPa) may be due to a subsequent cracking of volatiles and/or the promotion of some methanation reaction in gas phase. Regarding the H_2 release profile, it should be highlighted that the most part of which appeared when the main devolatilization step was already concluded. Given the fact that the mass-loss profile did not show any considerable change during the highest release of H_2 , we can suggest that the formation of H_2 can mainly be attributed to secondary homogeneous gas-phase reactions.

Fig. 5a displays the cumulative yields of the main gaseous species

Table 3
Main characteristics of the produced biochars.

	Pyrolysis conditions			
	0.1_N ₂	0.5_N ₂	0.1_N ₂ &CO ₂	0.5_N ₂ &CO ₂
Proximate analysis (wt. % in dry basis)				
Ash	12.8 ± 0.20	11.7 ± 0.14	13.1 ± 0.16	13.3 ± 0.03
Volatile matter	25.0 ± 0.65	18.3 ± 0.16	26.3 ± 1.78	25.7 ± 1.13
Fixed carbon	62.1 ± 0.42	70.0 ± 0.14	60.6 ± 1.83	61.0 ± 1.08
Ultimate analysis (wt. % in daf basis)				
C	86.0 ± 0.02	85.0 ± 0.13	87.7 ± 0.07	89.3 ± 0.13
H	3.87 ± 0.03	3.31 ± 0.15	3.66 ± 0.01	3.30 ± 0.22
N	1.82 ± 0.01	1.89 ± 0.01	1.93 ± 0.01	2.09 ± 0.02
O ^a	8.30	9.77	6.66	5.28
Other				
y _{FC} ^b	0.199	0.231	0.202	0.205
Molar H:C ratio	0.539	0.468	0.500	0.443
Molar O:C ratio	0.072	0.086	0.060	0.044
S _{BET} (m ² ·g ⁻¹)	200	196	380	226
Pore volume (V _{DR} ; cm ³ ·g ⁻¹)	0.112	0.110	0.197	0.129
Pore volume (V _{DFT} ; cm ³ ·g ⁻¹)	0.0814	0.0839	0.150	0.0962

^aCalculated by difference.

^bFixed-carbon yield calculated according to Eq. (1).

(in mmol g⁻¹ of feedstock in a daf basis) for the experiments conducted under a pure N₂ environment. All the yields notably increased when a pressure of 0.5 MPa was applied, partly as a result of the higher extent of secondary pyrolysis reactions, leading to a higher production of permanent gases from intermediate volatile organic compounds. This fact could explain the higher peaks observed in Fig. 3b (compared with those of Fig. 3a) for CO₂, CO and CH₄ during the devolatilization process (i.e., when the mass loss of biomass still continued). However, and as has been pointed out before, an additional formation of CH₄ at higher temperatures (i.e., the second peak of CH₄) is clearly enhanced at 0.5 MPa. From a thermodynamics point of view, the additional formation of CH₄ can be explained by an enhancement of methanation reactions (see reactions #3, #4, and #6 in Table 2). For its part, the higher production of CO₂ at 0.5 MPa could be explained by the promotion of reactions #2 (Boudouard) and #6 (reverse dry reforming). Nevertheless, the fact that the yield of CO also increased with pressure (in spite of its consumption through reactions #2, #3, and #6) suggests that further reactions are involved. One of them could be the above-mentioned steam gasification reaction (reaction #5 in Table 2), which can also partly explain the decreased yield of produced water at high pressure.

3.1.2. CO₂/N₂ atmosphere

Using a carrier gas composed of a mixture of CO₂ and N₂ (60:40 v/v) led to considerable changes in the pyrolysis behavior (as compared with that observed using pure N₂) at both 0.1 and 0.5 MPa. At atmospheric pressure, a higher exothermicity during the main devolatilization stage can be observed in Fig. 3c (in comparison to the temperature profiles at 0.1 MPa shown in Fig. 3a), leading to a higher value of T_{max} (300 °C instead of 263 °C). This observed higher exothermic behavior might be explained by a promotion of the secondary reactions of the primary volatile organic compounds. This finding is in agreement with a recent study focused on slow pyrolysis of red pepper stalk [39], in which the observed decrease in tar yield (in favor of produced gas) was attributed to an enhancement of the thermal cracking of volatiles when an atmosphere of CO₂ was used. Interestingly and as can be seen in Fig. 4b, the yield of biochar (y_{char}) was almost the same than that obtained

using pure N₂ at 0.1 MPa. In fact, the higher yield of produced gas (under an atmosphere of CO₂/N₂) was at the expense of the total production of liquid (y_{water} + y_{org}). The fact that the yield of produced water also decreased at 0.1 MPa, using a pyrolysis environment composed of a mixture of CO₂ and N₂, can suggest that CO₂ also promotes the further consumption of water through steam reforming and/or steam gasification reactions.

Regarding the yields of the main gaseous species obtained at 0.1 MPa (see Fig. 5b), it should be highlighted the higher yields of CO and CH₄ compared with those measured using an atmosphere of N₂. The increase in the yield of CH₄ (1.02 mmol g⁻¹, 86% higher than that using N₂), as well as in the yield of C₂ hydrocarbons (C₂H₄ + C₂H₆), could be related to the above-mentioned higher extent of the thermal cracking of volatile organic compounds [39]. In the case of the yield of CO (2.73 mmol g⁻¹, 127% higher than that using N₂ at 0.1 MPa), its increase could be due to different chemical processes: (1) thermal cracking of intermediate volatile compounds (such as carboxylic acids and phenolic compounds), (2) reverse water-gas-shift reaction, which is thermodynamically promoted and probably further enhanced by the relatively high partial pressure of CO₂, and (3) reverse Boudouard reaction, which can also be promoted by the high concentration of CO₂, despite the fact that this reaction is thermodynamically disfavored and extremely slow at the temperatures used here.

As expected, a further increase in the yield of produced gas at the expense of the yield of liquid (y_{water} + y_{org}) was observed when pressure raised to 0.5 MPa (see Fig. 4b). Nevertheless, the yields of gaseous species did not follow the expected trend. Fig. 5b shows a notably decrease in the yields of CO and CH₄ compared with those obtained at 0.1 MPa using a mixture of CO₂ and N₂. In other words, and unlike the trend observed for the pyrolysis experiments conducted in a pure N₂ environment, an increased pressure did not lead to any improvement in the pyrolysis gas composition when CO₂ was used as carrier gas. The observed increase in the yield of CO₂ (5.72 mmol g⁻¹, 31% higher than that using CO₂/N₂ at 0.1 MPa, and 15% higher than that using N₂ at 0.5 MPa) could be explained by a promotion of the Boudouard reaction at 0.5 MPa. A further evidence supporting this assumption is the observed decrease in the yield of CO (y_{CO}) when the absolute pressure was increased under a pyrolysis atmosphere of CO₂/N₂: from 2.73 mmol g⁻¹ at 0.1 MPa to 2.14 mmol g⁻¹ at 0.5 MPa. Furthermore, the CH₄ yield also decreased at 0.5 MPa (0.709 mmol g⁻¹, 30% lower than that using CO₂/N₂ at 0.1 MPa). This finding could be related to a certain enhancement of the dry reforming of CH₄ (reverse reaction #6 in Table 2), due to the high partial pressure of CO₂ [22,40].

The observed deterioration in the quality of the produced gas (at 0.5 MPa using a mixture of CO₂ and N₂) seems to be in disagreement with previous studies [5,25], in which an improvement in the pyrolysis gas (in terms of yield of CO and heating value) was reported when pyrolysis of biomass (vine shoots, olive mill waste, and corn stover) at a peak temperature of 600 °C was conducted at 1.0 MPa under an atmosphere composed of pure [5] or almost pure (95% vol [25]) CO₂. However, the discrepancies in the results can be explained by differences in the pyrolysis peak temperature (500 °C in the present study), and, to a lesser extent, partial pressure of CO₂ (which is lower here), and the biomass feedstock (having different contents of ash and different inorganic constituents). In this sense, the lower pyrolysis temperature used in the present study can lead to very different rates and extents of the involved reversible reactions.

3.2. Biochar properties

The main characteristics of the biochars produced under different operating conditions are reported in Table 3. The biochar having the highest fixed-carbon content (70.0% in dry basis, 79.3% in daf basis) was obtained under pure N₂ at 0.5 MPa. Given that the yields of biochar were practically the same, regardless of the pyrolysis conditions, the carbonization efficiency was also maximized at 0.5 MPa under an

atmosphere of pure N_2 ($y_{FC} = 0.231$; approximately 15% higher than that for the rest of pyrolysis runs). This result can be attributed to the role of pressure in the promotion of secondary reactions. As mentioned in Section 3.1.1, an increased pressure can delay the transfer of volatiles into the vapor phase and thereby promote liquid-phase coking reactions that enhance the formation of fixed carbon [29]. However, an increased pressure did not lead to any improvement in the fixed-carbon yield when an atmosphere of CO_2/N_2 was used. One possible explanation can be related to the finding recently reported by Lee et al. [39], who observed a faster thermal degradation of lignin when CO_2 was used as pyrolysis medium instead of N_2 . Given the fact that the content of lignin (in a given biomass feedstock) is directly correlated to the yield of fixed carbon [13], a higher degradation of this amorphous substance can lead to a lower fixed-carbon yield.

Concerning the atomic H:C and O:C ratios reported in Table 3, it should be pointed out that the values for all produced biochars were very low (0.44 – 0.54 and 0.04 – 0.09, respectively), in spite of the relatively low pyrolysis peak temperature (500 °C). For instance, Windeatt et al. [41] reported H:C ratio values in the range of 0.4 – 0.5 for biochars produced from several crop residues through atmospheric pyrolysis (under N_2) at a higher peak temperature of 600 °C. Furthermore, a slight decrease in the atomic ratios (at both 0.1 and 0.5 MPa) was observed when the pyrolysis atmosphere was a mixture of CO_2 and N_2 . However, these differences (which can be within experimental error, especially for the O:C ratio) are too small to be considered as improvement in the carbon sequestration potential. In fact, the biochar having the lowest H:C and O:C ratios (produced at 0.5 MPa and under CO_2/N_2) does not exhibit the highest fixed-carbon content. In other words, we cannot assume that using an atmosphere of CO_2/N_2 (instead of pure N_2) can lead to biochars with higher potential stability. This is consistent with the results from an earlier study [25], in which no significant statistical effects on the potential stability of biochar's carbon were observed for neither the absolute pressure (in the range of 0.1 – 1.0 MPa) nor the pyrolysis atmosphere (pure N_2 or a mixture CO_2/N_2 95:5 v/v).

Table 3 also lists the textural parameters deduced from the CO_2 adsorption isotherms at 0 °C (which are displayed in Fig. S7). In addition to the BET specific surface area (S_{BET}), the limiting micropore volumes from the Dubinin-Radushkevich equation (V_{DR}) and the ultra-micropore volume (V_{ultra}) are also reported in Table 3. Two considerations can be drawn from the reported textural parameters and the pore size distributions shown in Fig. 6: (1) under a pyrolysis medium composed of pure N_2 , the microporosity development of biochars was not affected by the absolute pressure for the range of operating conditions tested in this study,

and (2) using a mixture of CO_2/N_2 as pyrolysis environment at atmospheric pressure led to notably higher microporous biochars. The fact that the presence of CO_2 at 0.1 MPa favors the porosity development of biochars could be due to the promotion of the reverse Boudouard reaction under these conditions. This is consistent with the increased yield of CO , which we already mentioned in Section 3.1.2. It must be highlighted the high ultra-micropore volume (a key parameter for CO_2 adsorption capacity) measured for the biochar produced at 0.1 MPa under CO_2/N_2 : $0.150 \text{ cm}^3 \text{ g}^{-1}$. This value is within the range or even higher than the ultra-micropore volumes reported for biomass-derived physically or chemically activated carbons [42,43]. Further research in this direction seems to be highly interesting to produce “low-temperature” carbon-based adsorbents for the selective removal of CO_2 in gas phase.

4. Conclusions

From the analysis of results presented above, the following main conclusions can be drawn:

(1) An increased pressure considerably affects the mass-loss profiles during the pyrolysis process, leading to higher devolatilization rates in a shorter period of time. Regardless of the pyrolysis atmosphere, an increase in the absolute pressure led to higher yields of produced gas at the expense of produced water and condensable organic compounds. This finding is related to the fact that an increased pressure favors the exothermic secondary reactions of the intermediate volatile organic compounds in both liquid and vapor phases.

(2) The switch from pure N_2 to a mixture of CO_2 and N_2 at 0.1 MPa led to a remarkable increase in the yield of produced gas at the expense of both the produced water and condensable organic compounds. This could be mainly due to the promotion of the thermal cracking of the volatile organic compounds at a high partial pressure of CO_2 , which is also consistent with the measured higher yields of CH_4 and CO . The increased yield of CO can also be seen as a direct result of the enhanced reverse Boudouard reaction. However, increasing the absolute pressure can result in a promotion of the direct Boudouard reaction, leading to a higher production of CO_2 at the expense of CO .

(3) Interestingly, neither the pressure nor the pyrolysis atmosphere appeared to affect the yield of biochar for the range of operating conditions under consideration. Moreover, the potential stability of biochar's carbon was found to be similar, regardless of the operating parameters used. Nevertheless, a much higher porosity development (in terms of specific surface area and volume of ultra-micropores) was measured for the biochar produced at 0.1 MPa under an atmosphere of CO_2/N_2 .

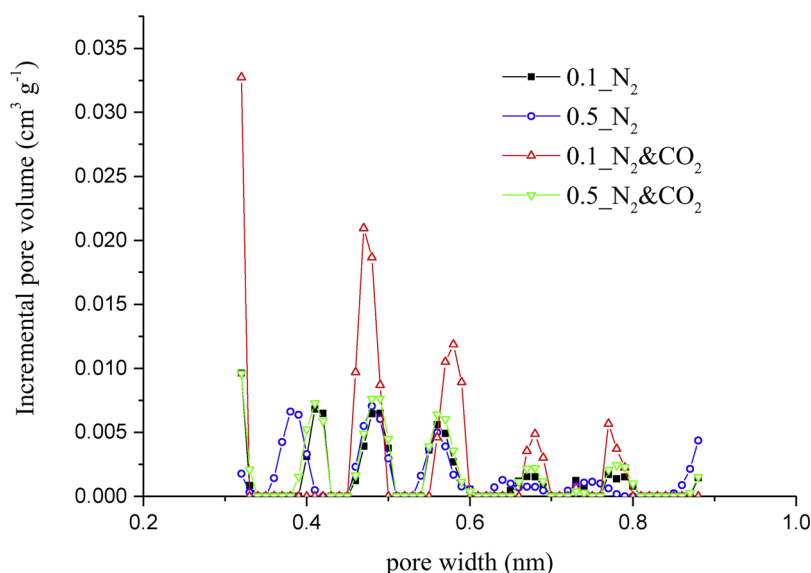


Fig. 6. Pore size distributions for the biochars obtained under different operating conditions (see legend) deduced from the CO_2 adsorption isotherms at 0 °C.

(4) We can conclude that, for the biomass feedstock used here at a pyrolysis peak temperature of 500 °C, using a mixture of CO₂ and N₂ (60:40 v/v) at atmospheric pressure is the most interesting way to simultaneously obtain a potentially recalcitrant and microporous biochar and an appropriate pyrolysis gas with relatively high contents of CH₄ and CO.

Acknowledgements

This project has received funding from the European Union's Horizon 2020 research and innovation programme under the Marie Skłodowska-Curie grant agreement No 721991. JJM also express his gratitude to the Aragon Government (GPT group) and the European Social Fund for additional financial support.

Appendix A. Supplementary data

Supplementary material related to this article can be found, in the online version, at doi:<https://doi.org/10.1016/j.jaap.2018.11.007>.

References

- [1] F. Li, X. Cao, L. Zhao, J. Wang, Z. Ding, Effects of mineral additives on biochar formation: carbon retention, stability, and properties, *Environ. Sci. Technol.* 48 (2014) 11211–11217, <https://doi.org/10.1021/es501885n>.
- [2] J.J. Manyà, Pyrolysis for biochar purposes: a review to establish current knowledge gaps and research needs, *Environ. Sci. Technol.* 46 (2012) 7939–7954, <https://doi.org/10.1021/es301029g>.
- [3] J. Lehmann, S. Joseph, *Biochar for environmental management: an introduction*, in: J. Lehmann, S. Joseph (Eds.), *Biochar Environ. Manag. Sci. Technol. Earthscan, London, 2009*, pp. 1–10.
- [4] J.J. Manyà, D. Alvira, M. Azuara, D. Bernin, N. Hedin, Effects of pressure and the addition of a rejected material from municipal waste composting on the pyrolysis of two-phase olive mill waste, *Energy Fuels* 30 (2016), <https://doi.org/10.1021/acs.energyfuels.6b01579>.
- [5] M. Azuara, E. Sáiz, J.A. Manso, F.J. García-Ramos, J.J. Manyà, Study on the effects of using a carbon dioxide atmosphere on the properties of vine shoots-derived biochar, *J. Anal. Appl. Pyrolysis* 124 (2017), <https://doi.org/10.1016/j.jaap.2016.11.022>.
- [6] V. Dhyani, T. Bhaskar, A comprehensive review on the pyrolysis of lignocellulosic biomass, *Renew. Energy* 129 (2018) 695–716, <https://doi.org/10.1016/j.renene.2017.04.035>.
- [7] W. Song, M. Guo, Quality variations of poultry litter biochar generated at different pyrolysis temperatures, *J. Anal. Appl. Pyrolysis* 94 (2012) 138–145, <https://doi.org/10.1016/j.jaap.2011.11.018>.
- [8] O. Mašek, P. Brownsort, A. Cross, S. Sohi, Influence of production conditions on the yield and environmental stability of biochar, *Fuel* 103 (2013) 151–155, <https://doi.org/10.1016/j.fuel.2011.08.044>.
- [9] F. Ronsse, S. van Hecke, D. Dickinson, W. Prins, Production and characterization of slow pyrolysis biochar: influence of feedstock type and pyrolysis conditions, *Gcb Bioenergy* 5 (2013) 104–115, <https://doi.org/10.1111/gcbb.12018>.
- [10] J.J. Manyà, S. Laguarda, M.A. Ortigosa, J.A. Manso, Biochar from slow pyrolysis of two-phase olive mill waste: effect of pressure and peak temperature on its potential stability, *Energy Fuels* 28 (2014) 3271–3280, <https://doi.org/10.1021/ef500654t>.
- [11] L. Wang, M. Trninić, Ø. Skreiberg, M. Gronli, R. Considine, M.J. Antal, Is elevated pressure required to achieve a high fixed-carbon yield of charcoal from biomass? Part 1: round-robin results for three different corncob materials, *Energy Fuels* 25 (2011) 3251–3265, <https://doi.org/10.1021/ef200450h>.
- [12] W.S.L. Mok, M.J. Antal Jr., Effects of pressure on biomass pyrolysis. I. Cellulose pyrolysis products, *Thermochim. Acta* 68 (1983) 155–164, [https://doi.org/10.1016/0040-6031\(83\)80221-4](https://doi.org/10.1016/0040-6031(83)80221-4).
- [13] M.J. Antal, S.G. Allen, X. Dai, B. Shimizu, M.S. Tam, M. Gronli, Attainment of the theoretical yield of carbon from biomass, *Ind. Eng. Chem. Res.* 39 (2000) 4024–4031, <https://doi.org/10.1021/ie000511u>.
- [14] M.J. Antal Jr., W.S.L. Mok, Review of Methods for Improving the Yield of Charcoal from Biomass, *Energy Fuels* 4 (1990) 221–225, <https://doi.org/10.1021/ef00021a001>.
- [15] P. Rousset, C. Figueiredo, M. De Souza, W. Quirino, Pressure effect on the quality of eucalyptus wood charcoal for the steel industry: a statistical analysis approach, *Fuel process. Technol.* 92 (2011) 1890–1897, <https://doi.org/10.1016/j.fuproc.2011.05.005>.
- [16] E.S. Noumi, J. Blin, J. Valette, P. Rousset, Combined effect of pyrolysis pressure and temperature on the yield and CO₂ gasification reactivity of Acacia wood in macro-TGA, *Energy Fuels* 29 (2015) 7301–7308, <https://doi.org/10.1021/acs.energyfuels.5b01454>.
- [17] M.J. Antal, E. Croiset, X. Dai, C. DeAlmeida, W.S.L. Mok, N. Norberg, J.-R. Richard, M. Al Majthoub, High-yield biomass charcoal, *Energy Fuels* 10 (1996) 652–658, <https://doi.org/10.1021/ef9501859>.
- [18] J. Recari, C. Berrueto, S. Abelló, D. Montané, X. Farriol, Effect of temperature and pressure on characteristics and reactivity of biomass-derived chars, *Bioresour. Technol.* 170 (2014) 204–210, <https://doi.org/10.1016/j.biortech.2014.07.080>.
- [19] Y. Qian, J. Zhang, J. Wang, Pressurized pyrolysis of rice husk in an inert gas sweeping fixed-bed reactor with a focus on bio-oil deoxygenation, *Bioresour. Technol.* 174 (2014) 95–102, <https://doi.org/10.1016/j.biortech.2014.10.012>.
- [20] F. Melligan, R. Aucaisse, E.H. Novotny, J.J. Leahy, M.H.B. Hayes, W. Kwapinski, Pressurized pyrolysis of Miscanthus using a fixed bed reactor, *Bioresour. Technol.* 102 (2011) 3466–3470, <https://doi.org/10.1016/j.biortech.2010.10.129>.
- [21] J.J. Manyà, F.X. Roca, J.F. Perales, TGA study examining the effect of pressure and peak temperature on biochar yield during pyrolysis of two-phase olive mill waste, *J. Anal. Appl. Pyrolysis* 103 (2013) 86–95, <https://doi.org/10.1016/j.jaap.2012.10.006>.
- [22] G. Pilon, J.-M. Lavoie, Pyrolysis of switchgrass (*Panicum virgatum* L.) at low temperatures within N₂ and CO₂ environments: Product yield study, *ACS Sustain. Chem. Eng.* 1 (2013) 198–204, <https://doi.org/10.1021/sc300098e>.
- [23] A. Enders, K. Hanley, T. Whitman, S. Joseph, J. Lehmann, A. Whitman, S. Joseph, J. Lehmann, Characterization of biochars to evaluate recalcitrance and agronomic performance, *Bioresour. Technol.* 114 (2012) 644–653, <https://doi.org/10.1016/j.biortech.2012.03.022>.
- [24] J.J. Manyà, M.A. Ortigosa, S. Laguarda, J.A. Manso, Experimental study on the effect of pyrolysis pressure, peak temperature, and particle size on the potential stability of vine shoots-derived biochar, *Fuel* 133 (2014) 163–172, <https://doi.org/10.1016/j.fuel.2014.05.019>.
- [25] J.J. Manyà, M. Azuara, J.A. Manso, Biochar production through slow pyrolysis of different biomass materials: seeking the best operating conditions, *Biomass Bioenergy* 117 (2018) 115–123, <https://doi.org/10.1016/j.biombioe.2018.07.019>.
- [26] K. Crombie, O. Masek, S.P. Sohi, P. Brownsort, A. Cross, The effect of pyrolysis conditions on biochar stability as determined by three methods, *Gcb Bioenergy* 5 (2013) 122–131, <https://doi.org/10.1111/gcbb.12030>.
- [27] O.R. Harvey, L.J. Kuo, A.R. Zimmerman, P. Louchouart, J.E. Amonette, B.E. Herbert, An index-based approach to assessing recalcitrance and soil carbon sequestration potential of engineered black carbons (biochars), *Environ. Sci. Technol.* 46 (2012) 1415–1421, <https://doi.org/10.1021/es2040398>.
- [28] A. Cross, S.P. Sohi, A method for screening the relative long-term stability of biochar, *Gcb Bioenergy* 5 (2013) 215–220, <https://doi.org/10.1111/gcbb.12035>.
- [29] L. Wang, O. Skreiberg, M. Gronli, G.P. Specht, M.J. Antal, Is elevated pressure required to achieve a high fixed-carbon yield of charcoal from biomass? Part 2: the importance of particle size, *Energy Fuels* 27 (2013) 2146–2156, <https://doi.org/10.1021/ef400041h>.
- [30] C. Di Blasi, G. Signorelli, C. Di Russo, G. Rea, Product distribution from pyrolysis of wood and agricultural residues, *Ind. Eng. Chem. Res.* 38 (1999) 2216–2224, <https://doi.org/10.1021/ie980711u>.
- [31] A. Demirbas, Effects of temperature and particle size on bio-char yield from pyrolysis of agricultural residues, *J. Anal. Appl. Pyrolysis* 72 (2004) 243–248, <https://doi.org/10.1016/j.jaap.2004.07.003>.
- [32] M. Azuara, B. Baguer, J.I. Villacampa, N. Hedin, J.J. Manyà, Influence of pressure and temperature on key physicochemical properties of corn stover-derived biochar, *Fuel* 186 (2016) 525–533, <https://doi.org/10.1016/j.fuel.2016.08.088>.
- [33] L. Zhao, X. Cao, O. Mašek, A. Zimmerman, Heterogeneity of biochar properties as a function of feedstock sources and production temperatures, *J. Hazard. Mater.* 256–257 (2013) 1–9, <https://doi.org/10.1016/j.jhazmat.2013.04.015>.
- [34] W. Suliman, J.B. Harsh, N.I. Abu-Lail, A.M. Fortuna, I. Dallmeyer, M. Garcia-Perez, Influence of feedstock source and pyrolysis temperature on biochar bulk and surface properties, *Biomass Bioenergy* 84 (2016) 37–48, <https://doi.org/10.1016/j.biombioe.2015.11.010>.
- [35] A.V. McBeath, C.M. Wurster, M.I. Bird, Influence of feedstock properties and pyrolysis conditions on biochar carbon stability as determined by hydrogen pyrolysis, *Biomass Bioenergy* 73 (2015) 155–173, <https://doi.org/10.1016/j.biombioe.2014.12.022>.
- [36] K.C. Kim, T.U. Yoon, Y.S. Bae, Applicability of using CO₂ adsorption isotherms to determine BET surface areas of microporous materials, *Microporous Mesoporous Mater.* 224 (2016) 294–301, <https://doi.org/10.1016/j.micromeso.2016.01.003>.
- [37] R. Ragucci, P. Giudicianni, A. Cavaliere, Cellulose slow pyrolysis products in a pressurized steam flow reactor, *Fuel* 107 (2013) 122–130, <https://doi.org/10.1016/j.fuel.2013.01.057>.
- [38] F. Ateş, N. Miskolczi, B. Saricaoglu, Pressurized pyrolysis of dried distillers grains with solubles and canola seed press cake in a fixed-bed reactor, *Bioresour. Technol.* 177 (2015) 149–158, <https://doi.org/10.1016/j.biortech.2014.10.163>.
- [39] J. Lee, X. Yang, S.H. Cho, J.K. Kim, S.S. Lee, D.C.W. Tsang, Y.S. Ok, E.E. Kwon, Pyrolysis process of agricultural waste using CO₂ for waste management, energy recovery, and biochar fabrication, *Appl. Energy* 185 (2017) 214–222, <https://doi.org/10.1016/j.apenergy.2016.10.092>.
- [40] C. Guizani, F.J. Escudero-Sanz, S. Salvador, Effects of CO₂ on biomass fast pyrolysis: reaction rate, gas yields and char reactivity properties, *Fuel* 116 (2014) 310–320, <https://doi.org/10.1016/j.fuel.2013.07.101>.
- [41] J.H. Windeatt, A.B. Ross, P.T. Williams, P.M. Forster, M.A. Nahil, S. Singh, Characteristics of biochars from crop residues: Potential for carbon sequestration and soil amendment, *J. Environ. Manage.* 146 (2014) 189–197, <https://doi.org/10.1016/j.jenvman.2014.08.003>.
- [42] W. Hao, E. Björkman, M. Lilliestråle, N. Hedin, Activated carbons prepared from hydrothermally carbonized waste biomass used as adsorbents for CO₂, *Appl. Energy* 112 (2013) 526–532, <https://doi.org/10.1016/j.apenergy.2013.02.028>.
- [43] J.J. Manyà, B. González, M. Azuara, G. Arner, Ultra-microporous adsorbents prepared from vine shoots-derived biochar with high CO₂ uptake and CO₂/N₂ selectivity, *Chem. Eng. J.* 345 (2018) 631–639, <https://doi.org/10.1016/j.cej.2018.01.092>.

Supplementary data

Evolution of the mass loss rate during atmospheric and pressurized slow pyrolysis of wheat straw in a bench-scale reactor

Gianluca Greco^a, María Videgain^a, Christian Di Stasi^a, Belén González^a, Joan J. Manyà^{a,b,*}

^a *Technological College of Huesca*, ^b *Aragón Institute of Engineering Research (I3A), University of Zaragoza, crta. Cuarte s/n, Huesca E-22071, Spain*

* Corresponding author. E-mail address: joanjoma@unizar.es.

Table S1. Products distribution and mass balance closure for all the pyrolysis runs

Run	mass of feedstock (g)	mass of biochar (g)	mass of total liquid (g)	mass of produced gas (g)	mass balance closure (%)
0.1_N2	400.5	119	192.1	86.5	99.2
0.5_N2	400.1	118.6	148.9	107.5	93.7
0.1_N2&CO2	406.2	121.4	169.2	80.2	91.3
0.5_N2&CO2	402.6	121.2	145.7	102.5	91.7

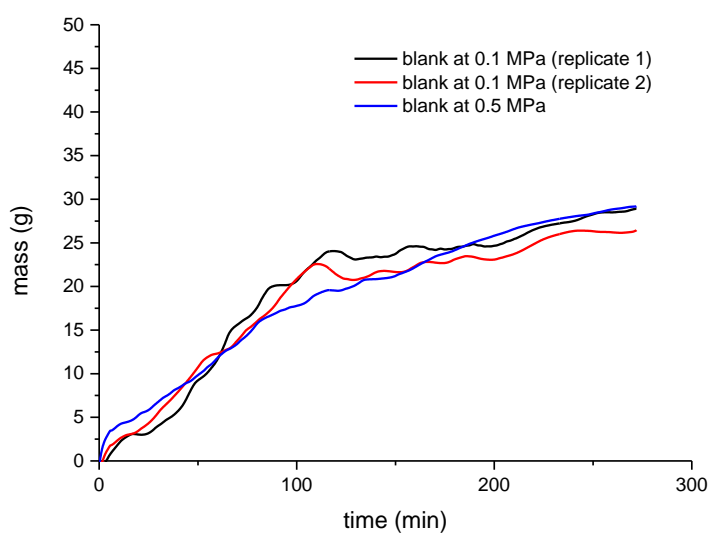


Fig. S1. Comparison of the mass-loss curves obtained for three blank tests.

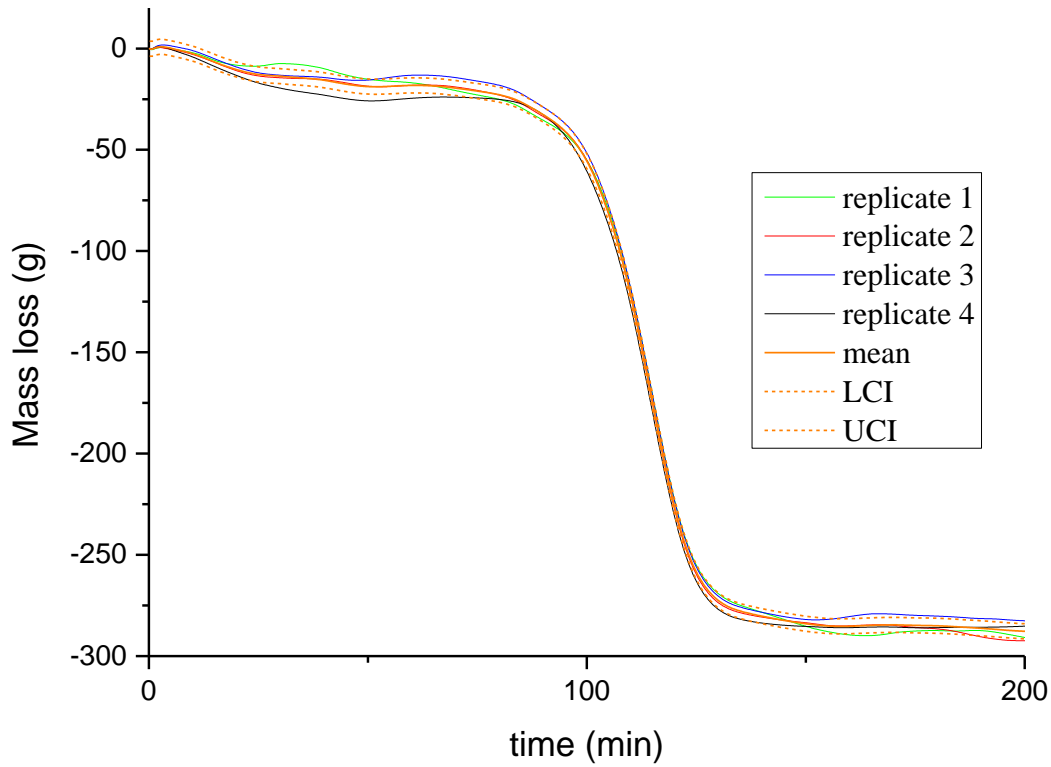


Fig. S2. Comparison of the mass-loss curves obtained for four replicates (at 0.1 MPa and using a mixture of CO₂ and N₂ as carrier gas). LCI and UCI correspond to lower and upper 95% confidence intervals.

Assessment of repeatability

The four repeated measurements shown in Fig. S2 were analyzed using a one-way ANOVA. Assuming normality and homogeneity of variances (since just 4 replicates at each level of factor is too low for conducting the appropriate tests), we computed the mean squares for the treatment and error terms (MS_t and MS_e , respectively). The intra-class correlation coefficient (ICC), which is commonly used as a measure of repeatability (R), was then estimated as follows [1]:

$$ICC = \frac{MS_t - MS_e}{MS_t + (n_0 - 1)MS_e} \quad (1)$$

where n_0 is the number of replicates (4). The obtained value of ICC was 0.9991, indicating high level of repeatability (99.91%).

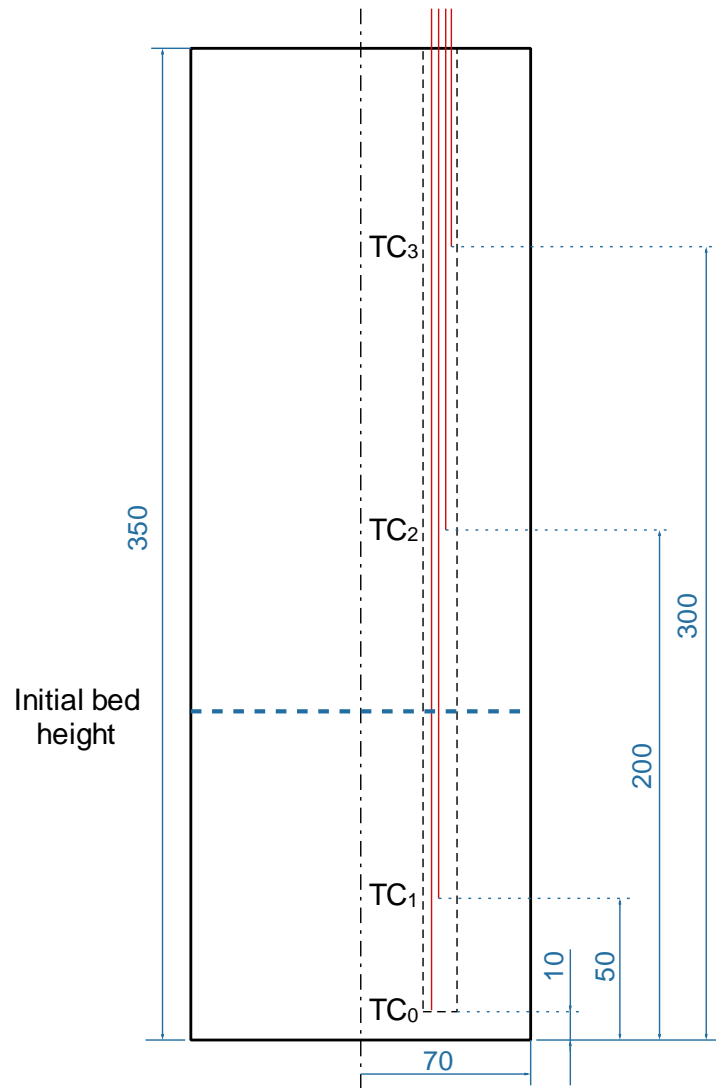


Fig. S3. Detail of the location of thermocouples TC₀, TC₁, TC₂, and TC₃ (all dimensions in mm).

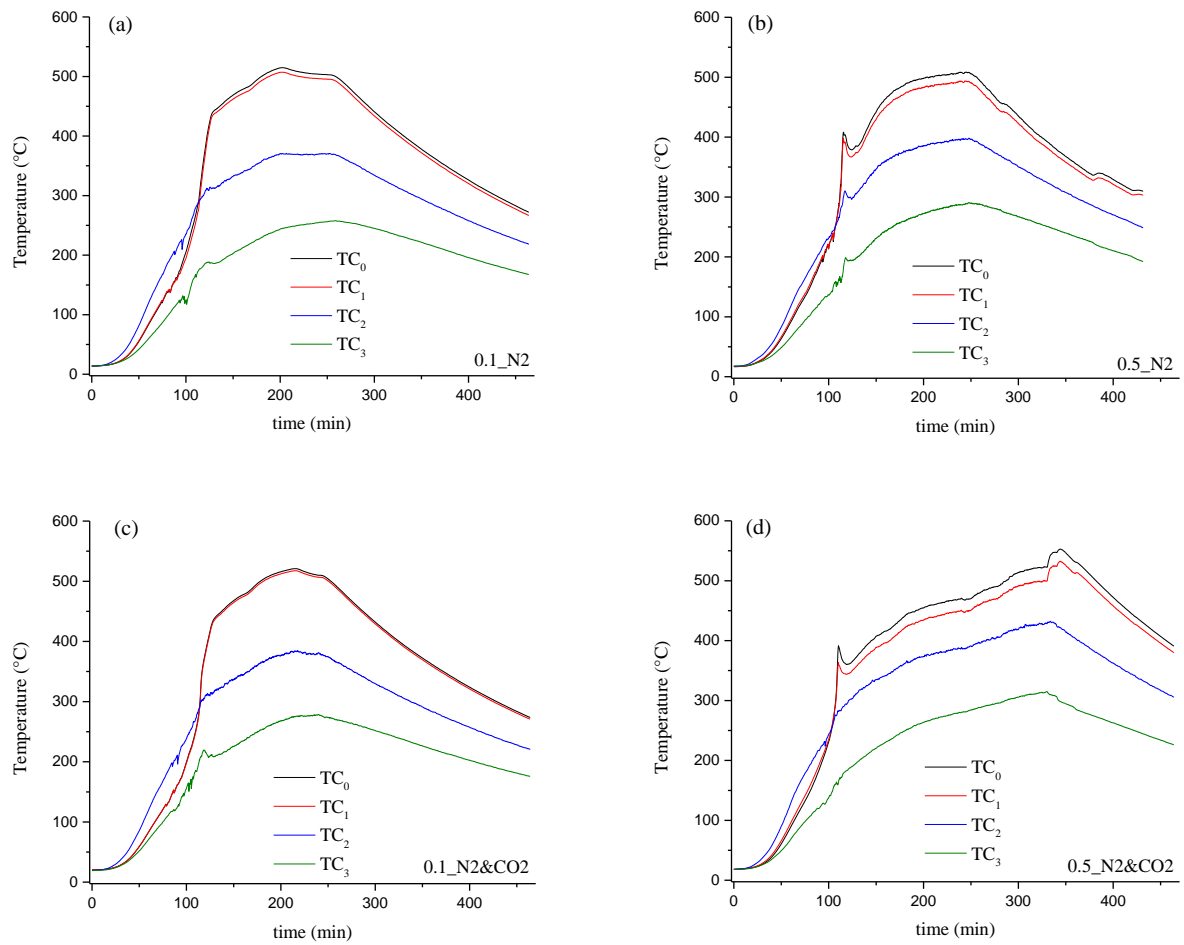


Fig. S4. Axial temperature profiles (at a radial location of 35 mm) in the bed (TC₀ and TC₁) and freeboard (TC₂ and TC₃) for each experiment: (a) 0.1 MPa in N₂, (b) 0.5 MPa in N₂, (c) 0.1 MPa in CO₂/N₂, and (d) 0.5 MPa in CO₂/N₂.

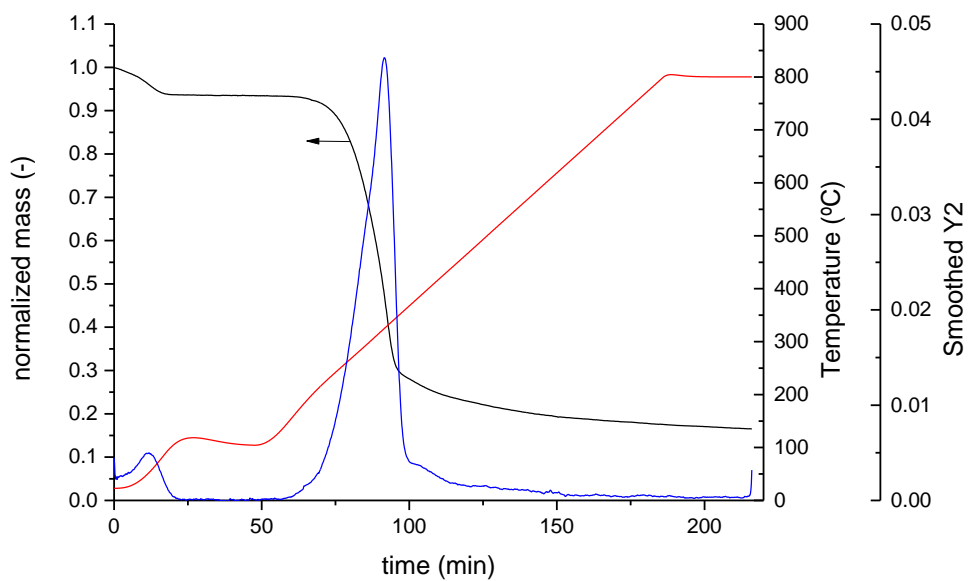


Fig. S5. Thermogravimetric curves obtained for the wheat straw pellets at a heating rate of 10 K min⁻¹.

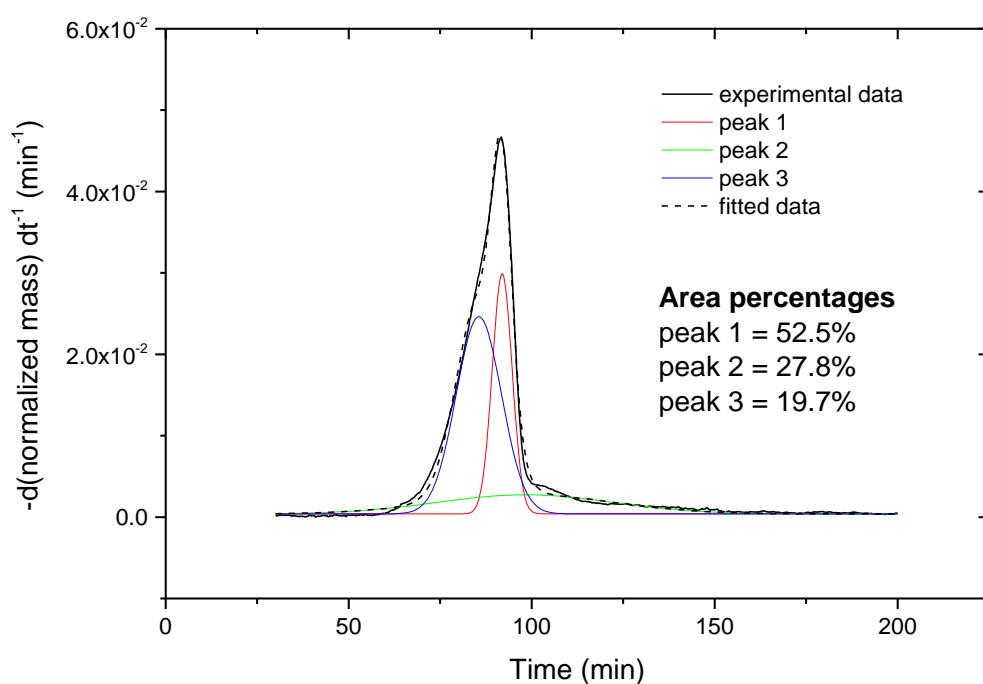


Fig. S6. Deconvolution of the derivative thermogravimetric curve (DTG) using three peaks.

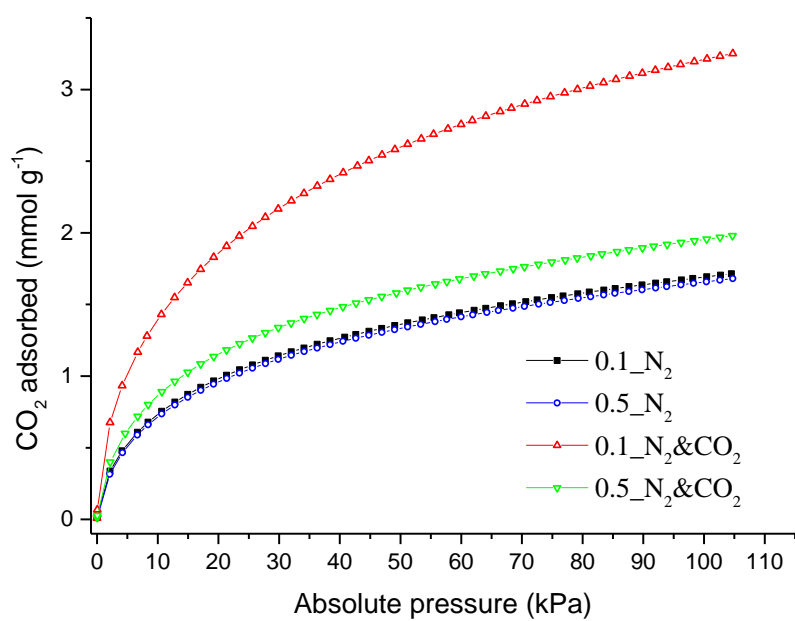


Fig. S7. CO₂ adsorption isotherms at 0 °C for the biochars produced under different operating conditions (see legend).

References

- [1] S. Nakagawa, H. Schielzeth, Repeatability for Gaussian and non-Gaussian data: A practical guide for biologists, *Biol. Rev.* 85 (2010) 935–956. <https://doi:10.1111/j.1469-185X.2010.00141.x>.

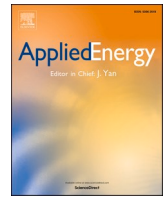
6.2. Theme II: study on the energy/exergy efficiency of the pyrolysis process

After assessing in the first instance how both absolute pressure and pyrolysis atmosphere could affect the pyrolysis behavior of wheat straw pellets (see *Theme I*), the next step was to expand the study including further pyrolysis operating conditions on more levels. Therefore, in the second part of the experimental work, a comprehensive study of the influence of peak temperature (400–550 °C), absolute pressure (0.2–0.9 MPa), gas residence time (100–200 s) and reactor atmosphere (pure N₂ or a 60/40 v/v mixture of CO₂/N₂) on the pyrolysis behavior of wheat straw pellets was conducted. Adopting a statistical approach through the implementation of an unreplicated full factorial design (with three replicates at the center point) resulted to be very helpful in order to assess the effects of the pyrolysis operating conditions on the pyrolysis products and the exergy efficiencies related to them, as well as the external energy demanded by the process. This research study was published in *Applied Energy* (article 2).

In agreement with previous findings available in the literature, peak temperature resulted to be the most influential factor on yields and distribution of the pyrolysis products. Its marked effect was visible also on the biochar properties, in terms of potential stability and pore size distribution. On the other side, an increase in pressure promoted the reaction kinetics related to the gas formation, penalizing the liquid products yield and keeping unaltered the final biochar yield. The switch from a pure N₂ atmosphere to the mixture of CO₂/N₂ resulted to be irrelevant on the pyrolysis behavior of wheat straw pellets, except for a slight increase in the yield of CO released, confirming the findings observed in the previous research theme. Furthermore, the presence of CO₂ in the carrier gas favored the availability of oxygenated functional groups on the surface of resulting biochars, regardless of the peak temperature and absolute pressure. These findings provide further evidence that using a flue gas stream to keep an oxygen-free atmosphere within the pyrolysis reactor represents a viable and cost-effective alternative.

From an energy efficiency point of view, it is important to note that an increase in the absolute pressure from 0.2 MPa to 0.9 MPa led to higher values of heat required by the pyrolysis process. This result, which seems to be contradictory to the typical more exothermic behavior of pyrolysis with increasing pressure, could be explained by a dilution of the exothermicity of the overall process, due to the increase in the carrier gas flow rate at high pressure (to guarantee the proper gas residence time), since the higher the flow rate, the higher the heat needed to be supplied to the system. Regarding the exergy efficiency related to the process, it was observed that high levels of absolute pressure favored the exergy efficiency of the process, even at

relatively high pyrolysis peak temperature. Indeed, the thermodynamic irreversibilities of pyrolysis process were notably reduced at 550 °C and 0.9 MPa under a mixture of CO₂ and N₂ as carrier gas at relatively short residence times (i.e., 100 s).



Effects of slow-pyrolysis conditions on the products yields and properties and on exergy efficiency: A comprehensive assessment for wheat straw

Gianluca Greco^{a,*}, Christian Di Stasi^a, Filipe Rego^b, Belén González^a, Joan J. Manyà^a

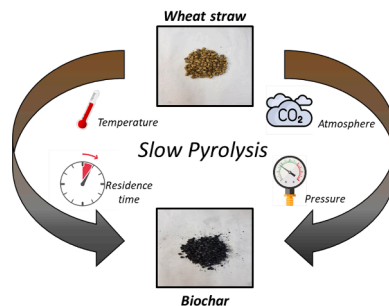
^a Aragón Institute of Engineering Research (I3A), Technological College of Huesca, University of Zaragoza, crta. Cuarte s/n, Huesca E-22071, Spain

^b Energy and Bioproducts Research Institute (EBRI), Aston University, Aston Triangle, B4-7ET Birmingham, United Kingdom

HIGHLIGHTS

- Pressure enhanced the release of gases without decreasing biochar yield.
- Gas residence time was the main factor affecting carbonization efficiency.
- Using CO₂/N₂ as carrier gas led to biochars with higher oxygen functionalities.
- Overall exergy efficiency was improved by two different sets of conditions.

GRAPHICAL ABSTRACT



ARTICLE INFO

Keywords:

Wheat straw
Slow pyrolysis
Char
Pyrolysis conditions
Energy and exergy analysis

ABSTRACT

In the present work, the effects of the peak temperature (400–550 °C), absolute pressure (0.2–0.9 MPa), gas residence time (100–200 s) and reactor atmosphere (pure N₂ or a mixture of CO₂/N₂) on the pyrolysis behavior of wheat straw pellets were investigated. A factorial design of experiments was adopted to assess the effects of the above-mentioned factors on the pyrolysis products, the exergy efficiencies related to them and to the overall process, and the heat required. The pyrolysis energy/exergy assessment is nowadays of great interest, for the scaling of the installations from lab-scale to commercial-scale. Results showed that, as expected, the peak temperature was the most influential factor on the yields and distributions of all the pyrolysis products as well as the char properties related to its potential stability and pore size distribution. However, an increased pressure enhanced the release of the gas species at the expense of the liquid products, without altering the final char yield. The char exergy efficiency was negatively affected by an increase in peak temperature, whereas its effect on the exergy efficiency of the produced gas resulted to be positive. It was also found that pressurized pyrolysis favored the exergy efficiency of the process, even at relatively high pyrolysis peak temperature. For the biomass feedstock and the range of operating conditions studied here, thermodynamic irreversibilities of the pyrolysis system were considerably lowered when the process was conducted at 550 °C, 0.9 MPa and using a mixture of CO₂ and N₂ as carrier gas at relatively short residence times.

* Corresponding author.

E-mail address: greco@unizar.es (G. Greco).

<https://doi.org/10.1016/j.apenergy.2020.115842>

Received 1 April 2020; Received in revised form 27 August 2020; Accepted 2 September 2020

Available online 14 September 2020

0306-2619/© 2020 Elsevier Ltd. All rights reserved.

Nomenclature	
$Area_{peak}$	area of the devolatilization peak (g)
DTG_{max}	peak of the time derivative ($g\ min^{-1}$)
$e_{out,i}$	exergy of the product i ($MJ\ kg^{-1}$)
h_{in}	input specific enthalpy ($MJ\ kg^{-1}$)
h_{out}	output specific enthalpy ($MJ\ kg^{-1}$)
$Q_{process}$	enthalpy required for the process that should be supplied externally ($MJ\ kg^{-1}$)
S_{BET}	Brunauer–Emmet–Teller specific surface area ($m^2\ g^{-1}$)
TC#	temperatures measured by the thermocouples placed within the reactor ($^{\circ}C$)
T_{max}	temperature peak of the devolatilization step ($^{\circ}C$)
V_{ultra}	ultra-micropore volume ($cm^3\ g^{-1}$)
x_{FC}	mass fraction of fixed-carbon in the char (daf basis)
y_{char}	mass yield of char in a dry and ash-free basis (–)
y_{FC}	fixed-carbon yield in a dry and ash-free basis (–)
y_{gas}	mass yield of produced gas in a dry and ash-free basis (–)
y_{org}	mass yield of condensable organics in a dry and ash-free basis (–)
y_{water}	mass yield of produced water in a dry and ash-free basis (–)
T	gas residence time
Ψ_{char}	exergy efficiency of the char (–)
Ψ_{gas}	exergy efficiency of the gas product (–)
$\Psi_{process}$	exergy efficiency of the overall process (–)
Σe_{in}	sum of the input exergies ($MJ\ kg^{-1}$)
Σe_{out}	sum of the output exergies ($MJ\ kg^{-1}$)
Acronyms	
AAEMs	alkali and alkaline Earth metal species
daf	dry-ash-free
FT-IR	Fourier Transform Infrared spectroscopy
GCMC	Grand Canonical Monte Carlo
GHSV	gas hourly space velocity (h^{-1})
HHV	High Heating Value ($MJ\ kg^{-1}$)
PID	proportional integral derivative
WS	wheat straw
XRF	X-Ray Fluorescence spectroscopy
μ -GC	micro gas chromatograph

1. Introduction

The term *char* refers to a carbon-rich, fine-grained, porous substance, produced from the thermal decomposition of biomass under oxygen-limited conditions and at relatively low temperatures [1]. It is otherwise known as biochar when obtained from plant biomasses and its use is addressed to soil applications. Nowadays, char can be used in a wide range of applications [2], such as solid fuel, reductant agent, soil amendment and as a precursor for activated carbons [3].

Among the wide range of thermochemical processes, slow pyrolysis is a promising route to produce char with relatively high yields, obtaining gas as a co-product for cogeneration use. As already stated by Mok and Antal [4], the pyrolysis process is very complex, since it comprises both endothermic (i.e., evaporation and tar formation) and exothermic (i.e., formation of char and gas) steps. Furthermore, the global amount of energy will depend on the operating conditions considered for the process. Hence, energy and exergy assessments are of great interest for scaling the process up to a commercial scale [5]. It is important to note that the energy analysis provides the amount of energy required for pyrolysis, while the exergy analysis gives information about the energy quality, since exergy accounts for the irreversibility of the process and the maximum work that can be obtained [6]. In other words, exergy shows a reverse relationship with energy sustainability: a decrease in energy quality loss corresponds to the incline of sustainability [7]. For this reason, its assessment could result to be of great relevance in order to evaluate and improve the efficiency related to the thermochemical routes of different biomasses [8].

Given the high number of variables affecting the pyrolysis process and the wide range of available biomass sources, a large variability in the char yield and properties should be expected. Therefore, one of the main challenges nowadays is to optimize the process conditions of pyrolysis in order to obtain the most appropriate char for a given application.

Peak temperature (also referred as highest treatment temperature) can be defined as the highest temperature reached during the pyrolysis process [9]. According to the general trend reported in literature (see, for instance, Duman *et al.* [10], Di Blasi *et al.* [11], and Demirbaş [12]), the char yield decreases when the peak temperature increases, whereas the fixed-carbon content in the final char gradually rises with an increasing temperature [13].

Another process parameter widely reported in literature, which markedly affects the final char yield, is the gas residence time. An

increase in the gas residence time (i.e., lower carrier gas flow rates) results in a prolonged contact between the solid and gas phases, leading to a further decomposition of the tarry vapors onto the solid carbonaceous matrix through secondary reactions such as condensation, re-polymerization and thermal cracking [14]. As a consequence, the char yield increases at the expense of the bio-oil yield, as reported by Heo *et al.* [15], Akhtar and Amin [16], and Guedes *et al.* [17].

The effect of the absolute pressure on the char properties results to be very interesting to study in deep. To date, relatively few studies have focused on the effect of the absolute pressure on the char yield and its properties [18]. In particular, many authors such as Antal *et al.* [19,20], Rousset *et al.* [21], Recari *et al.* [22] and Qian *et al.* [23] reported an increase in the char and gas yields at the expense of the condensable fraction when both absolute pressure and gas residence time increased. This increase in char yield can be explained by a major role of the secondary reactions [24]. Nevertheless, some recent studies reported a negligible [25] or even negative effect [26] of the absolute pressure on the char yield. Such effect could be attributed to a certain enhancement of the steam gasification rate with the pressure, which results in a certain consumption of char. The magnitude of its influence will depend on the nature of the feedstock (since a high content in alkaline metals will further promote gasification) as well as the selected operating conditions in terms of vapor residence time, reactor configuration, and partial pressure of volatiles.

Another important parameter that can affect the pyrolysis behavior of biomass is the type of carrier gas employed to maintain the oxygen-limited/free conditions [27]. The introduction of a potentially oxidative carrier gas such as CO_2 in a pyrolysis environment is promising in terms of energy recovery and ability to scale-up, since the flue gas generated by combustion of pyrolysis gas can be recycled into the pyrolysis process.

Keeping all the above-mentioned considerations in mind, the aim of the present study is to analyze the effects of peak temperature, absolute pressure, gas residence time and type of pyrolysis atmosphere (pure N_2 or a binary mixture of CO_2 and N_2 , 60:40 v/v) on the pyrolysis behavior of wheat straw pellets in a lab-scale fixed-bed reactor. A 2-level full factorial design was adopted in order to study the true effects of the parameters, even considering the interaction effects among them (if any). In addition, energy and exergy assessments of the slow pyrolysis system were carried out in order to investigate the influence of the above-mentioned operating parameters on the thermodynamic performance. The novelty of this work lies not only in our experimental

approach to simultaneously assess the effects of four operating conditions on the pyrolysis behavior and products properties, but also in the comparison of the operational efficiency (i.e., exergy balance) for several working conditions. To the best of our knowledge, only a few studies are found in literature reporting a comprehensive exergy assessment for different biomass sources at different pyrolysis temperatures [28], without considering any other process parameters (see, for instance, the excellent previous studies by Boateng *et al.* [29], Parvez *et al.* [30], and Atienza *et al.* [31]). Therefore, the present study is among the first ones to investigate the influence of the absolute pressure, which can certainly affect the pyrolysis exothermicity and, consequently, both the energy required for the pyrolysis process and its exergy efficiency.

2. Material and methods

2.1. Biomass feedstock

Wheat straw (WS) pellets (7 mm OD and approximately 12 mm long) were used as raw feedstock for the char production. The WS pellets were manufactured without using any binder. The as-received biomass was directly pyrolyzed without any preliminary milling step, in order to improve the carbonization efficiency, with a consequent augment of the fixed-carbon content in the final char [32]. The WS pellets were characterized by proximate analysis (performed in quadruplicate according to ASTM standards D3173 for moisture, D3174 for ash, and D3175 for volatile matter) as well as ultimate analysis, which was carried out in triplicate using a combustion elemental analyzer Leco CHN628 (Leco Corporation, USA). The high heating value (HHV) of the feedstock was estimated from the ultimate analysis using the Channiwala and Parikh correlation [33]. In addition, X-Ray Fluorescence (XRF) spectroscopy analysis (ADVANT^{XP} + XRF spectrometer from Thermo ARL, Switzerland) was performed in order to determine the inorganic constituents of the biomass ash.

The WS constituents were determined by leaching the biomass sample in a benzene/ethanol mixture, followed by a boiling step firstly in a NaOH solution, then in a H₂SO₄ solution. The description of the procedure is given in Appendix A.

2.2. Slow pyrolysis process

2.2.1. Design of pyrolysis experiments

An unreplicated 2-level full factorial design was adopted to evaluate the true effects of four factors: peak temperature (400–550 °C), absolute pressure (0.2–0.9 MPa), gas residence time (100–200 s) and type of pyrolysis environment (from pure N₂ to a binary mixture of 60:40 v/v of CO₂/N₂, respectively). The heating rate and the soaking time (at the peak temperature) were kept constant approximately at 5 °C min⁻¹ and 1 h, respectively. Three replicates at the center point (475 °C, 0.55 MPa, 150 s and 30:70 v/v of CO₂/N₂) were carried out to estimate both the experimental error and the overall curvature effect [34]. A special attention was paid on the analysis of the response variables related to the long-term stability of produced chars. Furthermore, the factorial design was also used to understand how the four factors could affect the evolution of the mass-loss rate along the pyrolysis process. For this purpose, the percentage of mass loss, the maximum value of the time-derivative of mass-loss (*DTG_{max}*), the area of the devolatilization peak (*Area_{peak}*) and the temperature at which *DTG_{max}* is attained (*T_{max}*) were considered as the main responses to be investigated. The structure of the regression model (using normalized values for factors in the range from -1 to 1) used during statistical analysis was the following:

$$\hat{y} = \beta_0 + \beta_1 T + \beta_2 P + \beta_3 \tau + \beta_4 CO_2 + \beta_{12} T \cdot P + \beta_{13} T \cdot \tau + \beta_{14} T \cdot CO_2 + \beta_{23} P \cdot \tau + \beta_{24} P \cdot CO_2 + \beta_{34} \tau \cdot CO_2 \quad (1)$$

where β_0 , β_i , β_{ij} are the intercept, linear, and 2-way interaction coefficients, respectively. All the statistical calculations were conducted

using Minitab software (v17). The estimated regression coefficients, the associated *p*-values (from *t*-tests) and the adjusted coefficients of determination (R_{adj}^2) were taken as indicators of the goodness of regression models.

2.2.2. Pyrolysis setup

Slow pyrolysis experiments were carried out in a bench-scale fixed-bed reactor, which was already described in a previous work [35]. A detailed outline of the pyrolysis plant is displayed in Fig. 1. Blank tests (i.e., empty reactor) were carried out in order to correct the thermal expansion effects (i.e., buoyancy effect). They were performed at the same ranges of peak temperature (400–550 °C) and absolute pressure (0.2–0.9 MPa) and using the same heating program than those conducted with biomass.

The temperature profiles inside the bed were measured by four thermocouples placed in two thermowells, located at the axis and at a radial distance of 35 mm from the axis, respectively. The thermocouples were placed two by two in the thermowells, at different heights from the bottom of the sample basket: 10 mm (TC₀ and TC₁) and 70 mm (TC₂ and TC₃). The proper residence time of the gas phase within the reactor (100–200 s at selected pyrolysis peak temperature and pressure values) as well as the pyrolysis environment (pure N₂ or a mixture CO₂/N₂) were guaranteed by adjusting the mass flow rates at STP conditions for both N₂ and CO₂. The real flow rate of the carrier gas within the reactor varied approximately between 1.60 and 3.30 L min⁻¹, which corresponded to gas-hourly space velocity (GHSV) values ranged from 18 to 36 h⁻¹ (assuming a void-volume fraction of 0.9 for the entire reactor).

After each experiment, the char produced was collected and weighted. The glass traps and their flexible connections were weighted before and after each run to estimate the total mass of liquid (organics + water). The pyrolysis liquid was recovered directly from the condensers without undergoing any washing step with solvents. The water content was evaluated by Karl Fischer titration, while the organic fraction was determined by difference from the total mass of liquid. The composition of the main components of the pyrolysis gas (i.e., CO₂, CO, CH₄ and H₂) was evaluated using a micro gas chromatograph (μ -GC, Agilent 490) equipped with two analytical columns: a PolarPlot U (He as carrier gas) and a Molsieve 5A (Ar as carrier gas).

2.2.3. Characterization of the pyrolysis products

The mass yield of char (y_{char}), produced gas (y_{gas}), organic condensable compounds (y_{org}) and produced water (y_{wat}) were calculated in a dry and ash-free (daf) basis. The produced char samples were characterized by proximate analysis and, additionally, ultimate analyses were performed on both chars and liquid products using the same procedures described for the biomass feedstock. The fixed-carbon yield (y_{FC}), firstly introduced by Antal and Gronli [9], was adopted to evaluate the carbonization efficiency. It was defined as following:

$$y_{FC} = x_{FC} \cdot y_{char} \quad (2)$$

where x_{FC} is the fixed-carbon content in mass fraction (daf basis). The fixed-carbon yield corresponds to the fraction of organic matter initially present in the biomass feedstock, which was converted into fixed carbon.

The BET specific surface areas (S_{BET}) of the chars were determined from the CO₂ adsorption isotherms at 0 °C, since chars typically present a highly ultra-microporous structure. The adsorption isotherms were obtained using an ASAP 2020 gas sorption analyzer (Micromeritics, USA). The samples (approximately 120 mg) were firstly degassed under dynamic conditions at 150 °C until constant weight was reached. Ultra-micropore volume (V_{ultra} , i.e. pore size lower than 0.7 nm) of the samples was calculated adopting a Grand Canonical Monte Carlo method (GCMC) for carbon slit-shaped pores. All the calculations related to the adsorption isotherms were carried out using the MicroActive software (Micromeritics). In addition, Fourier transform infrared analyses (FT-IR)

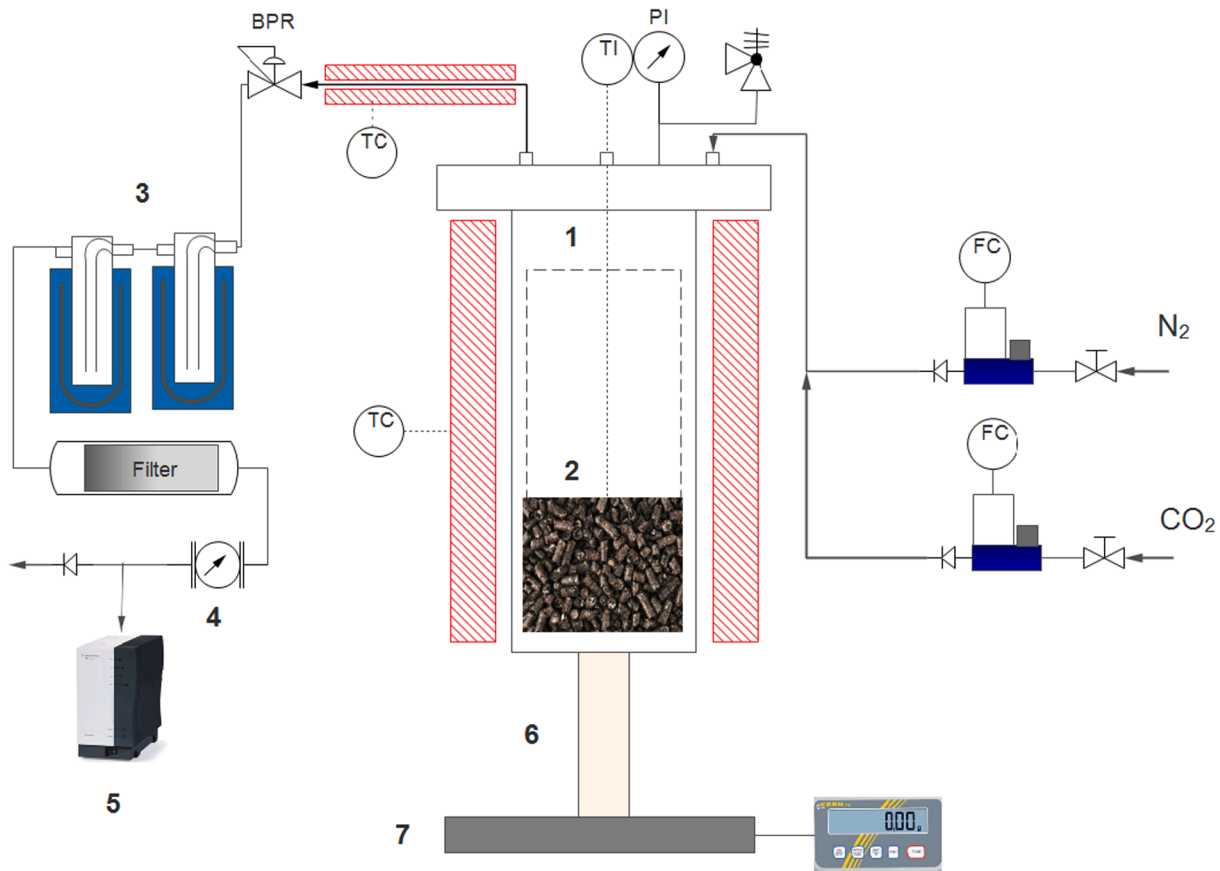


Fig. 1. Schematic layout of the pyrolysis plant: (1) pyrolysis reactor, (2) biomass bed, (3) condensation system, (4) volumetric gas meter, (5) micro-GC, (6) ceramic tube, (7) weighing platform.

were performed using a Perkin Elmer FT-IR Spectrometer with PIKE Technologies GladiATR and Spectrum software in order to determine the functional groups on the surface of the produced chars. The FT-IR analyses were performed at least in triplicate under a range of wave-number of 400 to 4000 cm^{-1} with a resolution of 4 cm^{-1} , doing 16 scans for each point in order to accomplish a reliable level of accuracy.

2.2.4. Energy and exergy assessment

The enthalpy required for the process that should be supplied externally ($Q_{process}$) and the exergy efficiencies related to the char (Ψ_{char}), produced gas (Ψ_{gas}) as well as the global exergy efficiency of the process ($\Psi_{process}$) were partly calculated using the process simulation software Aspen Plus v10 (Aspentech, USA). The pyrolysis reactor was simulated as a yield reactor block, in which the WS pellets (nonconventional component) were converted into char, CO_2 , CO , CH_4 , H_2 , water, and condensable tars. The mass flow rate of each stream was defined on the basis of the experimental data generated in the pyrolysis device. A layout of the control volume considered for simulations is illustrated in Fig. 2, where T_0 , T_p and P are the reference temperature ($25\text{ }^\circ\text{C}$), pyrolysis peak temperature (which was also considered as the process temperature) and process absolute pressure, respectively.

The methodology followed to calculate the energy and exergy balances was based on that reported by Atienza *et al.* [31]. Briefly, $Q_{process}$ was calculated according to Eq. (3), where h_{in} and h_{out} are the specific input and output enthalpies (in MJ kg^{-1}), respectively.

$$Q_{process} = h_{out} - h_{in} \quad (3)$$

On the other hand, the exergy efficiencies were calculated as following:

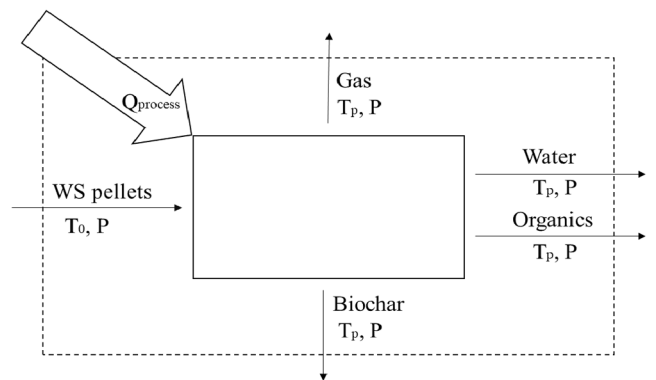


Fig. 2. A schematic layout of the control volume considered for energy and exergy assessment.

$$\psi_i = 100 \frac{e_{out,i}}{\sum e_{in}} \quad (4)$$

where $e_{out,i}$ is the exergy of the product (char or gas), and $\sum e_{in}$ is the sum of the input exergies (both physical and chemical). The exergy associated to the heat required for the process was also taken into account in Eq. (4). Calculations were conducted assuming the following considerations: (i) the standard reference was $T_0 = 25\text{ }^\circ\text{C}$ and $P_0 = 0.1\text{ MPa}$, (ii) chemical exergies for all the involved species were obtained from the literature [36], (iii) process heat losses as well as kinetic and potential exergies of the streams were considered to be negligible [37], (iv) the energy and exergy contents inherent to the carrier gas streams were

considered in the respective balances, and (v) the exergies of condensable tar streams were not calculated (due to the impossibility to know their real chemical composition) and thus they were taken as exergy losses.

3. Results and discussion

The full characterization of the wheat straw pellets (in terms of biomass constituents as well as proximate, ultimate and XRF analyses) is

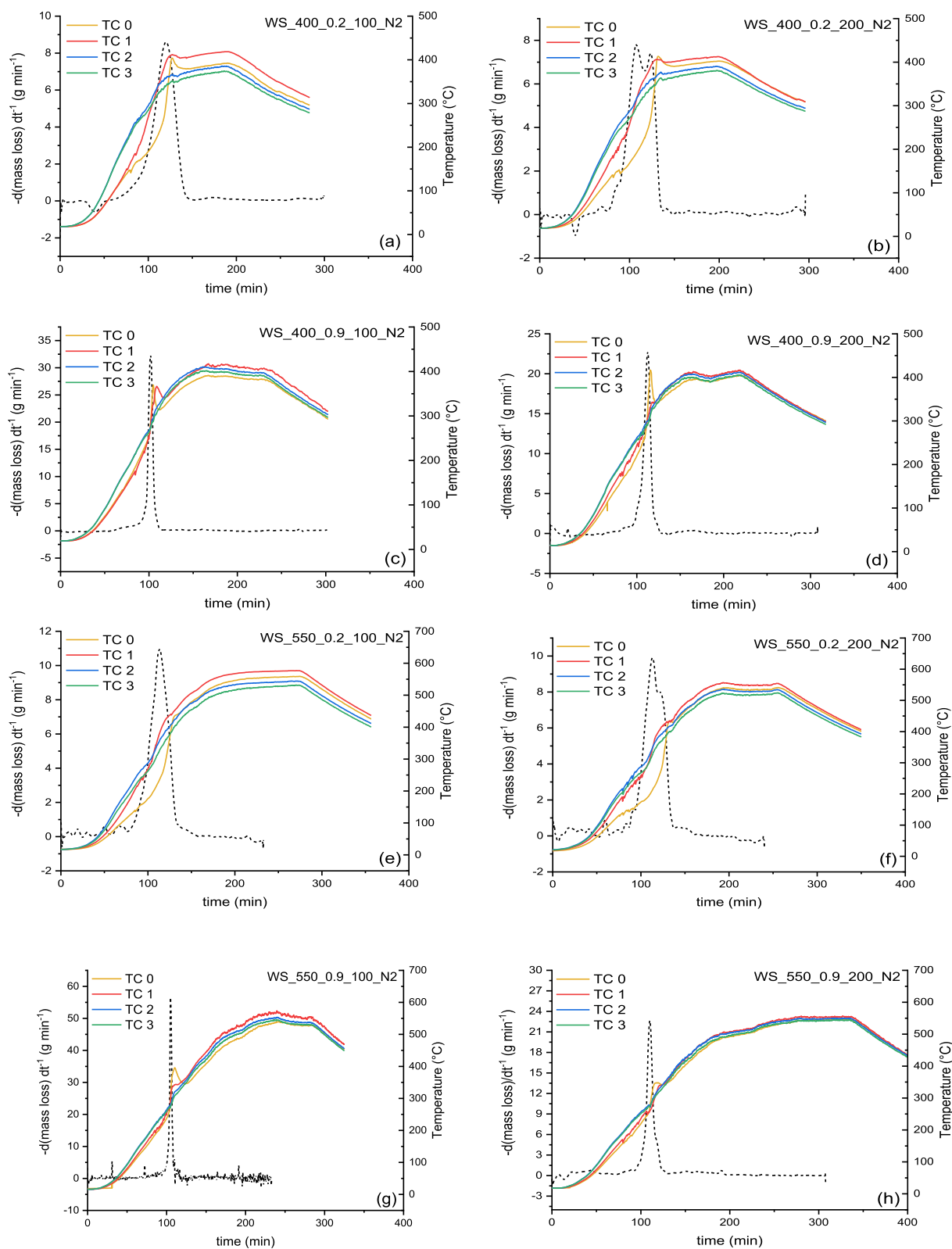


Fig. 3. Time derivative of the mass loss and evolution of the temperatures within the bed in axial (TC₀ and TC₃) and radial (TC₁ and TC₂) positions for the experiments conducted under N₂ at (a) 400 °C, 0.2 MPa and 100 s; (b) 400 °C, 0.2 MPa and 200 s; (c) 400 °C, 0.9 MPa and 100 s; (d) 400 °C, 0.9 MPa and 200 s; (e) 550 °C, 0.2 MPa and 100 s; (f) 550 °C, 0.2 MPa and 200 s; (g) 550 °C, 0.9 MPa and 100 s; and (h) 550 °C, 0.9 MPa and 200 s.

reported in Table A.1 (Appendix A). The mass-balance closures of all the pyrolysis tests were comprised between 85% and 99%. These marginal losses were attributed to errors in collecting the produced gases, especially due to the higher flow rates when the pressure increased. Therefore, the mass yields of the pyrolysis products were calculated attributing the error in the mass-balance closure to minor accuracies in determining the mass of produced gas. The repeatability of the mass-loss profiles was assessed by performing three replicates at the central point of the experimental design, which indicated a reasonable level of repeatability. Therefore, a blank test of the central point was carried out, and then subtracted to the raw mass-loss curves. Results from the analysis of repeatability are also given in Appendix A (Fig. A.1).

3.1. Pyrolysis behavior

Fig. 3 simultaneously shows the time derivative of the mass-loss and the temperature profiles, along the biomass bed at the axis (TC_0 and TC_3) and at a radial position of 35 mm (TC_1 and TC_2), for all the experiments conducted (at 400 and 550 °C, 0.2 and 0.9 MPa, and 100 and 200 s) under a pure N_2 atmosphere. As it can be seen from Fig. 3, the peak of the time derivative of the mass loss (dashed black line) was always recorded during the devolatilization step, which typically occurred between 200 and 400 °C. In this range of temperatures, exothermic peaks were visible in the temperature profiles, which are related to the heat of reaction released by the secondary reactions. According to a previous work [35], after increasing the pressure from 0.2 to 0.9 MPa, the devolatilization occurred in a narrower period of time. In other words, the devolatilization rate was higher. This was due to the effect of the absolute pressure, which greatly enhanced the kinetics of the reactions involved in the devolatilization. Also, the temperature profiles were affected by the increase in pressure, becoming more homogeneous and reducing the gradient between them, probably due to an enhanced convective heat transfer, as a consequence of a higher N_2 flow rate to ensure the proper vapor residence time. Furthermore, the secondary charring reactions were also promoted by an increased pressure, as proved by the more pronounced exothermic peaks measured at 0.9 MPa. The observed slight decrease in temperature (of about 30 °C) after attaining the exothermic peak at higher pressures was probably due to a transient response of the PID controller (i.e., a lower power was supplied to the furnace during a relatively short period).

Interestingly, a change in the gas residence time resulted in a different shape of the devolatilization peak. As shown in Fig. 3b and f, after increasing the gas residence time at lower pressure (0.2 MPa), a double peak appeared. This could be due to the longer contact time between the produced tarry vapors and the forming char, leading to simultaneous production of secondary char and permanent gases. However, when the gas residence time at higher pressures increased (Fig. 3d and h), the double peak disappeared, similarly to what seen at low residence times (Fig. 3a, b, e and g). However, these peaks resulted to be lower than the corresponding peaks recorded at the same conditions of peak temperature, absolute pressure and pyrolysis atmosphere but at higher residence times. This could be explained by a combined effect of pressure and gas residence time. On the one hand, the pressure could promote devolatilization, as mentioned above, enhancing the gas production; on the other hand, an increase in pressure together with an increase in the gas residence time, can also promote the secondary charring reactions, counterbalancing the release of volatiles during the devolatilization step.

The switch from a pure N_2 atmosphere to a mixture of 60 vol% of CO_2 and 40 vol% of N_2 in the pyrolysis environment resulted to be irrelevant on both the evolution of the mass-loss and the temperature profiles in the entire campaign of experiments. For this reason, the plots related to the mass loss along the experiments carried out under the mixture N_2/CO_2 are not shown.

The influence of the operating conditions on the evolution of the mass-loss rate of wheat straw pellets was also investigated using the full

factorial design described in Section 2.2.1. Fig. 4 displays the normal plot of the standardized effects of the operating conditions on the mass loss, T_{max} , DTG_{max} and $Area_{peak}$. As expected, the mass loss (see Fig. 4a) was favored by temperature, which promoted the thermal degradation of biomass. Furthermore, also pressure contributed to intensify the final mass loss, likely as a consequence of the relatively higher carrier flow rate, which swept the volatile species away from the reactor (thus suppressing the formation of secondary char), and, to a lesser extent, some steam gasification of char (which was promoted by the increased pressure). On the other side, an increase in the gas residence time reduced the mass loss, enhancing the secondary charring reactions, as explained above. The roles of the absolute pressure and gas residence time during the devolatilization process were confirmed from the results concerning DTG_{max} (see Fig. 4b), which resulted to be markedly enhanced by pressure and reduced when the gas residence time increased. In addition, the negative influence of the absolute pressure on $Area_{peak}$ (Fig. 4c) was completely in agreement with the observations described before (i.e., an increase in pressure results in a narrower peak). T_{max} (Fig. 4d) appeared to be positively affected by the peak temperature of the process. This could be attributed to the more severe heating when the peak temperature was higher. Furthermore, an interaction of effects between the peak temperature and the absolute pressure was responsible for a decrease in T_{max} , probably due to some convective effect related to the higher flow rate of carrier gas used at high pressure. More details about the statistics and the numerical results of this section are given in Tables A.2 and A.6.

3.2. Pyrolysis products distribution

The distributions of the pyrolysis products obtained along the experiments is listed in Table 1. In the next subsections, results concerning the yield of char, condensable organic compound and permanent gases are discussed. The statistical results related to this section are given in Table A.3.

3.2.1. Char yield

The normal plot of the standardized effects of the operating conditions on the resulting char yield is reported in Fig. 5. According to the results illustrated for the mass loss in Section 3.1, an increase in the peak temperature led to a decrease in the final char yield, whereas an increase in the gas residence time significantly improved it.

The effect of peak temperature was qualitatively in agreement with a large number of studies available in literature [11,38], which reported a higher thermal degradation of cellulose and hemicelluloses in the range of 250–450 °C [39], depending on the type of feedstock. Moreover, the effect of the gas residence time agreed with the results obtained for the mass loss. As mentioned above, an increase in the gas residence time resulted in a prolonged contact between the gas and solid phases, allowing the tarry vapors to repolymerize with a major extent instead of leaving the reaction zone as they were produced. As a consequence, the resulting char yield was higher. In addition, the char yield did not seem to be affected by the absolute pressure, according to Melligan *et al.* [25] and to one of our previous works [35]. However, this result is also in contrast with many earlier works; for instance, Manyà *et al.* [26,40] reported in both studies a negative effect of the absolute pressure on char yield, whereas Noumi *et al.* [41] observed a decrease in char yield when pressure increased. The reasons for this discrepancy could be various, such as the range chosen for the gas residence time, which may result too short to appreciate the pure effect of the pressure on the char yield. Another possible explanation could be that the effect of pressure, responsible of the formation of the secondary char, is counterbalanced by another effect of itself, which promotes a low (but certain) extent of the steam gasification. In other words, the additional char produced through secondary charring reactions could be compensated by a certain consumption of carbon via steam gasification. This theory is strengthened by the presence of alkali and alkaline earth metal species (AAEMs)

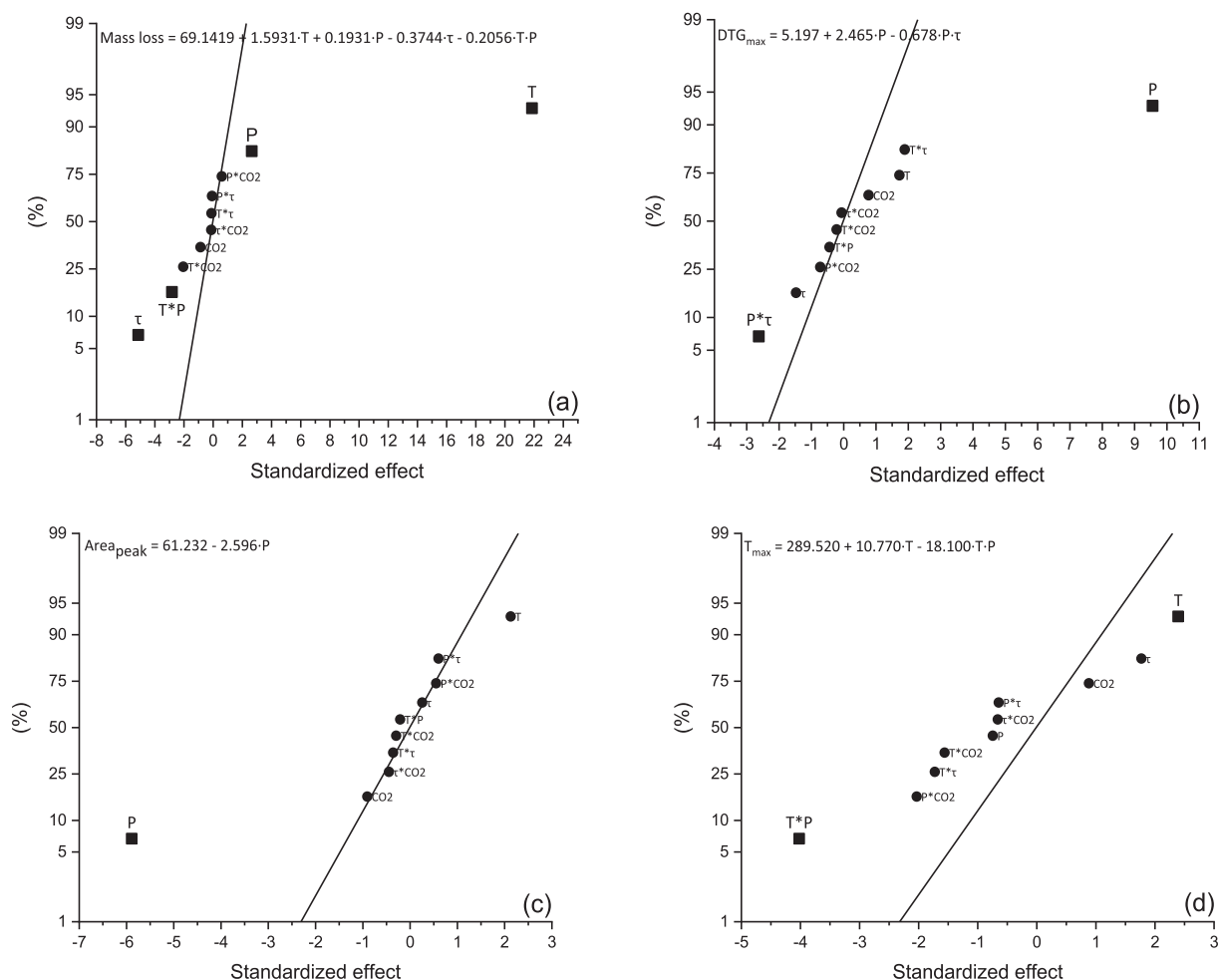


Fig. 4. Normal plots of standardized effects ($\alpha = 0.05$) for (a) the mass loss (%), (b) DTG_{\max} , (c) $Area_{\text{peak}}$, and (d) T_{\max} (square, significant effect; circle, non-significant effect). Regression models are given above each plot.

Table 1

Experimental distributions obtained respectively for y_{char} , y_{org} , y_{wat} , y_{gas} , y_{CO_2} , y_{CO} , y_{CH_4} and y_{H_2} .

Parameter				Response variable							
T (°C)	P (MPa)	τ (s)	CO ₂ (%v)	y_{char} (-)	y_{org} (-)	y_{wat} (-)	y_{gas} (-)	$y_{\text{CO}_2}^1$	y_{CO}^1	$y_{\text{CH}_4}^1$	$y_{\text{H}_2}^1$
550	0.2	100	0	0.276	0.084	0.307	0.334	5.365	2.917	0.215	1.333
475	0.55	150	30	0.294	0.125	0.291	0.360	5.310	3.606	0.975	0.387
550	0.9	100	0	0.276	0.105	0.207	0.413	7.099	1.877	1.939	1.546
400	0.9	100	0	0.317	0.098	0.163	0.421	7.174	3.115	0.520	0.092
400	0.2	100	0	0.311	0.133	0.240	0.316	5.037	2.896	0.457	0.057
475	0.55	150	30	0.290	0.102	0.227	0.380	3.970	3.478	0.934	0.377
550	0.2	200	60	0.288	0.111	0.290	0.311	3.881	3.694	1.431	0.942
400	0.2	100	60	0.293	0.146	0.311	0.251	3.949	2.374	0.345	0.043
400	0.9	200	0	0.324	0.094	0.199	0.383	6.543	2.637	0.636	0.105
550	0.2	100	60	0.280	0.123	0.283	0.314	2.872	5.180	1.732	1.326
550	0.2	200	0	0.285	0.112	0.268	0.335	5.176	2.690	1.371	1.133
550	0.9	100	60	0.279	0.093	0.202	0.425	7.324	3.168	0.419	0.447
400	0.9	200	60	0.317	0.096	0.190	0.397	7.562	1.787	0.515	0.070
400	0.2	200	60	0.332	0.137	0.275	0.257	3.763	2.790	0.428	0.049
475	0.55	150	30	0.297	0.101	0.238	0.364	5.427	3.391	1.026	0.421
550	0.9	200	60	0.288	0.109	0.251	0.352	5.763	2.677	0.988	0.395
400	0.2	200	0	0.327	0.122	0.265	0.286	4.699	2.363	0.410	0.043
400	0.9	100	60	0.309	0.084	0.167	0.440	7.678	2.724	0.979	0.108
550	0.9	200	0	0.284	0.085	0.216	0.414	6.832	2.465	1.770	1.574

¹ The gas yields are given in mmol g⁻¹ of daf biomass.

contained in the wheat straw pellets, which enhance the kinetics of the reaction under higher pressures [42]. The experimental char yields, which are reported in Table 1, varied from 0.276 to 0.332. As

expected, the lowest values were obtained from pyrolysis at 550 °C and a gas residence time of 100 s.

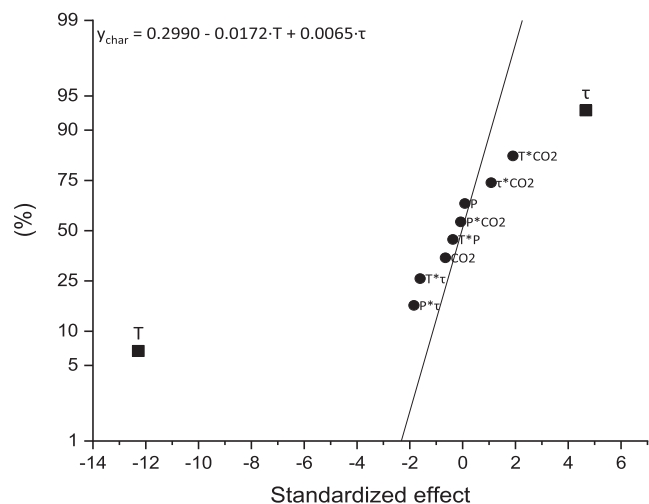


Fig. 5. Normal plot of the standardized effects ($\alpha = 0.05$) for y_{char} (square, significant effect; circle, non-significant effect). Regression models are given above each plot.

3.2.2. Organic condensable compounds and produced water yields

Fig. 6a shows the normal plot of the standardized effects of the selected parameters on the yield of organic condensable compounds. As expected, the absolute pressure had a remarkable, negative effect on it, since typically an increase in pressure favors the gas yield at the expense of the condensable products. In addition, the pressure promotes the formation of secondary char, leading to a higher consumption of volatiles and a further release of permanent gases (Fig. 6a). According to this, y_{org} decreased up to 0.084 (see Table 1) when pressure was high. The enhanced production of gases with high pressures also affected negatively the water yield (Fig. 6b), as already reported by Ates *et al.* [43], probably due to an enhancement of reaction kinetics such as that of the water gas shift (also thermodynamically favored at lower temperatures), which led to a higher consumption of water.

3.2.3. Non-condensable gases yield and their distributions

As visible in Fig. 7, the total gas yield was greatly affected by the absolute pressure, which boosted the release of gaseous species up to 0.440 (see Table 1). The yields of the main gas components (CO_2 , CO, CH_4 and H_2) have been analyzed and the normal plots of the standardized effects of the operating conditions on them are displayed in Fig. 8, whereas their yields are listed in Table 1. The yield of CO_2 (Fig. 8a)

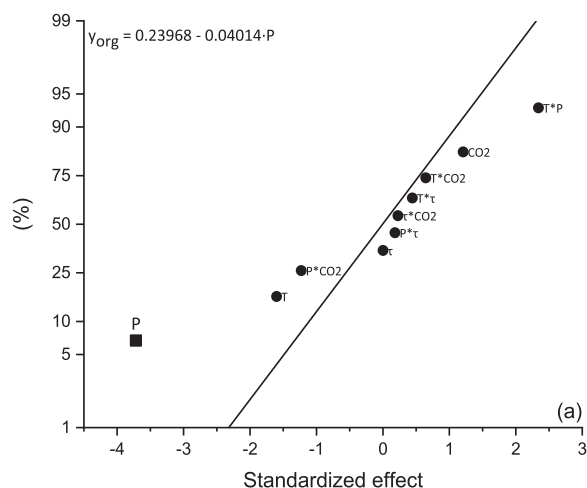


Fig. 6. Normal plots of the standardized effects ($\alpha = 0.05$) for (a) y_{org} and (b) y_{water} (square, significant effect; circle, non-significant effect). Regression models are given above each plot.

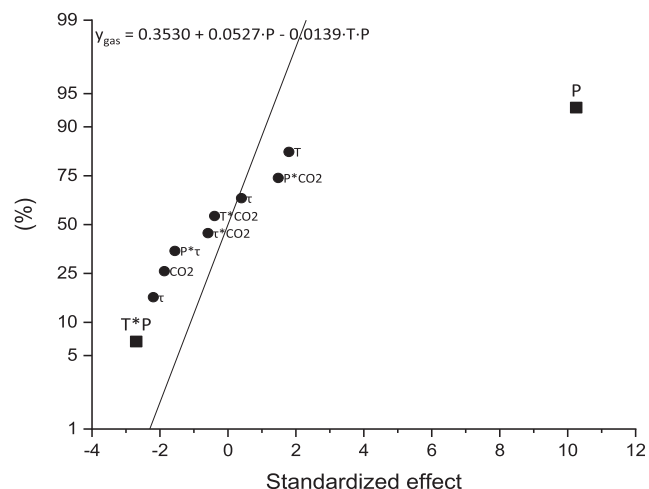


Fig. 7. Normal plots of the standardized effects ($\alpha = 0.05$) for y_{gas} (square, significant effect; circle, non-significant effect). Regression models are given above each plot.

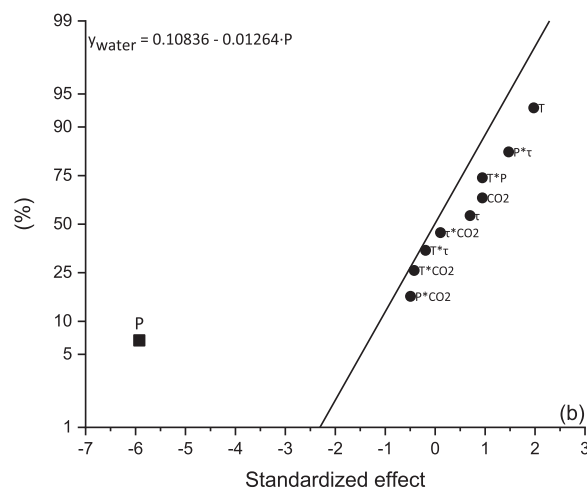
markedly increased with pressure, primarily due to the promoted decarboxylation of hemicelluloses and cellulose [23]. An increase in pressure also resulted in a lower yield of CO (Fig. 8b), likely due to the promotion of the water gas shift reaction kinetics. This was completely in agreement with the considerations related to the water content described above. An additional consumption of CO could be due to a certain extent of the Boudouard reaction at high pressure. In addition, and as deduced from Fig. 8b, the Boudouard equilibrium could be shifted towards the CO production when the peak temperature and CO_2 concentration in the pyrolysis atmosphere increased, thus leading to a higher y_{CO} . Regarding the CH_4 and H_2 releases (Fig. 8c and d), their yields notably increased with the peak temperature, as a consequence of a major extent of the methanation and dehydrogenation reactions at temperatures above 500 °C.

3.3. Char properties

The char properties related to its potential stability and textural properties are shown in Table 2. All the regression coefficients of the models related to this section are shown in Table A.4.

3.3.1. Potential stability and aromatic fraction

The fixed carbon content and the atomic H:C and O:C ratios were



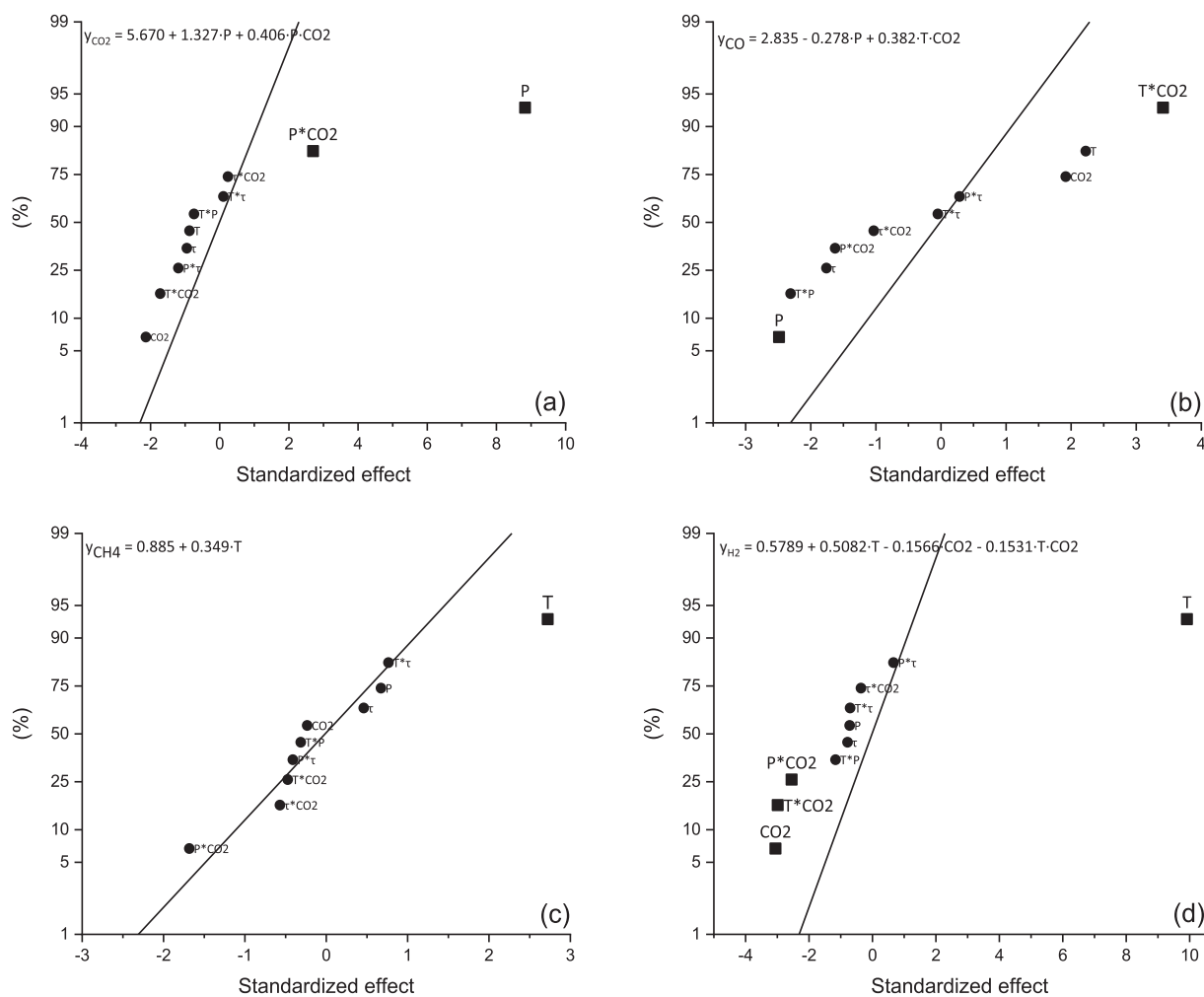


Fig. 8. Normal plots of standardized effects ($\alpha = 0.05$) for (a) y_{CO_2} , (b) y_{CO} , (c) y_{CH_4} and (d) y_{H_2} (square, significant effect; circle, non-significant effect). Regression models are given above each plot.

Table 2

Experimental results of H:C and O:C atomic ratios, x_{FC} , y_{FC} , S_{BET} and V_{ultra} related to the produced chars.

Parameter				Response variable					
T (°C)	P (MPa)	τ (s)	CO ₂ (%v)	H:C (–)	O:C (–)	x_{FC} (%)	y_{FC} (–)	S_{BET} (m ² g ⁻¹)	V_{ultra} (cm ³ g ⁻¹)
550	0.2	100	0	0.3683	0.0811	83.8538	0.230	229	0.085
475	0.55	150	30	0.4637	0.1066	81.9321	0.239	203	0.050
550	0.9	100	0	0.3527	0.0684	86.5415	0.238	214	0.080
400	0.9	100	0	0.6169	0.1125	72.5910	0.236	154	0.049
400	0.2	100	0	0.6720	0.1526	71.8470	0.220	157	0.052
475	0.55	150	30	0.4627	0.0931	80.4669	0.232	194	0.071
550	0.2	200	60	0.3650	0.0728	86.3462	0.248	217	0.081
400	0.2	100	60	0.6300	0.1357	72.9954	0.214	157	0.052
400	0.9	200	0	0.6081	0.1141	75.3153	0.243	160	0.052
550	0.2	100	60	0.3374	0.0734	86.1236	0.240	222	0.086
550	0.2	200	0	0.3662	0.0699	86.1469	0.244	216	0.082
550	0.9	100	60	0.3294	0.0679	85.5851	0.236	219	0.083
400	0.9	200	60	0.5696	0.1013	76.2568	0.242	158	0.050
400	0.2	200	60	0.6498	0.1299	72.4933	0.240	152	0.049
475	0.55	150	30	0.4739	0.0993	81.6941	0.242	187	0.067
550	0.9	200	60	0.3312	0.0633	85.8450	0.244	224	0.086
400	0.2	200	0	0.6350	0.1219	74.1738	0.242	152	0.049
400	0.9	100	60	0.5462	0.0992	76.8011	0.237	159	0.052
550	0.9	200	0	0.3422	0.0669	86.4768	0.245	213	0.082

considered as rough indicators of the potential stability (i.e., carbon sequestration potential) of the produced chars. In light of the results displayed in Fig. 9, it can be deduced that the potential stability was

markedly improved by both the peak temperature and, to a lesser extent, absolute pressure. In fact, the increase in peak temperature led to higher fixed carbon contents (up to 86.6%), due to the higher aromatization of

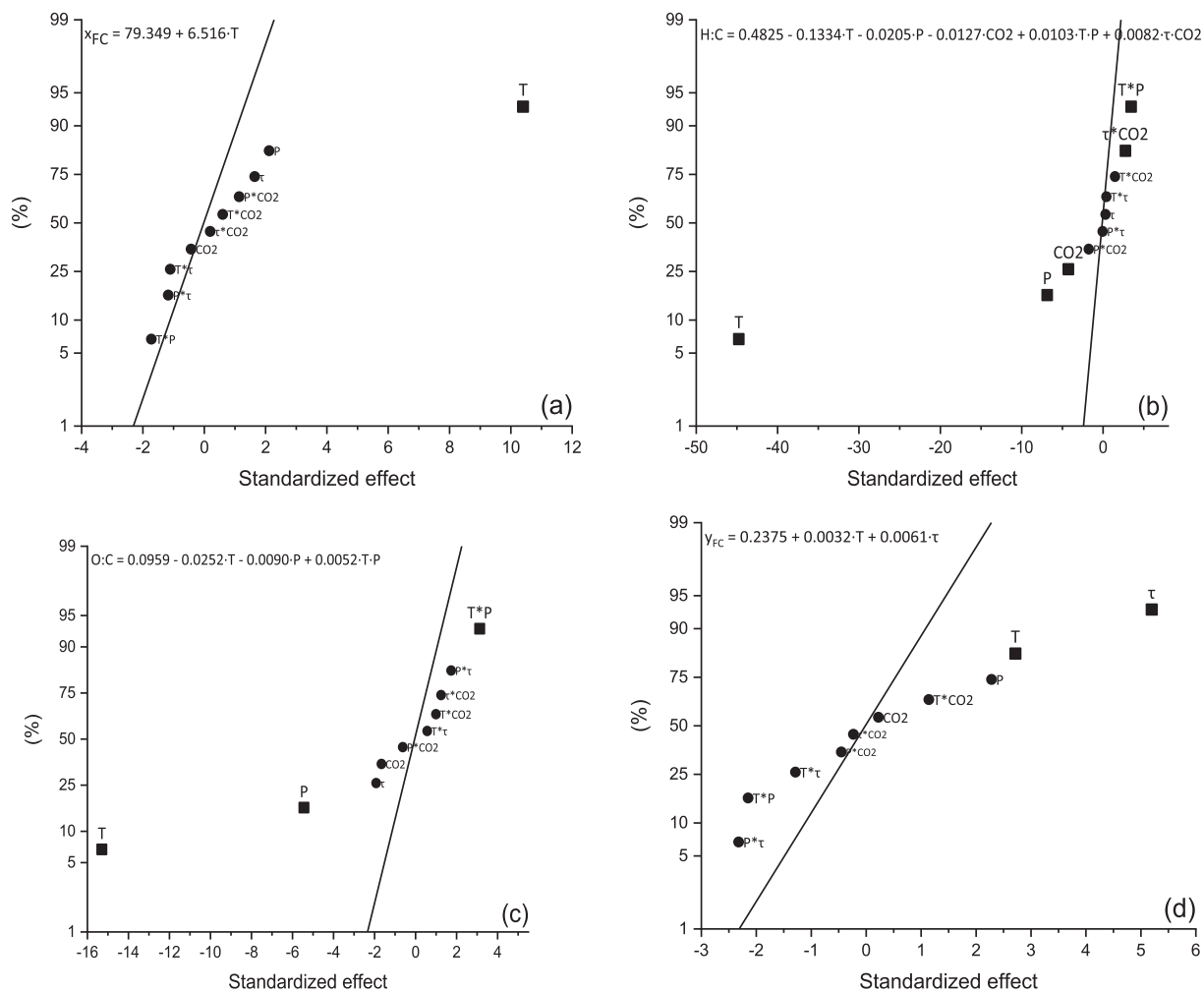


Fig. 9. Normal plots of standardized effects ($\alpha = 0.05$) for (a) x_{FC} , (b) atomic H:C ratio, (c) atomic O:C ratio and (d) y_{FC} (square, significant effect; circle, non-significant effect). Regression models are given above each plot.

the char structure, making it more stable. This is also confirmed by the reduction of both H and O contents in the char, as it could be deduced from Fig. 9b and c for the atomic H:C and O:C ratios, respectively. The positive effect of the absolute pressure on the char stability was a direct consequence of its role played in the production of secondary char (as

mentioned in Section 3.2.1), which is less reactive and more stable than the primary one.

From Fig. 9d, it can be seen that the fixed-carbon yield was positively affected by both the peak temperature and gas residence time. In particular, the effect of the latter resulted to be more significant, since

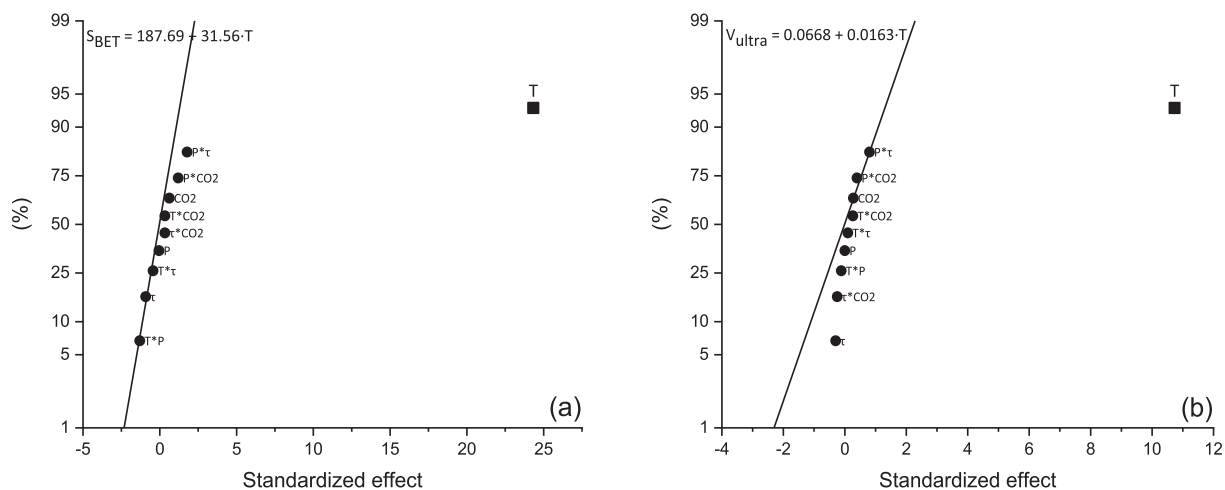


Fig. 10. Normal plots of standardized effects ($\alpha = 0.05$) for (a) S_{BET} and (b) V_{ultra} (square, significant effects; circle, non-significant effects). Regression models are given above each plot.

the effect of the peak temperature was the product of its positive contribution to the x_{FC} and its negative one to the y_{char} . In light of these results, it was possible to deduce that the highest value of y_{FC} was achieved for the experiments carried out at 550 °C and 200 s, with a value comprised between 0.24 and 0.25 (see Table 2).

3.3.2. Textural properties

Fig. 10 shows the normal plots of the standardized effects of the operating conditions on the BET surface area (S_{BET}) and the ultramicropore volume (V_{ultra}). It appeared that the peak temperature was the only factor to significantly affect both the surface area and the ultramicropore volume. This was probably due to a more extended thermal degradation of biomass at higher temperatures leading to a further release of the volatile species, thus leading to the formation of new pores. The ranges of values of S_{BET} and V_{ultra} were 152–229 m² g⁻¹ and 0.049–0.085 cm³ g⁻¹, respectively. Interestingly, the absolute pressure had no significant effect on the porosity development in the range of 0.2–0.9 MPa, in contrast with previous works [25,44], which reported a slight or even dramatic decrease in the BET surface area. This result was attributed to a clogging of the pores by tar deposits as a consequence of the high pressure. In this sense, the observed no significant effect of the absolute pressure on the textural properties analyzed here makes mild pressurized pyrolysis particularly attractive to produce wheat straw-derived chars with enhanced properties in terms of potential stability without affecting their porosity development.

3.3.3. FT-IR spectra and surface chemistry

Results from FT-IR spectra firstly showed that the gas residence time seemed to have no effect on the char surface chemistry. Hence, only the set of spectra for chars obtained at 200 s is shown in Fig. A.2. The switch from a pure N₂ atmosphere to the mixture CO₂/N₂ at 400 °C resulted into a slight increase in the bands at 1250, 1550 and 1750 cm⁻¹, which correspond to oxygen-containing groups, such as lactones, carboxyl groups, aldehydes and ketones. A substantial decrease in all the bands was observed when the temperature increased from 400 °C to 550 °C, as a consequence of a decrease in the volatile content and, thus, in the surface functionalities of the produced chars. The presence of CO₂ in the atmosphere at 550 °C, regardless of the pressure applied, led to higher bands visible in the spectra than those observed under a N₂ atmosphere, especially around 1250 cm⁻¹ (C—O vibrations), probably due to a certain surface oxidation.

3.4. Energy and exergy analysis

Fig. 11 shows the normal plot of the standardized effects of the selected operating factors on $Q_{process}$ and the exergy efficiencies, whereas the energy and exergy balances obtained along the whole set of experiments are summarized in Table 3. The statistics outcomes related to this section are reported in Table A.5.

First, it is important to note that the most part of the $Q_{process}$ values resulted to be slightly negative, in contrast with the values typically low but positive reported in literature for pyrolysis at atmospheric pressure

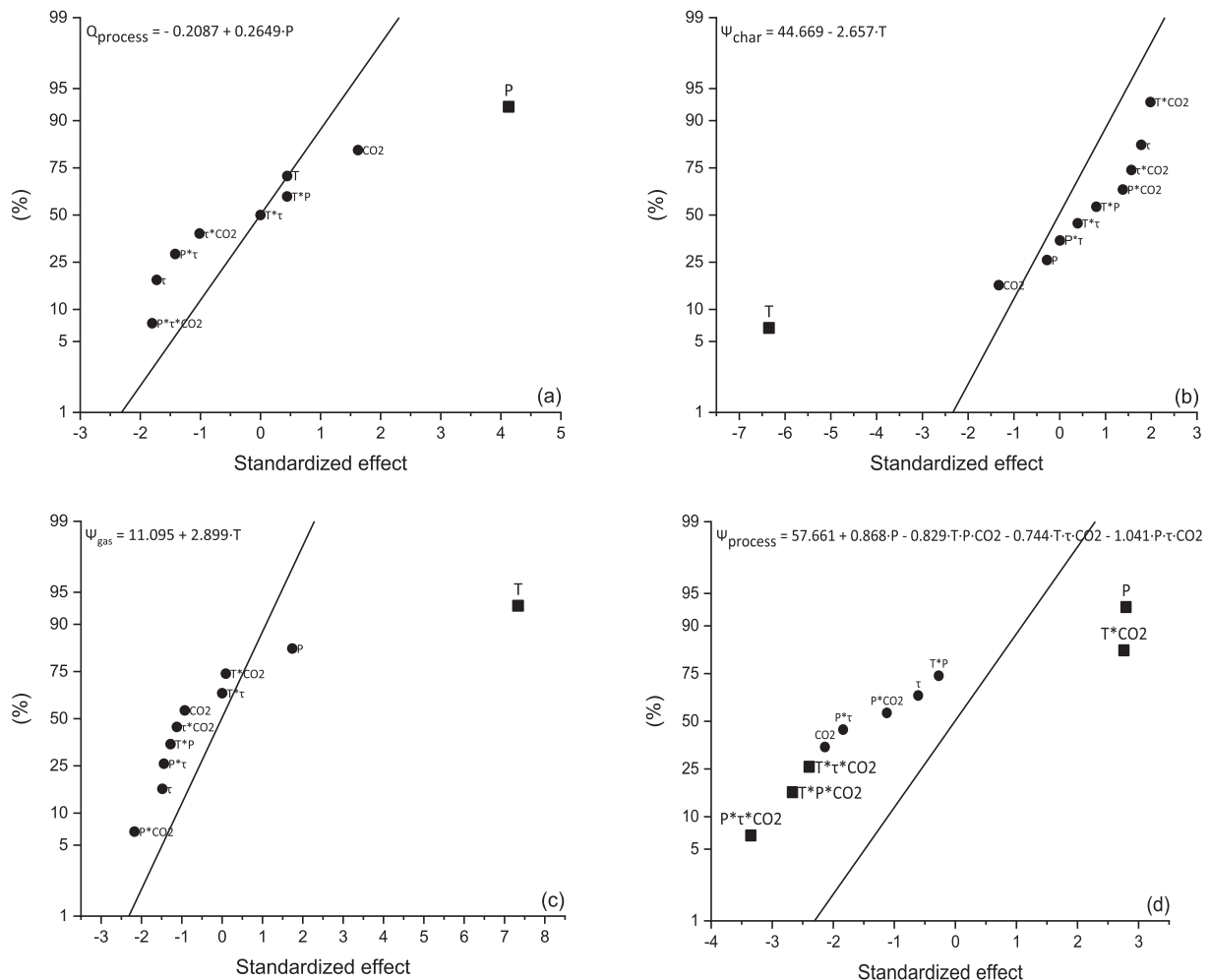


Fig. 11. Normal plots of standardized effects ($\alpha = 0.05$) for (a) $Q_{process}$; (b) Ψ_{char} ; (c) Ψ_{gas} ; and (d) $\Psi_{process}$ (square, significant effects; circle, non-significant effects). Regression models are given above each plot.

Table 3

Experimental results obtained for $Q_{process}$, Ψ_{char} , Ψ_{gas} and $\Psi_{process}$.

Parameter				Response variables			
T (°C)	P (MPa)	τ (s)	CO ₂ (%v)	$Q_{process}$ (MJ kg ⁻¹)	Ψ_{char} (%)	Ψ_{gas} (%)	$\Psi_{process}$ (%)
550	0.2	100	0	-0.50	40.94	12.27	54.94
475	0.55	150	30	-0.65	42.87	10.67	55.52
550	0.9	100	0	-0.18	40.90	16.19	58.99
400	0.9	100	0	0.01	46.70	10.32	59.55
400	0.2	100	0	-0.39	52.01	7.63	60.62
475	0.55	150	30	0.18	42.98	11.96	56.69
550	0.2	200	60	-0.48	42.93	14.55	58.91
400	0.2	100	60	-0.54	42.56	6.10	51.97
400	0.9	200	0	-0.21	48.06	9.42	59.24
550	0.2	100	60	-0.38	40.66	15.70	58.11
550	0.2	200	0	-0.53	42.65	12.74	56.59
550	0.9	100	60	0.79	41.92	14.16	59.53
400	0.9	200	60	-0.22	47.03	6.74	55.54
400	0.2	200	60	-0.32	48.45	7.26	56.92
475	0.55	150	30	-0.34	43.90	12.88	58.51
550	0.9	200	60	-0.10	43.63	10.26	55.92
400	0.2	200	0	-0.65	48.08	7.02	56.28
400	0.9	100	60	0.42	45.71	11.08	59.09
550	0.9	200	0	-0.05	42.47	16.10	60.38

[45]. This could be attributed to the reactor pyrolysis configuration (in which the carrier gas is not forced to pass through the bed) as well as the relatively large particle size of WS pellets. Both factors might result in enhanced secondary reactions, which are highly exothermic.

From Fig. 11a, it can be observed that a further increase in the absolute pressure from 0.2 MPa to 0.9 MPa led to higher values of $Q_{process}$. This result, which seems to be contradictory to the more exothermic peaks observed for experiments conducted at 0.9 MPa (see Fig. 3), could be explained by a dilution of the exothermicity of the overall process, due to the increase in the carrier gas flow rate at high pressure (to guarantee the proper gas residence time), since the higher the flow rate, the higher the heat needed to be supplied to the system.

An increase in the pyrolysis peak temperature resulted to be significantly negative for Ψ_{char} (Fig. 11b), meaning that the useful work obtained from chars produced at 550 °C was lower than that of chars produced at 400 °C. A reason to explain this finding is the lower yields of high-temperature chars. It is also important to highlight that, although the greater irreversibility, more severe conditions of temperature generally develops other important properties in the char, such as higher surface area and higher recalcitrance. In light of this, depending on the application that char addresses, it would be more or less appropriate to increase the temperature at the expense of a greater irreversibility.

The peak temperature positively affected Ψ_{gas} , since more refined gas products were released at higher pyrolysis temperatures. As seen from Fig. 11d, the absolute pressure was the only factor that had a significant (and positive) main effect on the exergy efficiency of the overall process. The available literature focused on the effects of pressure on the exergy efficiency is very limited and mainly restricted to gasification processes. Nonetheless, the positive effect of pressure on the exergy efficiency was already observed by Srinivas et al. [44]. The opposite trend was however observed by Prins et al. [45] and Wang et al. [28], who reported a negative effect of pressure on the exergy efficiency of the overall biomass gasification process. From the regression model for $\Psi_{process}$, which is given in Fig. 11d, it can be deduced that two sets of operating conditions (both at high pressure and peak temperature) led to the lowest extent of thermodynamic irreversibility involved in the process: (1) 550 °C, 0.9 MPa, 200 s, and pure N₂; and (2) 550 °C, 0.9 MPa, 100 s, and CO₂/N₂ 60:40 v/v. From a practical point of view, the second set of operating conditions appears to be the most convenient one, since relatively high flow rates of recycled CO₂-containing flue gas could easily be implemented in scaled-up process plants.

4. Conclusions

Despite the fact that there is not a unique combination of pyrolysis operating conditions capable to simultaneously optimize all the response variable analyzed here, some useful considerations can be drawn from the results above discussed:

- Although, as expected, the pyrolysis peak temperature was the most influential operating factor, the absolute pressure also played a key role during the devolatilization process of wheat straw, enhancing the release of the gas species at the expense of the liquid products and without affecting neither the yield of char nor its microporosity. An increased pressure also improved the potential stability of the resulting char, due to the greater extent of the secondary charring reactions. The gas residence time was also responsible to modify the course of the devolatilization, by prolonging the solid/gas phases contact and, consequently, further promoting the secondary char reactions. Its influence was reflected on the improved char yield and carbonization efficiency.
- The switch from a pure N₂ atmosphere to the mixture of CO₂/N₂ resulted to be irrelevant on the pyrolysis behavior of wheat straw pellets, except for a slight increase in the yield of CO released. This finding opens the possibility of recycling the flue gas stream as a gas carrier in the pyrolysis process instead of using a more expensive inert gas. Furthermore, the presence of CO₂ in the carrier gas favored the availability of oxygenated functional groups on the surface of resulting chars, regardless of the peak temperature and absolute pressure.
- From an applied research point of view, the most important finding from this study is the fact that pressurized pyrolysis—which implies a considerable reduction of the reactor vessel as well as the costly downstream compression steps—favors the exergy efficiency of the process, even at relatively high pyrolysis peak temperature. For the biomass feedstock and the range of operating conditions studied here, thermodynamic irreversibilities of the pyrolysis system were considerably lowered when the process was conducted at 550 °C, 0.9 MPa and using a mixture of CO₂ and N₂ as carrier gas at relatively short residence times. Under these same conditions, the release of more refined gases (with a higher exergy content) came with the production of a high-quality char with very good properties in terms of potential stability (which is essential for biochar purposes) as well as a considerable availability of oxygen-containing functionalities on surface with a certain microporosity development (being both properties valuable for further uses of chars in value-added applications).

CRedit authorship contribution statement

Gianluca Greco: Conceptualization, Methodology, Software, Validation, Formal analysis, Investigation, Data curation, Writing - original draft. **Christian Di Stasi:** Data curation, Methodology, Investigation, Resources. **Filipe Rego:** Data curation, Investigation. **Belén González:** Resources, Writing - review & editing, Project administration. **Joan J. Manyà:** Resources, Writing - review & editing, Visualization, Supervision, Project administration.

Declaration of Competing Interest

The authors declare that they have no known competing financial interests or personal relationships that could have appeared to influence the work reported in this paper.

Acknowledgements

This project has received funding from the European Union's Horizon 2020 research and innovation program under the Marie

Skłodowska-Curie grant agreement No 721991. JJM also acknowledge the funding from the Aragón Government (Ref. T22_20R), co-funded by FEDER 2014-2020 “Construyendo Europa desde Aragón”.

Appendix A. Supplementary material

Supplementary data to this article can be found online at <https://doi.org/10.1016/j.apenergy.2020.115842>.

References

- Lehmann J, Joseph S. Biochar for environmental management: an introduction. *Biochar Environ Manage*, Eartschan 2009;1–10. <https://doi.org/10.4324/9780203762264>.
- Basu P. Biomass gasification, pyrolysis and torrefaction. Burlington: Elsevier Applied Science; 2013. <https://doi.org/10.1016/C2011-0-07564-6>.
- Suhas Carrott PJM, Ribeiro Carrott MML. Lignin – from natural adsorbent to activated carbon: A review. *Bioresour Technol* 2007;98:2301–12. <https://doi.org/10.1016/J.BIORTECH.2006.08.008>.
- Mok WS-L, Antal MJ. Effects of pressure on biomass pyrolysis. II. Heats of reaction of cellulose pyrolysis. *Thermochim Acta* 1983;68:165–86. [https://doi.org/10.1016/0040-6031\(83\)80222-6](https://doi.org/10.1016/0040-6031(83)80222-6).
- Daugaard DE, Brown RC. Enthalpy for pyrolysis for several types of biomass. *Energy Fuels* 2003;17:934–9. <https://doi.org/10.1021/ef020260x>.
- Dincer I, Rosen MA. Exergy: energy, environment and sustainable development. 2nd Editio. Oxford, Great Britain: Elsevier; 2013. <https://doi.org/10.1016/B978-0-08-097089-9.00001-2>.
- Saidur R, BoroumandJazi G, Mekhilef S, Mohammed HA. A review on exergy analysis of biomass based fuels. *Renew Sustain Energy Rev* 2012;16:1217–22. <https://doi.org/10.1016/j.rser.2011.07.076>.
- Chaiwatanodom P, Vivanpatarakij S, Assabumrungrat S. Thermodynamic analysis of biomass gasification with CO₂ recycle for synthesis gas production. *Appl Energy* 2014;114:10–7. <https://doi.org/10.1016/j.apenergy.2013.09.052>.
- Antal MJ, Gronli M. The art, science, and technology of charcoal production. *Ind Eng Chem Res* 2003;42:1619–40. <https://doi.org/10.1021/ie0207919>.
- Duman G, Okutucu K, Ucar S, Stahl R, Yanik J. The slow and fast pyrolysis of cherry seed. *Bioresour Technol* 2011;102:1869–78. <https://doi.org/10.1016/j.biortech.2010.07.051>.
- Di Blasi C, Signorelli G, Di Russo C, Rea G. Product distribution from pyrolysis of wood and agricultural residues. *Ind Eng Chem Res* 1999;38:2216–24. <https://doi.org/10.1021/ie980711u>.
- Demirbaş A. Effects of temperature and particle size on bio-char yield from pyrolysis of agricultural residues. *J Anal Appl Pyrolysis* 2004;72:243–8. <https://doi.org/10.1016/j.jaap.2004.07.003>.
- Antal MJ, Allen SG, Dai X, Shimizu B, Tam MS, Gronli M. Attainment of the theoretical yield of carbon from biomass. *Ind Eng Chem Res* 2000;39:4024–31. <https://doi.org/10.1021/ie000511u>.
- Manyà JJ. Pyrolysis for biochar purposes: a review to establish current knowledge gaps and research needs. *Environ Sci Technol* 2012;46:7939–54. <https://doi.org/10.1021/es301029g>.
- Heo HS, Park HJ, Dong J-I, Park SH, Kim S, Suh DJ, et al. Fast pyrolysis of rice husk under different reaction conditions. *J Ind Eng Chem* 2010;16:27–31. <https://doi.org/10.1016/J.JIEC.2010.01.026>.
- Akhtar J, Saidina Amin N. A review on operating parameters for optimum liquid oil yield in biomass pyrolysis. *Renew Sustain Energy Rev* 2012;16:5101–9. <https://doi.org/10.1016/J.RSER.2012.05.033>.
- Guedes RE, Luna AS, Torres AR. Operating parameters for bio-oil production in biomass pyrolysis: A review. *J Anal Appl Pyrolysis* 2018;129:134–49. <https://doi.org/10.1016/J.JAAP.2017.11.019>.
- Manyà JJ, Alvira D, Azuara M, Bernin D, Hedin N. Effects of pressure and the addition of a rejected material from municipal waste composting on the pyrolysis of two-phase olive mill waste. *Energy Fuels* 2016;30:8055–64. <https://doi.org/10.1021/acs.energyfuels.6b01579>.
- Antal MJ, Croiset E, Dai X, DeAlmeida C, Mok WS-L, Norberg N, et al. High-yield biomass charcoal †. *Energy Fuels* 1996;10:652–8. <https://doi.org/10.1021/ef9501859>.
- Roussel P, Figueiredo C, De Souza M, Quirino W. Pressure effect on the quality of eucalyptus wood charcoal for the steel industry: A statistical analysis approach. *Fuel Process Technol* 2011;92:1890–7. <https://doi.org/10.1016/j.fuproc.2011.05.005>.
- Recari J, Berruoco C, Abelló S, Montané D, Farriol X. Effect of temperature and pressure on characteristics and reactivity of biomass-derived chars. *Bioresour Technol* 2014;170:204–10. <https://doi.org/10.1016/j.biortech.2014.07.080>.
- Qian Y, Zhang J, Wang J. Pressurized pyrolysis of rice husk in an inert gas sweeping fixed-bed reactor with a focus on bio-oil deoxygenation. *Bioresour Technol* 2014;174:95–102. <https://doi.org/10.1016/j.biortech.2014.10.012>.
- Bui H-H, Wang L, Tran K-Q, Skreiberg Ø. CO₂ gasification of charcoals produced at various pressures. *Fuel Process Technol* 2016;152:207–14. <https://doi.org/10.1016/J.FUPROC.2016.06.033>.
- Melligan F, Aucaille R, Novotny EH, Leahy JJ, Hayes MHB, Kwapinski W. Pressurized pyrolysis of Miscanthus using a fixed bed reactor. *Bioresour Technol* 2011;102:3466–70. <https://doi.org/10.1016/j.biortech.2010.10.129>.
- Manyà JJ, Roca FX, Perales JFJ. TGA study examining the effect of pressure and peak temperature on biochar yield during pyrolysis of two-phase olive mill waste. *Anal Appl Pyrolysis* 2013;103:86–95. <https://doi.org/10.1016/j.jaap.2012.10.006>.
- Azuara M, Sáiz E, Manso JA, García-Ramos FJ, Manyà JJ. Study on the effects of using a carbon dioxide atmosphere on the properties of vine shoots-derived biochar. *Anal Appl Pyrolysis* 2017;124:719–25. <https://doi.org/10.1016/j.jaap.2016.11.022>.
- Wang X, Lv W, Guo L, Zhai M, Dong P, Qi G. Energy and exergy analysis of rice husk high-temperature pyrolysis. *Int J Hydrogen Energy* 2016;41:21121–30. <https://doi.org/10.1016/J.IJHYDENE.2016.09.155>.
- Boateng AA, Mullen CA, Osgood-Jacobs L, Carlson P, Macken N. Mass balance, energy, and exergy analysis of bio-oil production by fast pyrolysis. *J Energy Resour Technol* 2012;134. <https://doi.org/10.1115/1.4007659>.
- Parvez AM, Wu T, Afzal MT, Mareta S, He T, Zhai M. Conventional and microwave-assisted pyrolysis of gumwood: A comparison study using thermodynamic evaluation and hydrogen production. *Fuel Process Technol* 2019;184:1–11. <https://doi.org/10.1016/J.FUPROC.2018.11.007>.
- Atienza-Martínez M, Ábrego J, Mastral JF, Ceamanos J, Gea G. Energy and exergy analyses of sewage sludge thermochemical treatment. *Energy* 2018;144:723–35. <https://doi.org/10.1016/J.ENERGY.2017.12.007>.
- Manyà JJ, Ortigosa MA, Laguarda S, Manso JA. Experimental study on the effect of pyrolysis pressure, peak temperature, and particle size on the potential stability of vine shoots-derived biochar. *Fuel* 2014;133:163–72. <https://doi.org/10.1016/j.fuel.2014.05.019>.
- Channiwala SA, Parikh PP. A unified correlation for estimating HHV of solid, liquid and gaseous fuels. *Fuel* 2002. [https://doi.org/10.1016/S0016-2361\(01\)00131-4](https://doi.org/10.1016/S0016-2361(01)00131-4).
- Montgomery DC. Design and Analysis of Experiments. 6th editio. Hoboken; 2005.
- Greco G, Videgain M, Di Stasi C, González B, Manyà JJ. Evolution of the mass-loss rate during atmospheric and pressurized slow pyrolysis of wheat straw in a bench-scale reactor. *J Anal Appl Pyrolysis* 2018;136:18–26. <https://doi.org/10.1016/j.jaap.2018.11.007>.
- Perry RH, Green DW. Perry's chemical engineers handbook. 7th Editio. Australia: McGraw Hill; 1998.
- Szargut J. Exergy method: technical and ecological applications. Outhampton, UK: WIT; 2005.
- Zhao L, Cao X, Mašek O, Zimmerman A. Heterogeneity of biochar properties as a function of feedstock sources and production temperatures. *J Hazard Mater* 2013; 256–257:1–9. <https://doi.org/10.1016/j.jhazmat.2013.04.015>.
- McBeath AV, Wurster CM, Bird MI. Influence of feedstock properties and pyrolysis conditions on biochar carbon stability as determined by hydrogen pyrolysis. *Biomass Bioenergy* 2015;73. <https://doi.org/10.1016/j.biombioe.2014.12.022>.
- Manyà JJ, Laguarda S, Ortigosa MA, Manso JA. Biochar from slow pyrolysis of two-phase olive mill waste: effect of pressure and peak temperature on its potential stability. *Energy Fuels* 2014;28:3271–80. <https://doi.org/10.1021/ef500654t>.
- Noumi ES, Blin J, Valette J, Rousset P. Combined effect of pyrolysis pressure and temperature on the yield and CO₂ gasification reactivity of Acacia Wood in macro-TG. *Energy Fuels* 2015;29:7301–8. <https://doi.org/10.1021/acs.energyfuels.5b01454>.
- Ates F, Miskolczi N, Saricaoglu B. Pressurized pyrolysis of dried distillers grains with solubles and canola seed press cake in a fixed-bed reactor. *Bioresour Technol* 2015;177:149–58. <https://doi.org/10.1016/j.biortech.2014.10.163>.
- Cetin E, Moghtaderi B, Gupta R, Wall T. Influence of pyrolysis conditions on the structure and gasification reactivity of biomass chars. *Fuel* 2004;83:2139–50. <https://doi.org/10.1016/J.FUEL.2004.05.008>.
- Ding H-S, Jiang H. Self-heating co-pyrolysis of excessive activated sludge with waste biomass: Energy balance and sludge reduction. *Bioresour Technol* 2013;133: 16–22. <https://doi.org/10.1016/J.BIORTECH.2013.01.090>.
- Srinivas T, Gupta AVSSKS, Reddy BV. Thermodynamic equilibrium model and exergy analysis of a Biomass gasifier. *J Energy Resour Technol Trans ASME* 2009. <https://doi.org/10.1115/1.3185354>.
- Prins MJ, Ptasiński KJ. Energy and exergy analyses of the oxidation and gasification of carbon. *Energy* 2005;30:982–1002. <https://doi.org/10.1016/J.ENERGY.2004.08.010>.

Appendix A: Supplementary material

Effects of slow-pyrolysis conditions on the products distribution and on exergy efficiency: a comprehensive assessment for wheat straw

Gianluca Greco^{1*}, Christian Di Stasi¹, Filipe Rego², Belén González¹, Joan J. Manyà¹

¹ *Aragón Institute of Engineering Research (I3A), Technological College of Huesca, University of Zaragoza, crta. Cuarte s/n, Huesca E-22071, Spain.*

² *Energy and Bioproducts Research Institute (EBRI), Aston University, Aston Triangle, B4-7ET, Birmingham, United Kingdom (UK).*

* Corresponding author. E-mail address: greco@unizar.es.

Analysis of wheat straw biomass constituents

The experimental procedure (reported in literature by Li et al. [1]) was conducted in duplicate and consisted of four main steps (which were performed in duplicate):

- The dried biomass was weighted (G_0) and added in a benzene/ethanol solution (2:1 v/v). Then, the residue obtained (G_1) was dried until a constant weight was reached. The extractive content was calculated as:

$$W_1(\text{wt. \%}) = \frac{G_0 - G_1}{G_0} \cdot 100\% \quad (\text{A.1})$$

- The residue G_1 from the extractive analysis was added in a NaOH solution and boiled for hours. Then it was filtered and washed of all the Na^+ ions left, and dried to a constant weight (G_2). The hemicellulose content was calculated as:

$$W_2(\text{wt. \%}) = \frac{G_1 - G_2}{G_0} \cdot 100\% \quad (\text{A.2})$$

- 1 g of the residue G_1 after the extractive analysis was dried to a constant weight (G_3). Successively, it was added in sulphuric acid solution and kept overnight. Then it was diluted with distilled water and boiled for 1 h. After cooling and filtration, the residue was washed of all the sulphate ions left, and dried to a constant weight (G_4). The lignin content was calculated as:

$$W_3(\text{wt. \%}) = \frac{G_4(1 - W_1)}{G_3} \cdot 100\% \quad (\text{A.3})$$

- The cellulose was determined by difference:

$$W_4(\text{wt. \%}) = 100 - (A_d + W_1 + W_2 + W_3) \quad (\text{A.4})$$

Pyrolysis plant

The reactor (140 mm ID and 465 mm long) was made of Sandvik 253 MA stainless steel (EN 1.4835). The biomass was placed in a basket of 4 L, made of AISI 316 (EN 1.4401) stainless steel wire mesh, which was in turn allocated into the reactor. The initial sample weight was approximately 400 g, which, according to the apparent density of the WS pellets, represented around 30% of the basket volume. A weighing platform (Kern, model DS with a measuring range up to 100 kg and a reading precision of 0.5 g) was collocated at the bottom of the reactor, in order to track the mass loss of the sample during the pyrolysis. A ceramic tube (117 mm OD and 330 mm long) connected the reactor with the weighing platform for thermal insulation purposes. Flexible stainless steel tubing (Swagelok, 10 mm OD) were employed as reactor connections to minimize any force

component. The pressure was maintained inside the bed at the desired value through a back-pressure regulator (BPR) located at the outlet of the reactor.

Assessment of repeatability

The three repeated measurements shown in Fig. A.1 were analyzed using a one-way ANOVA. Assuming normality and homogeneity of variances (since just three replicates at each level of factor is too low for conducting the appropriate tests), we computed the mean squares for the treatment and error terms (MS_t and MS_e , respectively). The intra-class correlation coefficient (ICC), which is commonly used as a measure of repeatability (R), was then estimated as follows [2]:

$$ICC = \frac{MS_t - MS_e}{MS_t + (n_0 - 1)MS_e} 100 \quad (A.5)$$

where n_0 is the number of replicates (3). The obtained value of ICC (99.27%) indicated a high level of repeatability.

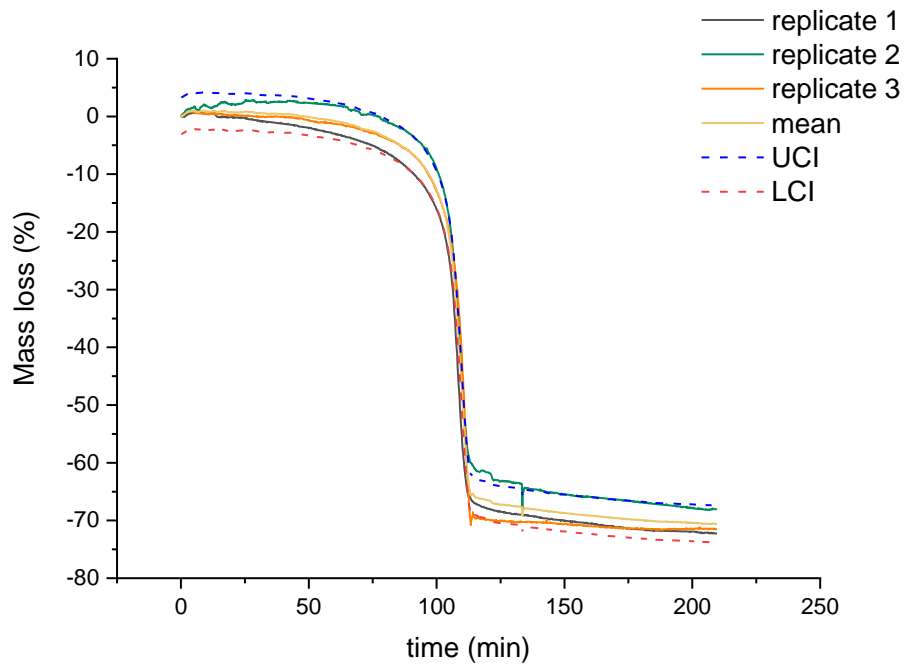


Fig. A.1. Comparison of the mass-loss curves obtained for three replicates of the central point of the experimental design. LCI and UCI correspond to lower and upper 95% confidence intervals.

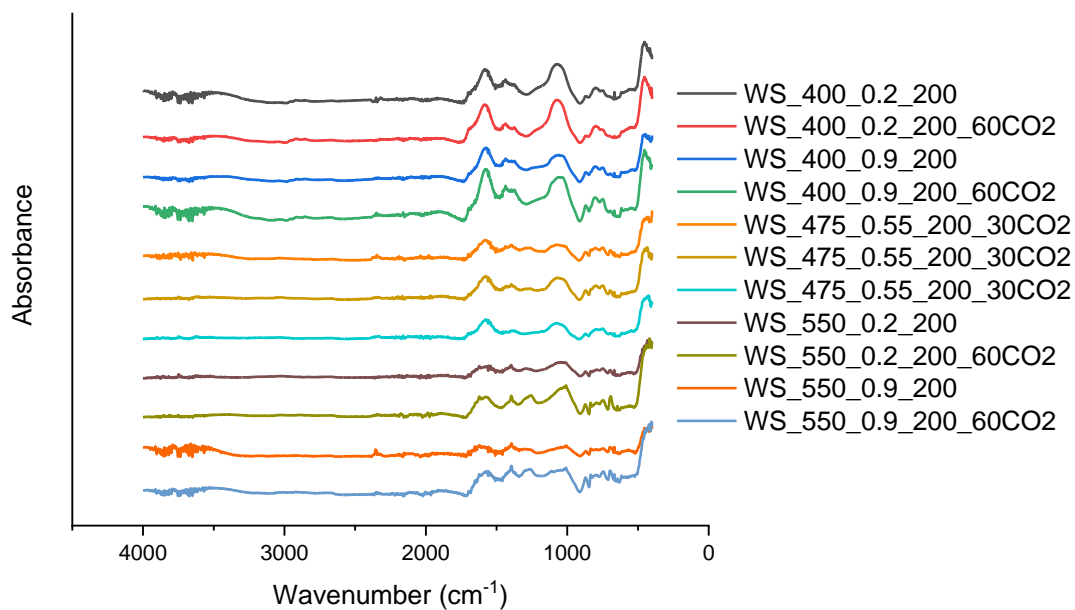


Fig A.2. FT-IR spectra of the biochars set produced under a gas residence time of 200 s. Biochars are notated as $WS_T_P_R_A$; where WS refers to a wheat straw-derived biochar (WS), T to the peak temperature, P to the absolute pressure, R to the gas residence time, and A to the type of reactor atmosphere.

Component (wt. %)	
Hemicellulose	33.0 ± 0.61
Cellulose	40.7 ± 0.50
Lignin	18.4 ± 0.54
Extractives	8.05 ± 0.28
Proximate (wt. %)	
Ash	3.87 ± 0.07
Moisture	7.27 ± 0.06
Volatile matter	74.99 ± 0.33
Fixed carbon	14.0 ± 0.29
Ultimate (wt. % in daf basis)	
C	49.0 ± 0.52
H	7.01 ± 0.04
N	0.704 ± 0.01
O	43.2 ¹
HHV (MJ kg⁻¹)	18.01
Inorganic matter as equivalent oxides (wt. % of ash)²	
K ₂ O	53.2
CaO	17.4
SiO ₂	16.9
P ₂ O ₅	4.46
Al ₂ O ₃	1.66
Cl (inorganic)	1.53
MgO	1.46
S (inorganic)	1.31
Fe ₂ O ₃	1.14

¹Oxygen was calculated by difference.

²Only listed components with a composition higher than 1%.

Table A.1. Lignocellulosic composition, proximate, ultimate and XRF analyses of wheat straw pellets.

	Mass loss	$Area_{peak}$	DTG_{max}	T_{max}
β_0	69.1419 (0.000)	61.232 (0.000)	5.197 (0.000)	289.520 (0.000)
$\beta_1 (T)$	1.5931 (0.000)	0.939 (0.071)	0.445 (0.128)	10.770 (0.048)
$\beta_2 (P)$	0.1931 (0.033)	-2.596 (0.001)	2.465 (0.000)	-3.350 (0.481)
$\beta_3 (\tau)$	-0.3744 (0.001)	0.114 (0.804)	-0.380 (0.184)	7.980 (0.120)
$\beta_4 (CO_2)$	-0.0631 (0.415)	-0.399 (0.396)	0.199 (0.466)	3.970 (0.407)
$\beta_{12} (T \cdot P)$	-0.2056 (0.026)	-0.093 (0.840)	-0.112 (0.676)	-18.100 (0.005)
$\beta_{13} (T \cdot \tau)$	-0.0081 (0.914)	-0.157 (0.731)	0.488 (0.101)	-7.770 (0.128)
$\beta_{14} (T \cdot CO_2)$	-0.1494 (0.080)	-0.130 (0.777)	-0.056 (0.834)	-7.020 (0.163)
$\beta_{23} (P \cdot \tau)$	-0.0056 (0.941)	0.265 (0.567)	-0.678 (0.034)	-2.900 (0.540)
$\beta_{24} (P \cdot CO_2)$	0.0431 (0.573)	0.242 (0.599)	-0.186 (0.494)	-9.150 (0.082)
$\beta_{34} (\tau \cdot CO_2)$	-0.0094 (0.901)	-0.197 (0.668)	-0.016 (0.952)	-2.970 (0.530)
R^2_{adj}	0.9666	0.6433	0.8511	0.6351
<i>Curvature</i>	(0.029)	(0.180)	(0.050)	(0.050)

Table A.2. Statistics of the regression model for the mass loss, $Area_{peak}$, DTG_{max} and T_{max} . The values in brackets correspond to the p -values resulting from the t -tests. The significant terms are marked in bold.

	y_{char}	y_{org}	y_{wat}	y_{gas}	y_{CO_2}	y_{CO}	y_{CH_4}	y_{H_2}
β_0	0.2990	0.23968	0.10836	0.3530	5.670	2.835	0.885	0.5789
	(0.000)	(0.000)	(0.000)	(0.000)	(0.000)	(0.000)	(0.000)	(0.000)
β_1	-0.0172	0.01338	-0.00544	0.0092	-0.131	0.249	0.349	0.5082
(T)	(0.000)	(0.089)	(0.154)	(0.115)	(0.413)	(0.061)	(0.030)	(0.000)
β_2	0.0001	-0.04014	-0.01264	0.0527	1.327	-0.278	0.086	-0.0368
(P)	(0.935)	(0.001)	(0.007)	(0.000)	(0.000)	(0.042)	(0.523)	(0.496)
β_3	0.0065	0.00474	0.00001	-0.0113	-0.142	-0.197	0.059	-0.0401
(τ)	(0.002)	(0.507)	(0.998)	(0.064)	(0.375)	(0.122)	(0.659)	(0.459)
β_4	-0.0009	0.00641	0.00411	-0.0096	-0.321	0.215	-0.030	-0.1566
(CO_2)	(0.536)	(0.376)	(0.266)	(0.104)	(0.070)	(0.097)	(0.822)	(0.018)
β_{12}	-0.0005	0.00641	0.00796	-0.0139	-0.112	-0.258	-0.040	-0.0596
($T \cdot P$)	(0.724)	(0.376)	(0.052)	(0.031)	(0.482)	(0.054)	(0.763)	(0.283)
β_{13}	-0.0022	-0.00131	0.00151	0.0020	0.016	-0.005	0.098	-0.0360
($T \cdot \tau$)	(0.151)	(0.853)	(0.671)	(0.702)	(0.916)	(0.963)	(0.469)	(0.506)
β_{14}	0.0027	-0.00285	0.00219	-0.0020	-0.258	0.382	-0.061	-0.1531
($T \cdot CO_2$)	(0.098)	(0.687)	(0.539)	(0.707)	(0.130)	(0.011)	(0.651)	(0.020)
β_{23}	-0.0026	0.00997	0.00062	-0.0080	-0.180	0.032	-0.052	0.0340
($P \cdot \tau$)	(0.108)	(0.184)	(0.861)	(0.163)	(0.271)	(0.783)	(0.694)	(0.528)
β_{24}	-0.0001	-0.00334	-0.00418	0.0076	0.406	-0.182	-0.215	-0.1306
($P \cdot CO_2$)	(0.943)	(0.637)	(0.259)	(0.182)	(0.031)	(0.148)	(0.136)	(0.038)
β_{34}	0.0015	0.00072	0.00077	-0.0030	0.036	-0.116	-0.073	-0.0184
($\tau \cdot CO_2$)	(0.315)	(0.918)	(0.827)	(0.577)	(0.819)	(0.336)	(0.587)	(0.730)
R^2_{adj}	0.9069	0.6500	0.4469	0.8692	0.8326	0.6480	0.6401	0.8673
Curvature	(0.179)	(0.494)	(0.909)	(0.276)	(0.082)	(0.052)	(0.780)	(0.198)

Table A.3. Statistics of the regression model for the pyrolysis products. The values in brackets correspond to the p -values resulting from the t -tests. The significant terms are marked in bold.

	H:C	O:C	x_{FC}	y_{FC}	S_{BET}	V_{ultra}
β_0	0.4825 (0.000)	0.0959 (0.000)	79.349 (0.000)	0.2375 (0.000)	187.69 (0.000)	0.0668 (0.000)
β_1	-0.1334 (0.000)	-0.0252 (0.000)	6.516 (0.000)	0.0032 (0.030)	31.56 (0.000)	0.0163 (0.000)
β_2	-0.0205 (0.000)	-0.0090 (0.001)	1.327 (0.072)	0.0027 (0.056)	-0.06 (0.963)	0.0000 (1.000)
β_3	0.0009 (0.774)	-0.0032 (0.096)	1.032 (0.143)	0.0061 (0.001)	-1.19 (0.390)	-0.0004 (0.776)
β_4	-0.0127 (0.004)	-0.0028 (0.140)	-0.269 (0.681)	0.0003 (0.830)	0.81 (0.551)	0.0004 (0.788)
β_{12}	0.0103 (0.011)	0.0052 (0.017)	-1.080 (0.128)	-0.0025 (0.069)	-1.69 (0.234)	-0.0002 (0.912)
β_{13}	0.0012 (0.695)	0.0009 (0.588)	-0.694 (0.305)	-0.0015 (0.239)	-0.56 (0.678)	0.0001 (0.924)
β_{14}	0.0044 (0.185)	0.0016 (0.353)	0.379 (0.564)	0.0013 (0.292)	0.44 (0.746)	0.0004 (0.800)
β_{23}	-0.0001 (0.960)	0.0029 (0.126)	-0.735 (0.279)	-0.0027 (0.053)	2.31 (0.118)	0.0012 (0.447)
β_{24}	-0.0053 (0.121)	-0.0010 (0.554)	0.714 (0.292)	-0.0005 (0.665)	1.56 (0.268)	0.0006 (0.705)
β_{34}	0.0082 (0.029)	0.0020 (0.253)	0.122 (0.851)	-0.0003 (0.823)	0.44 (0.746)	-0.0004 (0.812)
R^2_{adj}	0.9914	0.9388	0.8630	0.6994	0.9706	0.8556
Curvature	(0.074)	(0.368)	(0.242)	(0.978)	(0.070)	(0.286)

Table A.4. Statistics of the regression model for the char properties related to its potential stability and textural properties. The values in brackets correspond to the p -values resulting from the t -tests. The significant terms are marked in bold.

	$Q_{process}$	Ψ_{char}	Ψ_{gas}	$\Psi_{process}$
β_0	-0.2087 (0.012)	44.669 (0.000)	11.095 (0.000)	57.661 (0.000)
β_1	0.0285 (0.668)	-2.657 (0.000)	2.899 (0.000)	–
β_2	0.2649 (0.003)	-0.116 (0.789)	0.688 (0.125)	0.868 (0.027)
β	-0.1107 (0.122)	0.746 (0.118)	-0.585 (0.182)	-0.189 (0.562)
β_4	0.1041 (0.143)	-0.557 (0.225)	-0.365 (0.386)	-0.663 (0.070)
β_{12}	0.0284 (0.669)	0.334 (0.451)	-0.505 (0.242)	-0.085 (0.793)
β_{13}	0.0001 (0.999)	0.164 (0.707)	0.001 (0.999)	–
β_{14}	–	0.830 (0.088)	0.037 (0.929)	0.858 (0.028)
β_{23}	-0.091 (0.194)	0.002 (0.997)	-0.570 (0.192)	-0.571 (0.109)
β_{24}	–	0.577 (0.210)	-0.858 (0.066)	-0.349 (0.299)
β_{34}	-0.0650 (0.341)	0.655 (0.161)	-0.444 (0.299)	–
β_{124}	–	–	–	-0.829 (0.032)
β_{134}	–	–	–	-0.744 (0.048)
β_{234}	-0.1156 (0.109)	–	–	-1.041 (0.012)
R^2_{adj}	0.5203 (0.714)	0.7154 (0.080)	0.7667 (0.481)	0.6847 (0.366)
Curvature				

Table A.5. Statistics of the regression model for $Q_{process}$, Ψ_{char} , Ψ_{gas} and $\Psi_{process}$. The values in brackets correspond to the p -values resulting from the t -tests. The significant terms are marked in bold.

Parameter				Response variable				
T	P	τ	N ₂ /CO ₂	Mass balance closure (%)	Mass loss (%)	$Area_{peak}$ (g min ⁻¹)	DTG_{max} (min ⁻¹)	T_{max} (°C)
550	0.2	100	100/0	90	71.20	66.37	2.70	325.0
475	0.55	150	70/30	89	69.46	59.95	6.21	296.0
550	0.9	100	100/0	85	71.46	58.52	8.41	290.4
400	0.9	100	100/0	84	68.02	57.84	8.10	280.0
400	0.2	100	100/0	88	67.60	62.55	2.24	203.0
475	0.55	150	70/30	87	69.90	65.61	7.53	322.8
550	0.2	200	40/60	85	70.30	63.35	5.38	334.0
400	0.2	100	40/60	93	67.44	62.00	2.20	280.0
400	0.9	200	100/0	86	67.27	57.62	5.68	305.0
550	0.2	100	40/60	85	71.03	65.00	2.60	320.0
550	0.2	200	100/0	88	70.46	64.72	2.48	308.0
550	0.9	100	40/60	99	70.78	58.97	8.43	265.0
400	0.9	200	40/60	94	67.90	58.00	5.60	300.0
400	0.2	200	40/60	90	66.60	62.40	2.29	290.0
475	0.55	150	70/30	84	69.57	63.10	6.45	330.0
550	0.9	200	40/60	99	69.98	59.25	6.73	270.0
400	0.2	200	100/0	92	66.96	64.24	1.97	283.0
400	0.9	100	40/60	85	68.60	57.70	9.94	289.0
550	0.9	200	100/0	87	70.67	61.19	8.41	290.0

Table A.6. Mass balance closures and experimental results of the mass loss, $Area_{peak}$, DTG_{max} and T_{max} for all the pyrolysis runs.

References

- [1] Li S, Xu S, Liu S, Yang C, Lu Q. Fast pyrolysis of biomass in free-fall reactor for hydrogen-rich gas. *Fuel Process Technol* 2004; 85: 1201–11. <https://doi.org/10.1016/J.FUPROC.2003.11.043>.
- [2] Nakagawa S, Schielzeth H. Repeatability for Gaussian and non-Gaussian data: A practical guide for biologists. *Biol Rev* 2010; 85: 935–56. <https://doi.org/10.1111/j.1469-185X.2010.00141.x>.
- [3] Zhao Y, Feng D, Zhang Y, Huang Y, Sun S. Effect of pyrolysis temperature on char structure and chemical speciation of alkali and alkaline earth metallic species in biochar. *Fuel Process Technol* 2016; 141: 54–60. <https://doi.org/10.1016/J.FUPROC.2015.06.029>.
- [4] Lin X, Wang C, Ideta K, Miyawaki J, Nishiyama Y, Wang Y, et al. Insights into the functional group transformation of a chinese brown coal during slow pyrolysis by combining various experiments. *Fuel* 2014; 118: 257–64. <https://doi.org/10.1016/J.FUEL.2013.10.081>.

6.3. Theme III: assessment of the potential toxicity of biochar for soli application purposes

Once determined the wheat straw pyrolysis behavior in *Theme II*, the same design of experiments was performed using wood waste as biomass feedstock. A special emphasis was given to the effects of the above-mentioned process parameters on the final PAHs concentrations in biochar. PAHs assessment is an essential step when it comes the possibility to employ wasted biomass as soil amendment, with the double objective of improving the soil properties and promoting the circular economy of such biomaterials by increasing their value added. This research study was published in *Journal of Analytical and Applied Pyrolysis* (article 3).

From the results obtained in the framework of this theme, it can be deduced that wood waste exhibited a similar pyrolysis behavior to that of wheat straw, except for an observed minor influence of pressure on the devolatilization kinetics, which was attributed to the lower hemicellulose content of wood waste. The highest PAHs content was reached at the lowest temperature level (400 °C), suggesting that conversion of PAHs toward lighter hydrocarbons was promoted by temperature. This result, which appears to be contradictory to the literature, might be explained considering that the total PAHs content takes into account all the processes involved in the formation and consumption of PAHs, which occur throughout many phases in succession under different temperature levels. Consequently, PAHs may turn into lower molecular weight PAHs by breakage or into higher molecular weight PAHs through condensation and polymerization reactions, depending on the pyrolysis reactor configuration, operating process conditions and type of feedstock too. In addition, also the effect of absolute pressure resulted to be negative on total PAHs content, due to a massive dilution of reaction environment by the relatively high carrier gas flow rates employed in these experiments. This led to a minor interaction in the vapor-solid phase, hindering the formation of PAHs.

Once ensured the relatively low contents of hazardous PAH compounds in biochar, germination tests were performed to assess their short-term phytotoxicity on different seeds. The results obtained from the germination assessment suggest that PAHs were not the only ones responsible for the short-term phytotoxic effects related to biochars. In fact, the co-occurrence of low-molecular weight organic acids and phenolic compounds, which have high mobility and can be removed relatively easily by water washing, could partly explain the phytotoxic effects observed. Results also provided evidence on the efficiency of the water washing pretreatment as a means of diminishing the potential toxicity of WW-derived biochars for soil application purposes.



Importance of pyrolysis temperature and pressure in the concentration of polycyclic aromatic hydrocarbons in wood waste-derived biochars

Gianluca Greco^{a,*}, María Videgain^b, Christian Di Stasi^a, Elisabet Pires^c, Joan J. Manyà^{a,*}

^a Aragón Institute of Engineering Research (I3A), Thermochemical Processes Group, University of Zaragoza, Escuela Politécnica Superior, crta. Cuarte s/n, Huesca, E-22071, Spain

^b Escuela Politécnica Superior, University of Zaragoza, crta. Cuarte s/n, Huesca, E-22071, Spain

^c Departamento de Química Orgánica ISQCH, Facultad de Ciencias, Universidad de Zaragoza-CSIC, Pedro Cerbuna 12, Zaragoza, 50009, Spain

ARTICLE INFO

Keywords:

Biochar
Slow pyrolysis
Pressure
Untreated wood waste
PAH assessment
Phytotoxicity

ABSTRACT

Biochar addition to soil can lead to potential environmental risks due to its content of polycyclic aromatic hydrocarbons (PAHs). Until now, previous research focused on assessing the influence of pyrolysis peak temperature and feedstock on the formation and evolution of PAHs. Nevertheless, the effects of other important process parameters—such as pressure, gas residence time, and type of carrier gas—have not been comprehensively explored. To fill this gap, a 2-level full factorial design of experiments was conducted to assess the influence of the above-mentioned parameters on the pyrolysis behavior of an untreated wood waste as well as the properties of resulting biochars, including their PAHs contents. Results showed that the highest production of PAHs was reached at lower peak temperatures, whereas an increase in temperature led to a substantial reduction of the final PAHs content. An increased pressure also resulted in a marked decrease in PAHs, probably as a consequence of the higher carrier gas flow rates used under pressurized conditions, which could inhibit the generation of PAHs by condensation and polymerization. The outstanding results obtained from the phytotoxicity assessment for three plant species (barley, watercress, and basil) suggest that PAHs were not the major responsible for the observed short-term phytotoxic effects of biochars, since a considerable part of the phytotoxic compounds in biochar can be removed by a simple water washing step.

1. Introduction

Biochar is widely recognized as a potential soil amendment due to its unique properties, such as high stability, high nutrients content, alkalinity, and relatively high porosity [1]. Although the research in the field of biochar has been very intensive in the last years, a better understanding of its role in agricultural and environmental practices is still needed. Biochar addition to soil also entails potential environmental risks due to its content of polycyclic aromatic hydrocarbons (PAHs). Being the largest group of carcinogenic, teratogenic and mutagenic compounds, PAHs are nowadays recognized as priority pollutants [2]. Allowed levels of PAHs in biochar for soil applications have been proposed in the last years, defining basic- and premium-grade biochars: below 12 and 4 mg kg⁻¹, respectively, according to the European Biochar Certificate [3]; and below 20 and 6 mg kg⁻¹, respectively, in line with the International Biochar Initiative [4].

PAHs are highly condensed aromatic structures produced during the

pyrolysis process [5]. Their final concentrations in the produced biochar—which typically range from less than 0.1 to over 10,000 mg kg⁻¹ [6]—depend on both the pyrolysis operating conditions (especially pyrolysis peak temperature) and biomass feedstock [7]. However, the effect of pyrolysis peak temperature on the production and distribution of PAHs within the resulting biochar is still unclear, in light of the apparently contradictory findings available in the literature [8–10]. It is known that aromatization, cyclization, dehydrogenation and dealkylation are the main reactions involved in PAHs formation at relatively low peak temperatures [11] (i.e., below 500 °C), whereas a further recombination of reactive radicals occurs when more severe conditions are applied, leading to the formation of more condensed aromatic structures [12].

In addition to pyrolysis peak temperature, the gas residence time can also markedly affect the final PAHs content in biochar. Typically, its increase results in a prolonged contact between the solid and gas phases, leading to a further decomposition of the tarry vapors onto the solid carbonaceous matrix through secondary reactions such as condensation, repolymerization and thermal cracking [13]. In other words, longer gas

* Corresponding authors.

E-mail addresses: greco@unizar.es (G. Greco), joanjoma@unizar.es (J.J. Manyà).

<https://doi.org/10.1016/j.jaap.2021.105337>

Received 20 July 2021; Received in revised form 31 August 2021; Accepted 24 September 2021

Available online 28 September 2021

0165-2370/© 2021 The Author(s).

Published by Elsevier B.V. This is an open access article under the CC BY-NC-ND license

(<http://creativecommons.org/licenses/by-nc-nd/4.0/>).

Nomenclature	
<i>Abbreviations of 16 EPA PAHs</i>	
ANA	Acenaphthene
ANT	Anthracene
<i>&%Annotation-xml.content; Acenaphthylene</i>	
BaA	Benzo[a]anthracene
BaP	Benzo[a]pyrene
BbF	Benzo[b]fluoranthene
BkF	Benzo[k]fluoranthene
BPE	Benzo[ghi]perylene
CHR	Chrysene
DBA	Dibenz[a,h]anthracene
FLT	Fluoranthene
FLU	Fluorene
IPY	Indeno[1,2,3,-cd]pyrene
NAP	Naphthalene
PHE	Phenanthrene
PYR	Pyrene
<i>Variables</i>	
CO ₂	CO ₂ content in the pyrolysis carrier gas (vol. %)
G	Germination percentage
GI	Germination index (%)
L	Average root length (mm)
P	Absolute pressure during pyrolysis (MPa)
S _{BET}	Specific surface area according to the BET model (m ² g ⁻¹)
T	Pyrolysis peak temperature (°C)
τ	Gas residence time (s)
V _{ultra}	Volume of ultra-micropores (cm ³ g ⁻¹)
x _{FC}	Fixed-carbon content (wt. %)
y _{char}	Yield of char (mass fraction, daf basis)
y _{FC}	Fixed-carbon yield (mass fraction)
y _{gas}	Yield of produced gas (mass fraction, daf basis)
y _{org}	Yield of condensable organic compounds (mass fraction, daf basis)
y _{wat}	Yield of produced water (mass fraction, daf basis)
<i>Acronyms</i>	
daf	Dry- and ash-free basis
db	Dry basis
TTEC	Total toxic equivalent concentrations (μg kg ⁻¹ biochar, db)
<i>Subscript</i>	
w	Washed biochar samples

residences times could result in biochars with higher PAHs contents, since PAHs are predominantly synthesized in the gas phase [5]. In line with this, Madej et al. [14] observed that using relatively high carrier gas (N₂) flow rates during the pyrolysis of several biomass sources led to biochars with low PAHs contents (less than 1.5 mg kg⁻¹), regardless of the peak temperature used.

On the other hand, the effect of the absolute pressure on the production and distribution of PAHs has been much less explored. Since it was found that an increased pressure can significantly affect the pyrolysis process—leading to higher yields of gas at the expense of condensable organic products [15–19]—, a certain influence of this process parameter on the PAHs contents of produced biochars can be expected. At this point, it should be emphasized that pressurized pyrolysis coupled with CO₂-containing flue gas recirculation appears as a promising approach in terms of energy efficiency [16]. The presence of CO₂ in the pyrolysis atmosphere was previously tested in different works [15,16,20]. For instance, Azuara et al. [20] analyzed the effects of absolute pressure coupled with a CO₂ pyrolysis atmosphere during the slow pyrolysis of vine shoot biomass, demonstrating that the switch from N₂ to CO₂ did not affect neither the carbonization efficiency nor the properties of resulting biochar. In addition, under a CO₂ atmosphere, the yield of CO notably increased at the expense of the CO₂ yield, leading to the production of a more refined gas product, with a higher energy content. In light of these previous findings, which clearly appeared to be very appealing from an energy point of view, the role played by the content of CO₂ in the carrier gas in the genesis of PAHs results to be very interesting to assess.

It is estimated that the countries of the EU generate 50 million cubic meters of wood waste (WW) each year [21]. WW can be considered a valuable material, due to its potential for both recycling (e.g., particle-board) and energy recovery. However, WW could contain chemical impurities, such as heavy metals and persistent organic pollutants, including PAHs, which could be present in adhesives used in panels production [22]. Hence, and in order to produce high-quality biochars (with low PAHs levels), using untreated wood waste as precursor is encouraged.

Keeping in mind all the considerations given above, the present work aims at assessing the influence of four pyrolysis process parameters (peak temperature, absolute pressure, gas residence time, and content of

CO₂ in the carrier gas) on the pyrolysis behavior and physicochemical properties of resulting biochars, with a special emphasis on their PAHs contents. Phytotoxicity of WW-derived biochars was also evaluated through germination tests for different seeds (i.e., barley, watercress, and basil). To the best of our knowledge, the present study is among the first ones to assess the influence of a high number of process-related variables (not only peak temperature, which has been the most analyzed parameter so far) on the potential hazard of WW-derived biochar utilization.

2. Experimental section

2.1. Biomass feedstock

An untreated wood waste, which was basically a mixture of sawdust from sawmills and wood from used pallets and crates, was provided from a Belgian wood recycling company. The used WW, with a particle size in the range of 0.30–4.0 mm, was directly pyrolyzed without any preliminary treatment. Proximate analyses were performed in quadruplicate according to ASTM standards for moisture, volatile matter, and ash contents. Ultimate analyses were carried out in triplicate using a CHN628 elemental analyzer (Leco, USA). X-Ray Fluorescence (XRF) spectroscopy analysis (using an ADVANT^{XP} + XRF spectrometer from Thermo ARL, Switzerland) was also conducted to determine the inorganic constituents of the biomass ash. The procedure employed to determine the main constituents of WW (hemicelluloses, cellulose, lignin, and extractives) is reported in detail in a previous work [16].

2.2. Production and characterization of WW-derived biochars

The bench-scale fixed-bed pyrolysis unit used for biochar production was already described in an earlier study [15]. Pyrolysis experiments were performed by varying the peak temperature between 400 and 550 °C, whereas the ranges of absolute pressure and gas residence time were 0.2–0.9 MPa and 100–200 s, respectively. Moreover, the composition of the carrier gas varied from pure N₂ to a binary mixture of 60:40 v/v of CO₂/N₂. The initial mass of WW was 400 g and the mean heating rate and the soaking time (at the peak temperature) were kept constant at 5 °C min⁻¹ and 1 h, respectively. More details concerning the experimental

device and procedure are available in Appendix A.

The mass yields of biochar (y_{char}), produced gas (y_{gas}), organic condensable products (y_{org}) and produced water (y_{wat}) were calculated in a dry and ash-free (daf) basis. Produced biochars were characterized by proximate analysis and ultimate analyses using the same procedures as described above. The fixed-carbon yield (y_{FC}), which corresponds to the fraction of organic matter initially present in the biomass feedstock and converted into fixed carbon, was taken as a measure of carbonization efficiency.

Given the highly ultra-microporous structure of biochars, CO₂ adsorption isotherms at 0 °C were measured using an ASAP 2020 gas sorption analyzer (Micromeritics, USA). Approximately 120 mg of each sample were firstly degassed under dynamic conditions at 150 °C until constant weight was reached. From the obtained isotherms, the BET specific surface areas (S_{BET}) and the ultra-micropore volumes (V_{ultra} , pore size lower than 0.7 nm) were determined. For V_{ultra} , Grand Canonical Monte Carlo (GCMC) simulations for carbon slit-shaped pores were used.

The pH of biochars was measured in deionized water at a ratio of 1:10 (w/v) using a pH meter (SensION + pH3 from Hach, USA). For comparison purposes, pH of raw and water-washed biochars was measured. A large excess of distilled water (50 mL per g of biochar) was used for washing. The resulting mixture was gently stirred for 2 h at 300 rpm. The washed biochar particles were then separated by vacuum filtration and dried at 105 °C overnight.

2.3. PAHs contents in biochars

In line with the methodology described by De la Rosa et al. [23], 2 g of dried biochar underwent a Soxhlet extraction using 200 mL of toluene throughout 24 h without any clean-up treatment. The obtained extracts were concentrated to 1 – 2 mL by means of a rotary vacuum evaporator (R-210, Buchi, Switzerland). Prior to concentration, the biochar samples were spiked with 10 µL of toluene containing 400 ng of a PAH deuterated internal standard mix in order to detect any possible loss of analyte during sample preparation. The analysis of the 16 PAHs prioritized by the US EPA in the resulting extracts was performed using a 6890 GC coupled with a 5973i MS detector (Agilent, USA). More details on the procedure adopted to measure PAHs are available in Appendix A. The total toxic equivalent concentrations (TTEC) related to the carcinogenic risk assessment for each biochar sample was then calculated according to the procedure described by Dat and Chang [24].

2.4. Germination tests

Phytotoxicity tests were carried out in order to assess the hazard of employing WW-derived biochar as soil amendment. The procedure consisted of the incubation of 10 seeds (of barley, watercress, or basil) in 5 mL of an aqueous solution containing 0.5 g of biochar poured in a Petri dish over a sterile filter paper. All the samples were then covered and stored in an oven at 25 °C for 72 h. The root length of germinated seeds was measured using a Vernier caliper and the average values were calculated for each sample. According to Liang et al. [25], the germination index (GI) was calculated as follows:

$$GI = \frac{G}{G_0} \frac{L}{L_0} 100 \quad (1)$$

where G and L are the germination percentage and average root length, respectively. G_0 and L_0 refer to the control condition (i.e., Petri dish with 5 mL of deionized water).

2.5. Statistical approach

An unreplicated 2-level full factorial design was adopted to evaluate the effects of the four factors assessed —peak temperature (T , 400 and

550 °C), absolute pressure (P , 0.2 and 0.9 MPa), gas residence time (τ , 100 and 200 s), and CO₂ content in the carrier gas (CO₂, 0 and 60 vol. %). Three replicates at the center point (475 °C, 0.55 MPa, 150 s and 30:70 v/v of CO₂/N₂) were carried out to estimate the experimental error and the overall curvature effect [26]. The structure of the regression model for a given response variable —using normalized values for factors (x) in the range from -1 to 1 — was as follows:

$$\hat{y} = \beta_0 + \sum_{i=1}^4 \beta_i x_i + \sum_{i=1}^4 \sum_{j=1}^4 \beta_{ij} x_i x_j + \sum_{i=1}^4 \sum_{j=1}^4 \sum_{k=1}^4 \beta_{ijk} x_i x_j x_k \quad (2)$$

where β_0 , β_i , β_{ij} , β_{ijk} are the intercept, linear, 2-way interaction and 3-way interaction coefficients, respectively. All the statistical calculations were conducted using Minitab software (v17).

3. Results and discussion

3.1. Pyrolysis behavior

Results from proximate, ultimate, and XRF analyses —as well as lignocellulosic constituents— related to the WW feedstock are listed in Table 1. The relatively low content of nitrogen confirms the absence of nitrogen adhesives and/or melamine [27]. However, titanium was found in a non-negligible amount (67.0 mg kg⁻¹ db), probably due to the marginal presence of TiO₂-based paint pigments. In any case, the content of Ti was considerably lower than those reported for treated waste woods (e.g., 1600 [27] and 2140 mg kg⁻¹ db [28]).

From the analysis of the obtained pyrolysis mass loss curves and temperature profiles, it can be underlined that similar conclusions to those previously reported for wheat straw [16] can be drawn. In this regard, an increased pressure enhanced the kinetics of the reactions involved in the overall devolatilization process. For WW, however, kinetics was improved to a lesser extent in comparison with those corresponding to wheat straw, probably due to the lower hemicelluloses content in the WW feedstock, which is the first biomass fraction to

Table 1
Lignocellulosic composition, proximate, ultimate and XRF analyses of WW.

<i>Component (wt. %)</i>	
Hemicelluloses	18.0 ± 0.7
Cellulose	52.3 ± 0.3
Lignin	28.9 ± 0.2
Extractives	0.80 ± 0.2
<i>Proximate (wt. %)</i>	
Ash	0.36 ± 0.05
Moisture	7.61 ± 0.02
Volatile matter	80.2 ± 0.21
Fixed carbon	11.9 ± 0.23
<i>Ultimate (wt. % in daf basis)</i>	
C	45.9 ± 0.07
H	6.36 ± 0.02
N	0.36 ± 0.01
O (by difference)	47.0
<i>Inorganic matter (mg kg⁻¹ in dry basis)</i>	
Ca	400.0 ± 18
K	113.4 ± 5.8
Ti	67.0 ± 3.2
Fe	67.0 ± 3.2
Si	53.3 ± 2.5
S (inorganic)	43.2 ± 2.2
Mn	40.0 ± 2.2
Cl (inorganic)	39.6 ± 1.8
Mg	23.8 ± 2.3
Al	22.0 ± 1.1
Pb	21.9 ± 1.5
Zn	11.9 ± 0.7
Sn	10.6 ± 0.8

thermally decompose. Further details on this study are available in Appendix A.

The mass balance closures and the distributions of the pyrolysis products obtained for each experiment are listed in Table 2. The error in the mass-balance closure (which ranged from 78 % to 92 %) was attributed to the difficulty in accurately determining the mass of produced gas, especially at high carrier gas flow rates. The outcomes from the statistical analyses for the response variables related to the yields of pyrolysis products are given in Table A.2.

Fig. 1 displays the normal probability plots of the standardized effects on the yields of biochar, gas, condensable organics, and produced water. As expected and in line with previous studies [29–31], an increased peak temperature resulted in a lower yield of biochar, due to the higher extent of devolatilization at temperatures higher than 400 °C. To a much lesser extent than peak temperature, using a CO₂-containing carrier gas also led to a decreased yield of biochar. This can probably be ascribed to a slight gasification of the carbonaceous matrix with CO₂. In contrast, an increase in the absolute pressure resulted in a slight increase in y_{char} , probably as a result of the major extent of the secondary charring reactions. At this point, it should be pointed out that apparently contradictory results with regard to the effect of pressure on the yield of char have been reported. For instance, Melligan et al. [32] did not observe any significant correlation, whereas Manyà et al. even reported a slight negative effect of the absolute pressure in some studies [33,34]. A reason for this dissimilarity could be the fact that the present study incorporates the gas residence time as a parametric factor. This allowed us to separate properly the pure effects of the absolute pressure and the gas residence time. Another reason could be the influence of the processed biomass feedstock, especially in terms of biomass constituents and inorganic matter content and composition.

As can also be seen in Fig. 1, higher levels of pressure considerably promoted the yield of produced gas at the expense of the overall condensable products (y_{org} and y_{wat}). This could be explained by an enhancement of secondary reactions at pressurized conditions, with a consequent further consumption of volatiles and a higher release of non-condensable gases [16]. In fact, and as can be deduced from Fig. 1d, the main effect of the absolute pressure on y_{gas} was notably higher than that of the peak temperature. The observed decrease in the yield of produced water (see Fig. 1c) could probably be due to an enhancement of both water gas shift and reforming (of intermediate volatiles) reactions [18]. In addition, an increase in the gas residence time (i.e., lower carrier gas flow rates) positively affected the yields of water and condensable organic compounds at the expense of the produced gas, probably as a

result of a higher extent of both condensation and repolymerization reactions.

Regarding the yields of the main gaseous species released (i.e., CO₂, CO, H₂, and CH₄), some considerations can be drawn from the plot of the effects shown in Fig. A.3. The yield of CO₂ was greatly affected by pressure, which favored decarboxylation of both hemicelluloses and cellulose [17]. The yield of CO was positively affected by both the peak temperature and the presence of CO₂ in the carrier gas, probably as a result of the shift of the Boudouard reaction equilibrium towards CO production. An increased peak temperature also resulted in higher yields of hydrogen and methane, due to the higher extent of both the cracking and dehydrogenation reactions at temperatures higher than 500 °C [16]. Contrary to what was expected, an increased pressure did not result in any significant increase in y_{CH4} . This finding, which was also observed for wheat straw pellets [16], could be explained by the relatively narrow range of pressures applied in our study. For instance, Chen et al. [19] observed a marked increase in the yield of methane when pressure was raised above 1.0 MPa.

3.2. Properties of produced biochars

Table 3 reports the results of response variables related to potential stability (atomic H:C and O:C ratios, as well as the fixed-carbon content, x_{FC}), textural properties (S_{BET} and V_{ultra}), atomic C:N ratio, and pH. Fig. 2 displays the normal probability plots of the standardized effects for each response variable, whereas the regression coefficients of the statistical models are listed in Table A.3.

As can be seen in Fig. 2a, the fixed-carbon content was significantly improved by peak temperature, since its increase led to a higher aromatization of the biochar structure. The lower atomic H:C and O:C ratios measured for the biochars produced at the highest peak temperature confirmed their higher aromaticity (see Fig. 2b and c). The relatively high values of x_{FC} and low values of both the atomic H:C and O:C ratios for biochars produced at 550 °C highlight them as promising recalcitrant carbon sources for soil applications. In addition, Fig. 2d reveals that the absolute pressure was the most influential parameter on y_{FC} . The gas residence time and peak temperature also affected positively y_{FC} , albeit to a lesser extent. The highest fixed-carbon yield was 0.28, which is higher than that obtained for wheat straw pellets in the same range of operating conditions [16]. This can be due to the major content of lignin in the WW feedstock (28.9 vs 18.4 wt. %).

The peak temperature was by far the most influential factor on both the specific surface areas (S_{BET}) and ultra-micropore volumes (V_{ultra}) of

Table 2
Mass balance closures and experimental yields of pyrolysis products.

Factor				Response variable									
T ° C	P MPa	τ s	CO ₂ vol. %	Mass balance closure %	y_{char} mass fraction in dry basis	y_{org}	y_{wat}	y_{gas}	y_{CO2} mol kg ⁻¹ in daf basis	y_{CO}	y_{CH4}	y_{H2}	
550	0.2	200	0	88.9	0.304	0.095	0.302	0.299	4.844	2.345	0.564	0.828	
550	0.9	200	0	86.7	0.315	0.078	0.246	0.360	5.557	2.937	1.341	1.056	
475	0.55	150	30	85.6	0.327	0.083	0.285	0.305	3.765	3.656	1.602	0.414	
550	0.2	100	60	84.6	0.297	0.089	0.302	0.311	3.744	3.610	2.086	0.823	
475	0.55	150	30	83.7	0.323	0.076	0.282	0.320	3.993	3.682	1.765	0.484	
550	0.9	200	60	84.0	0.319	0.072	0.234	0.375	4.977	3.874	2.253	0.762	
400	0.2	200	0	91.5	0.369	0.102	0.254	0.275	4.445	2.275	0.638	0.089	
400	0.2	100	0	91.9	0.369	0.092	0.267	0.271	4.404	2.222	0.631	0.090	
400	0.9	100	0	80.0	0.362	0.056	0.175	0.407	6.642	3.296	0.860	0.223	
550	0.2	100	0	84.2	0.311	0.066	0.224	0.398	5.954	3.228	2.105	0.770	
400	0.9	100	60	78.0	0.357	0.050	0.160	0.433	7.520	2.895	0.851	0.214	
400	0.9	200	60	87.2	0.370	0.066	0.221	0.343	6.033	2.244	0.580	0.121	
550	0.9	100	0	80.5	0.314	0.067	0.189	0.430	6.437	3.708	1.719	1.441	
400	0.9	200	0	85.5	0.369	0.068	0.218	0.345	5.784	2.660	0.517	0.161	
400	0.2	200	60	90.8	0.352	0.108	0.299	0.241	3.319	2.726	0.700	0.122	
550	0.2	200	60	86.0	0.308	0.098	0.308	0.286	2.340	4.452	2.750	0.909	
400	0.2	100	60	88.0	0.352	0.108	0.258	0.282	4.316	2.635	0.774	0.094	
475	0.55	150	30	83.5	0.325	0.078	0.270	0.327	4.282	3.522	1.747	0.467	
550	0.9	100	60	82.7	0.314	0.057	0.194	0.435	6.325	4.248	1.688	0.857	

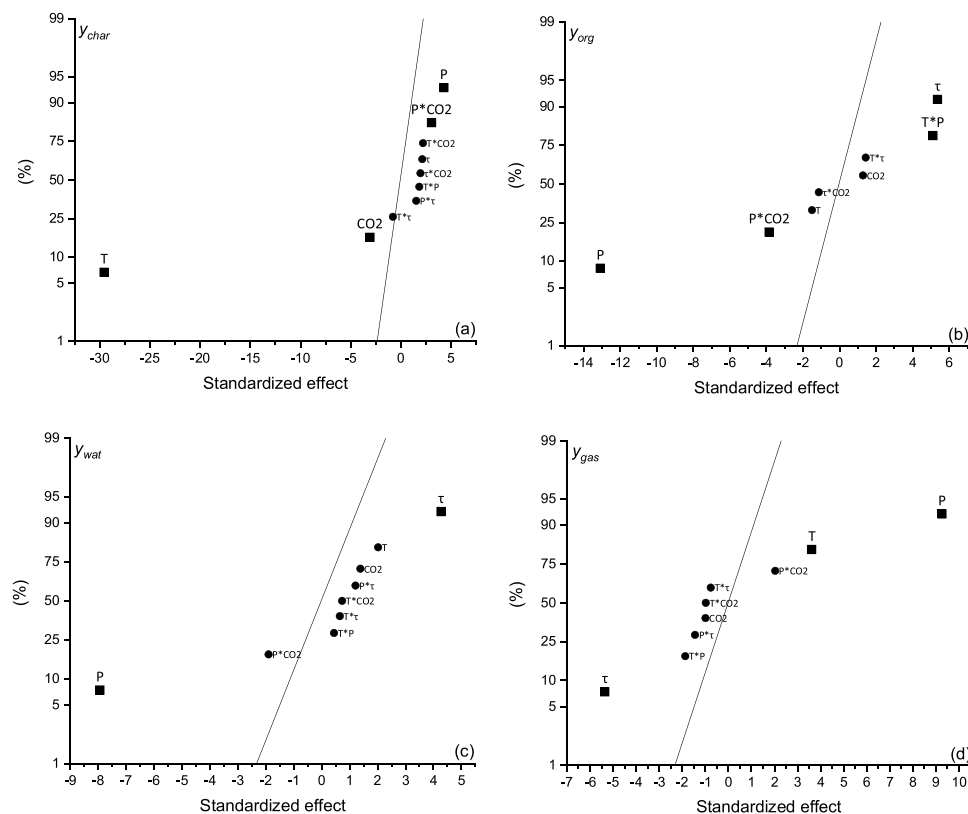


Fig. 1. Normal plot of the standardized effects ($\alpha = 0.05$) for (a) y_{char} , (b) y_{org} , (c) y_{water} , and (d) y_{gas} (square, significant effect; circle, non-significant effect).

Table 3

Physicochemical properties of produced biochars (the subscript “w” refers to the results obtained for water-washed biochars).

Factor				Response variable									
T °C	P MPa	τ s	CO_2 vol. %	H:C —	O:C	C:N	pH	pH_w	x_{FC} wt. %	y_{FC} —	S_{BET} $m^2 g^{-1}$	V_{ultra} $cm^3 g^{-1}$	
550	0.2	200	0	0.434	0.077	78.33	8.20	7.83	84.5	0.255	246	0.062	
550	0.9	200	0	0.388	0.066	85.77	8.36	7.76	86.6	0.271	246	0.063	
475	0.55	150	30	0.511	0.113	71.18	8.40	7.38	75.3	0.244	198	0.046	
550	0.2	100	60	0.377	0.054	76.70	8.36	7.70	85.3	0.250	255	0.064	
475	0.55	150	30	0.483	0.094	75.43	8.41	7.55	78.6	0.251	215	0.051	
550	0.9	200	60	0.356	0.056	76.21	8.42	7.50	88.2	0.279	256	0.067	
400	0.2	200	0	0.603	0.125	82.51	8.44	7.05	69.4	0.255	166	0.036	
400	0.2	100	0	0.640	0.142	71.04	8.34	7.06	68.5	0.251	159	0.034	
400	0.9	100	0	0.584	0.118	76.28	8.39	6.99	71.4	0.257	171	0.038	
550	0.2	100	0	0.415	0.073	73.97	8.42	7.30	83.4	0.256	242	0.060	
400	0.9	100	60	0.593	0.122	76.47	8.31	7.27	70.8	0.252	173	0.039	
400	0.9	200	60	0.616	0.131	78.60	8.29	6.76	69.3	0.256	163	0.036	
550	0.9	100	0	0.396	0.060	72.36	8.39	7.29	83.7	0.261	240	0.060	
400	0.9	200	0	0.586	0.117	83.04	8.42	6.73	73.0	0.269	172	0.038	
400	0.2	200	60	0.582	0.114	76.00	8.52	7.25	73.0	0.256	170	0.038	
550	0.2	200	60	0.428	0.103	76.88	8.35	7.76	85.4	0.261	243	0.091	
400	0.2	100	60	0.602	0.111	58.17	8.40	7.26	68.8	0.241	175	0.038	
475	0.55	150	30	0.475	0.087	73.06	8.40	7.77	79.2	0.256	218	0.052	
550	0.9	100	60	0.328	0.042	71.94	8.43	7.52	87.0	0.273	270	0.070	

the resulting biochars (see the corresponding plots of the effects in Fig. A.4). Higher temperatures induced a more extended thermal degradation of biomass, resulting in the formation of new pores. At a much lesser extent than temperature, feeding CO_2 in the pyrolysis reactor also positively influenced the development of ultra-micropores, as a consequence of the above-mentioned slight gasification. On the other hand, it is important to note that the influence of the absolute pressure resulted to be negligible on the porosity development in the range of 0.2–0.9 MPa, in contrast to the negative effects that were reported in the literature [32,35]. This encouraging result suggests that

pressurized pyrolysis at relatively low temperatures could be feasible for the production of engineered biochars with an ameliorated carbon sequestration potential without altering their porosity development.

From Table 3, it can be seen that biochars resulted to be moderately basic, since the values of pH were comprised between 8.20 and 8.52, which may indicate the availability of a certain level of both macro- and micro-nutrients [36], having been concentrated in the biochar matrix during the pyrolysis process. These pH values dropped down to 6.73–7.83 for water-washed biochars. This could be mainly ascribed to the loss of some water-soluble basic species (e.g., salts and minerals).

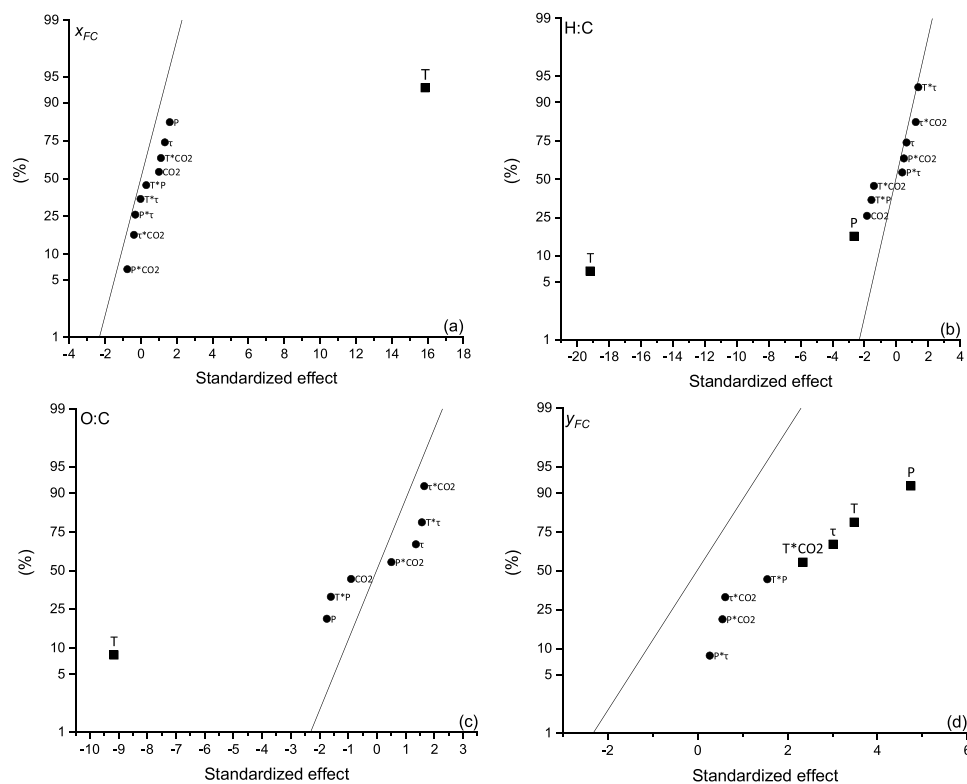


Fig. 2. Normal plots of the standardized effects ($\alpha = 0.05$) for (a) x_{FC} , (b) atomic H:C ratio, (c) atomic O:C ratio, and (d) y_{FC} (square, significant effect; circle, non-significant effect).

From the normal plot of the effects shown in Fig. A.5a, it can be deduced a significant interaction effect between peak temperature and pressure, which results in an increase in pH at the highest levels of both factors. This finding could probably be due to an enhanced consumption of volatiles (which typically show an acidic nature [6]) through secondary reactions. By contrast, the interaction effect between the gas residence time and peak temperature led to lower values of pH, likely due to the major extent of recondensation reactions at longer vapor residence times.

On the other hand, the atomic C:N ratio was mainly (and positively) affected by the gas residence time (see the corresponding plot of the effects in Fig. A.5b), probably due to a higher release of nitrogen-containing volatile compounds. All the biochars produced in this study showed atomic C:N ratios much higher than the threshold value of 30, indicating their high suitability for the mitigation of N_2O emissions from soil [37,38].

3.3. PAHs contents in biochars

Table 4 lists the PAHs contents and TTEC values of produced biochars (the regression coefficients of the statistical models are reported in Table A.4). For its part, Fig. 3 shows the normal probability plots of the effects of the selected factors on the PAHs contents. As can be seen in Fig. 3a, an increase in either the peak temperature or the absolute pressure led to a marked decrease in the concentration of total PAHs. Within the available literature, no clear consensus exists on the influence of pyrolysis peak temperature on PAHs content in biochar. For instance, Kloss et al. [39] did not observe any correlation in the range of 400 – 525 °C for wheat straw, poplar wood, and spruce wood biochars; however, Rogovska et al. [40] reported an increase in the PAHs contents with temperature (in the range between 450 and 850 °C) for biochars obtained from hardwood, corn and switchgrass. Nevertheless, the studies by Brown et al. [9] and Freddo et al. [41] yielded the opposite trend at temperatures ranging from 300 to 1000 °C. To explain these

apparently contradictory results, it is important to note that the total PAHs content takes into account all the processes involved in the formation and consumption of PAHs, which occurred at the solid-vapor interphase throughout different temperature phases in fast/slow succession until the peak temperature was reached [8]. In other words, PAHs may turn into lower molecular weight PAHs by breakage (which can subsequently be desorbed from the solid surface [42]) or into higher molecular weight PAHs through condensation and polymerization reactions [43,44]. Depending on the pyrolysis reactor configuration, operating process conditions and type of feedstock, different extents of the above-cited PAHs conversion pathways could be expected. In the present study, the highest PAHs content was reached at the lowest temperature level (400 °C), suggesting that conversion of PAH compounds toward lighter hydrocarbons was promoted by temperature.

At a first glance, the statistically significant negative effect of the absolute pressure on the total PAHs content could appear in disagreement with previous studies [45]. However, it might be explained by the relatively high carrier gas flow rates employed in order to ensure the proper gas residence time, which massively diluted the reaction environment, reducing the vapor-solid interaction and, consequently, preventing condensation and polymerization reactions and enhancing desorption of low-weight PAHs. Furthermore, a combined effect of the gas residence time and the presence of CO_2 in the carrier gas led to a slight increase in the total PAHs content. This appears to be in line with the findings reported in an earlier study [46].

The effects of factors on the contents of low-molecular weight PAHs (the sum of naphthalene, acenaphthylene, acenaphthene and fluorene contents, *PAH light* in Fig. 3b), medium-molecular weight PAHs (the sum of phenanthrene, anthracene and fluoranthene contents, *PAH medium* in Fig. 3c), and high-molecular weight PAHs (the sum of pyrene, benzo[a]anthracene and chrysene contents, *PAH heavy* in Fig. 3d) were also assessed. The criterion used to classify the PAH species in the three as-mentioned fractions was based on the number of aromatic rings in their structures, being this fact responsible for most of their

Table 4
16 EPA PAH contents and TTEC values for each biochar (see the Nomenclature section for abbreviations). "N.D." (not determined) refers to the PAH peaks visible but under quantification limit, whereas "n.d." (not detected) refers to those under the detection limit.

Factor	PAH content																						
	T °C	P MPa	τ s	CO ₂ vol. %	MAP $\mu\text{g kg}^{-1}$ biochar, db	%Amnotation-xml content;	ANA	FLU	PHE	ANT	FLT	PYR	BaA	CHR	BbF	BkF	BaP	IPY	DBA	BPE	Total	TTEC	
550	0.2	0.2	200	0	2344	n.d.	599	110	298	58	85	95	12	18	n.d.	n.d.	n.d.	n.d.	n.d.	n.d.	n.d.	3619	5.46
550	0.9	0.2	200	0	1901	n.d.	662	122	247	1034	70	46	N.D.	N.D.	n.d.	n.d.	n.d.	n.d.	n.d.	n.d.	n.d.	4083	14.18
475	0.55	150	30	30	3245	n.d.	775	271	396	74	107	65	28	50	n.d.	n.d.	n.d.	n.d.	n.d.	n.d.	n.d.	5010	8.85
550	0.2	100	60	30	2312	n.d.	787	179	477	110	114	72	N.D.	N.D.	n.d.	n.d.	n.d.	n.d.	n.d.	n.d.	n.d.	4051	5.53
475	0.55	150	30	30	2714	n.d.	774	217	618	133	127	102	47	72	n.d.	n.d.	n.d.	n.d.	n.d.	n.d.	n.d.	4804	11.33
550	0.9	200	60	60	1884	n.d.	632	149	296	110	75	50	n.d.	n.d.	n.d.	n.d.	n.d.	n.d.	n.d.	n.d.	n.d.	3197	4.19
400	0.2	200	0	0	1543	388	656	219	1180	137	427	392	54	75	n.d.	n.d.	n.d.	n.d.	n.d.	n.d.	n.d.	5071	12.37
400	0.2	100	0	0	1809	665	696	174	790	94	364	348	92	136	n.d.	n.d.	n.d.	n.d.	n.d.	n.d.	n.d.	5168	16.38
400	0.9	100	0	0	2367	416	485	278	747	82	151	130	89	114	n.d.	n.d.	n.d.	n.d.	n.d.	n.d.	n.d.	4860	15.45
550	0.2	100	0	0	3455	n.d.	598	127	410	66	128	70	10	22	n.d.	n.d.	n.d.	n.d.	n.d.	n.d.	n.d.	4886	6.70
400	0.9	100	60	60	1972	n.d.	735	145	438	118	147	113	43	71	n.d.	n.d.	n.d.	n.d.	n.d.	n.d.	n.d.	3782	9.76
400	0.9	200	60	60	2123	219	748	177	649	98	229	187	101	145	n.d.	n.d.	n.d.	n.d.	n.d.	n.d.	n.d.	4677	16.90
550	0.9	100	0	0	1717	n.d.	764	182	415	150	74	104	N.D.	15	n.d.	n.d.	n.d.	n.d.	n.d.	n.d.	n.d.	3421	5.19
400	0.9	200	0	0	1155	517	454	130	545	60	200	194	88	130	n.d.	n.d.	n.d.	n.d.	n.d.	n.d.	n.d.	3474	13.91
400	0.2	200	60	60	2103	362	632	291	1092	341	304	298	66	93	n.d.	n.d.	n.d.	n.d.	n.d.	n.d.	n.d.	5583	16.05
550	0.2	200	60	60	2380	n.d.	444	97	352	61	114	59	n.d.	14	n.d.	n.d.	n.d.	n.d.	n.d.	n.d.	n.d.	3522	4.20
400	0.2	100	60	60	1677	646	603	159	731	109	219	211	57	72	n.d.	n.d.	n.d.	n.d.	n.d.	n.d.	n.d.	4484	11.77
475	0.55	150	30	30	2464	n.d.	715	200	541	132	102	84	27	46	n.d.	n.d.	n.d.	n.d.	n.d.	n.d.	n.d.	4310	8.60
550	0.9	100	60	60	1987	n.d.	440	220	298	307	70	59	n.d.	n.d.	n.d.	n.d.	n.d.	n.d.	n.d.	n.d.	n.d.	3379	6.18

physicochemical properties [47]. It was observed that, among the three fractions, PAH light resulted to be the most affected by pressure, which seemed to promote further decomposition and desorption of PAH compounds and/or partly inhibit their formation. It is important to note that PAH light was the most abundant fraction in the produced biochars. On the other side, the operating parameter that mostly affected (negatively) both the PAH medium and PAH heavy groups was the peak temperature, whereas the effect of pressure was very low or even negligible for PAH medium and PAH heavy, respectively.

From the PAHs concentrations listed in Table 4, it can be seen that a highest value of 5583 $\mu\text{g kg}^{-1}$ was measured for the biochar produced at 400 °C, 0.2 MPa and 200 s, while the lowest value (3197 $\mu\text{g kg}^{-1}$) corresponded to the biochar produced at 550 °C, 0.9 MPa and 100 s. In both cases, a CO₂-containing carrier gas (60 vol. %) was used. From Table 4, it is also possible to observe that PAH compounds having ring structures more complex than chrysene were not detected for the range of operating conditions adopted in the present work. According to the European Biochar Certificate (EBC) guidelines [3], half of the produced biochars exceeded the limit concentration (4000 $\mu\text{g kg}^{-1}$) allowed for being considered as premium biochars. However, assuming the recommendations made by the International Biochar Initiative (IBI) [4], all the produced biochars can be marked as premium quality ones (i.e., PAHs content below 6000 $\mu\text{g kg}^{-1}$).

Concerning the TTEC values (which ranged from 4.19 to 16.9 $\mu\text{g kg}^{-1}$), the pyrolysis peak temperature was the most influential factor, leading to a marked decrease in this response variable when temperature was increased (see Fig. 3e). The effect of the absolute pressure was negligible in this case. These findings were perfectly in line with the considerations reported above, especially with those related to PAH medium and PAH heavy fractions, which represent the most toxic classes of PAHs.

The PAHs assessment was also conducted for water-washed biochars. As expected, the measured total PAHs contents (as well as those corresponding to the light, medium and heavy PAH fractions) were the same than those obtained for the unwashed biochars and, therefore, they are not reported herein.

3.4. Germination response

Once it has been ensured that the produced biochars had relatively low contents of hazardous PAH compounds, a germination assessment was performed to assess their short-term phytotoxicity. The germination index (calculated as in Eq. (1)) lower than 50 % indicates a high level of phytotoxicity, values comprised between 50 % and 80 % are representative of moderate phytotoxicity, whereas a lack of phytotoxicity is accomplished when *GI* falls between 80 % and 100 % [25]. Furthermore, the biochar could be defined as phytostimulant or phytonutrient when *GI* values exceed 100 %.

Table 5 shows the *GI* values obtained for the tested species (see Table A.5 for model regression coefficients). The germination response for barley was very sensitive to the pyrolysis operating conditions, showing a relatively wide response window: from low phytotoxicity (51.4 % as the lowest value) to moderate phytostimulation (up to 157 %). From Fig. 4a, it can be deduced a significant (and positive) interaction effect between peak temperature and pressure. The increase in *GI* when both factors were kept at their highest level could be explained by the relatively low contents of PAHs (as discussed above) as well as the higher extent of secondary reactions, which are promoted by either temperature or pressure and result in a higher consumption of volatile organic compounds. On the opposite side, the interaction effect between peak temperature and gas residence time on *GI* for barley was negative. This could be related to the higher contents of PAHs measured for biochars produced at the highest level of gas residence time.

Regarding the germination of watercress, the most part of the produced biochars resulted to be highly phytotoxic, regardless of the operating conditions adopted during pyrolysis (see Table 5). A possible

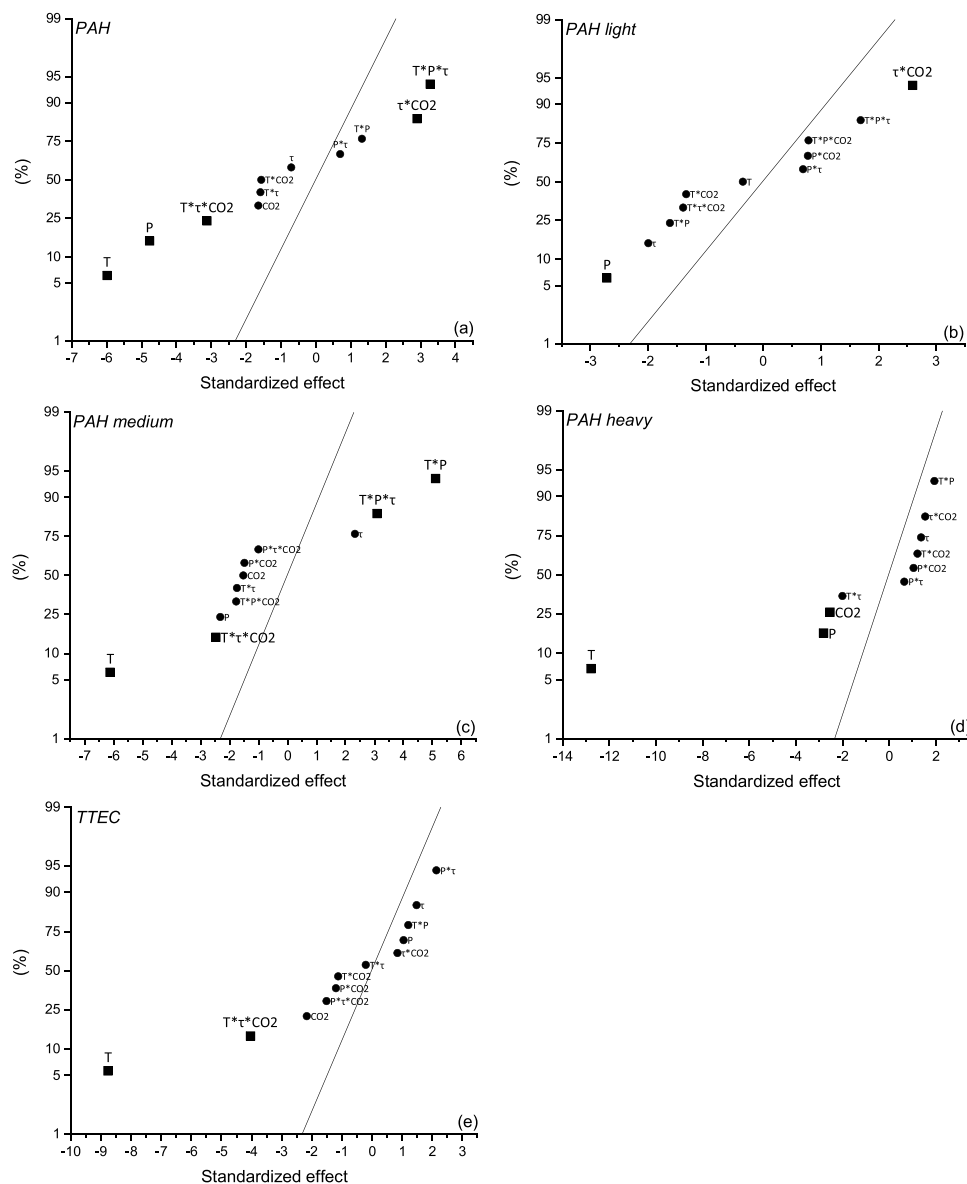


Fig. 3. Normal plots of the standardized effects ($\alpha = 0.05$) for (a) total PAHs content, (b) low molecular weight PAHs content, (c) medium molecular weight PAHs content, (d) high molecular weight PAHs content, and (e) TTEC (square, significant effect; circle, non-significant effect).

reason behind this could be the high sensitivity of watercress to the biochar ash content, which can cause salt stress in the plant [48]. As can be seen in Fig. 4b, an increased peak temperature resulted in lower *GI* values, whereas the absolute pressure had a positive effect on the germination response.

For basil, germination resulted to be the less sensitive to the different pyrolysis conditions. In fact, no significant effects were detected for any of the main or 2-way interaction effects assessed, as shown in Fig. 4c. The observed variability in the *GI* values (from 61.0% to 139.5%) was then mainly explained by factors outside the regression model.

As can also be observed from the data reported in Table 4, the levels of phytotoxicity were noticeably reduced after washing the biochars, especially in the case of watercress, for which outstanding values of *GI* (up to 228.8 %) were measured. An improvement in the germination behavior was also observed for barley. However, the effect of washing biochar on the germination response of basil was unclear (i.e., no evident trend can be deduced). Results from the germination assessment seem to suggest that PAHs were not the only ones responsible for the short-term phytotoxic effects related to biochars. In fact, and as suggested by Buss et al. [49], the co-occurrence of low-molecular weight

organic acids and phenolic compounds, which have high mobility and can be removed relatively easily by water washing, could partly explain the above-mentioned phytotoxic effects of biochars. In any case, the water washing pretreatment for wood waste-derived biochars appears to be a highly useful and low-cost means of diminishing their potential toxicity for soil application purposes.

4. Conclusions

Some useful considerations can be drawn from the results shown and discussed above:

- The total PAHs content in the produced biochars can be significantly reduced by increasing either the peak temperature or the absolute pressure (ideally both). The extent of PAHs volatilization could be promoted at higher temperatures, while an increased pressure (at high flow rates of carrier gas) could partly inhibit repolymerization and recondensation reactions (which lead to PAHs formation). Generally speaking, the resulting wood waste-derived biochars were

Table 5

GI values for watercress, barley, and basil. The subscript “w” refers to the results obtained when washed biochars were tested.

Factor				Germination index (GI)					
T	P	τ	CO2	GI barley	GI watercress	GI basil	GI _w barley	GI _w watercress	GI _w basil
°C	MPa	s	vol. %	%					
550	0.2	200	0	98.50	24.76	118.6	157.9	129.7	99.80
550	0.9	200	0	90.39	42.21	91.56	143.0	115.1	75.56
475	0.55	150	30	103.0	36.18	93.80	185.2	124.2	77.15
550	0.2	100	60	74.77	43.06	105.8	212.3	85.28	170.4
475	0.55	150	30	75.38	14.82	139.5	100.8	155.8	86.37
550	0.9	200	60	62.76	50.97	78.61	41.36	86.79	81.97
400	0.2	200	0	134.5	44.08	62.79	91.93	165.7	95.13
400	0.2	100	0	90.09	46.85	121.0	57.21	228.8	136.7
400	0.9	100	0	51.35	50.99	117.6	99.09	183.8	85.25
550	0.2	100	0	87.39	35.59	77.21	117.8	99.07	144.1
400	0.9	100	60	68.47	58.11	103.1	143.5	90.15	141.6
400	0.9	200	60	69.07	67.49	100.4	136.8	198.5	122.2
550	0.9	100	0	78.08	41.49	61.03	196.9	203.0	126.5
400	0.9	200	0	101.8	69.60	73.76	66.32	121.9	78.02
400	0.2	200	60	136.0	48.04	104.8	144.1	105.0	72.39
550	0.2	200	60	75.08	29.64	74.72	222.8	180.5	53.94
400	0.2	100	60	83.78	49.68	118.6	39.72	100.6	110.8
475	0.55	150	30	70.57	32.60	111.7	84.76	72.07	161.0
550	0.9	100	60	157.1	64.98	99.27	104.2	79.37	79.35

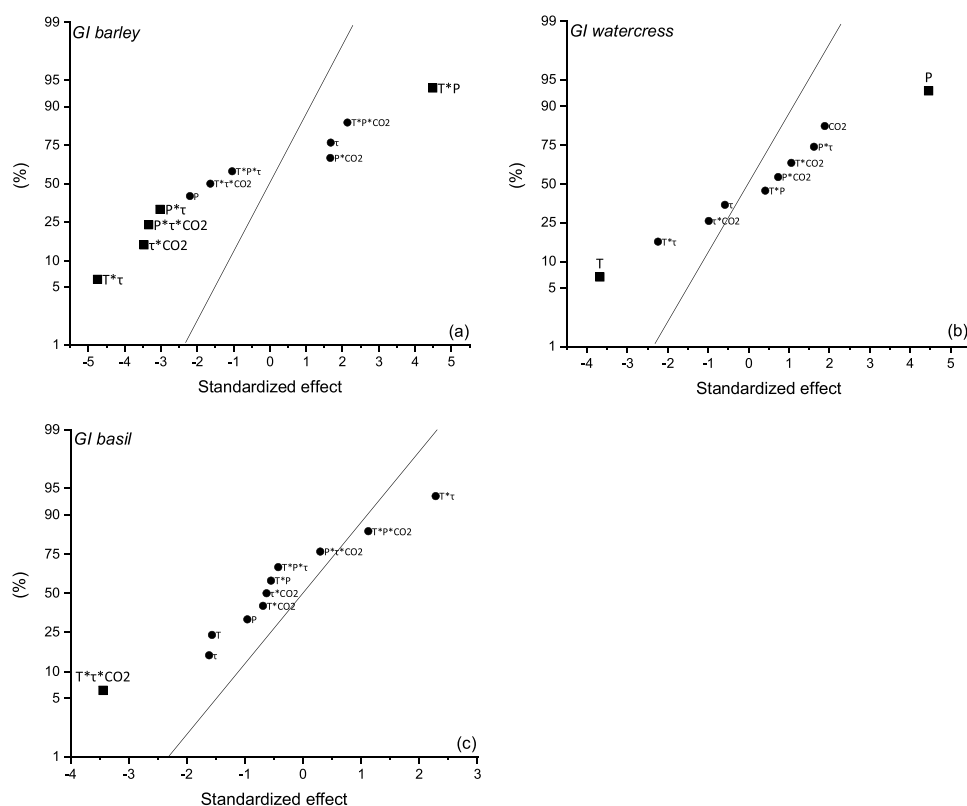


Fig. 4. Normal plots of standardized effects ($\alpha = 0.05$) for the germination index (GI) of (a) barley, (b) watercress, and (c) basil (square, significant effect; circle, non-significant effect).

of good quality in terms of PAH hazard, making them suitable for soil amendment purposes.

- The phytotoxic or phytostimulant effect of wood waste-derived biochar depended mainly on the process pyrolysis conditions as well as the seed species considered for the germination assay. In any case, germination indices notably increased (in some cases from phytotoxic to phytostimulant responses) when biochars were washed with water before being tested. This suggests that the acute phytotoxicity observed for some biochars can be ascribed to water-soluble acidic and phenolic compounds.

- From an applied research point of view, pressurized slow pyrolysis (at a moderate peak temperature of 550 °C and relatively high carrier gas flow rates) followed by an inexpensive water washing step appears as an interesting pathway to produce premium-quality and value-added biochars from wood waste.

CRediT authorship contribution statement

Gianluca Greco: Conceptualization, Methodology, Software, Validation, Formal analysis, Investigation, Data curation, Writing - original

draft. **María Videgain:** Data curation, Methodology, Investigation, Resources. **Christian Di Stasi:** Data curation, Methodology, Investigation, Resources. **Elisabet Pires:** Data curation, Methodology, Software, Validation, Investigation, Resources, Writing - review & editing, Supervision. **Joan J. Manyà:** Resources, Writing - review & editing, Visualization, Supervision, Project administration.

Declaration of Competing Interest

The authors declare that they have no known competing financial interests or personal relationships that could have appeared to influence the work reported in this paper.

Acknowledgements

This project has received funding from the European Union's Horizon 2020 research and innovation program under the Marie Skłodowska-Curie grant agreement No 721991. JJM and EP also acknowledge the funding from the Aragón Government (Refs. T22_20R and E37_20R, respectively), co-funded by FEDER 2014-2020 "Construyendo Europa desde Aragón". EP acknowledges the Spanish Ministerio de Ciencia, Innovación y Universidades (project number RTI2018-093431-B-I00). The authors gratefully thank the ISQCH Chromatography Service, José Antonio Manso and Eugenio Vispe Palacín for their help in the preparation and characterization of the samples.

Appendix A. Supplementary data

Supplementary material related to this article can be found, in the online version, at doi:<https://doi.org/10.1016/j.jaap.2021.105337>.

References

- S. Chandra, J. Bhattacharya, Influence of temperature and duration of pyrolysis on the property heterogeneity of rice straw biochar and optimization of pyrolysis conditions for its application in soils, *J. Clean. Prod.* 215 (2019) 1123–1139, <https://doi.org/10.1016/j.jclepro.2019.01.079>.
- European Commission Regulation (ECR) No 1881/2006, Setting Maximum Levels for Certain Contaminants in Foodstuffs, 2006. <https://eur-lex.europa.eu/homepage.html>.
- European Biochar Certificate (EBC), European Biochar Certificate – Guidelines for a Sustainable Production of Biochar, Arbaz, Switzerland, 2019, <https://www.european-biochar.org/biochar/media/doc/ebc-guidelines.pdf>.
- IBI, Standardized Product Definition and Product Testing Guidelines for Biochar that is Used in Soil, 2015. <https://biochar-international.org/>.
- H.P. Schmidt, I. Hilber, T.D. Bucheli, Polycyclic aromatic hydrocarbons and polychlorinated aromatic compounds in biochar. *Biochar Environ. Manag.*, 2nd edition, Routledge, London, 2015, p. 30.
- C. Wang, Y. Wang, H.M.S.K. Herath, Polycyclic aromatic hydrocarbons (PAHs) in biochar – their formation, occurrence and analysis: a review, *Org. Geochem.* 114 (2017) 1–11, <https://doi.org/10.1016/j.orggeochem.2017.09.001>.
- D. Fabbri, A.G. Rombolà, C. Torri, K.A. Spokas, Determination of polycyclic aromatic hydrocarbons in biochar and biochar amended soil, *J. Anal. Appl. Pyrolysis* 103 (2013) 60–67, <https://doi.org/10.1016/j.jaap.2012.10.003>.
- W. Buss, M.C. Graham, G. MacKinnon, O. Mašek, Strategies for producing biochars with minimum PAH contamination, *J. Anal. Appl. Pyrolysis* 119 (2016) 24–30, <https://doi.org/10.1016/j.jaap.2016.04.001>.
- R.A. Brown, A.K. Kercher, T.H. Nguyen, D.C. Nagle, W.P. Ball, Production and characterization of synthetic wood chars for use as surrogates for natural sorbents, *Org. Geochem.* 37 (2006) 321–333, <https://doi.org/10.1016/j.orggeochem.2005.10.008>.
- S.E. Hale, J. Lehmann, D. Rutherford, A.R. Zimmerman, R.T. Bachmann, V. Shitumbanuma, A. O'Toole, K.L. Sundqvist, H.P.H. Arp, G. Cornelissen, Quantifying the total and bioavailable polycyclic aromatic hydrocarbons and dioxins in biochars, *Environ. Sci. Technol.* 46 (2012) 2830–2838, <https://doi.org/10.1021/es203984k>.
- B.R.T. Simoneit, Biomarker PAHs in the environment. PAHs Relat. Compd. Handb. Environ. Chem. (Anthropogenic Compd.), Springer, Berlin, Heidelberg, 1998, https://doi.org/10.1007/978-3-540-49697-7_5.
- J.M. De la Rosa, H. Knicker, E. López-Capel, D.A.C. Manning, J.A. González-Perez, F.J. González-Vila, Direct detection of black carbon in soils by Py-GC/MS, carbon-13 NMR spectroscopy and thermogravimetric techniques, *Soil Sci. Soc. Am. J.* 72 (2008) 258–267, <https://doi.org/10.2136/sssaj2007.0031>.
- M.J. Antal, S.G. Allen, X. Dai, B. Shimizu, M.S. Tam, M. Gronli, Attainment of the theoretical yield of carbon from biomass, *Ind. Eng. Chem. Res.* 39 (2000) 4024–4031, <https://doi.org/10.1021/ie000511u>.
- J. Madej, I. Hilber, T.D. Bucheli, P. Oleszczuk, Biochars with low polycyclic aromatic hydrocarbon concentrations achievable by pyrolysis under high carrier gas flows irrespective of oxygen content or feedstock, *J. Anal. Appl. Pyrolysis* 122 (2016) 365–369, <https://doi.org/10.1016/j.jaap.2016.09.005>.
- G. Greco, M. Videgain, C. Di Stasi, B. González, J.J. Manyà, Evolution of the mass-loss rate during atmospheric and pressurized slow pyrolysis of wheat straw in a bench-scale reactor, *J. Anal. Appl. Pyrolysis* 136 (2018) 18–26, <https://doi.org/10.1016/j.jaap.2018.11.007>.
- G. Greco, C. Di Stasi, F. Rego, B. González, J.J. Manyà, Effects of slow-pyrolysis conditions on the products yields and properties and on energy efficiency: a comprehensive assessment for wheat straw, *Appl. Energy* 279 (2020), 115842, <https://doi.org/10.1016/j.apenergy.2020.115842>.
- Y. Qian, J. Zhang, J. Wang, Pressurized pyrolysis of rice husk in an inert gas sweeping fixed-bed reactor with a focus on bio-oil deoxygenation, *Bioresour. Technol.* 174 (2014) 95–102, <https://doi.org/10.1016/j.biortech.2014.10.012>.
- F. Ates, N. Miskolczi, B. Saricaoglu, Pressurized pyrolysis of dried distillers grains with solubles and canola seed press cake in a fixed-bed reactor, *Bioresour. Technol.* 177 (2015) 149–158, <https://doi.org/10.1016/j.biortech.2014.10.163>.
- Y. Chen, L. Zhang, Y. Zhang, A. Li, Pressurized pyrolysis of sewage sludge: process performance and products characterization, *J. Anal. Appl. Pyrolysis* 139 (2019) 205–212, <https://doi.org/10.1016/j.jaap.2019.02.007>.
- M. Azuara, E. Sáiz, J.A. Manso, F.J. García-Ramos, J.J. Manyà, Study on the effects of using a carbon dioxide atmosphere on the properties of vine shoots-derived biochar, *J. Anal. Appl. Pyrolysis* 124 (2017) 719–725, <https://doi.org/10.1016/j.jaap.2016.11.022>.
- U. Mantau, Wood Flows in Europe (EU 27), Proj. Report, Comm. by CEPI (Confederation Eur. Pap. Ind.) CEI-Bois (European Confed. Woodwork. Ind.), 2012.
- G. Faraca, A. Boldrin, T. Astrup, Resource quality of wood waste: the importance of physical and chemical impurities in wood waste for recycling, *Waste Manage.* 87 (2019) 135–147, <https://doi.org/10.1016/j.wasman.2019.02.005>.
- J.M. De la Rosa, Á.M. Sánchez-Martín, P. Campos, A.Z. Miller, Effect of pyrolysis conditions on the total contents of polycyclic aromatic hydrocarbons in biochars produced from organic residues: assessment of their hazard potential, *Sci. Total Environ.* 667 (2019) 578–585, <https://doi.org/10.1016/j.scitotenv.2019.02.421>.
- N.-D. Dat, M.B. Chang, Review on characteristics of PAHs in atmosphere, anthropogenic sources and control technologies, *Sci. Total Environ.* 609 (2017) 682–693, <https://doi.org/10.1016/j.scitotenv.2017.07.204>.
- C. Liang, G. Gascó, S. Fu, A. Méndez, J. Paz-Ferreiro, Biochar from pruning residues as a soil amendment: effects of pyrolysis temperature and particle size, *Soil Tillage Res.* 164 (2016) 3–10, <https://doi.org/10.1016/j.still.2015.10.002>.
- D.S. Montgomery, Design and Analysis of Experiments, 6th edition, John Wiley & Sons, New York, 2005.
- A.I. Moreno, R. Font, Pyrolysis of furniture wood waste: decomposition and gases evolved, *J. Anal. Appl. Pyrolysis* 113 (2015) 464–473, <https://doi.org/10.1016/J.JAAP.2015.03.008>.
- H.J. Gehrmann, H. Mätzing, P. Nowak, D. Baris, H. Seifert, C. Dupont, F. Defoort, M. Peyrot, F. Castagno, Waste wood characterization and combustion behaviour in pilot lab scale, *J. Energy Inst.* 93 (2020) 1634–1641, <https://doi.org/10.1016/J.JOEI.2020.02.001>.
- C. Di Blasi, G. Signorelli, C. Di Russo, G. Rea, Product distribution from pyrolysis of wood and agricultural residues, *Ind. Eng. Chem. Res.* 38 (1999) 2216–2224, <https://doi.org/10.1021/ie980711u>.
- L. Zhao, X. Cao, O. Mašek, A. Zimmerman, Heterogeneity of biochar properties as a function of feedstock sources and production temperatures, *J. Hazard. Mater.* 256–257 (2013) 1–9, <https://doi.org/10.1016/j.jhazmat.2013.04.015>.
- A.V. McBeath, C.M. Wurster, M.I. Bird, Influence of feedstock properties and pyrolysis conditions on biochar carbon stability as determined by hydrogen pyrolysis, *Biomass Bioenergy* 73 (2015) 155–173, <https://doi.org/10.1016/j.biombioe.2014.12.022>.
- F. Melligan, R. Aucaisse, E.H. Novotny, J.J. Leahy, M.H.B. Hayes, W. Kwapinski, Pressurized pyrolysis of Miscanthus using a fixed bed reactor, *Bioresour. Technol.* 102 (2011) 3466–3470, <https://doi.org/10.1016/j.biortech.2010.10.129>.
- J.J. Manyà, F.X. Roca, J.F. Perales, TGA study examining the effect of pressure and peak temperature on biochar yield during pyrolysis of two-phase olive mill waste, *J. Anal. Appl. Pyrolysis* 103 (2013) 86–95, <https://doi.org/10.1016/j.jaap.2012.10.006>.
- J.J. Manyà, S. Laguarda, M.A. Ortigosa, J.A. Manso, Biochar from slow pyrolysis of two-phase olive mill waste: effect of pressure and peak temperature on its potential stability, *Energy Fuels* 28 (2014) 3271–3280, <https://doi.org/10.1021/ef500654t>.
- E. Cetin, B. Moghtaderi, R. Gupta, T. Wall, Influence of pyrolysis conditions on the structure and gasification reactivity of biomass chars, *Fuel* 83 (2004) 2139–2150, <https://doi.org/10.1016/J.FUEL.2004.05.008>.
- L. Bouqbis, S. Daoud, H.W. Koyro, C.I. Kammann, F.Z. Ainhout, M.C. Harrouni, Phytotoxic effects of argan shell biochar on salad and barley germination, *Agric. Nat. Resour.* 51 (2017) 247–252, <https://doi.org/10.1016/j.anres.2017.04.001>.
- M.L. Cayuela, L. van Zwieten, B.P. Singh, S. Jeffery, A. Roig, M.A. Sánchez-Monedero, Biochar's role in mitigating soil nitrous oxide emissions: a review and meta-analysis, *Agric. Ecosyst. Environ.* 191 (2014) 5–16, <https://doi.org/10.1016/j.agee.2013.10.009>.
- P. Brassard, S. Godbout, V. Raghavan, Soil biochar amendment as a climate change mitigation tool: key parameters and mechanisms involved, *J. Environ. Manage.* 181 (2016) 484–497, <https://doi.org/10.1016/j.jenvman.2016.06.063>.
- S. Kloss, F. Zehetner, A. Dellantonio, R. Hamid, F. Ottner, V. Liedtke, M. Schwanninger, M.H. Gerzabek, G. Soja, Characterization of slow pyrolysis biochars: effects of feedstocks and pyrolysis temperature on biochar properties, *J. Environ. Qual.* 41 (2012) 990–1000, <https://doi.org/10.2134/jeq2011.0070>.

- [40] N. Rogovska, D. Laird, R.M. Cruse, S. Trabue, E. Heaton, Germination tests for assessing biochar quality, *J. Environ. Qual.* 41 (2012) 1014–1022, <https://doi.org/10.2134/jeq2011.0103>.
- [41] A. Freddo, C. Cai, B.J. Reid, Environmental contextualisation of potential toxic elements and polycyclic aromatic hydrocarbons in biochar, *Environ. Pollut.* 171 (2012) 18–24, <https://doi.org/10.1016/j.envpol.2012.07.009>.
- [42] T. McGrath, R. Sharma, M. Hajjaligol, An experimental investigation into the formation of polycyclic-aromatic hydrocarbons (PAH) from pyrolysis of biomass materials, *Fuel* 80 (2001) 1787–1797, [https://doi.org/10.1016/S0016-2361\(01\)00062-X](https://doi.org/10.1016/S0016-2361(01)00062-X).
- [43] M. Keiluweit, M. Kleber, M.A. Sparrow, B.R.T. Simoneit, F.G. Prah, Solvent-extractable polycyclic aromatic hydrocarbons in biochar: influence of pyrolysis temperature and feedstock, *Environ. Sci. Technol.* 46 (2012) 9333–9341, <https://doi.org/10.1021/es302125k>.
- [44] R.K. Sharma, M.R. Hajjaligol, Effect of pyrolysis conditions on the formation of polycyclic aromatic hydrocarbons (PAHs) from polyphenolic compounds, *J. Anal. Appl. Pyrolysis* 66 (2003) 123–144, [https://doi.org/10.1016/S0165-2370\(02\)00109-2](https://doi.org/10.1016/S0165-2370(02)00109-2).
- [45] T. Matamba, A. Tahmasebi, S. Khoshk Rish, J. Yu, Promotion effects of pressure on polycyclic aromatic hydrocarbons and H₂ formation during flash pyrolysis of palm kernel shell, *Energy Fuels* 34 (2020) 3346–3356, <https://doi.org/10.1021/acs.energyfuels.9b04409>.
- [46] Q. Chang, R. Gao, H. Li, G. Yu, F. Wang, Effect of CO₂ on the characteristics of soot derived from coal rapid pyrolysis, *Combust. Flame* 197 (2018) 328–339, <https://doi.org/10.1016/j.combustflame.2018.05.033>.
- [47] C. Achten, J.T. Andersson, Overview of polycyclic aromatic compounds (PAC), *Polycyclic Aromat. Compd.* 35 (2015) 177–186, <https://doi.org/10.1080/10406638.2014.994071>.
- [48] W. Buss, O. Mašek, Mobile organic compounds in biochar – a potential source of contamination – phytotoxic effects on cress seed (*Lepidium sativum*) germination, *J. Environ. Manage.* 137 (2014) 111–119, <https://doi.org/10.1016/j.jenvman.2014.01.045>.
- [49] W. Buss, O. Mašek, M. Graham, D. Wüst, Inherent organic compounds in biochar—their content, composition and potential toxic effects, *J. Environ. Manage.* 156 (2015) 150–157, <https://doi.org/10.1016/j.jenvman.2015.03.035>.

Appendix A. Supplementary data

Importance of pyrolysis temperature and pressure in the concentration of polycyclic aromatic hydrocarbons in wood waste-derived biochars

Gianluca Greco ^{a,*}, María Videgain ^b, Christian Di Stasi ^a, Elisabet Pires ^c, Joan J. Manyà ^{a,*}

^a *Aragón Institute of Engineering Research (I3A), Thermochemical Processes Group, University of Zaragoza, Escuela Politécnica Superior, crta. Cuarte s/n, Huesca E-22071, Spain*

^b *Escuela Politécnica Superior, University of Zaragoza crta. Cuarte s/n, Huesca E-22071, Spain*

^c *Departamento de Química Orgánica ISQCH. Facultad de Ciencias, Universidad de Zaragoza-CSIC, Pedro Cerbuna 12, Zaragoza 50009, Spain*

* Corresponding authors. E-mail addresses: greco@unizar.es (G. Greco), joanjoma@unizar.es (J. J. Manyà).

Reactor configuration and products gathering

The temperature profiles inside the bed were measured by four thermocouples placed in two thermowells, located at the axis (TC₀ and TC₃) and at a radial distance of 35 mm from the axis (TC₁ and TC₂), respectively. Furthermore, the thermocouples were placed at different heights from the bottom of the basket: 10 mm (TC₀ and TC₁) and 70 mm (TC₂ and TC₃).

The gas residence time and the pyrolysis environment desired for each experiment were guaranteed by tuning the mass flow rates at STP conditions for both N₂ and CO₂. The actual flow rate of the carrier gas varied approximately between 1.40 and 2.80 L min⁻¹, which corresponded to gas-hourly space velocity (GHSV) values ranged from 18 to 36 h⁻¹ (assuming a void-volume fraction of 0.5 for the entire reactor).

The resulting biochar was collected and weighted after each experiment. The total mass of liquid (organics + water) was calculated by weighing the glass traps and their flexible connections before and after each pyrolysis run. The produced liquid was recovered directly from the condensers without any washing steps with solvents. The water content was evaluated by Karl Fischer titration, whereas the organic fraction was determined by difference from the total mass of liquid. The composition of the main components of the non-condensable pyrolysis products (i.e., CO₂, CO, CH₄ and H₂) was detected using a micro gas chromatograph (model 490 from Agilent Technologies, USA).

GC/MS analytical procedure for PAHs quantification

The PAH deuterated internal standard mix used to detect any possible loss of analyte during sample preparation was PAH-Mix 31 (Dr. Ehrenstorfer, Germany), containing naphthalene-d8, acenaphthene-d10, phenanthrene-d10, chrysene-d12, and perylene-d12.

The extract (2 μL) was injected in splitless mode in a ZB-5HT Inferno capillary column (30 m, 0.25 mm ID, 0.25 μm film thickness), where the separation was carried out under a He constant flow rate of 1.2 mL min^{-1} . The oven temperature program was the following: 80 $^{\circ}\text{C}$ held for 1 min, then ramped at 6 $^{\circ}\text{C min}^{-1}$ to 175 $^{\circ}\text{C}$ (held for 4 min), then heated again at 3 $^{\circ}\text{C min}^{-1}$ to 270 $^{\circ}\text{C}$ (held for 1 min), and finally ramped at 1 $^{\circ}\text{C min}^{-1}$ to 290 $^{\circ}\text{C}$ (held for 3 min).

The PAHs detection and quantification were conducted in single ion monitoring (SIM) mode, in order to enhance the selectivity and sensitivity of the method. The standard mixture PAH-Mix 63 (Dr. Ehrenstorfer, Germany) containing the 16 US EPA PAHs¹ was used for the preparation of calibration curves, which were used for PAH quantification. Each calibration curve was built for eight concentration levels, and the quantification limit for the individual PAH was approximately 10 $\mu\text{g kg}^{-1}$. The entire procedure was performed in duplicate for each biochar and the resulting PAHs contents were given by the average. Table A.1 reports the monitored ion profiles and toxic equivalent factor (TEF) for each PAH compound.

¹ naphthalene (NAP), acenaphthylene (ANY), acenaphthene (ANA), fluorene (FLU), phenanthrene (PHE), anthracene (ANT), fluoranthene (FLT), pyrene (PYR), benzo[*a*]anthracene (BaA), chrysene (CHR), benzo[*b*]fluoranthene (BbF), benzo[*k*]fluoranthene (BkF), benzo[*a*]pyrene (BaP), indeno[1,2,3-*cd*]pyrene (IPY), dibenz[*a,h*]anthracene (DBA), and benzo[*ghi*]perylene (BPE).

Table A.1. Monitored ion profiles and toxic equivalent factor (TEF) for each PAH compound

Compounds	Monitored ions	MS retention time (min)	TEF
Naphthalene-d ₈	136–108	6–8	–
Naphthalene	128–129	6–8	0.001
Acenaphthylene	152–153	12–14	0.001
Acenaphthylene-d ₁₀	164–162	13–14	–
Acenaphthene	154–153	14–15	0.001
Fluorene	166–165	15–17	0.001
Phenanthrene-d ₁₀	188–189	19–21	–
Phenanthrene	178–179	20–21	0.001
Anthracene	178–179	20–21	0.01
Fluoranthene	202–203	28–31	0.001
Pyrene	202–203	28–31	0.001
Benzo[a]anthracene	228–226	39–40	0.1
Chrysene-d ₁₂	240–236	39–40	–
Chrysene	228–226	39–40	0.01
Benzo[b]fluoranthene	252–253	46–48	0.1
Benzo[k]fluoranthene	252–253	46–48	0.1
Benzo[a]pyrene	252–253	48–50	1
Perylene-d ₁₂	264–260	49–50	–
Indeno[1,2,3-cd]pyrene	276–277	55–57	0.1
Dibenz[a,h]anthracene	278–279	55–57	1
Benzo[g,h,i]perylene	276–277	58–59	0.01

Mass-loss evolution during pyrolysis

Repeatability assessment

Three replicates of the experiment corresponding to the center point of the factorial design were carried out, indicating an adequate degree of repeatability of the mass-loss profiles (see Fig. A.1). An intra-class correlation coefficient (ICC) of 95.6% was obtained. Consequently, a blank test at the operating conditions of the center point was performed, and then subtracted to the raw mass-loss curves.

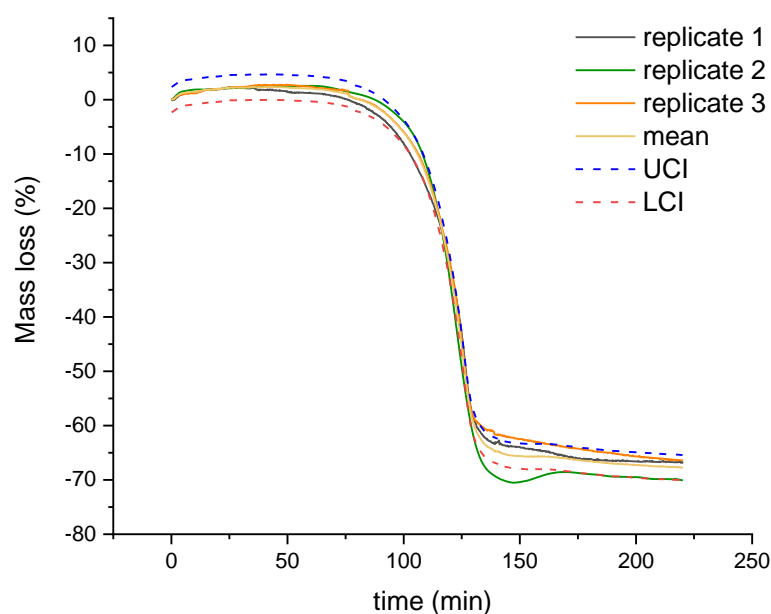


Fig. A.1. Comparison of the mass-loss curves obtained for three replicates of the central point of the experimental design (475 °C, 0.55 MPa, 150 s and 30:70 v/v of CO₂/N₂). LCI and UCI correspond to lower and upper 95% confidence intervals, respectively.

Mass-loss and temperature profiles

Fig. A.2 shows the time derivative of the mass-loss and the temperature profiles for the experiments conducted at 400–550 °C, 0.2–0.9 MPa, a gas residence time of 100 s, and using a pure N₂ carrier gas. As expected, the peak of the time derivative of the mass loss (dashed black line in Fig. A.2) was observed at temperatures ranging from 200 to approximately 400 °C. The observed exothermic behavior under these temperatures can be ascribed to the

extent of secondary reactions. In addition, an increased pressure enhanced the kinetics of the reactions involved in the overall devolatilization process. Furthermore, the increase in pressure also affected the temperature profiles, becoming more homogeneous across the reactor with a lower gradient between them, as a consequence of the higher carrier gas flow rates used at 0.9 MPa (to ensure the required gas residence time), which enhanced the convective heat transfer. The switch from a pure N₂ carrier gas to a mixture of CO₂/N₂ seemed to be irrelevant to both mass loss and temperature profiles. Therefore, the mass-loss plots for the rest of treatments (i.e., those not included in Fig. A.2) are not displayed.

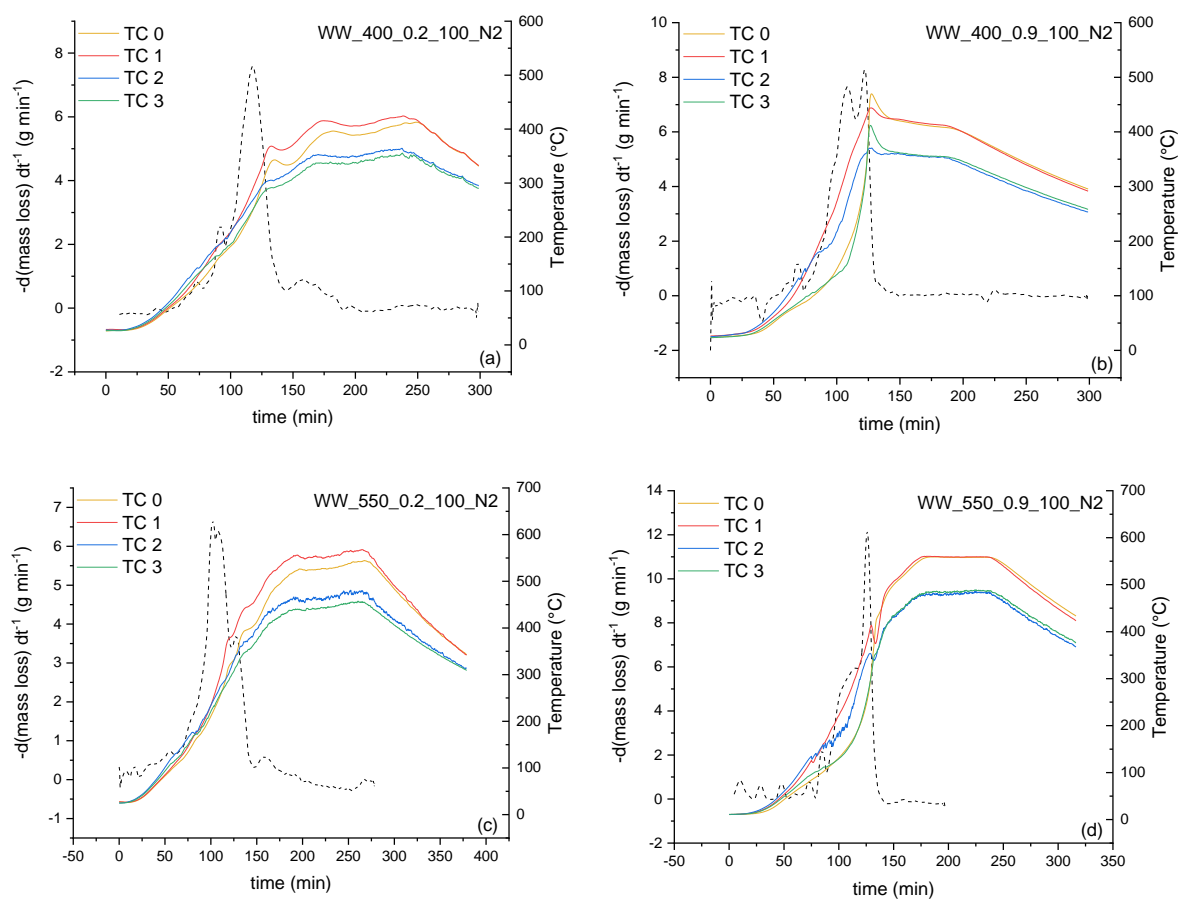


Fig. A.2. Time derivative of the mass loss and evolution of temperatures within the bed at axial (TC₀ and TC₃) and radial (TC₁ and TC₂) positions for the experiments conducted under N₂ at (a) 400 °C, 0.2 MPa and 100 s; (b) 400 °C, 0.9 MPa and 100 s; (c) 550 °C, 0.2 MPa and 100 s; and (d) 550 °C, 0.9 MPa and 100 s.

Table A.2. Results from the statistical tests of the regression model coefficients for the yields of the different pyrolysis products. The values in brackets correspond to the p -values resulting from the t -tests. The significant terms (p -values below 0.05) are marked in bold

	y_{char}	y_{org}	y_{wat}	y_{gas}	y_{CO2}	y_{CO}	y_{CH4}	y_{H2}
β_0	0.3365 (0.000)	0.0795 (0.000)	0.2408 (0.000)	0.3432 (0.000)	0.2589 (0.000)	3.0848 (0.000)	1.2538 (0.000)	0.5351 (0.000)
$\beta_1 (T)$	-0.0261 (0.000)	-0.0018 (0.166)	0.0092 (0.078)	0.0186 (0.007)	0.0043 (0.007)	0.4656 (0.000)	0.5596 (0.000)	0.3957 (0.000)
$\beta_2 (P)$	0.0038 (0.004)	-0.0154 (0.000)	-0.0362 (0.000)	0.0478 (0.000)	0.0059 (0.001)	0.1482 (0.040)	–	0.0693 (0.039)
$\beta_3 (\tau)$	0.0019 (0.070)	0.0063 (0.000)	0.0195 (0.003)	-0.0277 (0.001)	0.0037 (0.015)	-0.1456 (0.042)	-0.0857 (0.329)	-0.0290 (0.324)
$\beta_4 (CO2)$	-0.0027 (0.018)	0.0015 (0.231)	0.0063 (0.202)	-0.0051 (0.351)	–	0.2508 (0.003)	0.2067 (0.033)	-0.0471 (0.129)
$\beta_{12} (T\cdot P)$	0.0016 (0.109)	0.0060 (0.001)	0.0020 (0.670)	-0.0097 (0.099)	0.0019 (0.155)	–	–	0.0290 (0.324)
$\beta_{13} (T\cdot\tau)$	-0.0007 (0.453)	0.0017 (0.186)	0.0030 (0.534)	-0.0039 (0.467)	–	–	–	-0.0131 (0.647)
$\beta_{14} (T\cdot CO2)$	0.0019 (0.063)	–	0.0033 (0.485)	-0.0050 (0.357)	0.0029 (0.044)	0.2450 (0.003)	0.1743 (0.064)	-0.0458 (0.138)
$\beta_{23} (P\cdot\tau)$	0.0014 (0.168)	–	0.0055 (0.260)	-0.0075 (0.186)	0.0003 (0.793)	-0.1585 (0.030)	0.0322 (0.708)	-0.0503 (0.109)
$\beta_{24} (P\cdot CO2)$	0.0027 (0.018)	-0.0045 (0.004)	-0.0087 (0.094)	0.0105 (0.077)	0.0007 (0.593)	-0.1683 (0.023)	-0.0898 (0.308)	-0.0685 (0.041)
$\beta_{34} (\tau\cdot CO2)$	0.0017 (0.092)	-0.0013 (0.286)	–	–	0.0008 (0.553)	0.1341 (0.058)	0.1962 (0.041)	0.0197 (0.494)
R^2_{adj}	0.9813	0.9300	0.8401	0.8814	0.7405	0.8718	0.7688	0.9257
Curvature	(0.002)	(0.834)	(0.011)	(0.078)	(0.020)	(0.007)	(0.058)	(0.283)

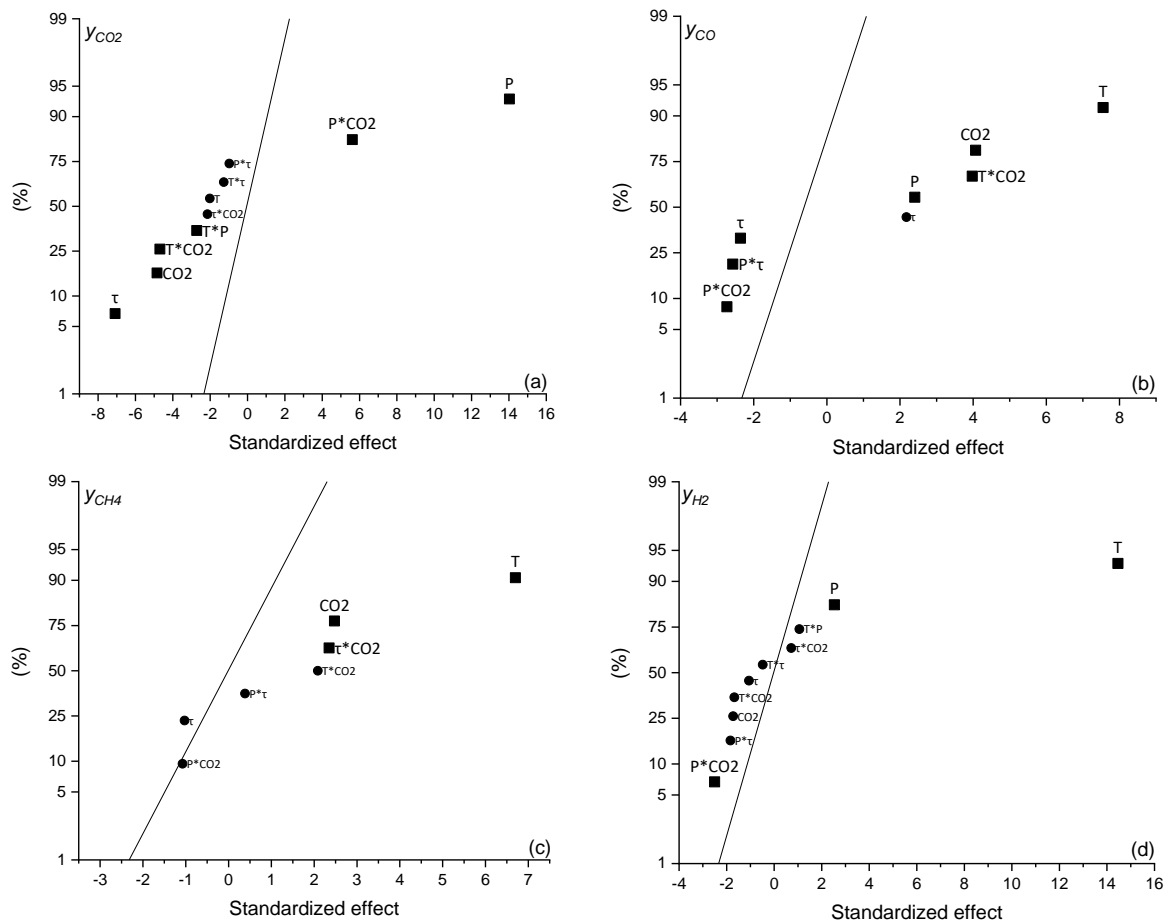


Fig. A.3. Normal plots of standardized effects ($\alpha = 0.05$) for (a) y_{CO_2} , (b) y_{CO} , (c) y_{CH_4} , and (d) y_{H_2} (square, significant effect; circle, non-significant effect).

Table A.3. Results from the statistical tests of the regression model coefficients for the variables listed in Table 3. The values in brackets correspond to the p -values resulting from the t -tests.

The significant terms (p -values below 0.05) are marked in bold

	H:C	O:C	C:N	pH	x_{FC}	y_{FC}	S_{BET}	V_{ultra}
β_0	0.4956 (0.000)	0.0945 (0.000)	75.89 (0.000)	8.378 (0.000)	78.04 (0.000)	0.2589 (0.000)	209.2 (0.000)	0.0523 (0.000)
$\beta_1(T)$	-0.1053 (0.000)	-0.0281 (0.000)	0.628 (0.215)	-0.0112 (0.016)	7.501 (0.000)	0.0043 (0.007)	40.56 (0.000)	0.0151 (0.000)
$\beta_2(P)$	-0.0145 (0.033)	-0.0053 (0.115)	1.691 (0.012)	–	0.7611 (0.152)	0.0059 (0.001)	2.190 (0.314)	–
$\beta_3(\tau)$	0.0035 (0.546)	0.0042 (0.207)	3.775 (0.000)	–	0.6323 (0.223)	0.0037 (0.015)	-1.440 (0.499)	0.0018 (0.224)
$\beta_4(CO_2)$	-0.0101 (0.108)	-0.0028 (0.392)	-2.021 (0.006)	0.0075 (0.070)	0.4751 (0.349)	–	3.941 (0.092)	0.0033 (0.038)
$\beta_{12}(T \cdot P)$	-0.0086 (0.162)	-0.0049 (0.143)	-1.642 (0.014)	0.0350 (0.000)	0.1422 (0.773)	0.0019 (0.155)	1.062 (0.615)	-0.0015 (0.309)
$\beta_{13}(T \cdot \tau)$	0.0075 (0.212)	0.0048 (0.151)	-0.9970 (0.074)	-0.0312 (0.000)	-0.0100 (0.983)	–	-0.5600 (0.788)	0.0019 (0.190)
$\beta_{14}(T \cdot CO_2)$	-0.0077 (0.201)	–	0.9310 (0.089)	0.0162 (0.003)	0.5280 (0.301)	0.0029 (0.044)	2.311 (0.289)	0.0026 (0.093)
$\beta_{23}(P \cdot \tau)$	0.0020 (0.728)	–	–	–	-0.1490 (0.762)	0.0003 (0.793)	-0.6901 (0.743)	-0.0020 (0.176)
$\beta_{24}(P \cdot CO_2)$	0.0026 (0.651)	0.0015 (0.624)	–	-0.0212 (0.001)	-0.3591 (0.473)	0.0007 (0.593)	0.1900 (0.929)	-0.0017 (0.239)
$\beta_{34}(\tau \cdot CO_2)$	0.0067 (0.264)	0.0051 (0.133)	-0.7240 (0.162)	0.0125 (0.011)	-0.1830 (0.711)	0.0008 (0.553)	-3.690 (0.110)	0.0009 (0.522)
$\beta_{123}(T \cdot P \cdot \tau)$	–	–	2.096 (0.005)	0.0250 (0.000)	–	–	–	–
$\beta_{124}(T \cdot P \cdot CO_2)$	–	–	-1.649 (0.014)	0.0225 (0.001)	–	–	–	–
$\beta_{234}(P \cdot \tau \cdot CO_2)$	–	–	-0.9390 (0.087)	0.0162 (0.003)	–	–	–	–
<i>Curvature</i>	–	–	-0.9980 (0.074)	-0.0162 (0.003)	–	–	–	–
R^2_{adj}	0.9544	0.8317	0.9068	0.9589	0.9324	0.7405	0.9573	0.8825

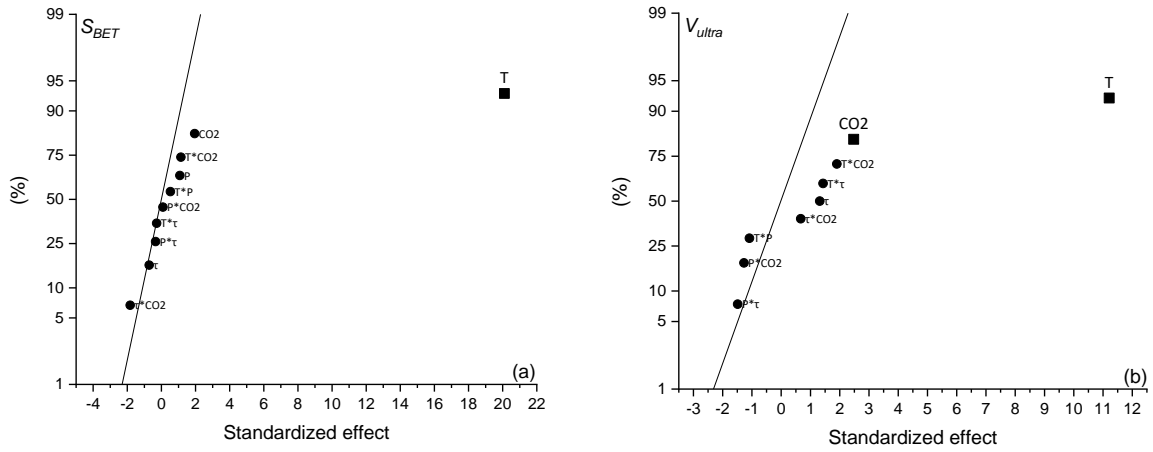


Fig. A.4. Normal plots of standardized effects ($\alpha = 0.05$) for (a) S_{BET} and (b) V_{ultra} (square, significant effect; circle, non-significant effect).

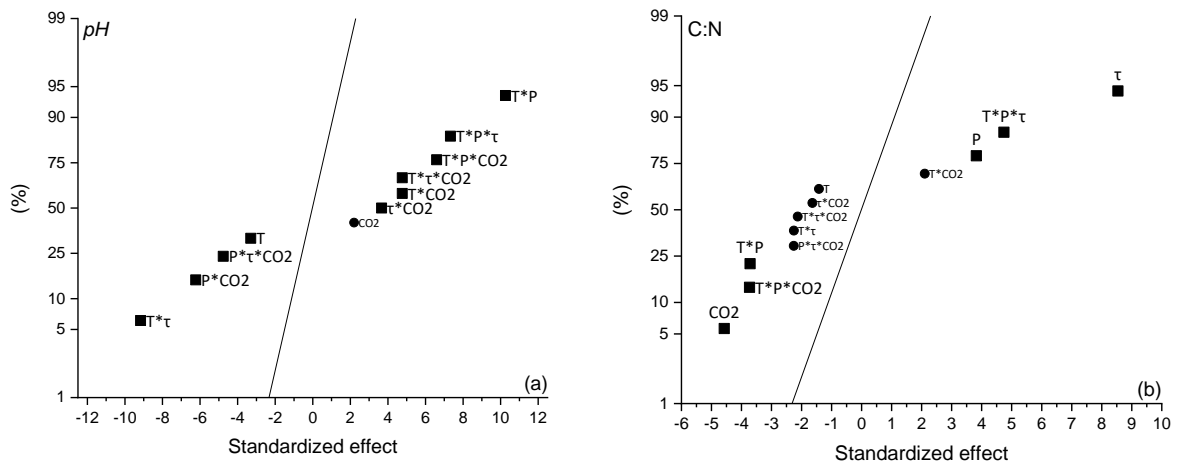


Fig. A.5. Normal plots of standardized effects ($\alpha = 0.05$) for (a) pH , and (b) atomic C:N ratio (square, significant effect; circle, non-significant effect).

Table A.4. Results from the statistical tests of the regression model coefficients for the total PAHs content (PAH), light-weight PAHs content (PAH light), medium-weight PAHs content (PAH medium), heavy-weight PAHs content (PAH heavy), and TTEC of the produced biochars. The values in brackets correspond to the p -values resulting from the t -tests (the significant terms are marked in bold)

	<i>PAH</i>	<i>PAH light</i>	<i>PAH medium</i>	<i>PAH heavy</i>	<i>TTEC</i>
β_0	4205 (0.000)	3040 (0.000)	916.7 (0.000)	248.8 (0.000)	10.26 (0.000)
$\beta_1(T)$	-431.9 (0.001)	-28.40 (0.735)	-239.4 (0.001)	-164.2 (0.000)	-3.810 (0.000)
$\beta_2(P)$	-344.0 (0.003)	-217.2 (0.035)	-90.60 (0.060)	-36.10 (0.026)	0.4560 (0.342)
$\beta_3(\tau)$	-51.00 (0.506)	-159.6 (0.093)	91.01 (0.059)	17.62 (0.212)	0.6443 (0.198)
$\beta_4(CO_2)$	-119.1 (0.150)	-	-59.60 (0.178)	-32.61 (0.039)	-0.9420 (0.082)
$\beta_{12}(T \cdot P)$	95.20 (0.235)	-129.5 (0.156)	199.8 (0.002)	25.02 (0.093)	0.5251 (0.281)
$\beta_{13}(T \cdot \tau)$	-114.8 (0.163)	-	-68.22 (0.132)	-25.71 (0.085)	-0.0891 (0.846)
$\beta_{14}(T \cdot CO_2)$	-113.1 (0.168)	-107.0 (0.229)	-	15.60 (0.263)	-0.4880 (0.312)
$\beta_{23}(P \cdot \tau)$	50.11 (0.513)	55.31 (0.515)	-	8.400 (0.536)	0.9302 (0.085)
$\beta_{24}(P \cdot CO_2)$	-	61.90 (0.468)	-58.12 (0.188)	13.53 (0.328)	-0.5201 (0.285)
$\beta_{34}(\tau \cdot CO_2)$	209.2 (0.027)	207.2 (0.041)	-	19.90 (0.165)	0.3680 (0.436)
$\beta_{123}(T \cdot P \cdot \tau)$	236.6 (0.017)	135.2 (0.142)	120.8 (0.021)	-	-
$\beta_{124}(T \cdot P \cdot CO_2)$	-	62.81 (0.462)	-69.20 (0.127)	-	-
$\beta_{134}(T \cdot \tau \cdot CO_2)$	-225.4 (0.020)	-111.2 (0.214)	-96.60 (0.048)	-	-1.753 (0.010)
$\beta_{234}(P \cdot \tau \cdot CO_2)$	-	-	-39.20 (0.354)	-	-0.6560 (0.191)
R^2_{adj}	0.8468	0.6328	0.8377	0.9123	0.8479
<i>Curvature</i>	(0.010)	(0.010)	(0.129)	(0.052)	(0.565)

Table A.5. Results from the statistical tests of the regression model coefficients for the germination index (*GI*) values obtained for watercress, barley, and basil. The values in brackets correspond to the *p*-values resulting from the *t*-tests (the significant terms are marked in bold)

	<i>GI watercress</i>	<i>GI barley</i>	<i>GI basil</i>
β_0	47.80 (0.000)	91.20 (0.000)	94.30 (0.000)
$\beta_1 (T)$	-6.55 (0.008)	–	-5.95 (0.168)
$\beta_2 (P)$	7.93 (0.003)	-6.33 (0.070)	-3.64 (0.375)
$\beta (\tau)$	-1.04 (0.577)	4.82 (0.144)	-6.14 (0.157)
$\beta_4 (CO_2)$	3.36 (0.101)	–	–
$\beta_{12} (T \cdot P)$	0.73 (0.692)	12.89 (0.004)	-2.09 (0.602)
$\beta_{13} (T \cdot \tau)$	-3.99 (0.060)	-13.65 (0.003)	8.67 (0.063)
$\beta_{14} (T \cdot CO_2)$	1.88 (0.325)	–	-2.62 (0.516)
$\beta_{23} (P \cdot \tau)$	2.88 (0.150)	-8.69 (0.023)	–
$\beta_{24} (P \cdot CO_2)$	1.30 (0.488)	4.79 (0.147)	–
$\beta_{34} (\tau \cdot CO_2)$	-1.76 (0.356)	-9.97 (0.013)	-2.39 (0.553)
$\beta_{123} (T \cdot P \cdot \tau)$	–	-2.98 (0.339)	-1.62 (0.685)
$\beta_{124} (T \cdot P \cdot CO_2)$	–	6.14 (0.077)	4.27 (0.304)
$\beta_{134} (T \cdot \tau \cdot CO_2)$	–	-4.71 (0.152)	-13.07 (0.014)
$\beta_{234} (P \cdot \tau \cdot CO_2)$	–	-9.59 (0.016)	1.13 (0.776)
R^2_{adj}	0.7588	0.8218	0.5057
<i>Curvature</i>	(0.003)	(0.299)	(0.074)

6.4. Theme IV: physically activated biomass-derived carbons for CH₄/CO₂ separation purposes

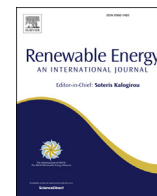
The evaluation of WW-based biochar feasibility for soil application purposes described in *Theme III* was followed by the assessment of wheat straw-derived biochar potential as precursor material for a second kind of application: biogas upgrading via CO₂ adsorption. The reason behind the choice of WS instead of WW in this applied topic was mainly due to its significant yearly production in many rural areas of Aragon (“Ministerio de Agricultura, Pesca y Alimentación, Gobierno de España,” 2020). Its utilization in any field of applications would be a glaring example of circular economy. In this specific type of application, its abundance opens to the possibility to synthesize large amounts of activated carbons for CO₂ adsorption. In addition, its added-value may impulse the economy of several sectors present in such rural areas.

In this research theme, wheat straw-derived activated carbons were produced by two-step or one-step physical activation pathways, aiming at their employment as sustainable adsorbents for CH₄/CO₂ separation. In addition, the effects of pyrolysis conditions on the properties of the resulting two-step activated carbons were carefully analyzed. This research study was published in *Renewable Energy* (article 4).

Among the most important results regarding the two-step production pathway, it should be highlighted the fact that the biochar precursors showing the best textural properties were obtained at 400 °C and 0.2 MPa, the least severe process conditions. In line with this finding, the effect of absolute pressure appeared to be negative on both the specific surface area and porosity development of resulting activated carbons, probably due to the formation of a more stable biochar during the pyrolysis step. An important consequence of an increased pressure might also be the clogging of biochar pores, due to a higher extent of recondensation of volatiles.

With regard to the one-step production process, the resulting activated carbons showed similar features—in terms of textural properties as well as CO₂ uptake and selectivity (up to 2.29 mol kg⁻¹ at 0.1 MPa and 6.9, respectively)—to those produced by the more conventional two-step process. Results obtained from breakthrough curve simulations highlighted that the best activated carbon in terms of CH₄ recovery under dynamic conditions was produced by one-step activation at 700 °C, 0.55 MPa, 100 s, and under a 37.5% v CO₂ atmosphere. Using the adsorbent produced under these conditions, a methane recovery of 95% at 0.1 MPa was

estimated. In conclusion, the one-step process appears to be an alternative route for engineered carbon materials production, which can lead to significant cost savings in large-scale production systems.



Biomass-derived carbons physically activated in one or two steps for CH₄/CO₂ separation

Gianluca Greco^{a,*}, Rafael L.S. Canevesi^b, Christian Di Stasi^a, Alain Celzard^b,
Vanessa Fierro^b, Joan J. Manyà^{a,**}

^a Aragon Institute of Engineering Research (I3A), Thermochemical Processes Group, University of Zaragoza, Escuela Politécnica Superior, crta. Cuarte s/n, Huesca, E-22071, Spain

^b Université de Lorraine, CNRS, IJL, Épinal, F-88000, France

ARTICLE INFO

Article history:

Received 4 October 2021

Received in revised form

19 March 2022

Accepted 5 April 2022

Available online 11 April 2022

Keywords:

Wheat straw

Pressurized slow pyrolysis

CO₂ activation

CO₂/CH₄ separation

CO₂/CH₄ selectivity

CH₄ recovery

ABSTRACT

The present study aims at evaluating the suitability of producing activated carbons (ACs) derived from wheat straw by a one-step synthesis approach, as an alternative to more conventional two steps production processes (i.e., pyrolysis and subsequent activation). The performance of the produced ACs, in one or two steps, as sustainable and selective CO₂ adsorbents for CH₄/CO₂ separation is compared. In addition, the influence of pyrolysis conditions on the properties of the resulting two-step ACs is carefully analyzed. We show that the biochar-based precursors of ACs presenting the best textural properties were obtained under mild conditions of maximum temperature and absolute pressure during pyrolysis. The one-step ACs were fully comparable—in terms of textural properties as well as CO₂ uptake and selectivity—to those produced by the more conventional two-step synthesis process. In addition, results obtained from breakthrough curve simulations highlight that the best AC in terms of CH₄ recovery under dynamic conditions was produced by a one-step activation. Therefore, the one-step process appears to be as an attractive route for the production of engineered carbon materials, which can lead to significant cost savings in large-scale production systems.

© 2022 The Authors. Published by Elsevier Ltd. This is an open access article under the CC BY-NC-ND license (<http://creativecommons.org/licenses/by-nc-nd/4.0/>).

1. Introduction

Serious concerns about climate change and the growing global energy demand have led to a great interest in renewable energies [1]. One of the most attractive options is to use biofuels as a valuable alternative to widely used fossil fuels. Having a low environmental impact, biofuels could contribute significantly to the reduction of hydrocarbons, SO_x and CO₂ emissions [2]. Biogas, mainly produced by anaerobic digestion processes [3], can certainly be considered as a biofuel, due to its significant methane content. Before being used as a biofuel, biogas needs to be refined by reducing its CO₂ content, in order to increase its heating value and bring it closer to that of natural gas [4], and to reduce the risk of pipeline corrosion in presence of water [5].

The most commonly used technologies for CO₂ separation are chemical absorption into aqueous amine blended solutions [6], multistage membrane separation using polymeric materials [7],

and adsorption into porous materials in fixed beds [8]. The former is considered the current benchmark technology, thanks to its level of maturity reached after sixty years [9]. However, the main drawback of this technology is the energy penalty associated with the regeneration step [10]. Adsorption in porous solids appears as an emerging alternative for CO₂ separation, due to its relatively low cost and high energy efficiency [11]. As potential adsorbents for large-scale systems, activated carbons (ACs) has attracted increasing interest in the last years, due to their relatively high CO₂ adsorption capacity (over 2 mol kg⁻¹ at ambient conditions [12–14]), fast kinetics, thermal stability, chemical resistance and relatively low costs (for production and regeneration) compared to other adsorbents such as zeolites and metal organic frameworks (MOFs) [5,15,16]. When used in biogas upgrading applications, ideal ACs should exhibit high selectivity towards CO₂, guaranteed by appropriate pore size distribution (PSD) and surface chemistry [17]. However, designing adsorbents based on kinetics could be very complex, as CO₂ and CH₄ molecules have very similar kinetic diameters (0.34 and 0.38 nm, respectively) [16]. On the other hand, CO₂ is a polar molecule with a quadrupole moment of 13.4

* Corresponding author.

** Corresponding author.

E-mail addresses: greco@unizar.es (G. Greco), joanjoma@unizar.es (J.J. Manyà).

10^{-40} cm², whereas CH₄ is non-polar. This significant difference in polarity makes the presence of polar functional groups on the adsorbent surface very useful to increase the CO₂ selectivity [18] to values higher than 8 [19,20].

Biomass is a sustainable way to produce ACs. In general, the process consists of two main steps: pyrolysis and subsequent activation. The former involves the thermal degradation of biomass, resulting in a solid carbon precursor known as biochar. Given the large number of variables influencing the pyrolysis process and the wide variety of biomass sources, there are significant differences in the final biochar properties [21,22]. With this in mind, optimization of pyrolysis conditions is necessary to obtain the most suitable biochar for its subsequent activation into porous carbon materials. Since pristine biochar typically has a low specific surface area (SSA) and a porous texture consisting mainly of narrow micropores [23], a secondary activation step (physical or chemical [24,25]) is required to accomplish further porosity development.

As an alternative to the two-step production process mentioned above, biomass-derived ACs can also be synthesized by a one-step thermochemical process. For this purpose, the highest pyrolysis temperature has to be raised to more than 650 °C and the inert gas atmosphere (usually N₂) has to be replaced by an atmosphere containing an activating agent (e.g., CO₂, H₂ or H₂O). This process is considered a very interesting solution in terms of energy recovery, especially for large-scale production systems. The results of the relatively few published studies on the production of ACs from biomass by a one-step process [26–29] are certainly encouraging, since similar or even better properties have been reported for ACs produced in one step compared to traditional ACs produced in two steps. For instance, González et al. [29], who produced olive stones-derived ACs by one-step physical activation (with CO₂ at 800 °C), reported excellent CO₂ uptakes (1.75 mmol g⁻¹ at 35 kPa and 25 °C). Bergna et al. [30] carried out a study based on the comparison between one-step and two-step production pathways, observing that ACs produced through one-step activation generally had higher surface areas as well as higher total pore volumes. In the same study, the authors reported that the final carbon yield was higher when ACs were prepared by two-step process, whereas no significant differences were detected in the total carbon content between the two types of activation.

In view of all the above, the aim of the present study is to contribute to fill the gaps that still exist in establishing the most suitable route for the conversion of biomass feedstock into ACs with tuned porosity. To this end, a systematic and parametric study of the effects of several pyrolysis conditions (maximum temperature, absolute pressure, gas residence time, and type of pyrolysis atmosphere) on the textural properties of the resulting wheat-straw-derived ACs —produced via pyrolysis and subsequent physical activation with CO₂ at 800 °C— was performed. In addition, several wheat straw-derived ACs were prepared through a one-step process under different operating conditions (maximum temperature, absolute pressure and CO₂ content in the carrier gas). The most promising ACs (i.e., those with the best textural properties for CO₂ adsorption from both one-step and two-step conversion processes) were then tested as selective adsorbents for CO₂/CH₄ separation.

2. Materials and methods

2.1. Biomass feedstock

The wheat straw (WS) pellets (7 mm OD and approximately 12 mm long, with an apparent density of 400 kg m⁻³) used as feedstock in this work were described elsewhere [31,32]. Demonstrating the real potential of WS pellets in biogas upgrading would be of great importance in terms of circular economy for this abundant,

autochthonous resource in Aragon (Spain), which represents a significant share of local agricultural disposals. The as-received biomass was directly pyrolyzed without any preliminary milling step in order to maximize the final carbonization efficiency [33,34]. WS pellets were characterized by proximate analysis (according to ASTM standards for moisture, ash, and volatiles), and X-Ray Fluorescence (XRF) spectroscopy analysis (ADVANT'XP + XRF spectrometer from Thermo ARL, Switzerland) to determine inorganic constituents. The contents of hemicelluloses, cellulose and lignin were determined following an analytical approach described previously [32].

2.2. One-step activation

The one-step activation process was performed using the same bench-scale fixed-bed reactor described in previous works [31,32]. The following ranges of operating conditions were considered: maximum temperature between 650 and 750 °C, absolute pressure between 0.2 and 0.9 MPa, reactor environment varying between pure N₂ and a binary CO₂/N₂ mixture (75:25 v/v), and constant gas residence time of 100 s. In order to study the pyrolysis behavior in this range of process parameters, experiments using a pure N₂ atmosphere were included in the experimental design (see Fig. 1). The heating rate and the dwell time (at the maximum temperature) were 5 °C min⁻¹ and 1 h, respectively.

2.3. Two-step activation

The pyrolysis step was performed using the same bench-scale fixed-bed reactor as for the one-step activation. The maximum temperature, absolute pressure, and gas residence time varied in the range of 400–550 °C, 0.2–0.9 MPa, and 100–200 s, respectively. In addition, the pyrolysis atmosphere adopted for these experiments varied from pure N₂ to a CO₂/N₂ mixture (60:40 v/v). As before, the heating rate and the dwell time (at the maximum temperature) were 5 °C min⁻¹ and 1 h, respectively. More details on the pyrolysis setup are available in Appendix A (see Fig. A1). The resulting material from pyrolysis step is called biochar (see Fig. 1).

All biochars obtained after pyrolysis were then physically activated at 800 °C and atmospheric pressure under a pure CO₂ atmosphere. The device used for activation [35] consisted of a tubular reactor (Inconel 600 alloy, 600 mm long and 28 mm ID), placed inside a vertical tubular furnace (model EVA 12/300 mm from Carbolite Gero, UK). A K-type thermocouple was placed along the longitudinal axis of the reactor to monitor the temperature inside the bed in real-time. Following the same procedure as in a previous work [35], the raw biochars were first ground and sieved to obtain particle sizes between 0.21 and 1.41 mm. Then, samples of 10 g were heated at 10 °C min⁻¹ under a constant flow of N₂. Once the activation temperature was reached (i.e., 800 °C), the gas feed was switched from N₂ to CO₂ and held isothermally for 1 h. Under these conditions, the gas-hourly space velocity (GHSV) was approximately 7000 h⁻¹. Fig. 1 summarizes the production process pathways and the range of operating conditions adopted in this study.

2.4. Characterization of activated carbons

The degree of burn-off (X_i) was estimated as follows:

$$X_{1S} = (m_{\text{biomass}} - m_f) / m_{\text{biomass}} \cdot 100 \quad (1)$$

$$X_{2S} = (m_{\text{biochar}} - m_f) / m_{\text{biochar}} \cdot 100 \quad (2)$$

where i refers to the type of activation process: one-step (1S) or

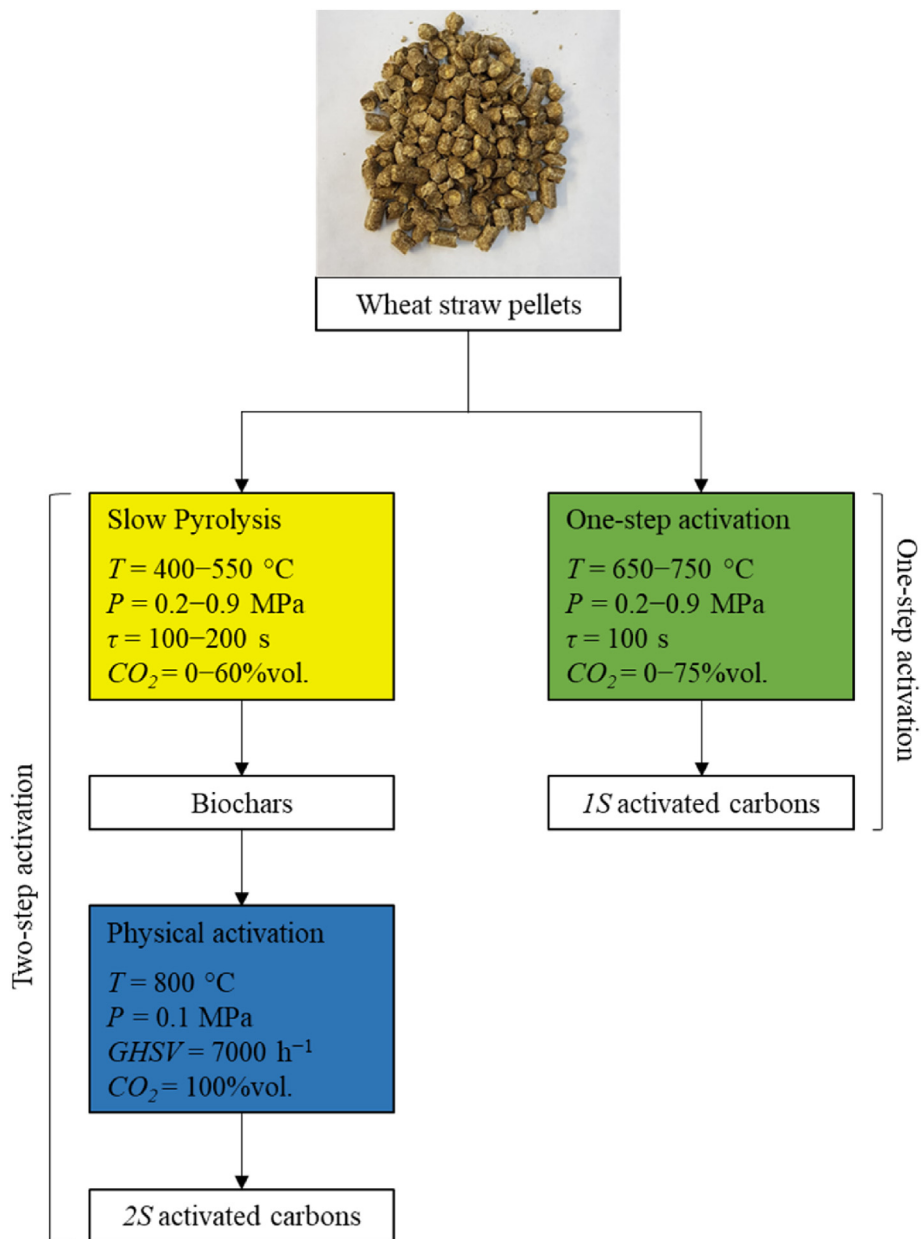


Fig. 1. Overview of the production pathways for one-step (1S) and two-step (2S) activated carbons.

two-step (2S). $m_{biomass}$, $m_{biochar}$, and m_f are the masses of biomass, biochar and final sample, respectively. It is important to note that, unlike the burn-off of 2S activated carbons (X_{2S}), which takes into account only the mass loss related to the physical activation, X_{1S} accounts for the mass loss during the whole one-step process from the biomass feedstock. Hence, the burn-offs corresponding to the one-step activation process are, in all cases, numerically higher than those related to the two-step activation. In order to compare both production pathways in terms of yield of AC, the overall mass yield (y_{2S}) for the 2S ACs was also calculated according to Eq. (3), where y_{char} is the mass yield of biochar (in mass fraction) after the pyrolysis step. The mass yield for 1S ACs (y_{1S}) was calculated using Eq. (4).

$$y_{2S} = y_{char} \cdot (100 - X_{2S}) \tag{3}$$

$$y_{1S} = (100 - X_{1S}) \tag{4}$$

The textural characterization of the carbon materials was performed by N₂ and H₂ adsorption at -196 °C using an ASAP 2020 automatic adsorption device from Micromeritics (USA). Samples were outgassed under secondary vacuum at 110 °C for at least 48 h and outgassing at the same temperature for at least 6 h was also carried out in the analysis port. Warm and cold volumes were determined after analysis to avoid He entrapment in ultramicropores. Processing of the adsorption isotherm data was performed using Microactive® and SAIEUS® software provided by Micromeritics. Pore size distributions (PSDs) and surface areas ($S_{2D-NLDFT}$) were calculated by applying the two-dimensional non-local density functional theory model for heterogeneous surfaces (2D-NLDFT-HS) [36] to N₂ and H₂ isotherms simultaneously. The total pore volume (V_{tot}), ultra-micropore volume (V_{ultra} , < 0.7 nm), micropore volume (V_{micro} , <2 nm) and mesopore volume (V_{meso} , 2–50 nm) were obtained by integrating the PSDs in the corresponding pore size ranges.

Infrared spectra were performed in the wavenumbers range of 600–4000 cm^{-1} using a Fourier-Transform Infrared (FTIR) spectrometer (Frontier Spotlight 400, PerkinElmer, Japan).

2.5. Statistical analysis

An unreplicated 2-level full factorial design was adopted to evaluate the effects of the assessed pyrolysis process parameters. Three replicates at the center point were carried out to estimate the experimental error and the overall curvature effect [37]. The structure of the regression model (using normalized values for factors in the range from -1 to 1) used during statistical analysis for the response variables (i.e., textural properties of 2S ACs) was as follows:

$$\begin{aligned} \hat{y} = & \beta_0 + \beta_1 T + \beta_2 P + \beta_3 \tau + \beta_4 \text{CO}_2 + \beta_{12} T \cdot P + \beta_{13} T \cdot \tau \\ & + \beta_{14} T \cdot \text{CO}_2 + \beta_{23} P \cdot \tau + \beta_{24} P \cdot \text{CO}_2 + \beta_{34} \tau \cdot \text{CO}_2 \\ & + \beta_{123} T \cdot P \cdot \tau + \beta_{124} T \cdot P \cdot \text{CO}_2 + \beta_{134} T \cdot \tau \cdot \text{CO}_2 \\ & + \beta_{234} P \cdot \tau \cdot \text{CO}_2 \end{aligned} \quad (5)$$

where β_0 , β_i , β_{ij} , and β_{ijk} are the intercept, linear, 2-way interaction and 3-way interaction coefficients, respectively. The regression models used for the response variables related to the textural properties of the 1S ACs were the same as those described in Eq. (5) without considering the gas residence time as a factor. Statistical calculations were conducted using Minitab software (v17).

2.6. Adsorption isotherms and breakthrough simulations

CO_2 and CH_4 adsorption isotherms were measured up to 3.5 MPa, at 25 and 50 °C, using a HPVA II high-pressure manometric device (from Micromeritics). The samples were firstly outgassed under secondary vacuum (5×10^{-7} Pa) at 110 °C for at least 48 h. Afterwards, the pressure was gradually increased from 0.005 to 3.5 MPa, and then decreased stepwise to 0.5 MPa. The amount of gas adsorbed was calculated as the difference between the amount of gas dosed and the amount of gas determined at each equilibrium pressure.

The transient pressure change prior to the first isotherm point was recorded to obtain the adsorption kinetics. The batch kinetic model presented in Appendix A was fitted to the experimental kinetic data to obtain an estimate of the diffusivity of methane and carbon dioxide on the solid adsorbents.

The experimental data obtained from the isotherms were described using the Sips model. The ideal adsorbed solution theory (IAST) was adopted to predict the adsorption behavior of CO_2/CH_4 binary mixtures at different volume concentrations (i.e., 10:90 v/v, 30:70 v/v, 50:50 v/v, and 70:30 v/v). The selectivity towards CO_2 over CH_4 , S , was then calculated as follows:

$$S = (x_{\text{CO}_2} y_{\text{CH}_4}) / (x_{\text{CH}_4} y_{\text{CO}_2}) \quad (6)$$

where x and y are the gas molar fractions in the adsorbed and gas phases, respectively.

Simulations of adsorption breakthrough curves were carried out at 0.1, 0.3, 0.5, 0.7 and 1.0 MPa considering an initial temperature of 30 °C and a total feed flow rate of 0.75 NL min^{-1} , with a molar composition of 40% CO_2 and 60% CH_4 . A simulated fixed-bed column with length and diameter of 60 cm and 2.8 cm, respectively, was considered to run the simulations using gPROMS ModelBuilder.

The samples tapped densities were obtained in an Autotap

equipment of Quantachrome®. The bed porosity was calculated using the bed and particle densities as follows:

$$\varepsilon_{\text{bed}} = 1 - \rho_{\text{bed}} / \rho_{\text{par}} \quad (7)$$

where ρ_{bed} and ρ_{par} are the bed and particle densities, respectively. The particle density and porosity were measured by mercury porosimetry (Autopore IV, Micromeritics). The average particle diameter was measured by laser diffraction using a Mastersizer Hydro 3000 analyzer (Malvern instruments Ltd.) equipped with a Hydro LV sampler and a measurement cell for liquid phase suspensions.

More details regarding the IAST-based approach and the carbon adsorbents parameters used to run the simulations under dynamic conditions are given in Appendix A.

3. Results and discussion

The complete characterization of the WS pellets (including lignocellulosic composition, proximate, ultimate, and XRF analyses) is reported in Table A.1 (Appendix A). Furthermore, Appendix A also provides details on the pyrolysis behavior of WS pellets under either a pure N_2 atmosphere or a mixture of CO_2/N_2 , including an assessment of repeatability and an analysis of mass loss profiles for the one-step activation experiments (see Figs. A.2 and A.3, respectively).

3.1. Conversion and textural properties of activated carbons

This section covers the results obtained from the full characterization of all ACs studied here. The numerical results are reported in Tables 1 and 2; more details on the statistics related to this section are given in Tables A.2 and A.3.

3.1.1. Two-step activation

When producing WS-derived ACs by slow pyrolysis and subsequent physical activation with CO_2 at 800 °C (two steps), the maximum pyrolysis temperature had a negative effect on the degree of burn-off (as shown in Fig. 2a). This could be explained by the fact that higher pyrolysis temperatures could lead to slightly more ordered carbon structures, making them less prone to reaction [38,39]. Similar conclusions can be drawn for the textural properties of the resulting ACs (see Fig. 2c–e), except for $V_{\text{ultra}}(2S)$, which appears to be positively affected by the maximum temperature and, to a greater extent, by the gas residence time. The effect of gas residence time also contributed to reduce the resulting X_{2S} , due to the importance of secondary charring reactions, which led to the formation of a more stable biochar structure. On the other hand, the effect of absolute pressure was found to be negative on both final specific surface area and porosity development (see Fig. 2b–e). This aspect could also be explained as a consequence of the formation of a more stable biochar during slow pyrolysis [40] and the clogging of its pores that would prevent the development of porosity during the activation step. It is important to note that it was not possible to develop mesoporosity under these activating conditions and, for this reason, $V_{\text{meso}}(2S)$ is not reported in Fig. 2. The presence of CO_2 as gas carrier in the pyrolysis environment did not affect the characteristics of the ACs, as well as the properties of the biochars produced, as previously reported [32]. This also indicates the possibility of recycling a flue gas stream by using it as a low-cost pyrolysis atmosphere, resulting in significant cost savings over N_2 on an industrial scale.

The values of surface areas and pore volumes obtained in this set of experiments were fully comparable to those obtained in a previous study [41] for WS-derived ACs produced by slow pyrolysis

Table 1

Experimental results of surface area ($S_{2D-NLDFT}$), ultramicropore volume (V_{ultra}), micropore volume (V_{micro}), mesopore volume (V_{meso}), total pore volume (V_{tot}) and burn-off (X) obtained in the two-step (2S) activation experiments.

Pyrolysis conditions				Response variable							
T (°C)	P (MPa)	τ (s)	CO ₂ (vol. %)	$S_{2D-NLDFT} (2S)$ (m ² g ⁻¹)	$V_{ultra} (2S)$ (cm ³ g ⁻¹)	$V_{micro} (2S)$ (cm ³ g ⁻¹)	$V_{meso} (2S)$ (cm ³ g ⁻¹)	$V_{tot} (2S)$ (cm ³ g ⁻¹)	X_{2S} (%)	y_{2S} (%)	
400	0.9	200	60	905	0.16	0.25	0.02	0.27	45.3	17.3	
400	0.9	100	60	837	0.11	0.24	0.02	0.26	51.3	15.1	
550	0.2	100	0	906	0.17	0.25	0.03	0.28	42.6	15.8	
400	0.2	100	60	986	0.11	0.30	0.05	0.35	63.7	10.6	
550	0.9	200	0	905	0.15	0.25	0.02	0.27	37.1	17.9	
550	0.2	100	60	865	0.15	0.24	0.02	0.26	45.4	15.3	
475	0.55	150	30	933	0.15	0.26	0.03	0.29	44.5	16.3	
400	0.9	100	0	782	0.09	0.25	0.02	0.27	56.0	14.6	
400	0.9	200	0	955	0.17	0.27	0.03	0.29	49.4	16.4	
400	0.2	100	0	919	0.15	0.25	0.02	0.27	49.4	15.7	
550	0.9	100	0	870	0.15	0.24	0.03	0.27	48.8	14.1	
550	0.2	200	0	945	0.17	0.26	0.02	0.28	38.5	17.5	
550	0.9	100	60	899	0.15	0.25	0.03	0.28	49.0	14.2	
475	0.55	150	30	915	0.17	0.25	0.04	0.28	48.5	15.0	
550	0.9	200	60	860	0.16	0.24	0.04	0.27	42.9	16.0	
475	0.55	150	30	940	0.17	0.26	0.03	0.28	45.0	16.3	
550	0.2	200	60	916	0.16	0.25	0.02	0.27	36.2	18.4	
400	0.2	200	60	998	0.17	0.28	0.02	0.30	47.9	17.3	
400	0.2	200	0	957	0.18	0.26	0.02	0.28	47.1	17.3	

Table 2

Same as Table 1, but for the one-step (1S) activation experiments.

Pyrolysis conditions			Response variable							
T (°C)	P (MPa)	CO ₂ (vol. %)	$S_{2D-NLDFT} (1S)$ (m ² g ⁻¹)	$V_{ultra} (1S)$ (cm ³ g ⁻¹)	$V_{micro} (1S)$ (cm ³ g ⁻¹)	$V_{meso} (1S)$ (cm ³ g ⁻¹)	$V_{tot} (1S)$ (cm ³ g ⁻¹)	X_{1S} (%)	y_{1S} (%)	
700	0.55	37.5	661	0.14	0.14	–	0.14	70.1	29.9	
750	0.9	75	882	0.14	0.26	0.02	0.28	78.5	21.5	
750	0.2	0	523	0.12	0.12	–	0.12	68.3	31.7	
750	0.2	75	760	0.14	0.19	0.01	0.20	71.3	28.7	
700	0.55	37.5	669	0.14	0.15	–	0.15	70.0	30.0	
650	0.9	0	537	0.12	0.12	–	0.12	68.2	31.8	
700	0.55	37.5	700	0.14	0.15	0.02	0.17	69.9	30.1	
650	0.9	75	606	0.13	0.13	–	0.13	69.2	30.8	
750	0.9	0	400	0.10	0.10	–	0.10	69.2	30.8	
650	0.2	0	574	0.12	0.12	–	0.12	67.9	32.1	
650	0.2	75	625	0.13	0.13	–	0.13	67.8	32.2	

(500 °C, atmospheric pressure, and 5 °C min⁻¹ as heating rate) and subsequent activation at 700–850 °C and 0.1–1.0 MPa under a pure CO₂ atmosphere. In particular, ACs obtained from biochars produced at 400 °C and 0.2 MPa showed, in some cases, better textural properties than those produced under similar conditions in the above-mentioned work (even when high pressures were applied to promote the extent of the reverse Boudouard reaction during the activation step). This finding seems to demonstrate the pivotal role that the pyrolysis operating conditions play in determining the textural properties of the resulting ACs. Table 1 shows that the AC with the highest surface area (998 cm² g⁻¹) and the most developed porosity was obtained from a biochar produced at 400 °C and 0.2 MPa, confirming the considerations explained in this section.

3.1.2. One-step activation

Fig. 3a shows the influence of the process operating conditions on the burn-off (X_{1S}) during the one-step production of ACs. As expected, the main factor affecting mass loss was the maximum temperature; its increase from 650 to 750 °C led to a higher carbonization degree, due to a more pronounced thermal degradation of the biomass constituents [42,43]. Even though the effect was smaller, the presence of CO₂ as an activating agent also contributed to increase the burn-off, as a clear consequence of the gasification of the carbonaceous matrix. Overall, the lowest value of X_{1S} was 67.8%, corresponding to the mildest temperature (650 °C),

whereas the highest value (78.5%) was obtained at 750 °C under an atmosphere containing CO₂. It is important to remember that the X_{1S} values took into account the mass loss related to the pyrolysis step too; for this reason, they resulted to be higher than the X_{2S} values.

According to a previous study conducted on the pyrolysis of WS pellets [32], it was confirmed that absolute pressure does not have a significant effect on the final yield of the resulting carbon material. The role of CO₂ atmosphere and, to a lesser extent, maximum temperature, was predominant for the development of porosity; indeed, their significant effects on the surface area and pores volumes are clearly visible in Fig. 3b–e. In contrast to the previous work [32], which was performed at lower maximum pyrolysis temperatures (400–550 °C), the ultra-micropore volume did not appear to be affected by the maximum temperature, which generally leads to greater thermal degradation of biomass, followed by additional evolution of volatiles, resulting in the creation of new pores. This discrepancy is probably due to the higher maximum temperatures used in this work; in particular, the higher the temperature, the lower its effect on $V_{ultra} (1S)$. Similar to what was observed for the two-step activation process, $V_{meso} (1S)$ was not reported in Fig. 3 due to the lack of mesopore formation. Even though the reactor configuration was designed for maximizing the biochar yield (i.e., enhancing secondary charring reactions through a slow release of primary volatiles at the inter-particle level) rather

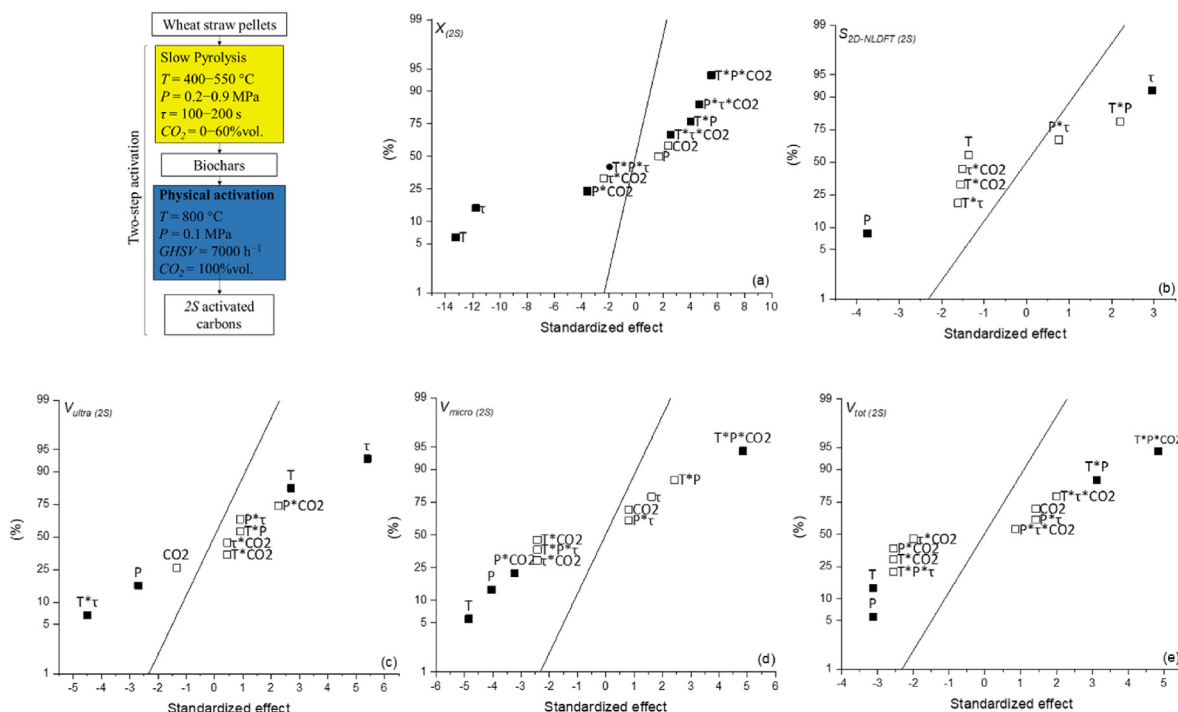


Fig. 2. Normal plot of the standardized effects ($\alpha = 0.05$) for ACs produced by two-step (2S) activation: (a) burn-off (X); (b) surface area ($S_{2D-NLDFT}$); (c) ultramicropore volume (V_{ultra}); (d) micropore volume (V_{micro}); and (e) total pore volume (V_{tot}) (squares = significant effect; empty squares = non-significant effect; the straight line represents the null-effect points).

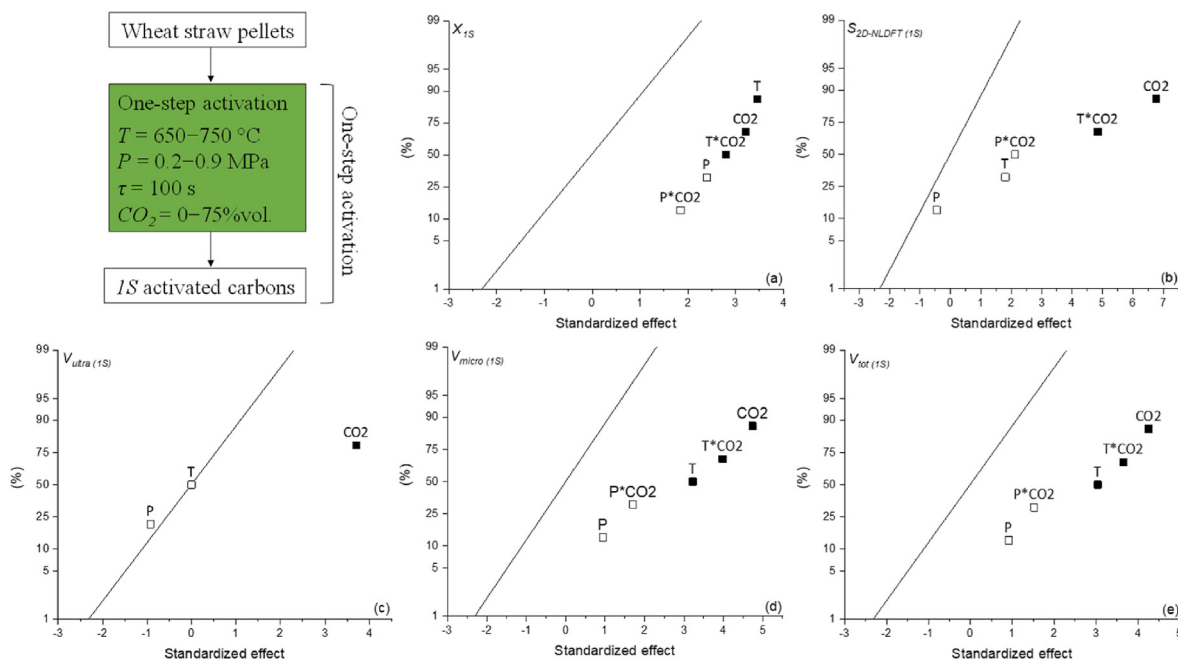


Fig. 3. Same as Fig. 2, but ACs produced by one-step (1S) activation: (a) burn-off (X), (b) ultramicropore volume (V_{ultra}), (c) micropore volume (V_{micro}), (d) mesopore volume (V_{meso}) and (e) total pore volume (V_{tot}) (square, significant effect; empty square, non-significant effect; the straight line represents the null-effect points).

than for activating the biochar, and keeping in mind the relatively milder temperatures employed, the surface areas as well as the porosity development of the 1S ACs were only slightly lower than those obtained for 2S ACs. In fact, the best one-step AC (produced at 750 °C and 0.9 MPa) showed textural properties very similar to those reported for the two-step ACs. Moreover, the 1S ACs showed a

higher final mass yield in comparison to that related to the 2S ACs, which resulted to be almost twice higher in all cases (see Tables 1 and 2, respectively). The reason behind this discrepancy between the two production routes is mainly due to the different activation conditions adopted, especially in terms of maximum temperature and CO₂ concentration in the reactor atmosphere, which were more

severe during the 2S activation process. These outstanding results demonstrate that one-step pressurized activation might be a valuable alternative to the conventional two-step activation, due to its lower energy cost and higher efficiency in terms of processing time and production capacity.

3.2. FT-IR spectra and surface chemistry

The results of FT-IR spectroscopy measurements for 2S ACs are shown in Fig. A.4a. The samples were mainly characterized by methylene groups (1460 cm^{-1}), aromatic rings ($1450\text{--}1600\text{ cm}^{-1}$) and, in some cases, OH groups (3500 cm^{-1}). The bands showed relatively small differences in intensity, meaning that the number of retained functional groups in the 2S ACs was not significantly influenced by the pyrolysis operating conditions. Conversely, more intense bands, for the aforementioned functional groups, were visible for 1S ACs (see Fig. A.4b), even at the highest maximum temperature ($750\text{ }^{\circ}\text{C}$). This finding may be ascribed to differences in the reactor configuration as well as in the different temperature conditions and CO_2 concentrations employed during the synthesis of 2S and 1S ACs.

3.3. CO_2 adsorption capacity and selectivity CO_2/CH_4

The ACs with the highest surface area and porosity (three 2S carbons and three 1S carbons) were selected for CO_2 and CH_4 adsorption experiments. The tested carbon materials are reported in Table 3. The Sips isotherm model (see Appendix A for further details) was fitted simultaneously to the experimental data at different temperature for each material. The parameters obtained by fitting the isotherm model are presented in Table A.4, and were used to perform the IAST-based and breakthrough simulations. The experimental isotherm data were also used to calculate the average heat of adsorption by means of the Clausius-Clapeyron equation. The average heat of adsorption is presented in Table A.8, and was then used to simulate the non-isothermal adsorption breakthrough curves.

According to the observations reported in Section 3.1.1, the combination of lower temperatures and pressures and higher gas residence time during the pyrolysis step proved to be crucial for obtaining 2S carbons with high surface areas and developed porosity. As expected, the molar amounts of CO_2 and CH_4 adsorbed at equilibrium conditions increased with pressure and decreased with temperature (see Fig. 4). Furthermore, the slope of the isotherm became less steep with increasing pressure because the adsorption sites are closer to saturation under these conditions. Fig. 4 also shows that the CO_2 and CH_4 adsorption isotherms were fully reversible, indicating physical adsorption [4]. All WS-derived ACs preferentially adsorbed CO_2 over CH_4 , due to the higher quadrupole moment of CO_2 [14,44], which promotes a stronger attraction between the adsorbate and the adsorbent surface.

Overall, 2S ACs reached higher CO_2 uptake capacity than 1S ACs

when the pressure was increased to 3.5 MPa. However, the performances of 2S and 1S ACs were perfectly comparable at lower pressures (0–0.5 MPa). The CO_2 uptake capacity at 0.1 MPa of the ACs produced in this study is compared with those of carbon-based adsorbents reported from previous studies in Table A.5. It is easy to observe that our ACs exhibited somewhat higher adsorbed amounts of CO_2 than many in the literature, regardless of their higher surface areas (up to $3000\text{ m}^2\text{ g}^{-1}$) and even though they were tested at lower temperatures (i.e., $20\text{ }^{\circ}\text{C}$) in some cases.

Fig. 5a shows the CO_2/CH_4 selectivity values under 10 vol % CO_2 , which were calculated using the IAST method after fitting the Sips equation to the isotherms. The selectivity profiles of the ACs were not visibly affected by the variation of the CO_2/CH_4 concentration ratio; for this reason, the selectivity profiles at higher CO_2 content are reported in Appendix A (see Fig. A.5). At pressures below 0.5 MPa, all samples showed high values of selectivity (up to more than 10) and these decreased with increasing pressure. Some authors have claimed that the predominant effect of the CO_2 -sorbent interaction due to the basic functionalities on the surface [45]. However, it has been shown that it is only true for working pressures below 0.5 MPa. The shift from surface chemistry-controlled to pore texture-controlled behavior occurs at 0.5 MPa [46]. The latter study is in good agreement with the present results. By increasing the pressure above 1.0 MPa, the 2S ACs showed a slight tendency to increase in selectivity, which was accentuated when the CO_2 concentration was higher. According to Castrillon et al. [4], the proportional increase in selectivity with pressure could probably be due to the intrinsic shape of the CO_2 and CH_4 isotherms; in other words, CO_2 uptake was positively affected by pressure to a greater extent than CH_4 uptake. On the other hand, the small increase in selectivity at higher CO_2 concentrations seems to be in disagreement with the reported literature [4]. This result is probably due to a combination of factors, such as PSD, micropore volume and surface area of the samples. The effect of CO_2 concentrations on selectivity at high pressures was even more visible for the 1S AC produced at $700\text{ }^{\circ}\text{C}$, 0.55 MPa, 100 s and 37.5 vol % CO_2 , whereas the selectivity related to the other 1S ACs remained approximately constant after the initial decrease. Overall, the 2S-3 sample appeared to be the best AC in terms of CO_2 retention, showing higher selectivity regardless of pressure and CO_2 content (see Fig. 5b for the corresponding set of selectivity profiles).

In conclusion, the resulting selectivity values were notably high for all ACs produced in this study, in most cases even higher than those reported in previous studies (see Table A.6) and examined under the same conditions. In addition, the CO_2/CH_4 selectivity profiles under 10, 30, 50 and 70 vol % CO_2 of a commercial AC (from *Brascarbo Agroindustrial Ltda.*, Brazil) [47] were also calculated using the IAST method (see Fig. A.6) for further comparison purposes. In line with the above-reported findings, the AC from *Brascarbo* showed slightly lower selectivity values, despite being examined under the same conditions and having a surface area totally comparable with those of 1S and 2S ACs.

Table 3
Activated carbons selected for CO_2 and CH_4 adsorption experiments.

Type of activation	AC	Slow Pyrolysis				CO_2 activation			
		T ($^{\circ}\text{C}$)	P (MPa)	τ (s)	CO_2 (vol. %)	T ($^{\circ}\text{C}$)	P (MPa)	τ (s)	CO_2 (vol. %)
One-Step	1S-1	–	–	–	–	700	0.55	100	37.5
	1S-2	–	–	–	–	750	0.2	100	75
	1S-3	–	–	–	–	750	0.9	100	75
Two-Step	2S-1	400	0.2	100	60	800	0.1	–	100
	2S-2	400	0.2	200	0	800	0.1	–	100
	2S-3	400	0.2	200	60	800	0.1	–	100

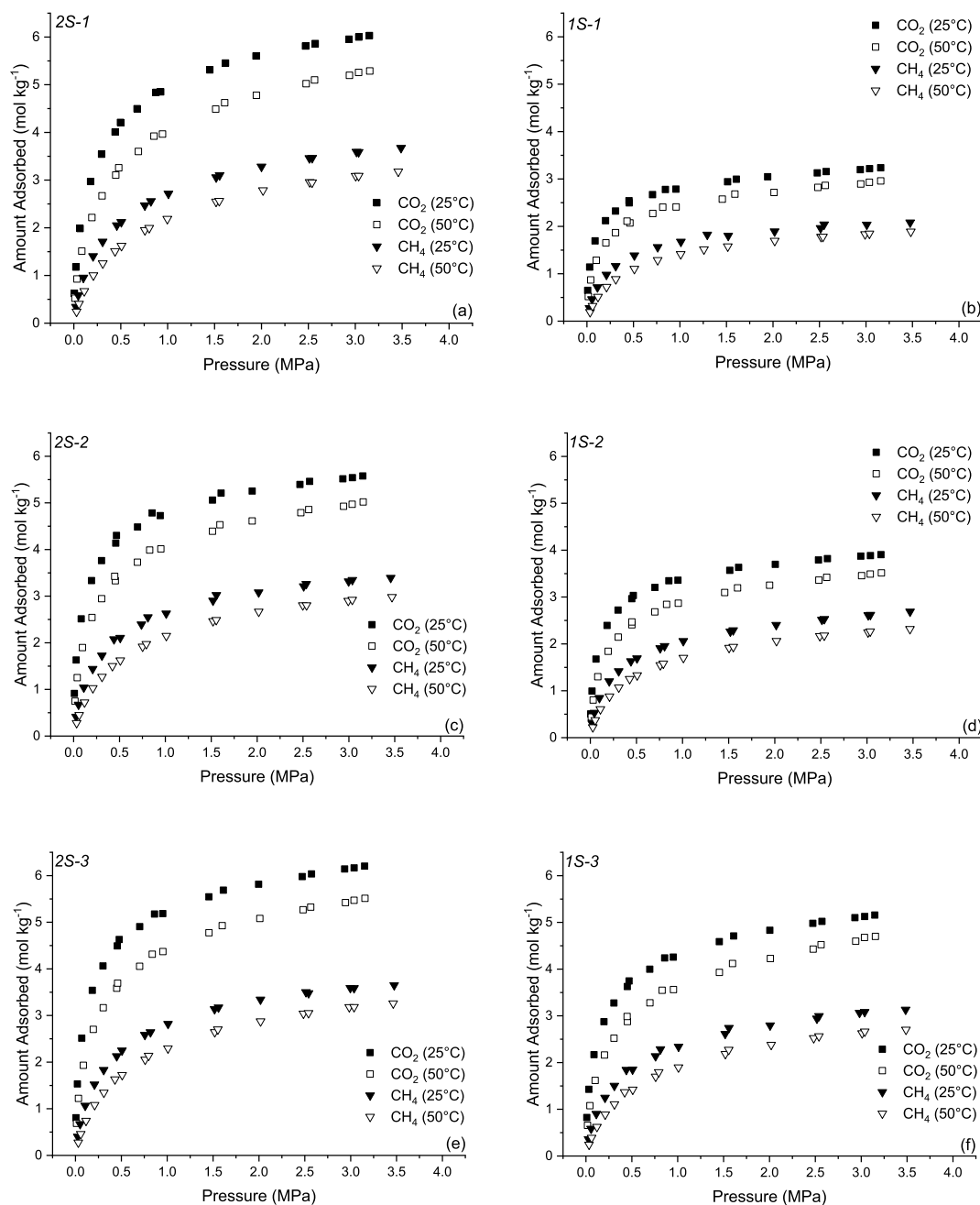


Fig. 4. CO₂ and CH₄ adsorption isotherms for selected 1S and 2S activated carbons (see Table 3 for details on production process conditions).

3.4. Simulated breakthrough curves

Although the IAST model is a suitable method to predict the separation selectivity of ACs, the study of their performance under dynamic conditions remains an essential step before any application. Fig. 6a–b show, respectively, the simulated CH₄ and CO₂ breakthrough curves at 0.5 MPa for each AC, whereas the fixed bed parameters used for the simulations are reported in Table 4. Additional parameters used in the simulation of the adsorption breakthrough, such as those related to the adsorption isotherms, kinetics, and thermodynamics, are given in Appendix A (Tables A.4, A.7 and A.8, respectively). The full set of breakthrough simulations for the selected ACs are available in Figs. A.7–A.12. In all simulations, methane breakthrough occurred before carbon dioxide

breakthrough, indicating the ability of all materials to achieve methane separation from mixtures with carbon dioxide. This is due to the fact that CH₄ is a completely non-polar molecule and interacts very weakly with most materials. While CO₂ has a quadrupolar moment and so it interacts, both physically and chemically, with the ACs surface. In addition, the adsorption breakthrough curves shown in Figs. A.7–A.12 indicated that the retention time of both gases increased with operating pressure.

As expected, Fig. 6a shows that the CH₄ stoichiometry time (i.e., the time needed to reach 50% of the feed flow rate at the reactor outlet, represented by $t_{CH_4}^*$) at 0.5 MPa was shorter, between 9 and 14 min, than that of CO₂, $t_{CO_2}^*$, which ranged from 34 to 43 min (Fig. 6b). In addition, in Fig. 6a, it is possible to observe the typical

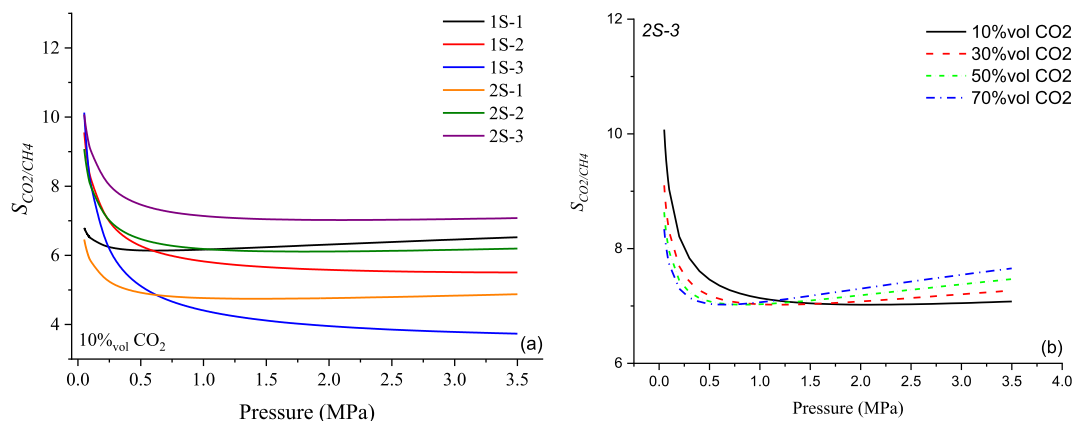


Fig. 5. (a) IAST-based selectivity values for ACs tested under 10 vol % CO₂; and (b) selectivity profiles of 2S-3 AC under 10, 30, 50, and 70 vol % CO₂.

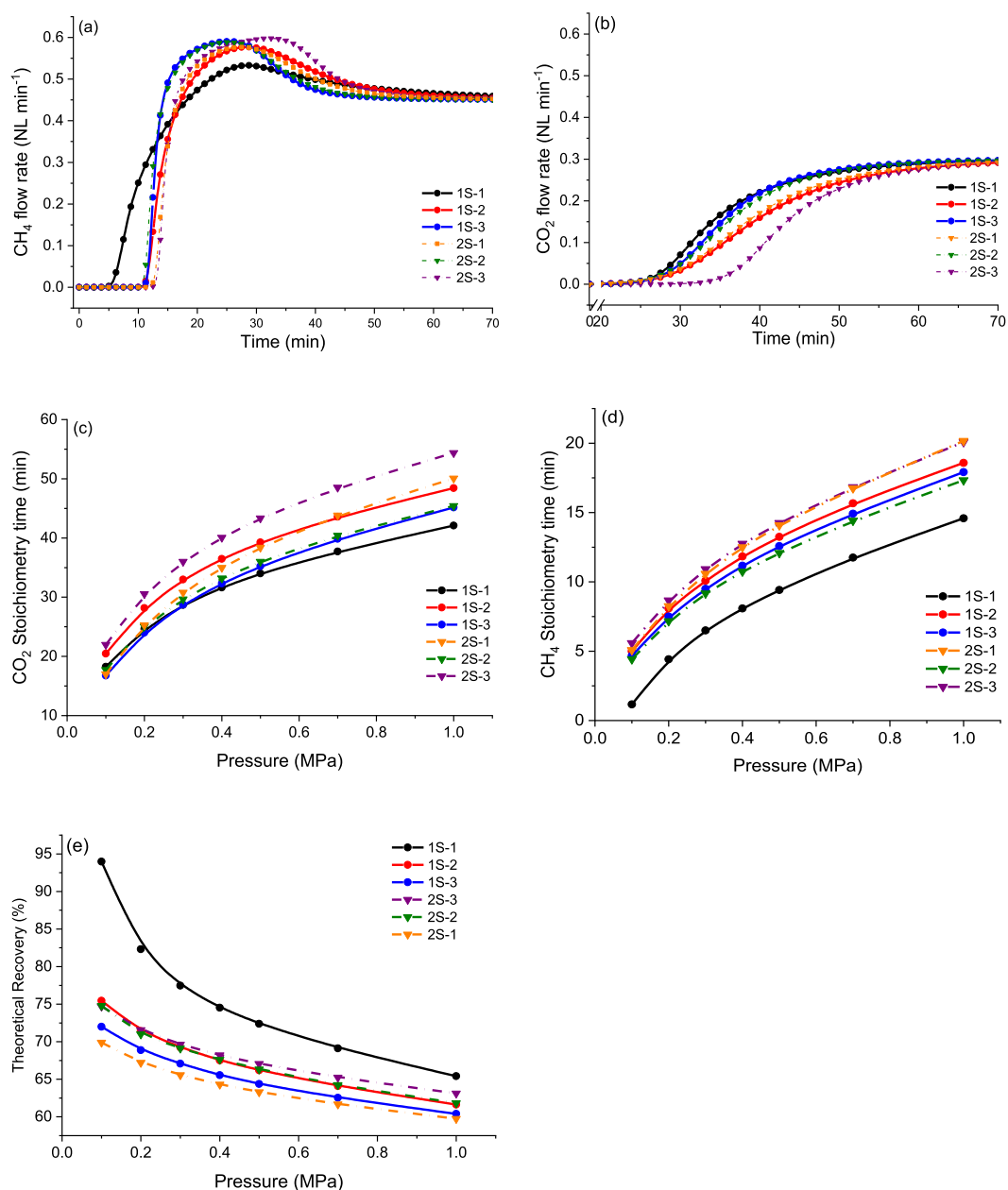


Fig. 6. Simulated results for (a) CH₄ and (b) CO₂ breakthrough curves at 0.5 MPa and 30 °C; (c) CH₄ and (d) CO₂ adsorption stoichiometry times as function of adsorption pressure; and (e) theoretical CH₄ recovery as a function of adsorption pressure.

Table 4
Fixed bed parameters used for the breakthrough simulations.

Activated carbon	Bed density (kg m ⁻³)	Bed porosity (-)	Particle density (kg m ⁻³)	Particle porosity (-)	Average particle diameter (mm)
1S-1	599	0.534	1285	0.431	0.14
1S-2	603	0.493	1190	0.474	0.30
1S-3	450	0.716	1586	0.298	0.22
2S-1	471	0.602	1184	0.476	0.32
2S-2	391	0.660	1149	0.491	0.41
2S-3	433	0.626	1158	0.488	0.34

roll-over phenomena, consisting of a temporary excess of CH₄ flow rate over the feed concentration, due to the replacement of CH₄ by CO₂ on the sorbent surface [5]. During an adsorption separation process, $t_{CO_2}^*$ and $t_{CH_4}^*$ represent the limits of the operation time; from an industrial point of view, longer CO₂ stoichiometry times are strongly desired in order to ensure longer operation times. Conversely, shorter values of $t_{CH_4}^*$ are required, as they are directly related to the amount of CH₄ desorbed from the solid phase. Given that both $t_{CO_2}^*$ and $t_{CH_4}^*$ are direct functions of the respective gas amounts adsorbed at equilibrium, they strictly depend on the breakthrough pressure, as shown in Fig. 6c–d. These figures also confirmed that CH₄ broke through earlier than CO₂, regardless of the pressure considered. Overall, the 2S AC obtained from the biochar produced at 400 °C, 0.2 MPa, 200 s under a 60 vol % CO₂ atmosphere (2S-3) showed the highest t^* values over the whole range of pressures adopted during all experiments, in line with its high selectivity observed in the previous section.

Since the pure CH₄ flow rate definitely leaves the adsorption column in the time interval between $t_{CO_2}^*$ and $t_{CH_4}^*$, the amount of pure CH₄ released during the adsorption process directly depends on both stoichiometric times. Taking this aspect into account, it is possible to calculate a theoretical CH₄ recovery from the adsorption process as:

$$Recovery_{CH_4} = (t_{CO_2}^* - t_{CH_4}^*) / t_{CO_2}^* \quad (6)$$

The theoretical CH₄ recovery values obtained for the examined ACs (see Fig. 6e) highlighted the 1S AC produced at 700 °C, 0.55 MPa, 100 s under a 37.5 vol % CO₂ atmosphere (1S-1) as the sorbent with the highest theoretical recovery, reaching around 95% at 0.1 MPa, and dropping to about 70% at 1.0 MPa. This result, clearly in contrast to the findings obtained by IAST methodology, is mainly due to the effects of various factors disregarded in the aforementioned IAST model, such as slow CH₄ diffusion and different packing densities (see Table 4). Furthermore, breakthrough simulations also predicted temperature increases around 25 °C inside the fixed-bed column (see Figs. A.6–A.11), which could also have a considerable effect on the adsorption process performance. Another parameter not considered in the IAST model, which certainly affected CH₄ recovery, was the average particle diameter, in particular, the smaller the particles, the higher the recovery. The CH₄ recovery values obtained for the 1S and 2S ACs were similar to many adsorbents reported in the literature (see Table A.9), although it is important to keep in mind that the operating pressures were milder than those employed in this work.

4. Conclusions

Sustainable activated carbons (ACs) from wheat straw (WS) biomass were produced by one-step (1S) and two-step (2S) physical activation processes. The obtained outcomes indicate that, for wheat straw and the range of operating conditions adopted, the one-step ACs exhibit similar textural features as ACs synthesized via a traditional two-step pathway. Interestingly, the 1S ACs can be

produced at considerably higher mass yields, which makes them attractive for commercial exploitation. Furthermore, 1S and 2S ACs exhibited even higher CO₂ uptakes and CO₂/CH₄ selectivity values than several adsorbents reported in the literature, proving that they are absolutely feasible for CH₄/CO₂ separation. In particular, the 2S AC produced at 400 °C, 0.2 MPa, 200 s and 60 vol % CO₂ showed the highest IAST-based selectivity, regardless of the CO₂ concentration and pressure conditions applied. However, breakthrough simulations revealed that the 1S AC produced at 700 °C, 0.55 MPa, 100 s and 37.5 vol % CO₂ showed the best CH₄ recovery performance under dynamic conditions. These notable findings highlighted 1S physical activation at moderate pressure as a promising route to produce carbon-based adsorbents, which may replace the conventional 2S physical activation process and lead to remarkable improvements, especially on an industrial scale. Indeed, 1S physical activation would allow a significant reduction in operating and installation costs as well as an improvement in productivity.

CRediT authorship contribution statement

Gianluca Greco: Conceptualization, Methodology, Software, Validation, Formal analysis, Investigation, Data curation, Writing – original draft, Resources. **Rafael L.S. Canevesi:** Conceptualization, Data curation, Methodology, Investigation, Resources, Software, Formal analysis, Writing – original draft. **Christian Di Stasi:** Data curation, Methodology, Investigation, Resources. **Alain Celzard:** Data curation, Resources, Supervision, Writing – review & editing. **Vanessa Fierro:** Data curation, Methodology, Resources, Supervision, Writing – review & editing. **Joan J. Manyà:** Resources, Writing – review & editing, Visualization, Supervision, Project administration.

Declaration of competing interest

The authors declare that they have no known competing financial interests or personal relationships that could have appeared to influence the work reported in this paper.

Acknowledgments

This project has received funding from the European Union's Horizon 2020 research and innovation program under the Marie Skłodowska-Curie grant agreement No 721991. JJM also acknowledge the funding from the Aragon Government (Ref. T22_20R), co-funded by FEDER 2014–2020 "Construyendo Europa desde Aragón". This study was partly supported by the TALiSMAN project (2019-000214), funded by the European Regional Development Fund (ERDF).

Appendix A. Supplementary data

Supplementary data to this article can be found online at <https://doi.org/10.1016/j.renene.2022.04.035>.

Nomenclature

m_{biochar}	mass of biochar
m_{biomass}	mass of biomass
m_f	final mass of the sample
$S_{2D-NLDFT}$	surface area
$S_{\text{CO}_2/\text{CH}_4}$	CO ₂ selectivity over CH ₄
V_{meso}	mesopore volume
V_{micro}	micropore volume
V_{tot}	total pore volume
V_{ultra}	ultra-micropore volume
X_i	burn-off
y_{char}	biochar yield
y_i	mass yield
ρ_{bed}	bed density
ρ_{par}	particle density

Acronyms

FT-IR	Fourier-Transform Infrared spectroscopy
GHSV	gas-hourly space velocity
IAST	Ideal Adsorbed Solution Theory
MEA	Mono-Ethanolamine
PSD	pore size distribution
1S	one-step activation
2S	two-step activation
XRF	X-Ray Fluorescence
WS	Wheat Straw

References

- N. Yang, R. Wang, Sustainable technologies for the reclamation of greenhouse gas CO₂, *J. Clean. Prod.* 103 (2015) 784–792, <https://doi.org/10.1016/j.jclepro.2014.10.025>.
- E.S. Shuba, D. Kifle, Microalgae as biofuels: 'Promising' alternative and renewable energy, review, *Renew. Sustain. Energy Rev.* 81 (2018) 743–755, <https://doi.org/10.1016/j.rser.2017.08.042>.
- G. Goula, V. Kioussis, L. Nalbandian, I. V. Ventekakis, Catalytic and electro-catalytic behavior of Ni-based cermet anodes under internal dry reforming of CH₄+CO₂ mixtures in SOFCs, *Solid State Ionics* 177 (2006) 2119–2123, <https://doi.org/10.1016/j.ssi.2006.03.040>.
- M.C. Castrillon, K.O. Moura, A.C. Alves, M. Bastos-Neto, D.C.S. Azevedo, J. Hofmann, J. Möllmer, W.-D. Einicke, R. Gläser, CO₂ and H₂S removal from CH₄-rich streams by adsorption on activated carbons modified with K₂CO₃, NaOH, or Fe₂O₃, *Energy Fuel*. 30 (2016) 9596–9604, <https://doi.org/10.1021/acs.energyfuels.6b01667>.
- I. Durán, N. Álvarez-Gutiérrez, F. Rubiera, C. Pevida, Biogas purification by means of adsorption on pine sawdust-based activated carbon: impact of water vapor, *Chem. Eng. J.* 353 (2018) 197–207, <https://doi.org/10.1016/j.cej.2018.07.100>.
- B.P. Spigarelli, S.K. Kawatra, Opportunities and challenges in carbon dioxide capture, *J. CO₂ Util.* 1 (2013) 69–87, <https://doi.org/10.1016/j.jcou.2013.03.002>.
- X. Zhang, X. He, T. Gundersen, Post-combustion carbon capture with a gas separation membrane: parametric study, capture cost, and exergy analysis, *Energy Fuel*. 27 (2013) 4137–4149, <https://doi.org/10.1021/ef3021798>.
- J. Baxter, Z. Bian, G. Chen, D. Danielson, M.S. Dresselhaus, A.G. Fedorov, T.S. Fisher, C.W. Jones, E. Maginn, U. Kortshagen, A. Manthiram, A. Nozik, D.R. Rolison, T. Sands, L. Shi, D. Sholl, Y. Wu, Nanoscale design to enable the revolution in renewable energy, *Energy Environ. Sci.* 2 (2009) 559–588, <https://doi.org/10.1039/B821698C>.
- R. Ben-Mansour, M.A. Habib, O.E. Bamidele, M. Basha, N.A.A. Qasem, A. Peedikakkal, T. Laoui, M. Ali, Carbon capture by physical adsorption: materials, experimental investigations and numerical modeling and simulations – a review, *Appl. Energy* 161 (2016) 225–255, <https://doi.org/10.1016/j.apenergy.2015.10.011>.
- N.A. Rashidi, S. Yusup, An overview of activated carbons utilization for the post-combustion carbon dioxide capture, *J. CO₂ Util.* 13 (2016) 1–16, <https://doi.org/10.1016/j.jcou.2015.11.002>.
- C.A. Grande, Advances in pressure swing adsorption for gas separation, *ISRN Chem. Eng.* 2012 (2012), 982934, <https://doi.org/10.5402/2012/982934>.
- F. Dreisbach, R. Staudt, J.U. Keller, High pressure adsorption data of methane, nitrogen, carbon dioxide and their binary and ternary mixtures on activated carbon, *Adsorption* 5 (1999) 215–227, <https://doi.org/10.1023/A:1008914703884>.
- J. McEwen, J.-D. Hayman, A. Ozgur Yazaydin, A comparative study of CO₂, CH₄ and N₂ adsorption in ZIF-8, Zeolite-13X and BPL activated carbon, *Chem. Phys.* 412 (2013) 72–76, <https://doi.org/10.1016/j.chemphys.2012.12.012>.
- M. Álvarez-Gutiérrez, N. Victoria Gil, F. Rubiera, C. Pevida, Cherry-stones-based activated carbons as potential adsorbents for CO₂/CH₄ separation: effect of the activation parameters, *Greenh. Gases Sci. Technol.* 5 (2015) 812–825, <https://doi.org/10.1002/ghg.1534>.
- Y. Zheng, Q. Li, C. Yuan, Q. Tao, Y. Zhao, G. Zhang, J. Liu, Influence of temperature on adsorption selectivity: coal-based activated carbon for CH₄ enrichment from coal mine methane, *Powder Technol.* 347 (2019) 42–49, <https://doi.org/10.1016/j.powtec.2019.02.042>.
- D. Peredo-Mancilla, C.M. Ghimbeu, B.-N. Ho, M. Jeguirim, C. Hort, D. Bessieres, Comparative study of the CH₄/CO₂ adsorption selectivity of activated carbons for biogas upgrading, *J. Environ. Chem. Eng.* 7 (2019), 103368, <https://doi.org/10.1016/j.jece.2019.103368>.
- Y. Zhao, X. Liu, Y. Han, Microporous carbonaceous adsorbents for CO₂ separation via selective adsorption, *RSC Adv.* 5 (2015) 30310–30330, <https://doi.org/10.1039/C5RA00569H>.
- J. Park, N.F. Attia, M. Jung, M.E. Lee, K. Lee, J. Chung, H. Oh, Sustainable nanoporous carbon for CO₂, CH₄, N₂, H₂ adsorption and CO₂/CH₄ and CO₂/N₂ separation, *Energy* 158 (2018) 9–16, <https://doi.org/10.1016/j.energy.2018.06.010>.
- P. Kluson, S. Scaife, Microporous adsorbents for a selective separation of carbon dioxide from mixtures with methane and nitrogen, *Chem. Biochem. Eng. Q.* 16 (2002) 97–103, <https://doi.org/10.15255/CABEQ.2014.635>.
- R.B. Rios, H.R. Stragliotto, F.M. Peixoto, A.E.B. Torres, J. Bastos-Neto, M. Azevedo, D.C.S. Cavalcante, C. L. Studies on the adsorption behavior of CO₂-CH₄ mixtures using activated carbon, *Braz. J. Chem. Eng.* 30 (2013) 939–951, <https://doi.org/10.1590/S0104-66322013000400024>.
- O. Mašek, P. Brownsort, A. Cross, S. Sohi, Influence of production conditions on the yield and environmental stability of biochar, *Fuel* 103 (2013) 151–155, <https://doi.org/10.1016/j.fuel.2011.08.044>.
- F. Ronse, S. van Hecke, D. Dickinson, W. Prins, Production and characterization of slow pyrolysis biochar: influence of feedstock type and pyrolysis conditions, *GCB Bioenergy* 5 (2013) 104–115, <https://doi.org/10.1111/gcbb.12018>.
- J.J. Manyà, B. González, M. Azuara, G. Arner, Ultra-microporous adsorbents prepared from vine shoots-derived biochar with high CO₂ uptake and CO₂/N₂ selectivity, *Chem. Eng. J.* 345 (2018) 631–639, <https://doi.org/10.1016/j.cej.2018.01.092>.
- M. Molina-Sabio, M.T. Gonzalez, F. Rodriguez-Reinoso, A. Sepúlveda-Escribano, Effect of steam and carbon dioxide activation in the micropore size distribution of activated carbon, *Carbon N. Y.* 34 (1996) 505–509, [https://doi.org/10.1016/0008-6223\(96\)00006-1](https://doi.org/10.1016/0008-6223(96)00006-1).
- M.G. Plaza, A.S. González, J.J. Pis, F. Rubiera, C. Pevida, Production of microporous biochars by single-step oxidation: effect of activation conditions on CO₂ capture, *Appl. Energy* 114 (2014) 551–562, <https://doi.org/10.1016/j.apenergy.2013.09.058>.
- A. Linares-Solano, J. De D. López-González, M. Molina-Sabio, F. Rodriguez-Reinoso, Active carbons from almond shells as adsorbents in gas and liquid phases, *J. Chem. Technol. Biotechnol.* 30 (1980) 65–72, <https://doi.org/10.1002/jctb.503300109>.
- A.C. Lua, J. Guo, Activated carbon prepared from oil palm stone by one-step CO₂ activation for gaseous pollutant removal, *Carbon N. Y.* 38 (2000) 1089–1097, [https://doi.org/10.1016/S0008-6223\(99\)00231-6](https://doi.org/10.1016/S0008-6223(99)00231-6).
- K. Yang, J. Peng, H. Xia, L. Zhang, C. Srinivasakannan, S. Guo, Textural characteristics of activated carbon by single step CO₂ activation from coconut shells, *J. Taiwan Inst. Chem. Eng.* 41 (2010) 367–372, <https://doi.org/10.1016/j.jtice.2009.09.004>.
- A.S. González, M.G. Plaza, F. Rubiera, C. Pevida, Sustainable biomass-based carbon adsorbents for post-combustion CO₂ capture, *Chem. Eng. J.* 230 (2013) 456–465, <https://doi.org/10.1016/j.cej.2013.06.118>.
- D. Bergna, T. Varila, H. Romar, U. Lassi, Comparison of the properties of activated carbons produced in one-stage and two-stage processes, *J. Carbon Res.* 4 (2018), <https://doi.org/10.3390/c4030041>.
- G. Greco, M. Videgain, C. Di Stasi, B. González, J.J. Manyà, Evolution of the mass-loss rate during atmospheric and pressurized slow pyrolysis of wheat straw in a bench-scale reactor, *J. Anal. Appl. Pyrolysis* 136 (2018) 18–26, <https://doi.org/10.1016/j.jaap.2018.11.007>.
- G. Greco, C. Di Stasi, F. Rego, B. González, J.J. Manyà, Effects of slow-pyrolysis conditions on the products yields and properties and on exergy efficiency: a comprehensive assessment for wheat straw, *Appl. Energy* 279 (2020), <https://doi.org/10.1016/j.apenergy.2020.115842>.
- J.J. Manyà, M.A. Ortigosa, S. Laguarda, J.A. Manso, Experimental study on the effect of pyrolysis pressure, peak temperature, and particle size on the potential stability of vine shoots-derived biochar, *Fuel* 133 (2014) 163–172, <https://doi.org/10.1016/j.fuel.2014.05.019>.
- L. Wang, Ø. Skreiberg, M. Gronli, G.P. Specht, M.J. Antal, Is elevated pressure required to achieve a high fixed-carbon yield of charcoal from biomass? Part 2: the importance of particle size, *Energy Fuels* 27 (2013) 2146–2156, <https://doi.org/10.1021/ef400041h>.
- C. Di Stasi, D. Alvira, G. Greco, B. González, J.J. Manyà, Physically activated wheat straw-derived biochar for biomass pyrolysis vapors upgrading with high resistance against coke deactivation, *Fuel* 255 (2019), 115807, <https://doi.org/10.1016/j.fuel.2019.115807>.
- J. Jagiello, J. Kenvin, C.O. Ania, J.B. Parra, A. Celzard, V. Fierro, Exploiting the

- adsorption of simple gases O₂ and H₂ with minimal quadrupole moments for the dual gas characterization of nanoporous carbons using 2D-NLDFT models, *Carbon* N. Y. 160 (2020) 164–175, <https://doi.org/10.1016/j.carbon.2020.01.013>.
- [37] D.C. Montgomery, *Design and Analysis of Experiments*, sixth ed., 2005. Hoboken.
- [38] F. Min, M. Zhang, Y. Zhang, Y. Cao, W.-P. Pan, An experimental investigation into the gasification reactivity and structure of agricultural waste chars, *J. Anal. Appl. Pyrolysis* 92 (2011) 250–257, <https://doi.org/10.1016/j.jaap.2011.06.005>.
- [39] W. Zhu, W. Song, W. Lin, Catalytic gasification of char from co-pyrolysis of coal and biomass, *Fuel Process. Technol.* 89 (2008) 890–896, <https://doi.org/10.1016/j.fuproc.2008.03.001>.
- [40] C.R. Correa, M. Stollovsky, T. Hehr, Y. Rauscher, B. Rolli, A. Kruse, Influence of the carbonization process on activated carbon properties from lignin and lignin-rich biomasses, *ACS Sustain. Chem. Eng.* 5 (2017) 8222–8233, <https://doi.org/10.1021/acsschemeng.7b01895>.
- [41] C. Di Stasi, G. Greco, R.L.S. Canevesi, M.T. Izquierdo, V. Fierro, A. Celzard, B. González, J.J. Manyà, Influence of activation conditions on textural properties and performance of activated biochars for pyrolysis vapors upgrading, *Fuel* 289 (2021), 119759, <https://doi.org/10.1016/j.fuel.2020.119759>.
- [42] C. Di Blasi, G. Signorelli, C. Di Russo, G. Rea, Product distribution from pyrolysis of wood and agricultural residues, *Ind. Eng. Chem. Res.* 38 (1999) 2216–2224, <https://doi.org/10.1021/ie980711u>.
- [43] A.V. McBeath, C.M. Wurster, M.I. Bird, Influence of feedstock properties and pyrolysis conditions on biochar carbon stability as determined by hydrogen pyrolysis, *Biomass Bioenergy* 73 (2015), <https://doi.org/10.1016/j.biombioe.2014.12.022>.
- [44] E. Buss, Gravimetric measurement of binary gas adsorption equilibria of methane–carbon dioxide mixtures on activated carbon, *Gas Separ. Purif.* 9 (1995) 189–197, [https://doi.org/10.1016/0950-4214\(95\)98226-B](https://doi.org/10.1016/0950-4214(95)98226-B).
- [45] S. Furmaniak, P. Kowalczyk, A.P. Terzyk, P.A. Gauden, P.J.F. Harris, Synergetic effect of carbon nanopore size and surface oxidation on CO₂ capture from CO₂/CH₄ mixtures, *J. Colloid Interface Sci.* 397 (2013) 144–153, <https://doi.org/10.1016/j.jcis.2013.01.044>.
- [46] R.L.S. Canevesi, S. Schaefer, M.T. Izquierdo, A. Celzard, V. Fierro, Roles of surface chemistry and texture of nanoporous activated carbons in CO₂ capture, *ACS Appl. Nano Mater.* (2022), <https://doi.org/10.1021/acsnm.1c04474>.
- [47] Brascarbo agroindustrial Ltda., n.d. <https://brascarbo.com.br/carvao/>. (Accessed 15 March 2022).

Appendix A: Supplementary material

Biomass-derived carbons physically activated in one or two steps for CH₄/CO₂ separation

Gianluca Greco^{a,*}, Rafael L. S. Canevesi^b, Christian Di Stasi^a, Alain Celzard^b, Vanessa Fierro^b, Joan J. Manyà^{a,*}

^a *Aragón Institute of Engineering Research (I3A), Thermochemical Processes Group, University of Zaragoza, Escuela Politécnica Superior, crta. Cuarte s/n, Huesca E-22071, Spain.*

^b *Université de Lorraine, CNRS, IJL, Épinal F-88000, France*

* Corresponding authors. E-mail addresses greco@unizar.es (Gianluca Greco); joanjoma@unizar.es (Joan J. Manyà).

Pyrolysis reactor configuration

The detailed diagram of the pyrolysis and activation plant is shown in Fig. A.1. Four thermocouples were placed in two thermowells, located at the axis (TC_0 and TC_3) and 35 mm radial distance from the axis (TC_1 and TC_2), to monitor the temperature profiles during the experiments. The thermocouples were placed at different heights from the bottom of the basket: 10 mm (TC_0 and TC_1), and 70 mm (TC_2 and TC_3). The proper conditions for each experiment of gas residence time and pyrolysis environment were ensured by varying the mass flow rates at STP conditions for both N_2 and CO_2 between 1.60 and 3.30 $L\ min^{-1}$. These values correspond to a gas-hourly space velocity (GHSV) ranging from 18 to 36 h^{-1} (assuming a void-volume fraction of 0.9 for the entire reactor).

In addition, the pyrolysis device was equipped with a weighing platform, which was used to monitor the real-time mass loss of the biomass during the one-step activation process.

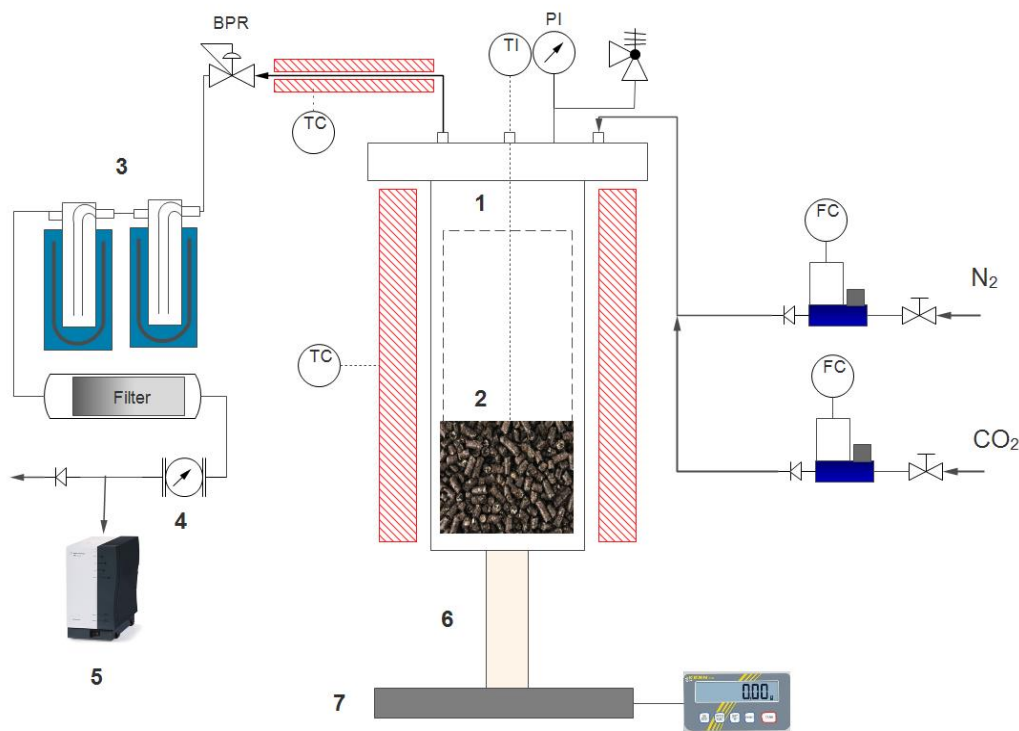


Fig. A.1. Schematic layout of the pyrolysis plant: (1) pyrolysis reactor, (2) biomass bed, (3) condensation system, (4) volumetric gas meter, (5) micro-GC, (6) ceramic tube, (7) weighing platform.

Adsorption equilibrium

The Sips model, a combination of Langmuir [1] and Freundlich [2] isotherms, was used to describe the resulting experimental data. The model can be described by the following equation:

$$q_{eq} = \frac{q_s b_s P^{1/n_s}}{1 + b_s P^{1/n_s}} \quad (\text{A.1})$$

where q is the adsorbed amount (mol kg⁻¹), P (bar) the equilibrium pressure, q_{eq} (mol kg⁻¹) is a constant reflecting the saturation adsorption capacity, b_s (bar⁻¹) is the Sips constant or affinity constant, and $1/n_s$ is the heterogeneity factor. All model parameters were fitted in Maplesoft using the sum of square error and the Dunhill simplex method [3] as objective functions.

The Ideal Adsorption Solution Theory (IAST), initially proposed by Myers and Prausnitz [4], is found to be a good tool to predict the adsorption of mixed gas using data from single-compound isotherms. This theory is based on an ideal relationship mathematically represented by:

$$P y_i = P_i^0 (\pi_i) x_i \quad (\text{A.2})$$

where P (bar) and P_i^0 (bar) are the total pressure and the theoretical pressure giving the same spreading pressure as observed in the single gas adsorption study, y_i and x_i are the molar fractions at the gas and adsorbed phases, and π_i is the spreading pressure of component i in the mixture. The Gibbs adsorption isotherm is used to obtain π_i as follows:

$$z = \frac{\pi_i}{RT} = \int_0^{P_i^0} \frac{q_i^{pure}(P)}{P} dP \quad (\text{A.3})$$

where R is the ideal gas constant, T (K) is the temperature and q_i^{pure} (mol kg⁻¹) is the molar concentration of compound i in the adsorbed phase from the single compound isotherm. Note that, under equilibrium conditions, the spreading pressure of each component must be the same:

$$\pi_1 = \pi_2 = \dots = \pi_n \quad (\text{A.4})$$

The total adsorbed amount, q_T (mol kg⁻¹), is calculated as follows:

$$\frac{1}{q_T} = \sum_{i=1}^n \frac{x_i}{q_i^0} \quad (\text{A.5})$$

where q_i^0 (mol kg⁻¹) is the adsorbed amount at the pressure giving the same spreading pressure as observed when studying the adsorption of a single gas.

Adsorption kinetics

The diffusion of the adsorbate on the adsorbent was estimated from the adsorption kinetics by means of mathematic modeling. The adopted kinetic model considers that the adsorbent particle was approximated by a sphere in order to describe the transport phenomena by the diffusion equation in spherical coordinates. In addition, further assumptions were made: (i) isothermal behavior and (ii) linearity of the isotherm at the kinetic point condition. The resulting equation is as follows.

$$\frac{\partial q}{\partial t} = \frac{1}{r^2} \frac{\partial}{\partial r} \left(r^2 D_c \frac{\partial q}{\partial r} \right) \quad (\text{A.6})$$

where D_c ($\text{m}^2 \text{s}^{-1}$) is the intraparticle diffusion coefficient and q (mol kg^{-1}) is the adsorbed phase concentration. When the bulk phase concentration is not constant and the boundary condition is time-dependent, the analytical solution of the equation A.6 is:

$$\frac{q}{q_{eq}} = 1 - 6 \sum_{n=1}^{\infty} \frac{\exp(-p_n^2 D_c / r_c^2 t)}{9 \frac{\Lambda}{1-\Lambda} + (1-\Lambda) p_n^2} \quad (\text{A.7})$$

where q_{eq} (mol kg^{-1}) is the adsorbed amount at equilibrium, r_c (m) is the particle radius, Λ (dimensionless) is the fraction of sorbate ultimately adsorbed by the adsorbent ($\Lambda \equiv (P_0 - P_{\infty}) / P_0$), and p_n (dimensionless) are the non-zero roots of the following equation:

$$\tan(p_n) = \frac{3p_n}{3 + \left(\frac{1}{\Lambda} - 1\right) p_n^2} \quad (\text{A.8})$$

At least 40 different roots of Eq. A.8 should be used in order to obtain meaningful results. The diffusion parameters were obtained by non-linear fits of the equations described above using the Dunhill simplex method in a calculation routine implemented in Python.

Mathematical model for simulation of breakthrough curves

The mathematical model adopted for the simulation of breakthrough curves is based on the following assumptions:

- Ideal gas behavior
- Heat, mass, and momentum transport are considered negligible in the radial directions;
- The momentum balance was described by the Ergun equation;
- The dual Linear Driving Force (LDF) model was used to simplify the macropore and micropore diffusion equations;
- The mass transfer resistance surrounding the pellets was taken into account;
- The void fraction, cross-sectional area and adsorbent properties were constant along the column;
- The heat transfer in different phases (gas, solid and wall) was described by different energy balances.

The mass balance for each component in the fluid phase was given by:

$$\frac{\partial C_i}{\partial t} = -\frac{\partial(uC_i)}{\partial z} + \frac{\partial}{\partial z} \left(D_{ax,i} C_T \frac{\partial Y_i}{\partial z} \right) - \frac{(1-\varepsilon_c) a_p k_{f,i}}{\varepsilon_c \left(\frac{Bi}{5} - 1 \right)} (C_i - Cp_i) \quad (\text{A.9})$$

where C_i (mol m⁻³) is the gas phase concentration, D_{ax} (mol m² s⁻¹) is the axial dispersion coefficient, u (m s⁻¹) is the surface velocity, y_i (dimensionless) is the molar fraction, $k_{f,i}$ (m s⁻¹) is the film mass transfer resistance, Cp_i (mol m⁻³) is the averaged concentration in the macropores, C_t (mol m⁻³) is the total gas concentrations, ε_c (dimensionless) is the column void fraction, a_p (m⁻¹) is the pellet specific surface area, and Bi (dimensionless) is the Biot number.

The mass balance in the macropores is described by:

$$\frac{\partial Cp_i}{\partial t} = \frac{15D_{p,i}(Bi/5)}{r_p^2(Bi/5+1)} (C_i - Cp_i) - \frac{\rho_p}{\varepsilon_p} \frac{\partial q_i}{\partial t} \quad (\text{A.10})$$

where $D_{p,i}$ (m² s⁻¹) is the macropore diffusivity, r_p (m) is the pellet radius, ε_p (dimensionless) is the pellet void fraction, ρ_p (kg m⁻³) is the pellet density, and q_i (mol kg⁻¹) is the averaged adsorbed concentration. On the other hand, the mass balance in the micropores was modeled as follows:

$$\frac{\partial q_i}{\partial t} = D_\mu (q_{eq,i} - q_i) \quad (\text{A.11})$$

where D_μ (s^{-1}) is the micropore diffusivity.

The Ergun equation was used to describe the pressure drop behavior along the column:

$$\frac{\partial P}{\partial z} = -150 \frac{\mu_G (1-\varepsilon_C)^2}{\varepsilon_C^3 d_p^2} u - 1.75 \frac{\rho_G (1-\varepsilon_C)}{\varepsilon_C^3 d_p} u \cdot |u| \quad (\text{A.12})$$

where P (bar) is the total pressure, μ_G (bar s^{-1}) the gas viscosity, ρ_G (kg m^{-3}) the mass density and d_p (m) is the pellet diameter.

The energy balance in the gas phase was calculated by equation A.13:

$$-\varepsilon_C C_T C_{Vg} \frac{\partial T}{\partial t} = \frac{\partial}{\partial z} \left(\lambda \frac{\partial T}{\partial z} \right) - C_T C_{Pg} \frac{\partial (uT)}{\partial z} + \varepsilon R T \frac{\partial C_T}{\partial t} - (1-\varepsilon) a_p h_f (T - T_S) - \frac{2h_w}{r_w} (T - T_W) \quad (\text{A.13})$$

where T , T_s and T_W (K) are the temperature in the gas phase, adsorbent and column wall, respectively, C_{Pg} ($\text{kJ mol}^{-1} \text{K}^{-1}$) and C_{Vg} ($\text{kJ mol}^{-1} \text{K}^{-1}$) are the molar specific heats of the gas at constant pressure and volume, respectively, r_w (m) is the inner wall radius, R ($\text{kJ mol}^{-1} \text{K}^{-1}$) is again the ideal gas constant, λ ($\text{kJ K}^{-1} \text{m}^{-1} \text{s}^{-1}$) is the axial heat dispersion coefficient, and h_w and h_f ($\text{kJ K}^{-1} \text{m}^{-2}$) are the film heat transfer coefficients at the gas-wall and gas-adsorbent interphases, respectively.

The energy balance in the solid phase was estimated as follows:

$$\left[\varepsilon_P \sum_{i=1}^{nc} (\bar{c}_i C_{V,i}) + \rho_P \sum_{i=1}^{nc} (q_i C_{V,ads,i}) + \rho_P C_{Ps} \right] \frac{\partial T_S}{\partial t} = \left[\varepsilon_P R \cdot T_S \sum_{i=1}^{nc} \left(\frac{\partial \bar{c}_i}{\partial t} \right) + a_p h_f (T - T_S) \right] + \frac{\rho_L}{(1-\varepsilon)} \sum_{i=1}^{nc} \left(-\Delta H_i \frac{\partial q_i}{\partial t} \right) \quad (\text{A.14})$$

where $C_{V,ads,i}$ ($\text{kJ mol}^{-1} \text{K}^{-1}$) is the molar specific heat at constant volume of adsorbed phase, and C_{Ps} ($\text{kJ kg}^{-1} \text{K}^{-1}$) is the mass heat capacity of the column.

Finally, the energy balance of the column was given by:

$$\rho_W C_{Pw} \frac{\partial T_W}{\partial t} = \alpha_w h_w (T - T_W) - \alpha_{wL} U (T_W - T_\infty) \quad (\text{A.15})$$

where C_{Pw} ($\text{kJ kg}^{-1} \text{K}^{-1}$) is the wall specific heat, U ($\text{kJ K}^{-1} \text{s}^{-1}$) is the overall heat transfer coefficient, T_∞ (K) is the external temperature, ρ_w (kg m^{-3}) is the wall density, α_w (m^{-1}) is the ratio of the internal surface area to the volume of the column wall, and α_{wl} (m^{-1}) is the ratio of the logarithmic mean surface area of the column shell to the volume of the column wall.

Table A.1. Lignocellulosic composition, proximate, ultimate and XRF analyses of wheat straw pellets

Component	Content (wt. %)
Hemicellulose	33.0 ± 0.61
Cellulose	40.7 ± 0.50
Lignin	18.4 ± 0.54
Extractives	8.05 ± 0.28
Proximate analysis	(wt. %)
Ash	3.87 ± 0.07
Moisture	7.27 ± 0.06
Volatile matter	74.9 ± 0.33
Fixed carbon	14.0 ± 0.29
Ultimate analysis	(on a d.a.f. basis)
C	49.0 ± 0.52
H	7.01 ± 0.04
N	0.704 ± 0.01
O	43.2 ¹
Inorganic matter as equivalent oxides	(wt. % of ash) ²
K ₂ O	53.2
CaO	17.4
SiO ₂	16.9
P ₂ O ₅	4.46
Al ₂ O ₃	1.66
Cl (inorganic)	1.53
MgO	1.46
S (inorganic)	1.31
Fe ₂ O ₃	1.14

¹Oxygen was calculated by difference.

²Only components with a content higher than 1% are listed.

Assessment of the repeatability of pyrolysis experiments

The three repeated measurements of central point were analyzed using a one-way ANOVA. Assuming normality and homogeneity of variances, the mean squares for the treatment and error terms (MS_t and MS_e , respectively) were computed. The intra-class correlation coefficient (ICC), which is commonly used as a measure of repeatability [5], was calculated as follows:

$$ICC = \frac{MS_t - MS_e}{MS_t + (n_0 - 1)MS_e} 100 \quad (\text{A.16})$$

where n_0 is the number of replicates (3). The obtained value of ICC (99.69%) indicated a high level of repeatability.

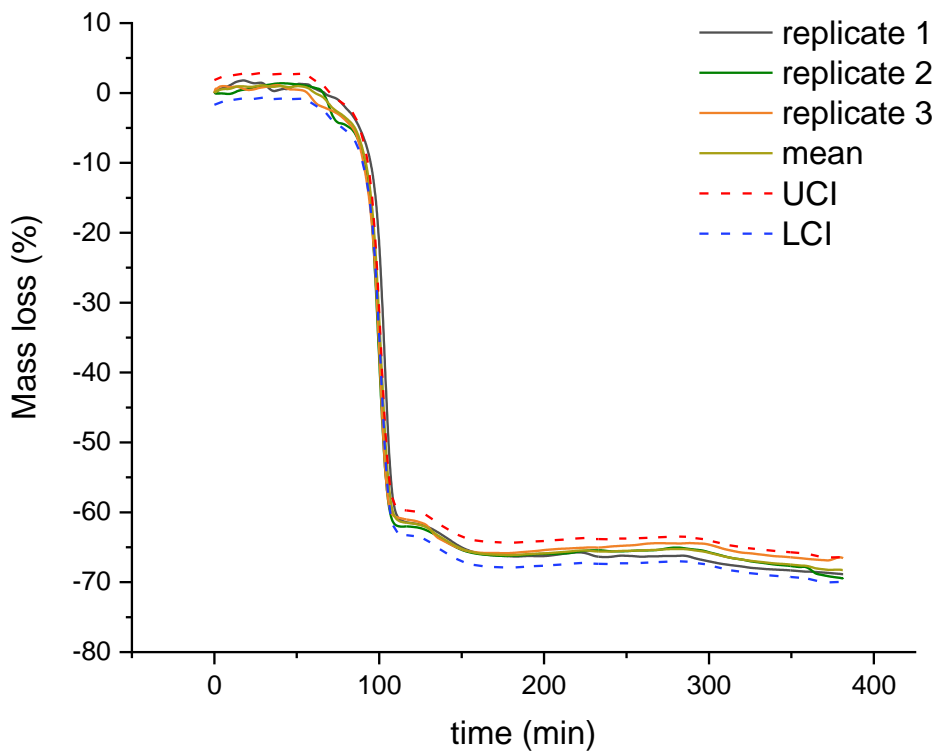


Fig. A.2. Comparison of the mass-loss curves obtained for three replicates of the central point of the experimental design. LCI and UCI correspond to lower and upper 95% confidence intervals.

Analysis on mass-loss profiles during the one-step production process

Fig. A.3 shows the mass loss time derivative and temperature profiles for the experiments conducted at 750 °C in the 0.2–0.9 MPa range, ensuring a gas residence time of 100 s under a pure N₂ atmosphere or a binary mixture of CO₂ and N₂ (75:25 v/v). According to our previous study [6] on WS pyrolysis behavior, the mass loss time derivative reached its peak in the range of 200–400 °C (dashed black line in Fig. A.3). As expected, an exothermic behavior was observed in this range of temperature, when secondary reactions occurred. Higher pressures contributed to enhance the kinetics of the reactions involved in the devolatilization step [7]. As a result, the faster and more intense devolatilization is visible in Fig. A.3c–d as a higher and narrower peak.

In line with the observations previously reported for WS pellets [6], the switch from a pure N₂ atmosphere to a CO₂/N₂ mixture in the pyrolysis environment confirmed to be irrelevant to the evolution of mass loss, even when the temperature was sufficiently high for the physical activation of the biochar with CO₂. A possible explanation for this could be the sensitivity of the weighing platform, which could be too low to detect small, very gradual changes in mass loss associated with some degree of biochar gasification. On the other hand, the temperature profiles became visibly more homogeneous in the presence of CO₂, probably due to an additional release of volatiles, which enhanced convective heat transfer during the process.

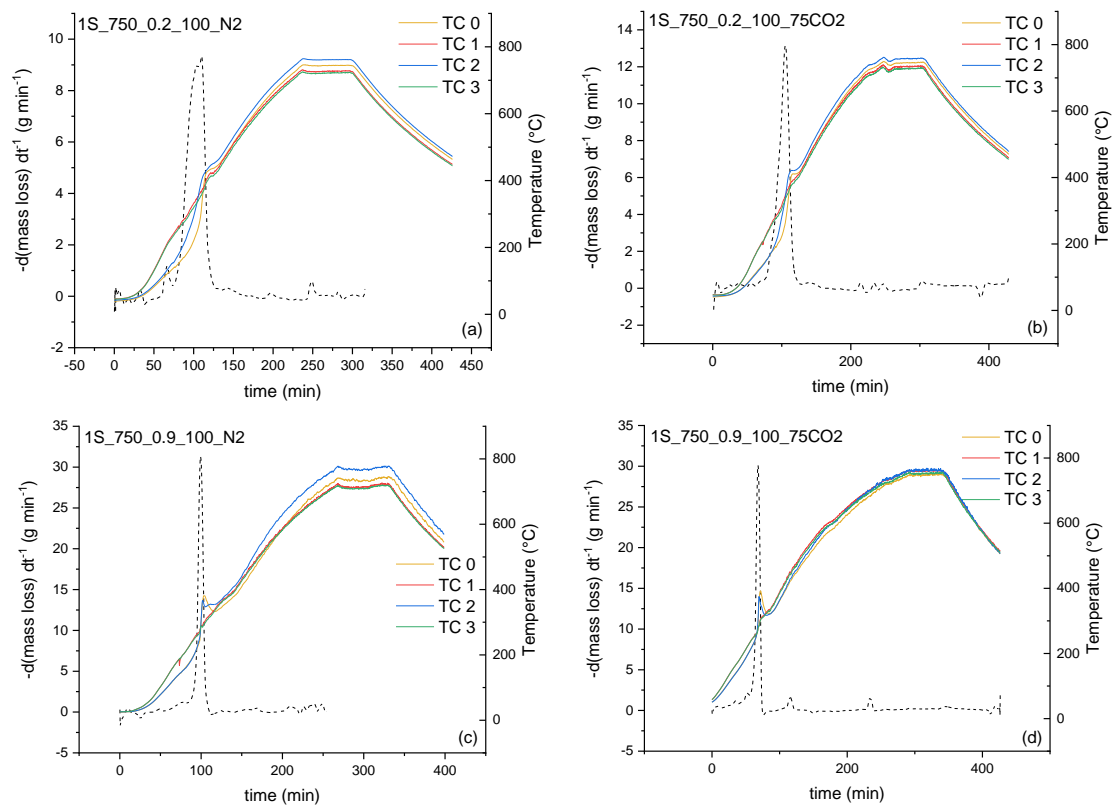


Fig. A.3. Time derivative of the mass loss and evolution of temperatures within the bed at axial (TC₀ and TC₃) and radial (TC₁ and TC₂) positions for the experiments conducted at 750 °C and 100 s under: (a) 0.2 MPa and N₂ atmosphere; (b) 0.2 MPa and 75 vol. % CO₂ atmosphere; (c) 0.9 MPa and N₂ atmosphere; and (d) 0.9 MPa and 75 vol. % CO₂ atmosphere. The samples are denoted *IS_T_P_R_A*, where *IS* refers to the carbons obtained by one-step activation, *T*, *P*, *R* and *A* are the maximum temperature (°C), absolute pressure (MPa), gas residence time (s) and the type of reactor atmosphere, respectively.

Table A.2. Results of statistical tests of regression model coefficients for textural properties of 2S activated carbons. The values in brackets correspond to the p-values resulting from the t-tests. The significant terms (p-values below 0.05) are marked in bold

	$S_{2D-NLDFT} (2S)$	$V_{ultra} (2S)$	$V_{micro} (2S)$	$V_{tot} (2S)$	X_{2S}
β_0	906.73 (0.000)	0.15 (0.000)	0.255 (0.000)	0.27938 (0.000)	46.92 (0.000)
β_1 (T)	-10.86 (0.207)	0.0075 (0.031)	-0.0075 (0.005)	-0.00687 (0.026)	-4.35 (0.000)
β_2 (P)	-29.93 (0.005)	-0.0075 (0.0031)	-0.00625 (0.010)	-0.00687 (0.026)	0.554 (0.143)
β_3 (τ)	23.53 (0.016)	0.015 (0.001)	0.0025 (0.167)	–	-3.859 (0.000)
β_4 (CO ₂)	–	-0.00375 (0.220)	0.00125 (0.456)	0.00312 (0.214)	0.794 (0.052)
β_{12} (T·P)	17.63 (0.055)	0.0025 (0.399)	0.00375 (0.060)	0.00688 (0.026)	1.325 (0.007)
β_{13} (T· τ)	-12,91 (0.141)	-0.0125 (0.003)	–	–	–
β_{14} (T·CO ₂)	-12.41 (0.155)	0.00125 (0.667)	-0.00375 (0.060)	-0.00562 (0.050)	–
β_{23} (P· τ)	6.07 (0.467)	0.0025 (0.399)	0.00125 (0.456)	0.00312 (0.214)	–
β_{24} (P·CO ₂)	–	0.00625 (0.059)	-0.005 (0.023)	-0.00562 (0.050)	-1.162 (0.012)
β_{34} (τ ·CO ₂)	-12.07 (0.165)	0.00125 (0.667)	-0.00375 (0.060)	-0.00438 (0.103)	-0.772 (0.057)
β_{123} (T·P· τ)	–	–	-0.00375 (0.060)	-0.00562 (0.050)	-0.628 (0.105)
β_{124} (T·P·CO ₂)	–	–	0.0075 (0.005)	0.01062 (0.005)	1.829 (0.001)
β_{134} (T· τ ·CO ₂)	–	–	–	0.00437 (0.103)	0.838 (0.044)
β_{234} (P· τ ·CO ₂)	–	–	–	0.00188 (0.432)	1.541 (0.003)
R^2_{adj}	0.6216	0.7840	0.8306	0.9324	0.9578
Curvature	(0.285)	(0.099)	(0.687)	(0.777)	(0.315)

Table A.3. Same as Table A.2, but for *IS* activated carbons

	$S_{2D-NLDFT} (IS)$	$V_{ultra} (IS)$	$V_{micro} (IS)$	$V_{tot} (IS)$	X_{IS}
β_0	613.5 (0.000)	0.125 (0.000)	0.14625 (0.000)	0.1500 (0.000)	70.069 (0.000)
β_1 (T)	27.9 (0.145)	–	0.02125 (0.032)	0.0250 (0.038)	1.770 (0.026)
β_2 (P)	–6.9 (0.678)	–0.0025 (0.390)	0.00625 (0.397)	0.0075 (0.414)	1.229 (0.074)
β_3 (CO ₂)	104.7 (0.002)	0.0100 (0.010)	0.03125 (0.009)	0.0350 (0.013)	1.647 (0.032)
β_{12} (T·P)	–	–	–	–	–
β_{13} (T·CO ₂)	74.9 (0.008)	–	0.02625 (0.016)	0.0300 (0.022)	1.443 (0.049)
β_{23} (P·CO ₂)	32.9 (0.100)	–	0.01125 (0.163)	0.0125 (0.203)	0.947 (0.138)
R^2_{adj}	0.8836	0.6550	0.8230	0.7790	0.7688
Curvature	(0.100)	(0.027)	(0.975)	(0.850)	(0.947)

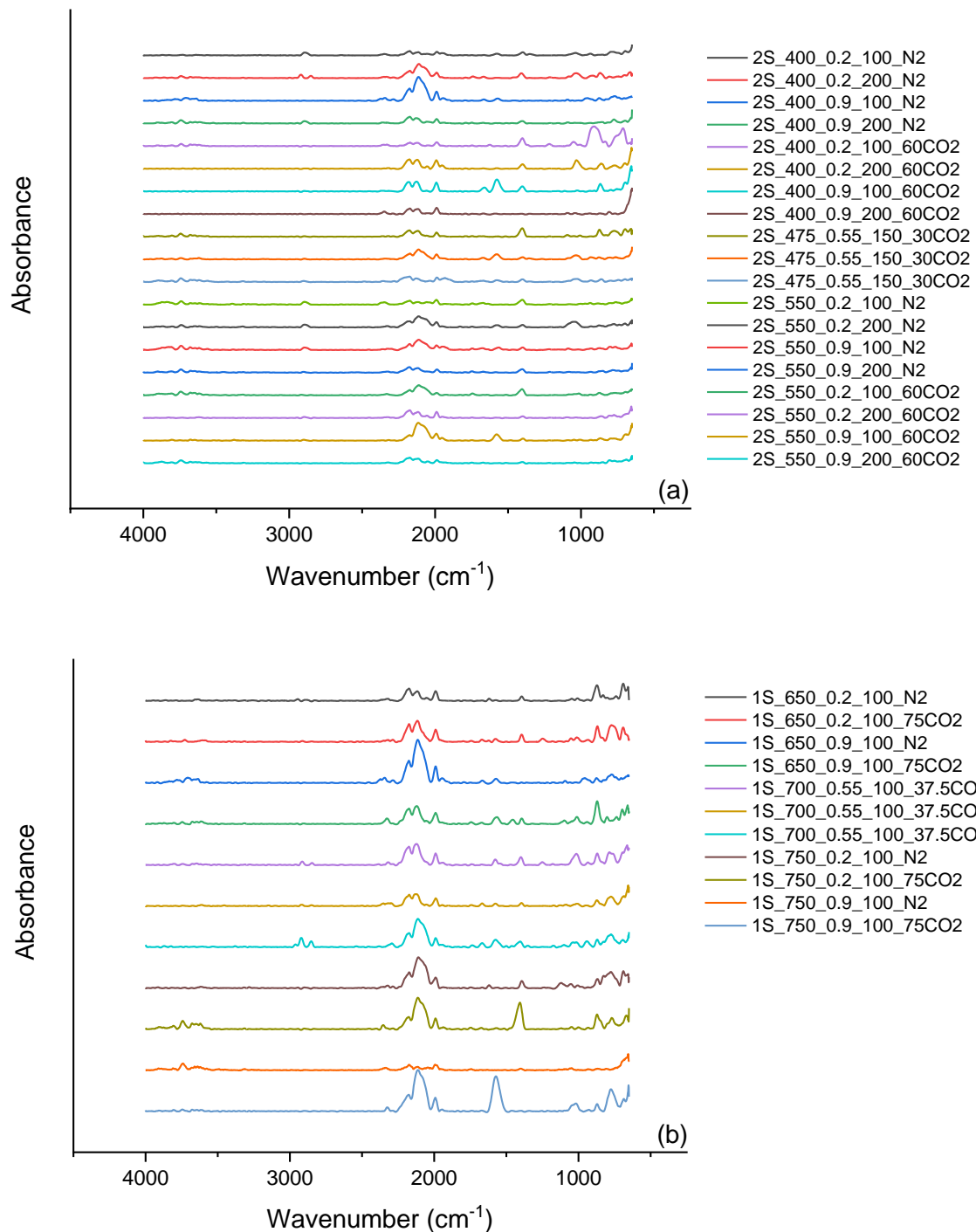


Fig. A.4. FT-IR spectra of activated carbons produced. The samples are denoted as $X_T_P_R_A$, where X refers to the carbons obtained by two-step (2S) or one-step (1S) activation, and T , P , R and A are the maximum temperature ($^{\circ}\text{C}$), absolute pressure (MPa), gas residence time (s) and the type of reactor atmosphere, respectively, adopted during the pyrolysis step ((a) for 2S carbons) or during the one-step activation ((b) for 1S carbons).

Table A.4. Isotherm parameters fitted from the isotherm experimental data.

AC	25 °C				50 °C			
	q_s (mol kg ⁻¹)	b_s (bar ^{-n_s})	n_s	R ²	q_s (mol kg ⁻¹)	b_s (bar ^{-n_s})	n_s	R ²
Methane								
<i>1S-1</i>	2.42	0.37	1.27	0.998	2.30	0.25	1.24	1.000
<i>1S-2</i>	3.33	0.33	1.45	0.999	3.15	0.24	1.43	1.000
<i>1S-3</i>	3.89	0.28	1.33	0.998	3.69	0.19	1.31	0.999
<i>2S-1</i>	4.74	0.25	1.35	1.000	4.51	0.16	1.31	1.000
<i>2S-2</i>	4.08	0.31	1.29	0.999	3.89	0.20	1.26	1.000
<i>2S-3</i>	4.84	0.26	1.38	0.999	4.04	0.20	1.22	0.999
Carbon Dioxide								
<i>1S-1</i>	3.66	0.89	1.67	0.999	3.49	0.61	1.65	0.998
<i>1S-2</i>	4.45	0.79	1.60	1.000	4.24	0.53	1.60	0.999
<i>1S-3</i>	7.30	0.44	1.98	0.997	5.85	0.40	1.57	0.997
<i>2S-1</i>	7.65	0.45	1.63	1.000	7.29	0.30	1.59	1.000
<i>2S-2</i>	6.50	0.71	1.63	0.999	6.20	0.46	1.60	0.999
<i>2S-3</i>	7.45	0.63	1.70	1.000	7.09	0.42	1.66	1.000

Table A.5. Specific surface areas and CO₂ uptakes of various carbon-based adsorbents

Name	AC description	Type of Activation	Surface Area (m ² g ⁻¹)	Temperature (°C)	CO ₂ uptake at 0.1 MPa (mol kg ⁻¹)	Reference
AC Norit R1	Commercial	—	3000	20	2.23	[8]
WV1050	Commercial	—	1615	20	1.69	[9]
Desorex K43-BG	Commercial	—	1005	25	1.88	[10]
Desorex K43-Fe	Commercial	—	952	25	1.61	[10]
Desorex K43-Na	Commercial	—	815	25	1.67	[10]
BPL	Commercial	—	985	25	2.10	[11]
Cherry stone AC	Lab-made AC from cherry stone	One-step	906	25	2.20	[12]
KLB1	Lab-made AC from Arundo donax stem	One-step	637	0	4.0	[13]
KLB2	Lab-made AC from Arundo donax stem	One-step	1122	0	6.3	[13]
AC A35/4	Commercial	—	—	20	2.00	[14]
EFB-600	Lab-made AC from empty fruit bunch	Two-step	1080	25	1.12	[15]
EFB-800	Lab-made AC from empty fruit bunch	Two-step	1120	25	2.63	[15]
H350-800	Lab-made hydrochar from empty fruit bunch	Two-step	2100	25	2.81	[15]
ACGR-4800	Lab-made hydrochar from Jujun grass	Two-step	2957	25	2.80	[16]
Brascarbo	Commercial	Two-step	967	25	2.92	[17]
2S-1	Lab-made AC from wheat straw pellets	Two-step	986	25	2.42	This work
2S-2	Lab-made AC from wheat straw pellets	Two-step	957	25	2.75	This work
2S-3	Lab-made AC from wheat straw pellets	Two-step	998	25	2.94	This work
1S-1	Lab-made AC from wheat straw pellets	One-step	700	25	1.75	This work
1S-2	Lab-made AC from wheat straw pellets	One-step	760	25	2.00	This work
1S-3	Lab-made AC from wheat straw pellets	One-step	882	25	2.29	This work

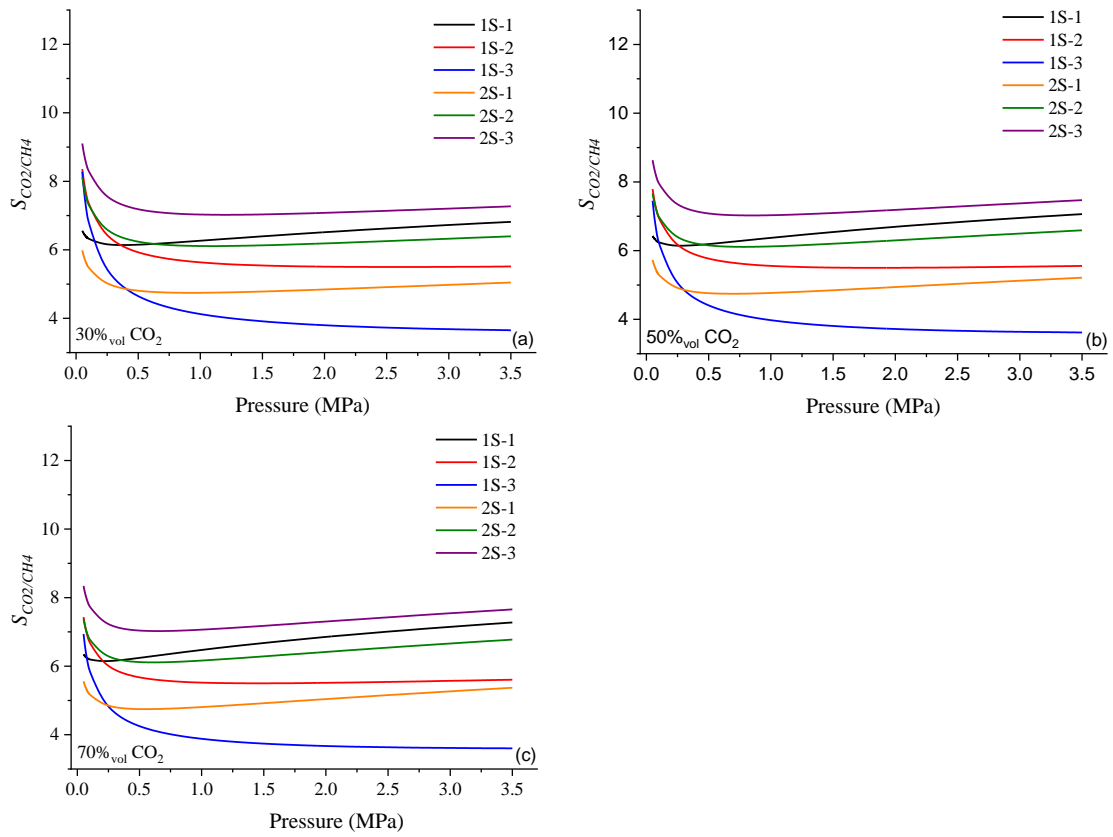


Fig. A.5. IAST-based selectivity values for ACs tested under: (a) 30; (b) 50; and (c) 70 vol. % CO_2 .

Table A.6. CO₂/CH₄ IAST-based selectivity values for various carbon-based adsorbents

Name	AC description	Type of Activation	CO ₂ molar fraction in gas feed	Pressure (MPa)	Temperature (°C)	S_{CO_2/CH_4}	Reference
AC (AX21)	Commercial	—	0.50	0.1	20	8.0	[18]
WV150	Commercial	—	0.69	0.1	20	8.7	[9]
Activated carbon beads	Lab-made AC from beads	—	0.50	0.1	30	3.6	[19]
Desorex K43-BG	Commercial	—	0.30	0.1	25	1.4	[10]
BPL	Commercial	—	0.50	0.1	25	3.8	[11]
Cherry stone AC	Lab-made AC from cherry stone	One-step	0.50	0.3	30	3.2	[12]
Norit R1 Extra	Commercial	—	0.57	0.1	25	1.4	[8]
Activated carbon	Lab-made AC from beads	Two-step	0.70	0.1	25	2.0	[20]
Brascarbo	Commercial	Two-step	0.50	0.1	25	4.49	[17]
CS-CO ₂	Lab-made AC from cherry stone	One-step	0.50	0.1	30	4.35	[21]
CS-H ₂ O	Lab-made AC from cherry stone	One-step	0.50	0.1	30	4.39	[21]
Mesoporous carbon	Lab-made mesoporous ordered carbon	One-step	0.50	0.1	25	3.0	[22]
Monolith activated carbon	Commercial	—	—	0.1	30	6.5	[23]
2S-1	Lab-made AC from wheat straw pellets	Two-step	0.5	0.1	25	5.3	This work
2S-2	Lab-made AC from wheat straw pellets	Two-step	0.5	0.1	25	6.8	This work
2S-3	Lab-made AC from wheat straw pellets	Two-step	0.5	0.1	25	7.9	This work
1S-1	Lab-made AC from wheat straw pellets	One-step	0.5	0.1	25	6.2	This work
1S-2	Lab-made AC from wheat straw pellets	One-step	0.5	0.1	25	6.9	This work
1S-3	Lab-made AC from wheat straw pellets	One-step	0.5	0.1	25	6.2	This work

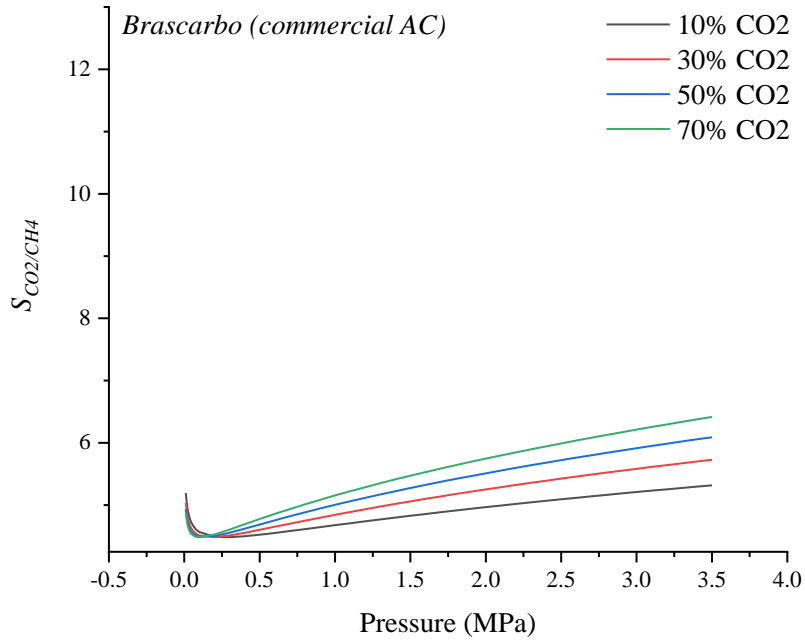
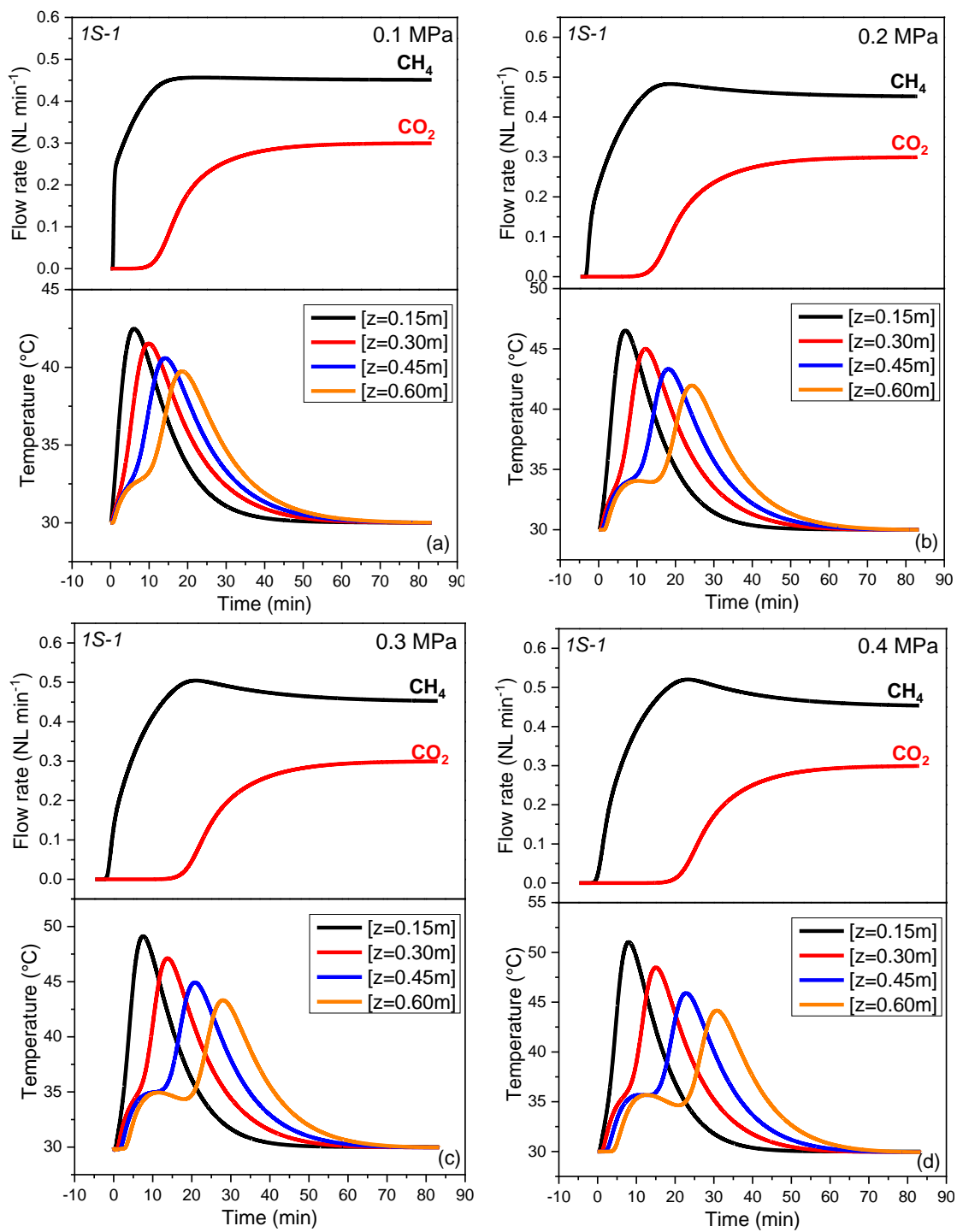


Fig. A.6. IAST-based selectivity profiles of commercial *Brascarbo* AC under 10, 30, 50, and 70 vol. % CO₂.

Table A.7. Kinetic parameters fitted from the first point of the isotherm measurements

Activated carbon	Gas diffusivity at the solid adsorbent normalized to the particle diameter: D_c/r_c (s ⁻¹)			
	25 °C		50 °C	
	CH ₄	CO ₂	CH ₄	CO ₂
<i>1S-1</i>	0.24	1.09	0.33	1.72
<i>1S-2</i>	0.64	0.98	0.65	0.98
<i>1S-3</i>	0.91	1.11	1.74	1.47
<i>2S-1</i>	0.81	1.04	0.90	1.04
<i>2S-2</i>	1.41	1.22	1.41	1.32
<i>2S-3</i>	1.03	1.38	1.55	1.38



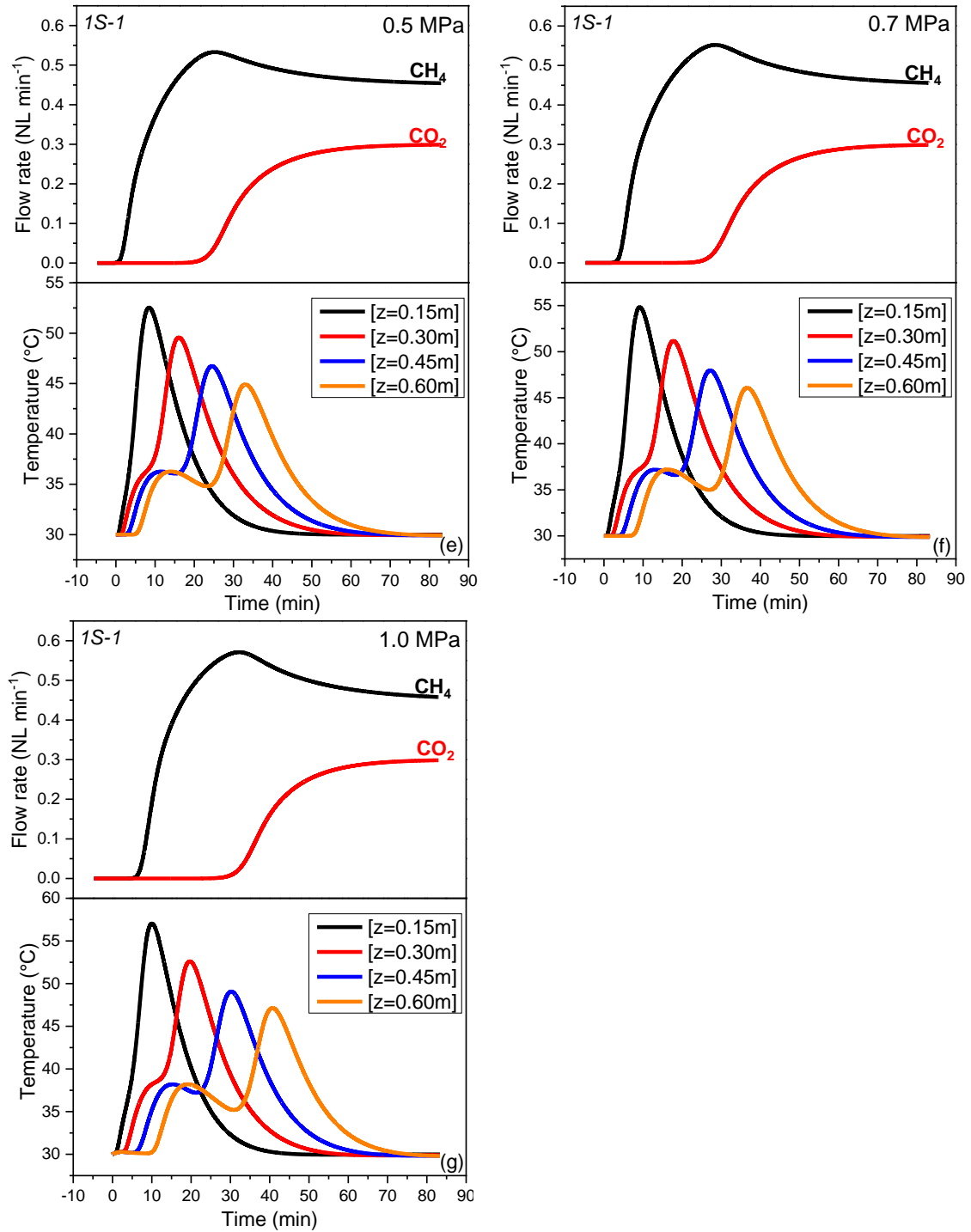
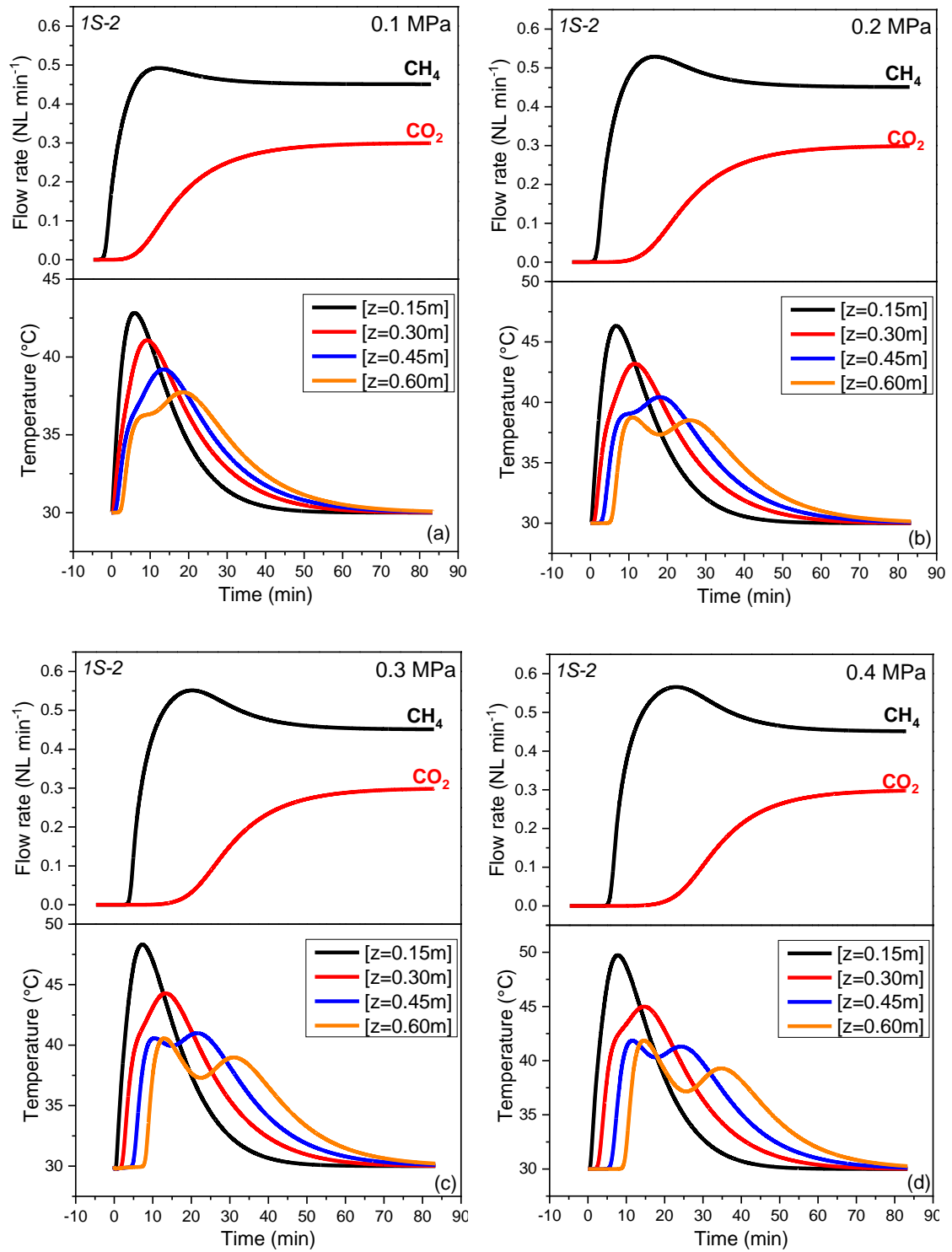


Fig. A.7. Flow rate and temperature profiles at: (a) 0.1 MPa; (b) 0.2 MPa; (c) 0.3 MPa; (d) 0.4 MPa; (e) 0.5 MPa; (f) 0.7 MPa; and (g) 1.0 MPa for the 1S activated carbon produced at 700 °C, 0.55 MPa, 100 s and 37.5 vol. % CO₂.



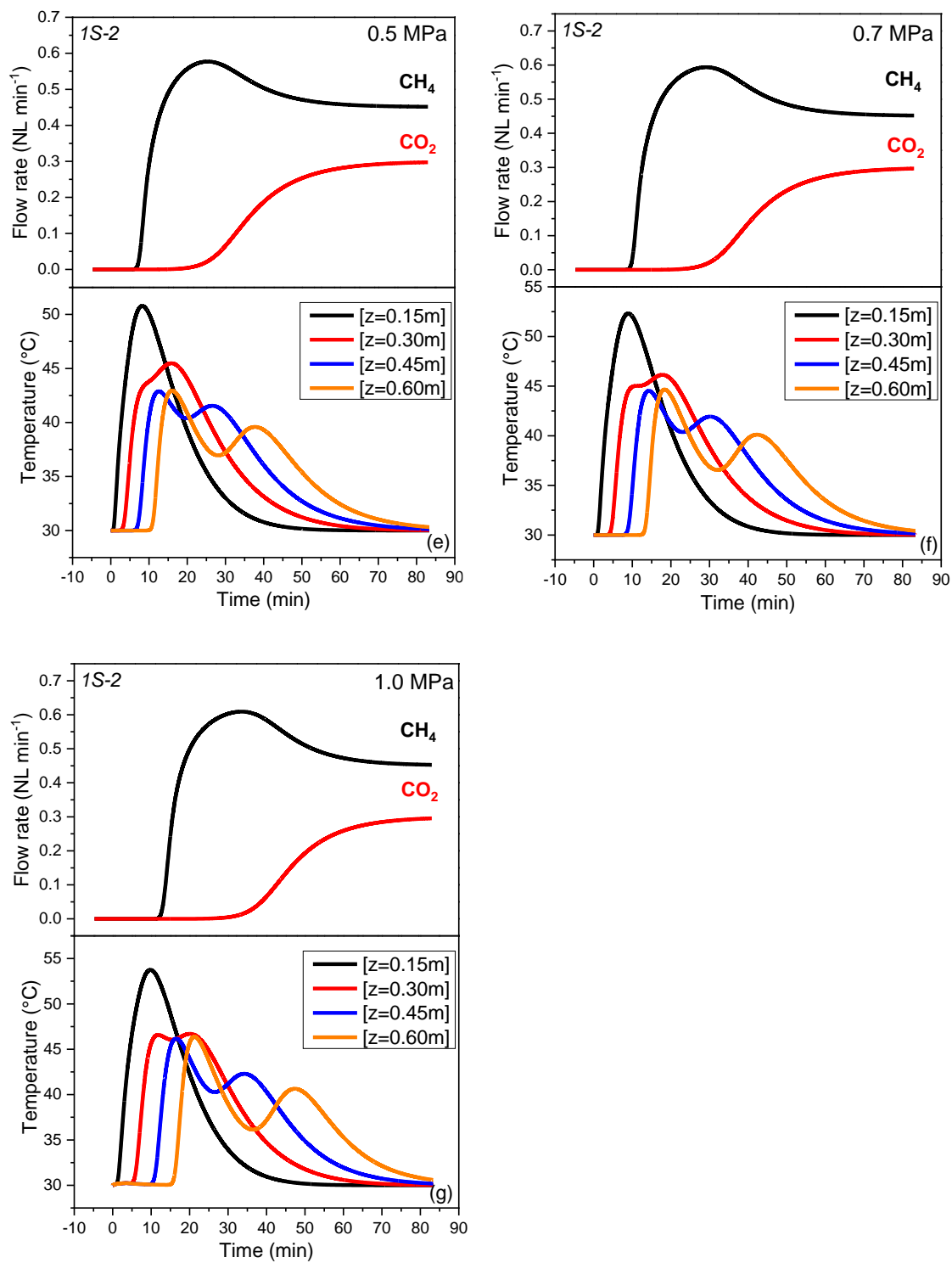
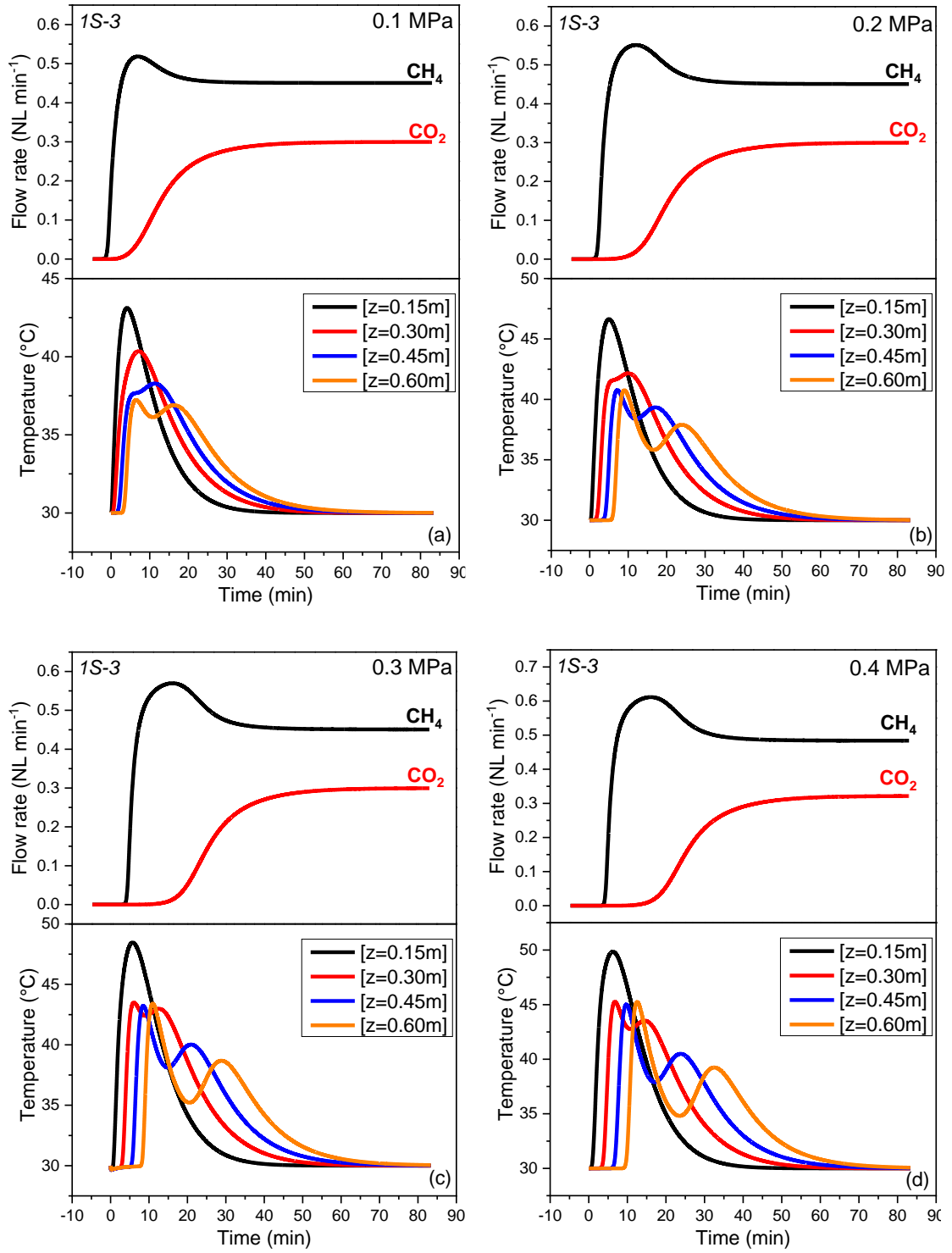


Fig. A.8. Same as Fig. A.7, but for the *IS* activated carbon produced at 750 °C, 0.2 MPa, 100 s and 75 vol. % CO₂.



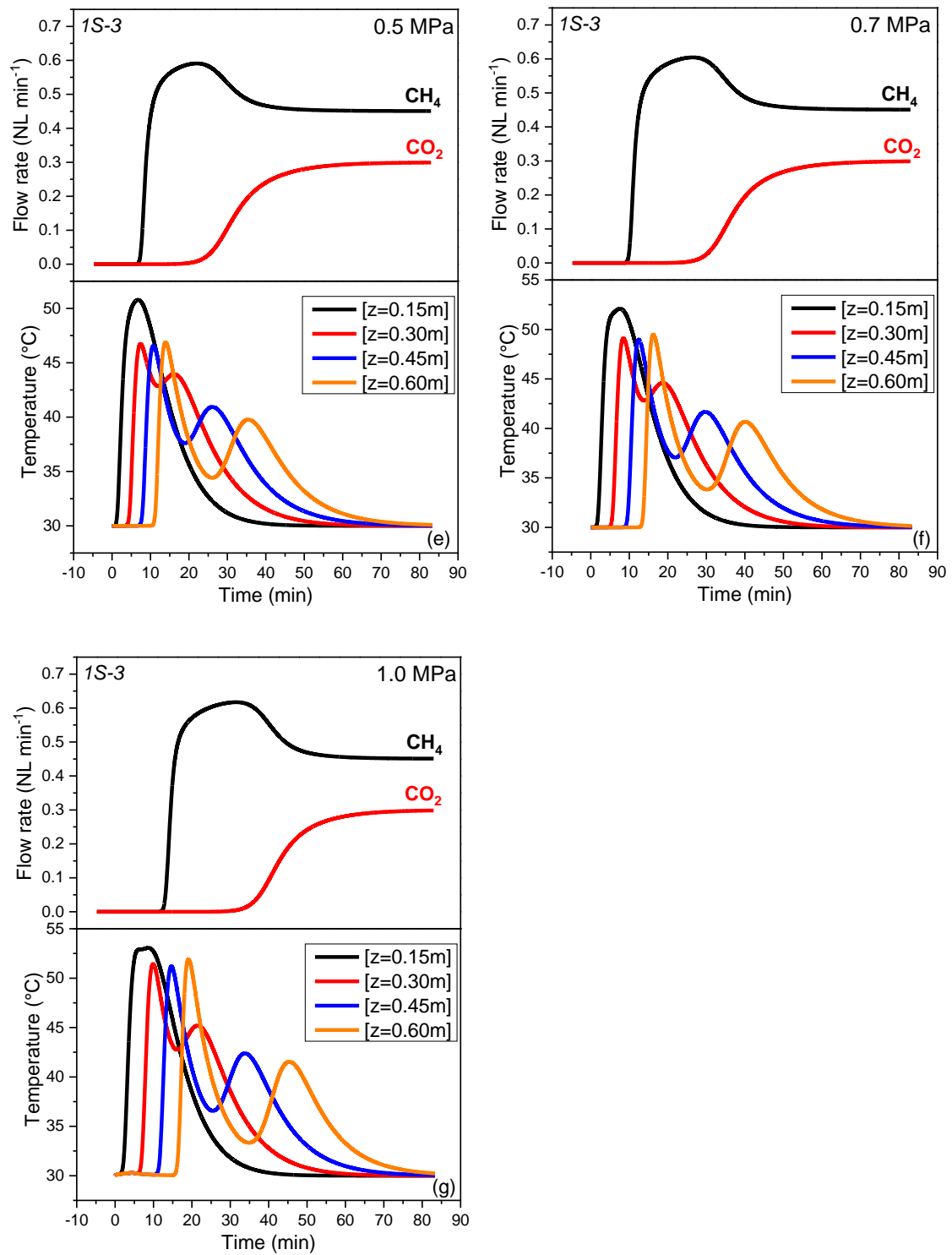
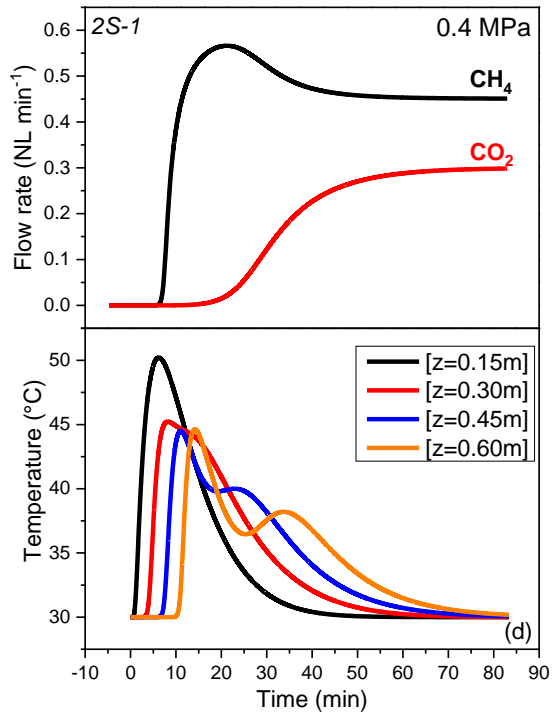
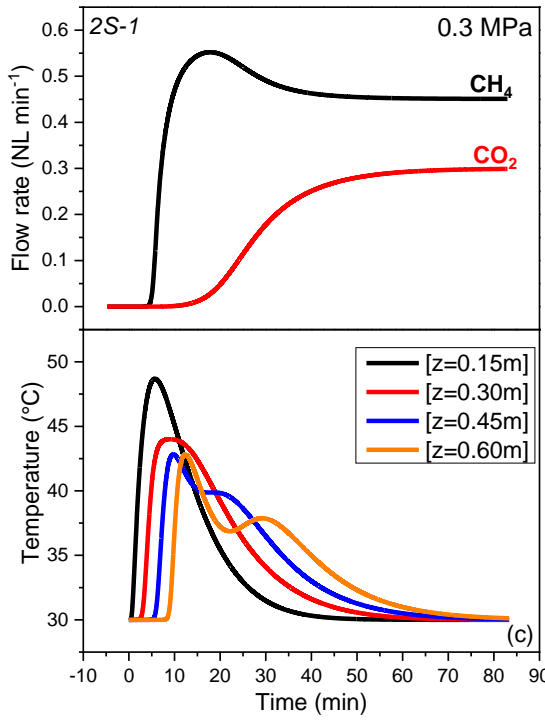
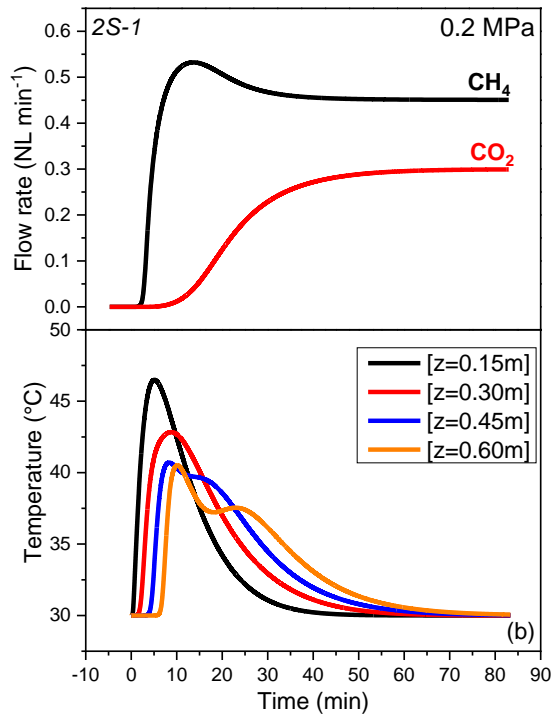
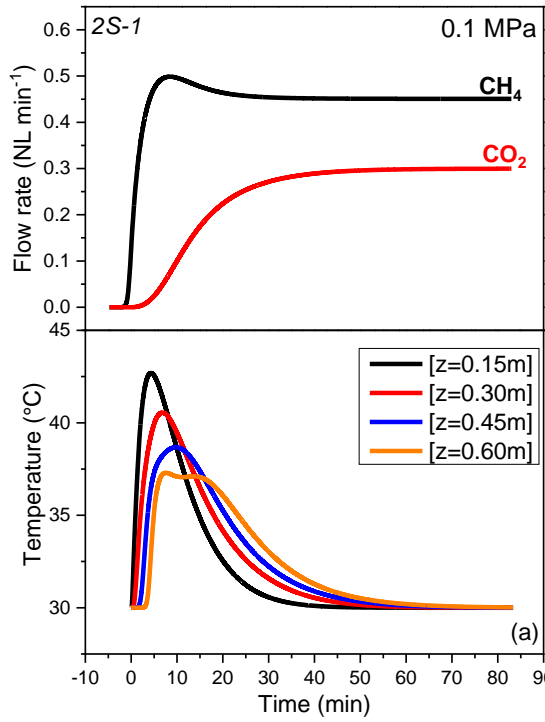


Fig. A.9. Same as Fig. A.7 but for the *1S* activated carbon produced at 750 °C, 0.9 MPa, 100 s and 75 vol. % CO₂.



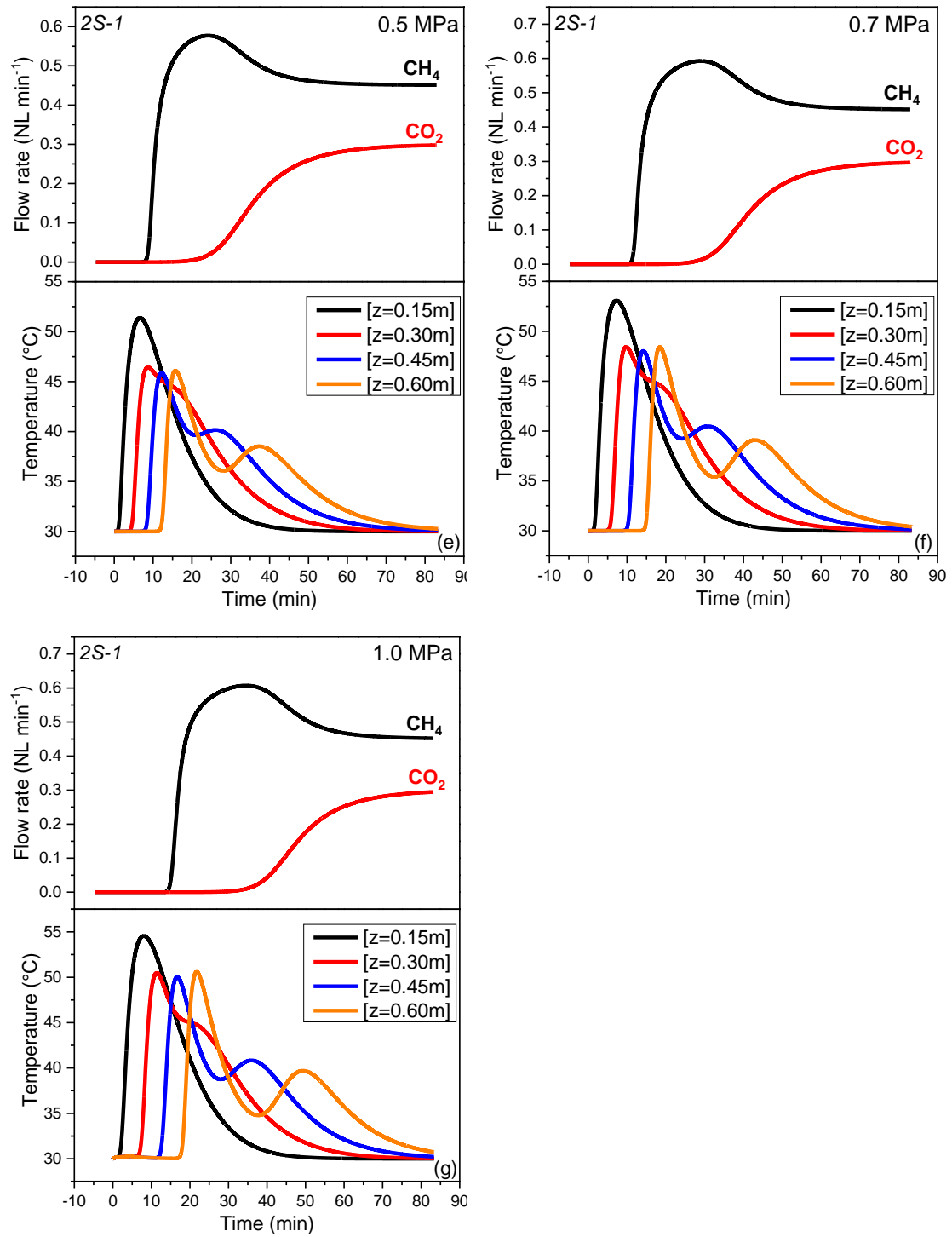
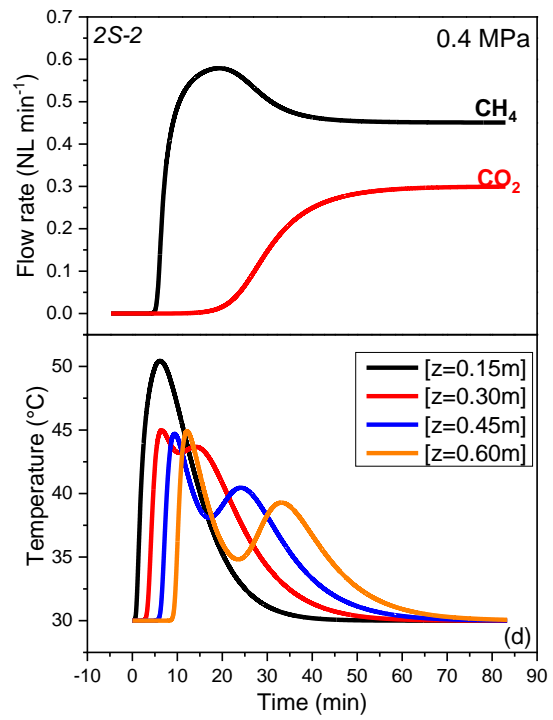
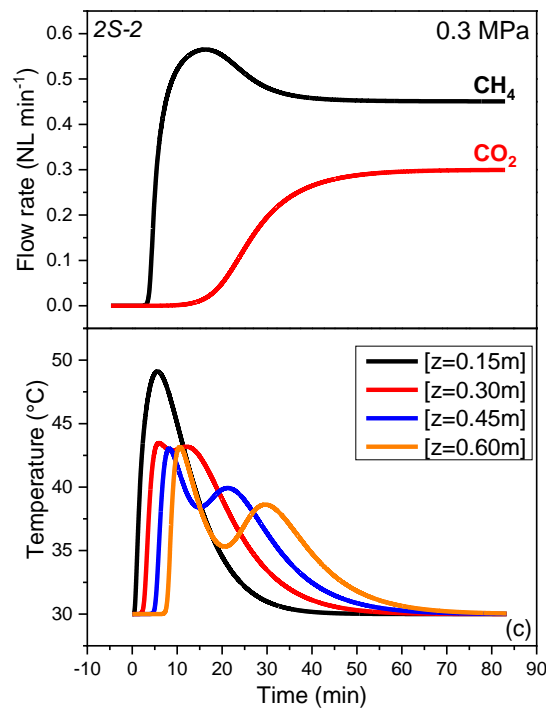
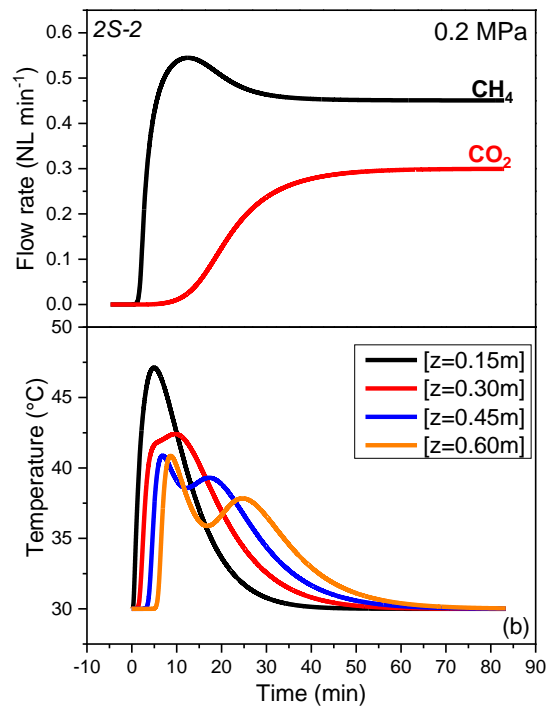
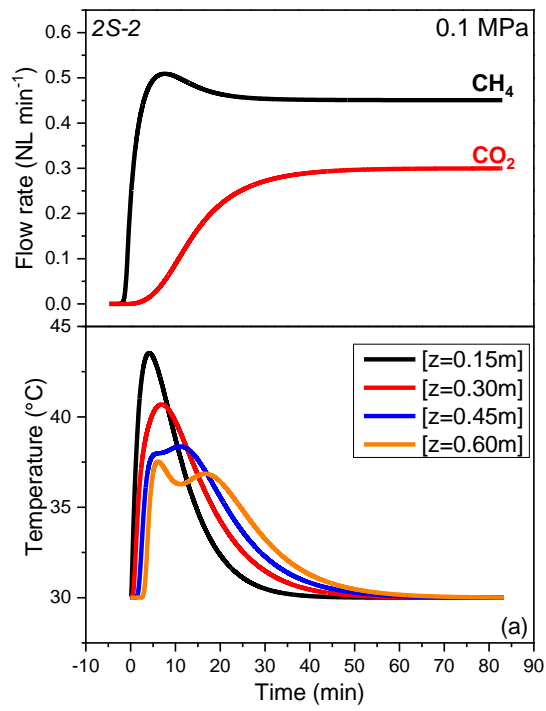


Fig. A.10. Same as Fig. A.7 but for the 2S activated carbon obtained from the biochar produced at 400 °C, 0.2 MPa, 100 s and 60 vol. % CO₂.



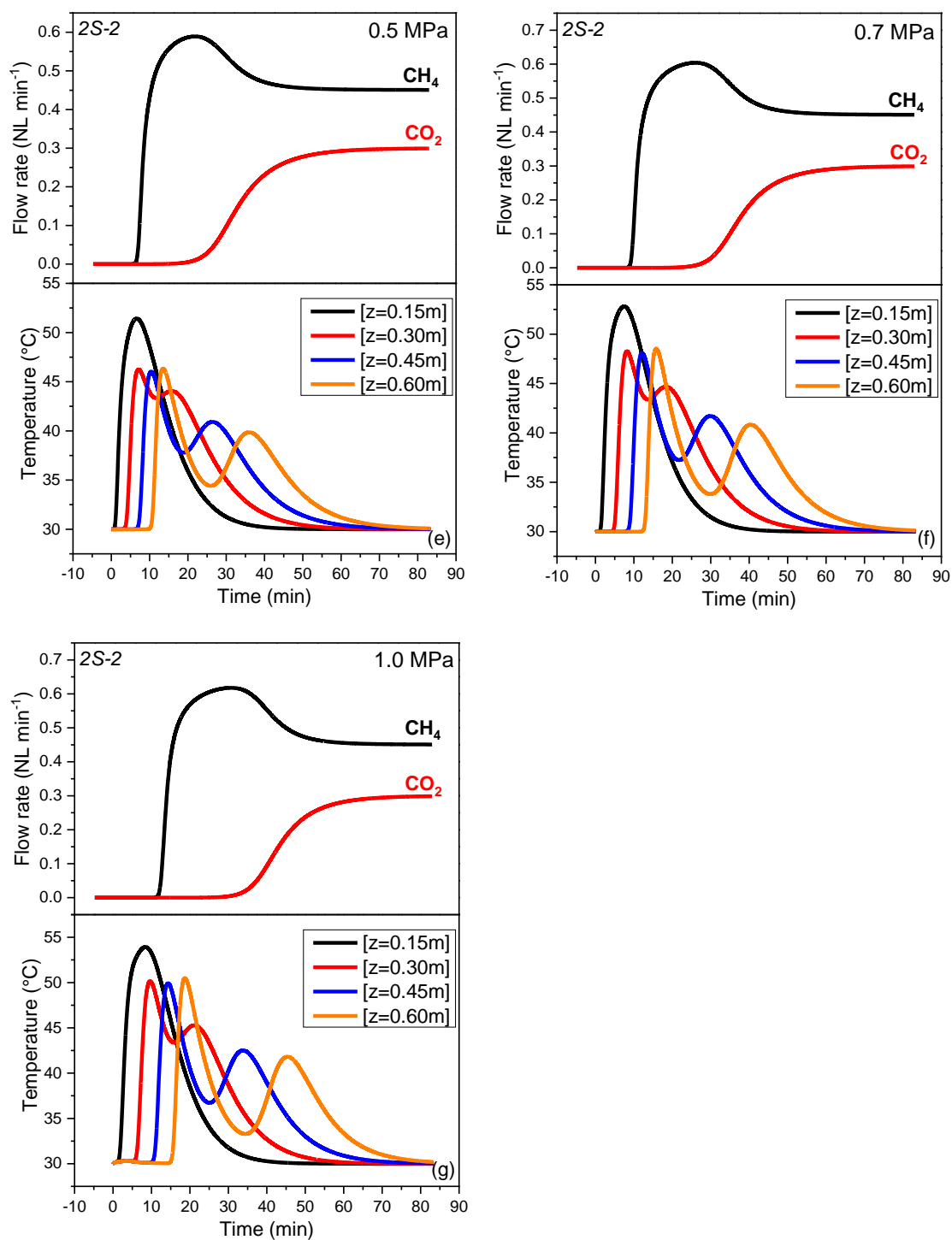
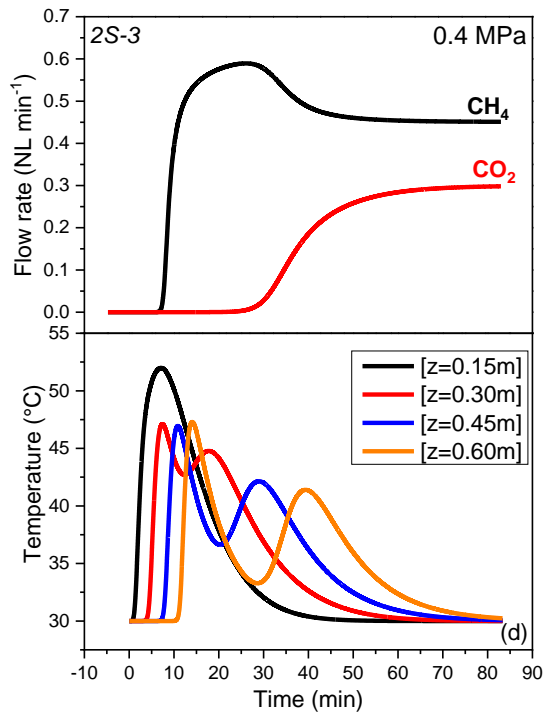
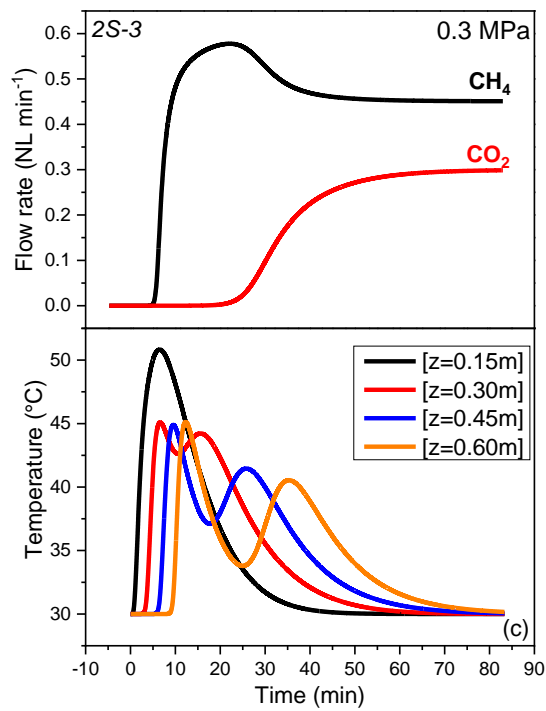
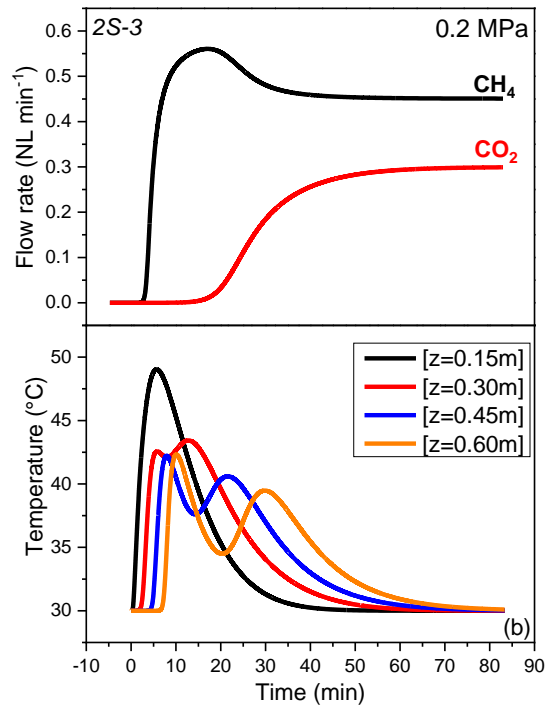
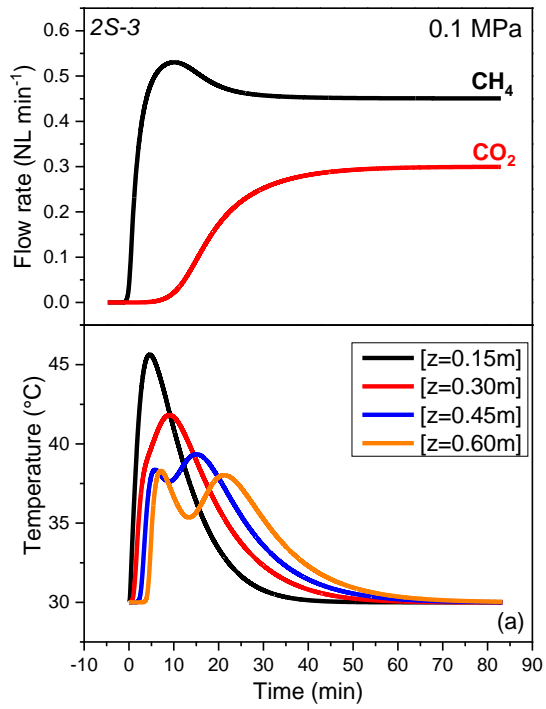


Fig. A.11. Same as Fig. A.7 but for the 2S activated carbon obtained from the biochar produced at 400 °C, 0.2 MPa, 200 s under a pure N₂ atmosphere.



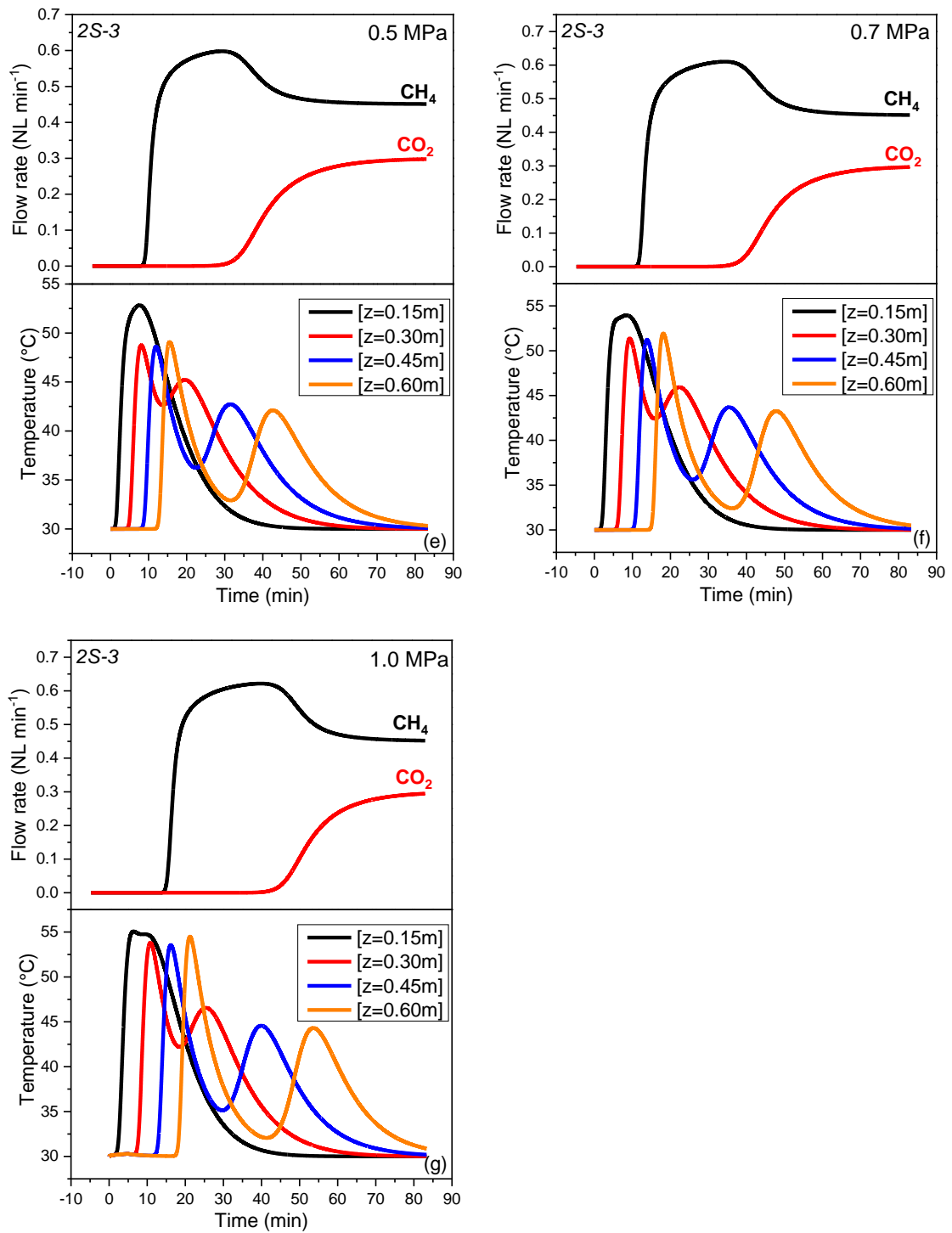


Fig. A.12. Same as Fig. A.7 but for the 2S activated carbon obtained from the biochar produced at 400 °C, 0.2 MPa, 200 s and 60 vol. % CO₂.

Table A.8. Average heat of adsorption (Q_{st}) obtained for the selected ACs

Activated carbon	Q_{st} (kJ mol ⁻¹)	
	CH ₄	CO ₂
<i>1S-1</i>	19.6	30.2
<i>1S-2</i>	21.7	29.2
<i>1S-3</i>	20.5	27.0
<i>2S-1</i>	20.1	26.5
<i>2S-2</i>	20.9	28.1
<i>2S-3</i>	20.6	28.2

Table A.9. CH₄ recovery for various adsorbents reported in literature and in this work

Name	Adsorbent description	Type of Activation	CO ₂ /CH ₄ molar percentage in gas feed	Feed flow rate (L STP min ⁻¹)	High pressure/Low pressure (MPa)	CH ₄ recovery (%)	Reference
	Commercial						
CMS 3A	carbon molecular sieve	—	50/50	3.76	0.4/0.1	71.2	[24]
	Commercial						
CMS 3K	carbon molecular sieve	—	45/55	1.4	0.3/0.01	83.6	[25]
KZ10-04	Commercial zeolite	—	42/58	—	0.15/0.01	84	[26]
NaUSY	Commercial zeolite	—	42/58	—	0.15/0.01	86	[26]
Z10-04	Commercial zeolite	—	42/58	—	0.15/0.01	93	[26]
	Lab-made AC						
2S-1	from wheat straw pellets	Two-step	40/60	0.75	1.0/0.1	75	This work
	Lab-made AC						
2S-2	from wheat straw pellets	Two-step	40/60	0.75	1.0/0.1	75	This work
	Lab-made AC						
2S-3	from wheat straw pellets	Two-step	40/60	0.75	1.0/0.1	70	This work
	Lab-made AC						
1S-1	from wheat straw pellets	One-step	40/60	0.75	1.0/0.1	94	This work
	Lab-made AC						
1S-2	from wheat straw pellets	One-step	40/60	0.75	1.0/0.1	75	This work
	Lab-made AC						
1S-3	from wheat straw pellets	One-step	40/60	0.75	1.0/0.1	72	This work

References

- [1] I. Langmuir, The Constitution and Fundamental Properties of Solids and Liquids. Part I. Solids., *J. Am. Chem. Soc.* 38 (1916) 2221–2295. <https://doi.org/10.1021/ja02268a002>.
- [2] H. Freundlich, Über Die Adsorption in Lösungen, *Zeitschrift Für Phys. Chemie.* 57 (1907) 285–470. <https://doi.org/10.1515/zpch-1907-5723>.
- [3] J.A. Nelder, R. Mead, A Simplex Method for Function Minimization., *Comput. J.* 7 (1964). <https://doi.org/10.1093/comjnl/7.4.308>.
- [4] A.L. Myers, J.M. Prausnitz, Thermodynamics of Mixed-Gas Adsorption., *AIChE J.* 11 (1965) 121–127. <https://doi.org/10.1002/aic.690110125>.
- [5] S. Nakagawa, H. Schielzeth, Repeatability for Gaussian and non-Gaussian data: A practical guide for biologists, *Biol. Rev.* 85 (2010) 935–956. <https://doi.org/10.1111/j.1469-185X.2010.00141.x>.
- [6] G. Greco, C. Di Stasi, F. Rego, B. González, J.J. Manyà, Effects of slow-pyrolysis conditions on the products yields and properties and on exergy efficiency: A comprehensive assessment for wheat straw, *Appl. Energy.* 279 (2020). <https://doi.org/10.1016/j.apenergy.2020.115842>.
- [7] G. Greco, M. Videgain, C. Di Stasi, B. González, J.J. Manyà, Evolution of the mass-loss rate during atmospheric and pressurized slow pyrolysis of wheat straw in a bench-scale reactor, *J. Anal. Appl. Pyrolysis.* 136 (2018) 18–26. <https://doi.org/10.1016/j.jaap.2018.11.007>.
- [8] F. Dreisbach, R. Staudt, J.U. Keller, High Pressure Adsorption Data of Methane, Nitrogen, Carbon Dioxide and their Binary and Ternary Mixtures on Activated Carbon, *Adsorption.* 5 (1999) 215–227. <https://doi.org/10.1023/A:1008914703884>.
- [9] R.B. Rios, H.R. Stragliotto, F. M. Peixoto, A.E.B. Torres, J. Bastos-Neto, M. Azevedo, D. C. S. Cavalcante, C. L., Studies on the Adsorption Behavior of CO₂-CH₄Mixtures Using Activated Carbon., *Brazilian J. Chem. Eng.* 30 (2013) 939–951. <https://doi.org/10.1590/S0104-66322013000400024>.

- [10] M.C. Castrillon, K.O. Moura, C.A. Alves, M. Bastos-Neto, D.C.S. Azevedo, J. Hofmann, J. Möllmer, W.-D. Einicke, R. Gläser, CO₂ and H₂S Removal from CH₄-Rich Streams by Adsorption on Activated Carbons Modified with K₂CO₃, NaOH, or Fe₂O₃, *Energy & Fuels*. 30 (2016) 9596–9604. <https://doi.org/10.1021/acs.energyfuels.6b01667>.
- [11] J. McEwen, J.-D. Hayman, A. Ozgur Yazaydin, A comparative study of CO₂, CH₄ and N₂ adsorption in ZIF-8, Zeolite-13X and BPL activated carbon, *Chem. Phys.* 412 (2013) 72–76. <https://doi.org/10.1016/j.chemphys.2012.12.012>.
- [12] M. Álvarez-Gutiérrez, N. Victoria Gil, F. Rubiera, C. Pevida, Cherry-stones-based activated carbons as potential adsorbents for CO₂/CH₄ separation: effect of the activation parameters, *Greenh. Gases Sci. Technol.* 5 (2015) 812–825. <https://doi.org/10.1002/ghg.1534>.
- [13] G. Singh, I.Y. Kim, K.S. Lakhi, P. Srivastava, R. Naidu, A. Vinu, Single step synthesis of activated bio-carbons with a high surface area and their excellent CO₂ adsorption capacity, *Carbon N. Y.* 116 (2017) 448–455. <https://doi.org/10.1016/j.carbon.2017.02.015>.
- [14] M. Heuchel, G.M. Davies, E. Buss, N.A. Seaton, Adsorption of Carbon Dioxide and Methane and Their Mixtures on an Activated Carbon: Simulation and Experiment, *Langmuir*. 15 (1999) 8695–8705. <https://doi.org/10.1021/la9904298>.
- [15] G.K. Parshetti, S. Chowdhury, R. Balasubramanian, Biomass derived low-cost microporous adsorbents for efficient CO₂ capture, *Fuel*. 148 (2015) 246–254. <https://doi.org/10.1016/j.fuel.2015.01.032>.
- [16] H.M. Coromina, D.A. Walsh, R. Mokaya, Biomass-derived activated carbon with simultaneously enhanced CO₂ uptake for both pre and post combustion capture applications, *J. Mater. Chem. A*. 4 (2016) 280–289. <https://doi.org/10.1039/C5TA09202G>.
- [17] Brascarbo Agroindustrial Ltda., (n.d.). <https://brascarbo.com.br/carvao/> (accessed March 15, 2022).
- [18] P. Kluson, S. Scaife, Microporous adsorbents for a selective separation of carbon

- dioxide from mixtures with methane and nitrogen., *Chem. Biochem. Eng. Q.* 16 (2002) 97–103. <https://doi.org/10.15255/CABEQ.2014.635>.
- [19] Y.-J. Wu, Y. Yang, X.-M. Kong, P. Li, J.-G. Yu, A.M. Ribeiro, A.E. Rodrigues, Adsorption of Pure and Binary CO₂, CH₄, and N₂ Gas Components on Activated Carbon Beads, *J. Chem. Eng. Data.* 60 (2015) 2684–2693. <https://doi.org/10.1021/acs.jced.5b00321>.
- [20] X. Shao, Z. Feng, R. Xue, C. Ma, W. Wang, X. Peng, D. Cao, Adsorption of CO₂, CH₄, CO₂/N₂ and CO₂/CH₄ in novel activated carbon beads: Preparation, measurements and simulation, *AIChE J.* 57 (2011) 3042–3051. <https://doi.org/10.1002/aic.12515>.
- [21] N. Álvarez-Gutiérrez, M. V Gil, F. Rubiera, C. Pevida, Adsorption performance indicators for the CO₂/CH₄ separation: Application to biomass-based activated carbons, *Fuel Process. Technol.* 142 (2016) 361–369. <https://doi.org/10.1016/j.fuproc.2015.10.038>.
- [22] B. Yuan, X. Wu, Y. Chen, J. Huang, H. Luo, S. Deng, Adsorption of CO₂, CH₄, and N₂ on Ordered Mesoporous Carbon: Approach for Greenhouse Gases Capture and Biogas Upgrading, *Environ. Sci. Technol.* 47 (2013) 5474–5480. <https://doi.org/10.1021/es4000643>.
- [23] R.P. Ribeiro, T.P. Sauer, F. V Lopes, R.F. Moreira, C.A. Grande, A.E. Rodrigues, Adsorption of CO₂, CH₄, and N₂ in Activated Carbon Honeycomb Monolith, *J. Chem. Eng. Data.* 53 (2008) 2311–2317. <https://doi.org/10.1021/jc800161m>.
- [24] M.-B. Kim, Y.-S. Bae, D.-K. Choi, C.-H. Lee, Kinetic Separation of Landfill Gas by a Two-Bed Pressure Swing Adsorption Process Packed with Carbon Molecular Sieve: Nonisothermal Operation, *Ind. Eng. Chem. Res.* 45 (2006) 5050–5058. <https://doi.org/10.1021/ie0511074>.
- [25] S. Cavenati, C.A. Grande, A.E. Rodrigues, Upgrade of Methane from Landfill Gas by Pressure Swing Adsorption, *Energy & Fuels.* 19 (2005) 2545–2555. <https://doi.org/10.1021/ef050072h>.
- [26] A. Arya, S. Divekar, R. Rawat, P. Gupta, M.O. Garg, S. Dasgupta, A. Nanoti, R.

Singh, P. Xiao, P.A. Webley, Upgrading Biogas at Low Pressure by Vacuum Swing Adsorption, *Ind. Eng. Chem. Res.* 54 (2015) 404–413.
<https://doi.org/10.1021/ie503243f>.

7. Conclusions / Conclusiones

Bearing in mind the objectives of the PhD project and the accomplished results, the following main conclusions can be drawn:

- The effects of peak temperature, absolute pressure, gas residence time and pyrolysis atmosphere have been deeply investigated during slow pyrolysis process. Although the pyrolysis peak temperature is the most influential operating factor, the absolute pressure plays a remarkable role on improving the potential stability of the resulting biochar, due to the greater extent of the secondary charring reactions. Such kind of reactions are also promoted by longer gas residence times, as a consequence of prolonged solid/gas phases contact, which is reflected on higher biochar yields and carbonization efficiency. On the other hand, the switch from a pure N₂ atmosphere to the mixture of CO₂/N₂ resulted to be irrelevant on the pyrolysis behavior of the biomass feedstocks adopted in this work, except for a slight increase in the yield of CO released. This important result opens the possibility of recycling the flue gas stream as a carrier gas in the pyrolysis process instead of using a more expensive inert gas.
- An increase in the absolute pressure clearly improves the exergy efficiency of the pyrolysis process for wheat straw pellets, even at relatively high pyrolysis peak temperature. The most significant finding is that the thermodynamic irreversibilities linked to biochar production were markedly reduced when pyrolysis was carried out at 550 °C, 0.9 MPa and relatively short gas residence times under a mixture of CO₂ and N₂ as carrier gas.
- The total PAHs content in the produced wood waste-derived biochars can be significantly reduced by increasing either the peak temperature or the absolute pressure. Indeed, the extent of PAHs volatilization could be promoted at higher temperatures, while an increased pressure could partly inhibit repolymerization and recondensation reactions, as a result of the high carrier gas mass flows used at high pressure. The resulting biochars were of good quality in terms of PAHs hazard, making them suitable for soil amendment purposes.

- Germination indices notably increased (in some cases from phytotoxic to phytostimulant responses) when WW-derived biochars were previously washed with water. Therefore, it is possible to conclude that the acute phytotoxicity observed for some biochars can be ascribed to water-soluble acidic and phenolic compounds. In light of this result, pressurized slow pyrolysis followed by an inexpensive water washing step appears as an interesting pathway to produce premium-quality and value-added biochars from wood waste.
- Activated carbons physically activated with CO₂ via a one-step process showed similar textural properties and CO₂ adsorption performance as those produced via a more conventional two-step process. Results obtained from breakthrough curve simulations indicated that the best activated carbon—in terms of CH₄ recovery under dynamic conditions—was produced by a one-step activation process at moderate pressure. This encouraging result indicates the one-step process as a potential, alternative way for the synthesis of tailored carbon materials, having the important advantage of evident cost savings when applied on large-scale systems.

In light of the above-mentioned results, it is possible to state that the main objectives initially set (in line with the goals of the GreenCarbon European Training Network) have been accomplished.

Teniendo en cuenta los objetivos propuestos en este proyecto de Tesis Doctoral y los resultados conseguidos, se pueden deducir las siguientes conclusiones:

- Se han estudiado en profundidad los efectos de temperatura máxima, presión absoluta, tiempo de residencia de gas y tipo de atmósfera durante el proceso de pirólisis lenta. Aunque la temperatura máxima durante la pirólisis es el factor operacional más importante, la presión absoluta juega un papel notable en el incremento de la estabilidad del biochar obtenido, debido a que potencia las reacciones de formación de char secundario. Este tipo de reacciones se ven también favorecidas a mayores tiempos de residencia de la fase gas, como consecuencia al aumento de tiempo de contacto entre fases, lo cual se ve reflejado en un mayor rendimiento en la producción de biochar y una mayor eficiencia de carbonización. Por otro lado, el proceso de pirólisis para las biomásas utilizadas en este trabajo no se ha visto significativamente alterado por el cambio de atmósfera pura de N_2 a una mezcla de CO_2/N_2 , a excepción de un ligero incremento en el rendimiento de CO cuando se utilizó la atmósfera oxidante. Este importante resultado confirma que la recirculación de los gases de combustión es una opción atractiva para su utilización como atmósfera de pirólisis, dado el importante ahorro que supone prescindir del uso de gas inerte.
- La eficiencia exergética del procesos de pirólisis de pellets de paja de trigo mejora sensiblemente con el incremento de la presión absoluta, incluso a temperaturas máximas relativamente elevadas. Es importante destacar que las irreversibilidades termodinámicas se vieron reducidas significativamente a 550 °C, 0.9 MPa, tiempos de residencia de la fase gas reducidos y usando la mezcla de CO_2 y N_2 como gas portador.
- El aumento de la temperatura máxima y/o de la presión absoluta durante la pirólisis de residuos de madera se ha traducido en una notable reducción de PAHs en el biochar obtenido. Esto se debe a que la aplicación de altas temperaturas facilita la volatilización de PAHs, mientras que el aumento de presión inhibe parcialmente las reacciones de repolimerización y de recondensación, a causa de los elevados caudales utilizados para el gas portador a presiones elevadas. En las condiciones antes señaladas, el biochar obtenido mostró una muy buena calidad en términos de riesgo por contenido en PAHs, haciéndolos idóneos para su uso como enmiendas en suelos.

- El lavado previo con agua del biochar se ha traducido en incremento notable de los índices de germinación (desde respuestas fitotóxicas a fitoestimulantes en algunos casos). Por este motivo, es posible concluir que la fitotoxicidad aguda observada en algunos biochar puede ser causada por ácidos hidrosolubles o compuestos fenólicos. A la vista de estos resultados, la pirólisis lenta presurizada y el lavado posterior del biochar resultante con agua se posiciona como una vía de tratamiento prometedora para producir biochar a partir de residuos de madera, con calidad premium y alto valor añadido.
- El carbón activado físicamente con CO₂ mediante una única etapa presenta propiedades texturales y capacidades de adsorción de CO₂ similares al producido utilizando el proceso de dos etapas. La activación en una única etapa a presión moderada ha facilitado la obtención del mejor carbón activado en términos de recuperación de CH₄ bajo condiciones dinámicas, de acuerdo a los resultados obtenidos de las simulaciones de las curvas de ruptura. Este buen resultado impulsa el proceso de etapa única como una alternativa prometedora para la síntesis de materiales carbonosos a medida, mostrando una importante ventaja en su aplicación en sistemas de gran escala, dada la evidente reducción de costes.

A la luz de los resultados mencionados, es posible afirmar que se han alcanzado los objetivos principales inicialmente propuestos, en línea con los objetivos planteados en el marco de la red ETN GreenCarbon.

8. Future Perspectives

The comprehensive and detailed study reported herein on the influence of the most important pyrolysis process conditions on the products yields and distributions, with a special emphasis on the resulting biochar properties, represents a valuable contribution to the field. Nonetheless, special care should be taken when attempting to extrapolate the results from this study to other biomass feedstocks and/or ranges of process conditions. Therefore, further efforts must be made to assess the effect of other variables, which still need to be clarified in order to allow the definitive launch of biochar-based materials at market conditions for the applications studied in this PhD thesis. In line with this, the following research themes would be addressed in the short and medium terms:

- Pressurized pyrolysis experiments are typically performed in reactors operating under a continuing carrier gas flow, which partially or totally sweeps away reactive vapors from the reactor. In such configuration, it is not possible to determine the truly effect of pressure on biochar, since it is strictly inter-related with other variables (i.e., gas residence time and pyrolysis environment). Other reactor configurations, such as the constant-volume carbonization (CVC) reactors, may allow to decouple the effect of pressure from that related to the gas residence time. Aligning the future research to this field of investigation will definitely clarify the influence of absolute pressure during pyrolysis process.
- The effect of absolute pressure on the overall energy and exergy efficiencies of pressurized pyrolysis process should be investigated by using different reactor configurations and biomass feedstocks, in order to determine more precise relationships.
- Evaluating the effects of both absolute pressure and pyrolysis environment on the final PAHs concentration in biochar resulted to be a very complex task, due to the large number of interactions among the factors related to the pyrolysis process conditions. In this sense, it would be interesting to enrich the available literature with a more relevant number of studies, which may definitively clarify the influence of the cited factors, guarantying a reasonable level of consistency.

- Despite the encouraging results for wheat straw-derived carbon materials produced through one-step physical activation, further research is needed on assessing the feasibility of large-scale production systems. In this sense, experimental trials using continuous reactor setups (e.g., those based on rotary or screw configurations, which are relatively easy to scale-up) should be conducted under the best operating conditions established for the reactor used here, or under a set of operating as similar as possible.

9. References

- Abdullah, H., Wu, H., 2009. Biochar as a fuel: 1. Properties and grindability of biochars produced from the pyrolysis of mallee wood under slow-heating conditions. *Energy Fuels* 23, 4174–4181. <https://doi.org/10.1021/ef900494t>.
- Abián, M., Millera, A., Bilbao, R., Alzueta, M.U., 2012. Effect of Recirculation Gases on Soot Formed from Ethylene Pyrolysis. *Combust. Sci. Technol.* 184, 980–994. <https://doi.org/10.1080/00102202.2012.663990>.
- Abián, M., Millera, A., Bilbao, R., Alzueta, M.U., 2012. Experimental study on the effect of different CO₂ concentrations on soot and gas products from ethylene thermal decomposition. *Fuel* 91, 307–312. <https://doi.org/10.1016/j.fuel.2011.06.064>.
- Akhtar, J., Saidina Amin, N., 2012. A review on operating parameters for optimum liquid oil yield in biomass pyrolysis. *Renew. Sustain. Energy Rev.* 16, 5101–5109. <https://doi.org/10.1016/J.RSER.2012.05.033>.
- Al-Wabel, M.I., Al-Omran, A., El-Naggar, A.H., Nadeem, M., Usman, A.R.A., 2013. Pyrolysis temperature induced changes in characteristics and chemical composition of biochar produced from conocarpus wastes. *Bioresour. Technol.* 131, 374–379. <https://doi.org/10.1016/j.biortech.2012.12.165>.
- AlAmeri, K., Giwa, A., Yousef, L., Alraeesi, A., Taher, H., 2019. Sorption and removal of crude oil spills from seawater using peat-derived biochar: An optimization study. *J. Environ. Manage.* 250, 109465. <https://doi.org/10.1016/j.jenvman.2019.109465>.
- Antal, M. J., J., Allen, S.G., Dai, X., Shimizu, B., Tam, M.S., Gronli, M., 2000. Attainment of the Theoretical Yield of Carbon from Biomass. *Ind. Eng. Chem. Res.* 39, 4024–4031. <https://doi.org/10.1021/ie000511u>.
- Antal, M.J., Croiset, E., Dai, X., DeAlmeida, C., Mok, W.S.-L., Norberg, N., Richard, J.-R., Al Majthoub, M., 1996. High-Yield Biomass Charcoal †. *Energy & Fuels* 10, 652–658. <https://doi.org/10.1021/ef9501859>.
- Antal, M.J., Gronli, M., 2003. The Art, Science, and Technology of Charcoal Production. *Ind. Eng. Chem. Res.* 42, 1619–1640. <https://doi.org/10.1021/ie0207919>.
- Antal, M.J., Mochidzuki, K., Paredes, L.S., 2003. Flash carbonization of biomass. *Ind. Eng. Chem. Res.* 42, 3690–3699. <https://doi.org/10.1021/ie0301839>.
- Aracil, I., Font, R., Conesa, J.A., 2005. Semivolatile and volatile compounds from the pyrolysis and combustion of polyvinyl chloride. *J. Anal. Appl. Pyrolysis* 74, 465–478. <https://doi.org/10.1016/j.jaap.2004.09.008>.

- Arias, B., Pevida, C., Feroso, J., Plaza, M.G., Rubiera, F., Pis, J.J., 2008. Influence of torrefaction on the grindability and reactivity of woody biomass. *Fuel Process. Technol.* 89, 169–175. <https://doi.org/10.1016/j.fuproc.2007.09.002>.
- Arrhenius, S., 1896. On the influence of carbonic acid in the air upon the temperature of the ground. *Philos. Mag. J. Sci.* 41, 237–276. <https://doi.org/10.1080/14786449608620846>.
- Atienza-Martínez, M., Ábrego, J., Mastral, J.F., Ceamanos, J., Gea, G., 2018. Energy and exergy analyses of sewage sludge thermochemical treatment. *Energy* 144, 723–735. <https://doi.org/10.1016/J.ENERGY.2017.12.007>.
- Aysu, T., Küçük, M.M., 2014. Biomass pyrolysis in a fixed-bed reactor: Effects of pyrolysis parameters on product yields and characterization of products. *Energy* 64, 1002–1025. <https://doi.org/10.1016/j.energy.2013.11.053>.
- Azuara, M., Sáiz, E., Manso, J.A., García-Ramos, F.J., Manyà, J.J., 2017. Study on the effects of using a carbon dioxide atmosphere on the properties of vine shoots-derived biochar. *Anal. Appl. Pyrolysis* 124, 719–725. <https://doi.org/10.1016/j.jaap.2016.11.022>.
- Bagreev, A., Bashkova, S., Locke, D.C., Bandosz, T.J., 2001. Sewage sludge-derived materials as efficient adsorbents for removal of hydrogen sulfide. *Environ. Sci. Technol.* 35, 1537–1543. <https://doi.org/10.1021/es001678h>.
- Banerjee, S., Joshi, S.R., Mandal, T., Halder, G., 2018. Application of zirconium caged activated biochar alginate beads towards deionization of Cr(VI) laden water in a fixed bed column reactor. *J. Environ. Chem. Eng.* 6, 4018–4029. <https://doi.org/10.1016/j.jece.2018.06.011>.
- Barisano, D., Canneto, G., Nanna, F., Alvino, E., Pinto, G., Villone, A., Carnevale, M., Valerio, V., Battafarano, A., Braccio, G., 2016. Steam/oxygen biomass gasification at pilot scale in an internally circulating bubbling fluidized bed reactor. *Fuel Process. Technol.* 141, 74–81. <https://doi.org/10.1016/j.fuproc.2015.06.008>.
- Bartoli, M., Giorcelli, M., Jagdale, P., Rovere, M., Tagliaferro, A., 2020. A Review of Non-Soil Biochar Applications. *Materials (Basel)*. <https://doi.org/10.3390/ma13020261>.
- Basu, P., 2013. *Biomass Gasification, Pyrolysis and Torrefaction*. Elsevier Applied Science, Burlington. <https://doi.org/10.1016/C2011-0-07564-6>.
- Biswas, B., Singh, R., Kumar, J., Singh, R., Gupta, P., Krishna, B.B., Bhaskar, T., 2018. Pyrolysis behavior of rice straw under carbon dioxide for production of bio-oil. *Renew. Energy* 129, 678–685. <https://doi.org/10.1016/j.renene.2017.04.048>.

- Brassard, P., Godbout, S., Lévesque, V., Palacios, J.H., Raghavan, V., Ahmed, A., Hogue, R., Jeanne, T., Verma, M., 2019. 4 - Biochar for soil amendment, in: Jeguirim, M., Limousy, L.B.T.-C. and C.M.D. from B. (Eds.), . Elsevier, pp. 109–146. <https://doi.org/10.1016/B978-0-12-814893-8.00004-3>.
- Brewer, C.E., Schmidt-Rohr, K., Satrio, J.A., Brown, R.C., 2009. Characterization of biochar from fast pyrolysis and gasification systems. *Environ. Prog. Sustain. Energy* 28, 386–396. <https://doi.org/10.1002/ep.10378>.
- Bridgwater, A. V., 2012. Review of fast pyrolysis of biomass and product upgrading. *Biomass and Bioenergy* 38, 68–94. <https://doi.org/10.1016/j.biombioe.2011.01.048>.
- Brown, R.A., Kercher, A.K., Nguyen, T.H., Nagle, D.C., Ball, W.P., 2006. Production and characterization of synthetic wood chars for use as surrogates for natural sorbents. *Org. Geochem.* 37, 321–333. <https://doi.org/10.1016/j.orggeochem.2005.10.008>.
- Bruun, E.W., Hauggaard-Nielsen, H., Ibrahim, N., Egsgaard, H., Ambus, P., Jensen, P.A., Dam-Johansen, K., 2011. Influence of fast pyrolysis temperature on biochar labile fraction and short-term carbon loss in a loamy soil. *Biomass and Bioenergy* 35, 1182–1189. <https://doi.org/10.1016/j.biombioe.2010.12.008>.
- Bui, H.-H., Wang, L., Tran, K.-Q., Skreiberg, Ø., 2016. CO₂ gasification of charcoals produced at various pressures. *Fuel Process. Technol.* 152, 207–214. <https://doi.org/10.1016/J.FUPROC.2016.06.033>.
- Buss, W., Graham, M.C., MacKinnon, G., Mašek, O., 2016. Strategies for producing biochars with minimum PAH contamination. *J. Anal. Appl. Pyrolysis* 119, 24–30. <https://doi.org/10.1016/j.jaap.2016.04.001>.
- Cahn, M.D., Bouldin, D.R., Cravo, M.S., Bowen, W.T., 1993. Cation and nitrate leaching in an oxisol of the Brazilian Amazon. *Agron. J.* 85, 334–340. <https://doi.org/10.2134/agronj1993.00021962008500020032x>.
- Cao, C.T.N., Farrell, C., Kristiansen, P.E., Rayner, J.P., 2014. Biochar makes green roof substrates lighter and improves water supply to plants. *Ecol. Eng.* 71, 368–374. <https://doi.org/10.1016/j.ecoleng.2014.06.017>.
- Carrier, M., Loppinet-serani, A., Aymonier, C., 2011. Thermogravimetric analysis as a new method to determine the lignocellulosic composition of biomass. *Biomass and Bioenergy* 35, 298–307. <https://doi.org/10.1016/j.biombioe.2010.08.067>.

- Castrillon, M.C., Moura, K.O., Alves, C.A., Bastos-Neto, M., Azevedo, D.C.S., Hofmann, J., Möllmer, J., Einicke, W.-D., Gläser, R., 2016. CO₂ and H₂S Removal from CH₄-Rich Streams by Adsorption on Activated Carbons Modified with K₂CO₃, NaOH, or Fe₂O₃. *Energy & Fuels* 30, 9596–9604. <https://doi.org/10.1021/acs.energyfuels.6b01667>.
- Chaiwatanodom, P., Vivanpatarakij, S., Assabumrungrat, S., 2014. Thermodynamic analysis of biomass gasification with CO₂ recycle for synthesis gas production. *Appl. Energy* 114, 10–17. <https://doi.org/10.1016/j.apenergy.2013.09.052>.
- Chang, Q., Gao, R., Li, H., Yu, G., Wang, F., 2018. Effect of CO₂ on the characteristics of soot derived from coal rapid pyrolysis. *Combust. Flame* 197, 328–339. <https://doi.org/10.1016/j.combustflame.2018.05.033>.
- Channiwala, S.A., Parikh, P.P., 2002. A unified correlation for estimating HHV of solid, liquid and gaseous fuels. *Fuel* 81, 1051–1063. [https://doi.org/10.1016/S0016-2361\(01\)00131-4](https://doi.org/10.1016/S0016-2361(01)00131-4).
- Chatterjee, R., Sajjadi, B., Mattern, D.L., Chen, W.-Y., Zubatiuk, T., Leszczynska, D., Leszczynski, J., Egiebor, N.O., Hammer, N., 2018. Ultrasound cavitation intensified amine functionalization: A feasible strategy for enhancing CO₂ capture capacity of biochar. *Fuel* 225, 287–298. <https://doi.org/10.1016/j.fuel.2018.03.145>.
- Chen, J., Yang, J., Hu, G., Hu, X., Li, Z., Shen, S., Radosz, M., Fan, M., 2016. Enhanced CO₂ Capture Capacity of Nitrogen-Doped Biomass-Derived Porous Carbons. *ACS Sustain. Chem. Eng.* 4, 1439–1445. <https://doi.org/10.1021/acssuschemeng.5b01425>.
- Church, T.L., Szego, A.E., Hedin, N., 2021. Biochar-based Carbon Materials for Adsorptive Separation and Applications in Catalysis, in: *Biochar as a Renewable-Based Material: With Applications in Agriculture, the Environment and Energy*. p. 224. <https://doi.org/10.1142/q0262>.
- Cochrane, T.T., Sanchez, P.A., 1980. Land resources, soil properties and their management in the Amazon region: a state of knowledge report, in: *International Conference on Amazon Land Use and Agricultural Research*.
- Collard, F.-X., Blin, J., 2014. A review on pyrolysis of biomass constituents: Mechanisms and composition of the products obtained from the conversion of cellulose, hemicelluloses and lignin. *Renew. Sustain. Energy Rev.* 38, 594–608. <https://doi.org/10.1016/j.rser.2014.06.013>.
- Coromina, H.M., Walsh, D.A., Mokaya, R., 2016. Biomass-derived activated carbon with simultaneously enhanced CO₂ uptake for both pre and post combustion capture applications. *J. Mater. Chem. A* 4, 280–289. <https://doi.org/10.1039/C5TA09202G>.

- Cotton, A.M., 2013. Engineering Scale-Up and Environmental Effects of the Calcium Looping Cycle for Post-Combustion CO₂ Capture.
- Dai, X., Antal, M.J., 1999. Synthesis of a high-yield activated carbon by air gasification of macadamia nut shell charcoal. *Ind. Eng. Chem. Res.* 38, 3386–3395. <https://doi.org/10.1021/ie990063u>.
- Dat, N.-D., Chang, M.B., 2017. Review on characteristics of PAHs in atmosphere, anthropogenic sources and control technologies. *Sci. Total Environ.* 609, 682–693. <https://doi.org/10.1016/j.scitotenv.2017.07.204>.
- Daugaard, D.E., Brown, R.C., 2003. Enthalpy for pyrolysis for several types of biomass. *Energy and Fuels* 17, 934–939. <https://doi.org/10.1021/ef020260x>.
- Dayton, D.C., Hlebak, J., Carpenter, J.R., Wang, K., Mante, O.D., Peters, J.E., 2016. Biomass Hydrolysis in a Fluidized Bed Reactor. *Energy & Fuels* 30, 4879–4887. <https://doi.org/10.1021/acs.energyfuels.6b00373>.
- De la Rosa, J.M., Knicker, H., López-Capel, E., Manning, D.A.C., González-Perez, J.A., González-Vila, F.J., 2008. Direct Detection of Black Carbon in Soils by Py-GC/MS, Carbon-13 NMR Spectroscopy and Thermogravimetric Techniques. *Soil Sci. Soc. Am. J.* 72, 258–267. <https://doi.org/10.2136/sssaj2007.0031>.
- De la Rosa, J.M., Sánchez-Martín, Á.M., Campos, P., Miller, A.Z., 2019. Effect of pyrolysis conditions on the total contents of polycyclic aromatic hydrocarbons in biochars produced from organic residues: Assessment of their hazard potential. *Sci. Total Environ.* 667, 578–585. <https://doi.org/10.1016/j.scitotenv.2019.02.421>.
- Dean, C.C., Dugwell, D., Fennell, P.S., 2011. Investigation into potential synergy between power generation, cement manufacture and CO₂ abatement using the calcium looping cycle. *Energy Environ. Sci.* 4, 2050. <https://doi.org/10.1039/c1ee01282g>.
- Demirbaş, A., 2004. Effects of temperature and particle size on bio-char yield from pyrolysis of agricultural residues. *J. Anal. Appl. Pyrolysis* 72, 243–248. <https://doi.org/10.1016/j.jaap.2004.07.003>.
- Demirbaş, A.H., Demirbaş, A.S., Demirbaş, A., 2010. Liquid fuels from agricultural residues via conventional pyrolysis. *Energy Sources* 26, 821–827. <https://doi.org/10.1080/00908310490451637>.
- Deng, S., Wei, H., Chen, T., Wang, B., Huang, J., Yu, G., 2014. Superior CO₂ adsorption on pine nut shell-derived activated carbons and the effective micropores at different temperatures. *Chem. Eng. J.* 253, 46–54. <https://doi.org/10.1016/j.cej.2014.04.115>.

- Dhyani, V., Bhaskar, T., 2017. A comprehensive review on the pyrolysis of lignocellulosic biomass. *Renew. Energy*. <https://doi.org/10.1016/j.renene.2017.04.035>.
- Di Blasi, C., Branca, C., Santoro, A., Hernandez, E.G., 2001. Pyrolytic behavior and products of some wood varieties. *Combust. Flame* 124, 165–177. [https://doi.org/10.1016/S0010-2180\(00\)00191-7](https://doi.org/10.1016/S0010-2180(00)00191-7).
- Di Blasi, C., Galgano, A., Branca, C., 2009. Effects of Potassium Hydroxide Impregnation on Wood Pyrolysis. *Energy & Fuels* 23, 1045–1054. <https://doi.org/10.1021/ef800827q>.
- Di Blasi, C., Signorelli, G., Di Russo, C., Rea, G., 1999. Product distribution from pyrolysis of wood and agricultural residues. *Ind. Eng. Chem. Res.* 38, 2216–2224. <https://doi.org/10.1021/ie980711u>.
- Di Stasi, C., Alvira, D., Greco, G., González, B., Manyà, J.J.J.J., 2019. Physically activated wheat straw-derived biochar for biomass pyrolysis vapors upgrading with high resistance against coke deactivation. *Fuel* 255, 115807. <https://doi.org/10.1016/j.fuel.2019.115807>.
- Di Stasi, C., Greco, G., Canevesi, R.L.S., Izquierdo, M.T., Fierro, V., Celzard, A., González, B., Manyà, J.J., 2021. Influence of activation conditions on textural properties and performance of activated biochars for pyrolysis vapors upgrading. *Fuel* 289, 119759. <https://doi.org/10.1016/j.fuel.2020.119759>.
- Dincer, I., Rosen, M.A., 2013. *Exergy: energy, environment and sustainable development*, 2nd Editio. ed. Elsevier, Oxford, Great Britain. <https://doi.org/10.1016/B978-0-08-097089-9.00001-2>.
- Dong, Q., Li, H., Niu, M., Luo, C., Zhang, J., Qi, B., Li, X., Zhong, W., 2018. Microwave pyrolysis of moso bamboo for syngas production and bio-oil upgrading over bamboo-based biochar catalyst. *Bioresour. Technol.* 266, 284–290. <https://doi.org/10.1016/j.biortech.2018.06.104>.
- Duman, G., Okutucu, C., Ucar, S., Stahl, R., Yanik, J., 2011. The slow and fast pyrolysis of cherry seed. *Bioresour. Technol.* 102, 1869–1878. <https://doi.org/10.1016/j.biortech.2010.07.051>.
- Durán, I., Álvarez-Gutiérrez, N., Rubiera, F., Pevida, C., 2018. Biogas purification by means of adsorption on pine sawdust-based activated carbon: Impact of water vapor. *Chem. Eng. J.* 353, 197–207. <https://doi.org/10.1016/j.cej.2018.07.100>.
- Encinar, J.M., Beltrán, F.J., Bernalte, A., Ramiro, A., González, J.F., 1996. Pyrolysis of two agricultural residues: Olive and grape bagasse. Influence of particle size and temperature. *Biomass and Bioenergy* 11, 397–409. [https://doi.org/10.1016/S0961-9534\(96\)00029-3](https://doi.org/10.1016/S0961-9534(96)00029-3).

- Encinar, J.M., Gonzalez, J.F., 2000. Fixed-bed pyrolysis of *Cynara carduncules* L., product yields and compositions. *Fuel Process. Technol.* 68, 209–222. [https://doi.org/10.1016/S0378-3820\(00\)00125-9](https://doi.org/10.1016/S0378-3820(00)00125-9).
- Enders, A., Hanley, K., Whitman, A., Joseph, S., Lehmann, J., Whitman, T., Joseph, S., Lehmann, J., Whitman, A., Joseph, S., Lehmann, J., 2012. Characterization of biochars to evaluate recalcitrance and agronomic performance. *Bioresour. Technol.* 114, 644–653. <https://doi.org/10.1016/j.biortech.2012.03.022>.
- European Biochar Certificate (EBC), 2019. European Biochar Certificate – Guidelines for a Sustainable Production of Biochar. Arbaz, Switzerland.
- European Commission Regulation (ECR), 2006. Setting maximum levels for certain contaminants in foodstuffs.
- Fabbri, D., Rombolà, A.G., Torri, C., Spokas, K.A., 2013. Determination of polycyclic aromatic hydrocarbons in biochar and biochar amended soil, in: *Journal of Analytical and Applied Pyrolysis*. pp. 60–67. <https://doi.org/10.1016/j.jaap.2012.10.003>.
- Fearnside, P.M., 2000. Global warming and tropical land-use change: greenhouse gas emissions from biomass burning, decomposition and soils in forest conversion, shifting cultivation and secondary vegetation. *Clim. Change* 46, 115–158. <https://doi.org/10.1023/A:1005569915357>.
- Fearnside, P.M., Graca, P.M.L., Filho, N.L., Rodrigues, F.J.A., Robinson, J.M., 1999. Tropical forest burning in Brazilian Amazonia: measurement of biomass loading, burning efficiency and charcoal formation at Altamira, Pará. *For. Ecol. Manage.* 123, 65–79. [https://doi.org/10.1016/S0378-1127\(99\)00016-X](https://doi.org/10.1016/S0378-1127(99)00016-X).
- Fennell, P., 2015. Calcium and Chemical Looping Technology for Power Generation and Carbon Dioxide (CO₂) Capture, Calcium and Chemical Looping Technology for Power Generation and Carbon Dioxide (CO₂) Capture. Elsevier. <https://doi.org/10.1016/B978-0-85709-243-4.00003-3>.
- Font, R., Aracil, I., Fullana, A., Martín-Gullón, I., Conesa, J.A., 2003. Semivolatile compounds in pyrolysis of polyethylene. *J. Anal. Appl. Pyrolysis* 68–69, 599–611. [https://doi.org/10.1016/S0165-2370\(03\)00038-X](https://doi.org/10.1016/S0165-2370(03)00038-X).
- Fowles, M., 2007. Black carbon sequestration as an alternative to bioenergy. *Biomass and Bioenergy* 31, 426–432. <https://doi.org/10.1016/j.biombioe.2007.01.012>.
- Freundlich, H., 1907. Über Die Adsorption in Lösungen. *Zeitschrift für Phys. Chemie* 57, 285–470. <https://doi.org/10.1515/zpch-1907-5723>.

- Furuhata, T., Kobayashi, Y., Hayashida, K., Arai, M., 2012. Behavior of PAHs and PM in a diffusion flame of paraffin fuels. *Fuel* 91, 16–25. <https://doi.org/10.1016/j.fuel.2011.07.014>.
- Gascó, G., Paz-Ferreiro, J., Álvarez, M.L., Saa, A., Méndez, A., 2018. Biochars and hydrochars prepared by pyrolysis and hydrothermal carbonisation of pig manure. *Waste Manag.* 79, 395–403. <https://doi.org/10.1016/j.wasman.2018.08.015>.
- Gaunt, J.L., Lehmann, J., 2008. Energy balance and emissions associated with biochar sequestration and pyrolysis bioenergy production. *Environ. Sci. Technol.* 42, 4152–4158. <https://doi.org/10.1021/es071361i>.
- Ghani, W.A.W.A.K., Mohd, A., da Silva, G., Bachmann, R.T., Taufiq-Yap, Y.H., Rashid, U., Al-Muhtaseb, A.H., 2013. Biochar production from waste rubber-wood-sawdust and its potential use in C sequestration: Chemical and physical characterization. *Ind. Crops Prod.* 44, 18–24. <https://doi.org/10.1016/j.indcrop.2012.10.017>.
- Glaser, B., Balashov, E., Haumaier, L., Guggenberger, G., Zech, W., 2000. Black carbon in density fractions of anthropogenic soils of the Brazilian Amazon region. *Org. Geochem.* 31, 669–678. [https://doi.org/10.1016/S0146-6380\(00\)00044-9](https://doi.org/10.1016/S0146-6380(00)00044-9).
- Glaser, B., Haumaier, L., Guggenberger, G., Zech, W., 2001. The Terra Preta phenomenon - a model for sustainable agriculture in the humid tropics. *Sci. Nat.* 88, 37–41. <https://doi.org/10.1007/s001140000193>.
- Glaser, B., Lehmann, J., Zech, W., 2002. Ameliorating physical and chemical properties of highly weathered soils in the tropics with charcoal - a review. *Biol. Fertil. Soils* 35, 219–230. <https://doi.org/10.1007/s00374-002-0466-4>.
- González, A.S., Plaza, M.G., Rubiera, F., Pevida, C., 2013. Sustainable biomass-based carbon adsorbents for post-combustion CO₂ capture. *Chem. Eng. J.* 230, 456–465. <https://doi.org/10.1016/j.cej.2013.06.118>.
- Goula, G., Kioussis, V., Nalbandian, L., Yentekakis, I. V, 2006. Catalytic and electrocatalytic behavior of Ni-based cermet anodes under internal dry reforming of CH₄+CO₂ mixtures in SOFCs. *Solid State Ionics* 177, 2119–2123. <https://doi.org/10.1016/j.ssi.2006.03.040>.
- Grande, C.A., 2012. Advances in Pressure Swing Adsorption for Gas Separation. *ISRN Chem. Eng.* 2012, 982934. <https://doi.org/10.5402/2012/982934>.
- Greco, G., Videgain, M., Di Stasi, C., Pires, E., Manyà, J.J., 2021. Importance of pyrolysis temperature and pressure in the concentration of polycyclic aromatic hydrocarbons in wood waste-derived biochars. *J. Anal. Appl. Pyrolysis* 159, 105337. <https://doi.org/10.1016/j.jaap.2021.105337>.

- Guedes, R.E., Luna, A.S., Torres, A.R., 2018. Operating parameters for bio-oil production in biomass pyrolysis: A review. *J. Anal. Appl. Pyrolysis* 129, 134–149. <https://doi.org/10.1016/J.JAAP.2017.11.019>.
- Guizani, C., Escudero Sanz, F.J., Salvador, S., 2015. Influence of temperature and particle size on the single and mixed atmosphere gasification of biomass char with H₂O and CO₂. *Fuel Process. Technol.* 134, 175–188. <https://doi.org/10.1016/j.fuproc.2015.01.031>.
- Guo, L., Yang, J., Hu, G., Hu, X., Wang, L., Dong, Y., DaCosta, H., Fan, M., 2016. Role of Hydrogen Peroxide Preoxidizing on CO₂ Adsorption of Nitrogen-Doped Carbons Produced from Coconut Shell. *ACS Sustain. Chem. Eng.* 4, 2806–2813. <https://doi.org/10.1021/acssuschemeng.6b00327>.
- Hale, S.E., Lehmann, J., Rutherford, D., Zimmerman, A.R., Bachmann, R.T., Shitumbanuma, V., O'Toole, A., Sundqvist, K.L., Arp, H.P.H., Cornelissen, G., 2012. Quantifying the Total and Bioavailable Polycyclic Aromatic Hydrocarbons and Dioxins in Biochars. *Environ. Sci. Technol.* 46, 2830–2838. <https://doi.org/10.1021/es203984k>.
- Hao, W., Björkman, E., Lilliestråle, M., Hedin, N., 2013. Activated carbons prepared from hydrothermally carbonized waste biomass used as adsorbents for CO₂. *Appl. Energy* 112, 526–532. <https://doi.org/10.1016/J.APENERGY.2013.02.028>.
- Heo, H.S., Park, H.J., Dong, J.-I., Park, S.H., Kim, S., Suh, D.J., Suh, Y.-W., Kim, S.-S., Park, Y.-K., 2010. Fast pyrolysis of rice husk under different reaction conditions. *J. Ind. Eng. Chem.* 16, 27–31. <https://doi.org/10.1016/J.JIEC.2010.01.026>.
- Hervy, M., Pham Minh, D., Gérente, C., Weiss-Hortala, E., Nzihou, A., Villot, A., Le Coq, L., 2018. H₂S removal from syngas using wastes pyrolysis chars. *Chem. Eng. J.* 334, 2179–2189. <https://doi.org/10.1016/j.cej.2017.11.162>.
- Hou, Y., Huang, G., Li, J., Yang, Q., Huang, S., Cai, J., 2019. Hydrothermal conversion of bamboo shoot shell to biochar: Preliminary studies of adsorption equilibrium and kinetics for rhodamine B removal. *J. Anal. Appl. Pyrolysis* 143, 104694. <https://doi.org/10.1016/j.jaap.2019.104694>.
- Huang, Y.-F., Chiueh, P.-T., Lo, S.-L., 2019. CO₂ adsorption on biochar from co-torrefaction of sewage sludge and leucaena wood using microwave heating. *Energy Procedia* 158, 4435–4440. <https://doi.org/10.1016/j.egypro.2019.01.772>.
- Huggins, T.M., Haeger, A., Biffinger, J.C., Ren, Z.J., 2016. Granular biochar compared with activated carbon for wastewater treatment and resource recovery. *Water Res.* 94, 225–232. <https://doi.org/10.1016/j.watres.2016.02.059>.

- Initial Biochar Initiative (IBI), 2015. Standardized Product Definition and Product Testing Guidelines for Biochar that is Used in Soil.
- IPCC, 2000. Summary for Policymakers: Emissions Scenarios. A Special Report of Working Group III of the Intergovernmental Panel on Climate Change. Group 20. <https://doi.org/92-9169-113-5>.
- Jagiello, J., Kenvin, J., Ania, C.O., Parra, J.B., Celzard, A., Fierro, V., 2020. Exploiting the adsorption of simple gases O₂ and H₂ with minimal quadrupole moments for the dual gas characterization of nanoporous carbons using 2D-NLDFT models. *Carbon N. Y.* 160, 164–175. <https://doi.org/10.1016/j.carbon.2020.01.013>.
- Jayawardhana, Y., Gunatilake, S.R., Mahatantila, K., Ginige, M.P., Vithanage, M., 2019. Sorptive removal of toluene and m-xylene by municipal solid waste biochar: Simultaneous municipal solid waste management and remediation of volatile organic compounds. *J. Environ. Manage.* 238, 323–330. <https://doi.org/10.1016/j.jenvman.2019.02.097>.
- Kauffman, J.B., Cummings, D.L., Ward, D.E., Babbitt, R., 1995. Fire in the Brazilian Amazon: 1. Biomass, nutrient pools, and losses in slashed primary forests. *Oecologia* 104, 397–408. <https://doi.org/10.1007/BF00341336>.
- Kleinman, P.J.A., Pimentel, D., Bryant, R.B., 1995. The Ecological Sustainability of Slash-and-burn Agriculture. *Agric. Ecosyst. Environ.* 52, 235–249. [https://doi.org/10.1016/0167-8809\(94\)00531-I](https://doi.org/10.1016/0167-8809(94)00531-I).
- Kolokolova, O., Levi, T., Pang, S., 2013. Torrefaction and Pyrolysis of biomass waste in continuous reactors, in: *Proceedings of the 13th International Conference on Environmental Science and Technology*.
- Krishna, B.B., Biswas, B., Ohri, P., Kumar, J., Singh, R., Bhaskar, T., 2016. Pyrolysis of Cedrus deodara saw mill shavings in hydrogen and nitrogen atmosphere for the production of bio-oil. *Renew. Energy* 98, 238–244. <https://doi.org/10.1016/j.renene.2016.02.056>.
- Laird, A.D., 2008. The charcoal vision: a win-win-win scenario for simultaneously producing bioenergy, permanently sequestering carbon, while improving soil and water quality. *Agron. J.* 100, 178–181. <https://doi.org/10.2134/agronj2007.0161>.
- Langmuir, I., 1916. The Constitution and Fundamental Properties of Solids and Liquids. Part I. Solids. *J. Am. Chem. Soc.* 38, 2221–2295. <https://doi.org/10.1021/ja02268a002>.

- Lee, J., Yang, X., Cho, S.H., Kim, J.K., Lee, S.S., Tsang, D.C.W., Ok, Y.S., Kwon, E.E., 2017. Pyrolysis process of agricultural waste using CO₂ for waste management, energy recovery, and biochar fabrication. *Appl. Energy* 185, 214–222. <https://doi.org/10.1016/j.apenergy.2016.10.092>.
- Legarra, M., Morgan, T., Turn, S., Wang, L., Skreiberg, Ø., Antal, M. J., J., 2018. Carbonization of Biomass in Constant-Volume Reactors. *Energy & Fuels* 32, 475–489. <https://doi.org/10.1021/acs.energyfuels.7b02982>.
- Lehmann, J., 2007. A handful of carbon. *Nature* 447, 143–144. <https://doi.org/10.1038/447143a>.
- Lehmann, J., Joseph, S., 2009. Biochar for Environmental Management: An Introduction, in: *Biochar for Environmental Management*. Eartschan, pp. 1–10. <https://doi.org/10.4324/9780203762264>.
- Li, D., Ma, T., Zhang, R., Tian, Y., Qiao, Y., 2015. Preparation of porous carbons with high low-pressure CO₂ uptake by KOH activation of rice husk char. *Fuel* 139, 68–70. <https://doi.org/10.1016/j.fuel.2014.08.027>.
- Li, M., Liu, C., Cao, H., Zhao, H., Zhang, Y., Fan, Z., 2014. KOH self-templating synthesis of three-dimensional hierarchical porous carbon materials for high performance supercapacitors. *J. Mater. Chem. A* 2, 14844–14851. <https://doi.org/10.1039/C4TA02167C>.
- Li, S., Xu, S., Liu, S., Yang, C., Lu, Q., 2004. Fast pyrolysis of biomass in free-fall reactor for hydrogen-rich gas. *Fuel Process. Technol.* 85, 1201–1211. <https://doi.org/10.1016/J.FUPROC.2003.11.043>.
- Liang, C., Gascó, G., Fu, S., Méndez, A., Paz-Ferreiro, J., 2016. Biochar from pruning residues as a soil amendment: Effects of pyrolysis temperature and particle size. *Soil Tillage Res.* 164, 3–10. <https://doi.org/10.1016/j.still.2015.10.002>.
- Linares-Solano, A., De D. López-González, J., Molina-Sabio, M., Rodríguez-Reinoso, F., 1980. Active carbons from almond shells as adsorbents in gas and liquid phases. *J. Chem. Technol. Biotechnol.* 30, 65–72. <https://doi.org/10.1002/jctb.503300109>.
- Lingamdinne, L.P., Roh, H., Choi, Y.-L., Koduru, J.R., Yang, J.-K., Chang, Y.-Y., 2015. Influencing factors on sorption of TNT and RDX using rice husk biochar. *J. Ind. Eng. Chem.* 32, 178–186. <https://doi.org/10.1016/j.jiec.2015.08.012>.
- Liu, Q., Wang, S., Zheng, Y., Luo, Z., Cen, K., 2008. Mechanism study of wood lignin pyrolysis by using TG-FTIR analysis. *J. Anal. Appl. Pyrolysis* 82, 170–177. <https://doi.org/10.1016/j.jaap.2008.03.007>.

- Liu, S.-H., Huang, Y.-Y., 2018. Valorization of coffee grounds to biochar-derived adsorbents for CO₂ adsorption. *J. Clean. Prod.* 175, 354–360. <https://doi.org/10.1016/j.jclepro.2017.12.076>.
- Liu, W.-J., Jiang, H., Yu, H.-Q., 2015. Development of Biochar-Based Functional Materials: Toward a Sustainable Platform Carbon Material. *Chem. Rev.* 22, 12251–12285. <https://doi.org/10.1021/acs.chemrev.5b00195>.
- Lu, Q., Yang, X., Dong, C., Zhang, Z., Zhang, X., Zhu, X., 2011. Influence of pyrolysis temperature and time on the cellulose fast pyrolysis products: Analytical Py-GC/MS study. *J. Anal. Appl. Pyrolysis* 92, 430–438. <https://doi.org/10.1016/j.jaap.2011.08.006>.
- Lua, A.C., Guo, J., 2000. Activated carbon prepared from oil palm stone by one-step CO₂ activation for gaseous pollutant removal. *Carbon N. Y.* 38, 1089–1097. [https://doi.org/10.1016/S0008-6223\(99\)00231-6](https://doi.org/10.1016/S0008-6223(99)00231-6).
- Madej, J., Hilber, I., Bucheli, T.D., Oleszczuk, P., 2016. Biochars with low polycyclic aromatic hydrocarbon concentrations achievable by pyrolysis under high carrier gas flows irrespective of oxygen content or feedstock. *J. Anal. Appl. Pyrolysis* 122, 365–369. <https://doi.org/10.1016/j.jaap.2016.09.005>.
- Manyà, J.J., 2012. Pyrolysis for Biochar Purposes: A Review to Establish Current Knowledge Gaps and Research Needs. *Environ. Sci. Technol.* 46, 7939–7954. <https://doi.org/10.1021/es301029g>.
- Manyà, J.J., Alvira, D., Azuara, M., Bernin, D., Hedin, N., 2016. Effects of Pressure and the Addition of a Rejected Material from Municipal Waste Composting on the Pyrolysis of Two-Phase Olive Mill Waste. *Energy & Fuels* 30, 8055–8064. <https://doi.org/10.1021/acs.energyfuels.6b01579>.
- Manyà, J.J., Gascó, G., 2021. Biochar as a Sustainable Resource to Drive Innovative Green Technologies, in: *Biochar as a Renewable-Based Material: With Applications in Agriculture, the Environment and Energy*. pp. 1–33. <https://doi.org/10.1142/q0262>.
- Manyà, J.J., González, B., Azuara, M., Arner, G., 2018. Ultra-microporous adsorbents prepared from vine shoots-derived biochar with high CO₂ uptake and CO₂/N₂ selectivity. *Chem. Eng. J.* 345, 631–639. <https://doi.org/10.1016/j.cej.2018.01.092>.
- Manyà, J.J., Laguarda, S., Ortigosa, M.A., Manso, J.A., 2014a. Biochar from Slow Pyrolysis of Two-Phase Olive Mill Waste: Effect of Pressure and Peak Temperature on its Potential Stability. *Energy & Fuels* 28, 3271–3280. <https://doi.org/10.1021/ef500654t>.

- Manyà, J.J., Ortigosa, M.A., Laguarda, S., Manso, J.A., 2014b. Experimental study on the effect of pyrolysis pressure, peak temperature, and particle size on the potential stability of vine shoots-derived biochar. *Fuel* 133, 163–172. <https://doi.org/10.1016/j.fuel.2014.05.019>.
- Manyà, J.J., Roca, F.X., Perales, J.F.J., 2013. TGA study examining the effect of pressure and peak temperature on biochar yield during pyrolysis of two-phase olive mill waste. *Anal. Appl. Pyrolysis* 103, 86–95. <https://doi.org/10.1016/j.jaap.2012.10.006>.
- Manyà, J.J., Ruiz, J., Arauzo, J., 2007. Some peculiarities of conventional pyrolysis of several agricultural residues in a packed bed reactor. *Ind. Eng. Chem. Res.* 46, 9061–9070. <https://doi.org/10.1021/ie070811c>.
- Maroušek, J., 2014. Significant breakthrough in biochar cost reduction. *Clean Technol. Environ. Policy* 16, 1821–1825. <https://doi.org/10.1007/s10098-014-0730-y>.
- Maroušek, J., Strunecký, O., Stehel, V., 2019. Biochar farming: defining economically perspective applications. *Clean Technol. Environ. Policy* 21, 1389–1395. <https://doi.org/10.1007/s10098-019-01728-7>.
- Mašek, O., Brownsort, P., Cross, A., Sohi, S., 2013. Influence of production conditions on the yield and environmental stability of biochar. *Fuel* 103, 151–155. <https://doi.org/10.1016/j.fuel.2011.08.044>.
- Mastral, A.M., Callén, M.S., García, T., 2000. Polyaromatic Environmental Impact in Coal–Tire Blend Atmospheric Fluidized Bed (AFB) Combustion. *Energy & Fuels* 14, 164–168. <https://doi.org/10.1021/ef990101m>.
- Mastral, A.M., Callén, M.S., García, T., Lopez, J.M., 2001. Benzo(a)pyrene, Benzo(a)anthracene, and Dibenzo(a,h)anthracene Emissions from Coal and Waste Tire Energy Generation at Atmospheric Fluidized Bed Combustion (AFBC). *Environ. Sci. Technol.* 35, 2645–2649. <https://doi.org/10.1021/es0015850>.
- Matamba, T., Tahmasebi, A., Khoshk Rish, S., Yu, J., 2020. Promotion Effects of Pressure on Polycyclic Aromatic Hydrocarbons and H₂ Formation during Flash Pyrolysis of Palm Kernel Shell. *Energy & Fuels* 34, 3346–3356. <https://doi.org/10.1021/acs.energyfuels.9b04409>.
- McBeath, A. V., Smernik, R.J., Schneider, M.P.W., Schmidt, M.W.I., Plant, E.L., 2011. Determination of the aromaticity and the degree of aromatic condensation of a thermosequence of wood charcoal using NMR. *Org. Geochem.* 42, 1194–1202. <https://doi.org/10.1016/j.orggeochem.2011.08.008>.

- McBeath, A. V., Wurster, C.M., Bird, M.I., 2015. Influence of feedstock properties and pyrolysis conditions on biochar carbon stability as determined by hydrogen pyrolysis. *Biomass Bioenergy* 73. <https://doi.org/10.1016/j.biombioe.2014.12.022>.
- McHenry, M.P., 2009. Agricultural bio-char production, renewable energy generation and farm carbon sequestration in Western Australia: certainty, uncertainty and risk. *Agric. Ecosyst. Environ.* 129, 1–7. <https://doi.org/10.1016/j.agee.2008.08.006>.
- McKendry, P., 2002. Energy production from biomass (part 1): overview of biomass. *Bioresour. Technol.* 83, 37–46. [https://doi.org/10.1016/S0960-8524\(01\)00118-3](https://doi.org/10.1016/S0960-8524(01)00118-3).
- Melgar, R.J., Smyth, T.J., Sanchez, P.A., Cravo, M.S., 1992. Fertilizer nitrogen movement in a Central Amazon Oxisol and Entisol cropped to corn. *Fertil. Res.* 31, 241–252. <https://doi.org/10.1007/BF01063298>.
- Melligan, F., Hayes, M.H.B., Kwapinski, W., Leahy, J.J., 2013. A study of hydrogen pressure during hydrolysis of *Miscanthus x giganteus* and online catalytic vapour upgrading with Ni on ZSM-5. *J. Anal. Appl. Pyrolysis* 103, 369–377. <https://doi.org/10.1016/j.jaap.2013.01.005>.
- Méndez, A., Barriga, S., Fidalgo, J.M., Gascó, G., 2009. Adsorbent materials from paper industry waste materials and their use in Cu(II) removal from water. *J. Hazard. Mater.* 165, 736–743. <https://doi.org/10.1016/j.jhazmat.2008.10.055>.
- Méndez, A., Gómez, A., Paz-Ferreiro, J., Gascó, G., 2012. Effects of sewage sludge biochar on plant metal availability after application to a Mediterranean soil. *Chemosphere* 89, 1354–1359. <https://doi.org/10.1016/j.chemosphere.2012.05.092>.
- Méndez, A., Paz-Ferreiro, J., Gil, E., Gascó, G., 2015. The effect of paper sludge and biochar addition on brown peat and coir based growing media properties. *Sci. Hortic. (Amsterdam)*. 193, 225–230. <https://doi.org/10.1016/j.scienta.2015.07.032>.
- Méndez, A., Terradillos, M., Gascó, G., 2013. Physicochemical and agronomic properties of biochar from sewage sludge pyrolysed at different temperatures. *J. Anal. Appl. Pyrolysis* 102, 124–130. <https://doi.org/10.1016/j.jaap.2013.03.006>.
- Ministerio de Agricultura, Pesca y Alimentación, Gobierno de España [WWW Document], 2020. URL <https://www.mapa.gob.es/es/estadistica/temas/estadisticas-agrarias/agricultura/superficies-producciones-anuales-cultivos/>.
- Mohan, D., Pittman, C.U., Steele, P.H., 2006. Pyrolysis of wood/biomass for bio-oil: a critical review. *Energy & Fuels* 20, 848–889. <https://doi.org/10.1021/ef0502397>.

- Mok, W.S.-L., Antal, M.J., 1983. Effects of pressure on biomass pyrolysis. II. Heats of reaction of cellulose pyrolysis. *Thermochim. Acta* 68, 165–186. [https://doi.org/10.1016/0040-6031\(83\)80222-6](https://doi.org/10.1016/0040-6031(83)80222-6).
- Mok, W.S., Antal, M.J., Szabo, P., Varhegyi, G., Zelei, B., 1992. Formation of charcoal from biomass in a sealed reactor. *Ind. Eng. Chem. Res.* 31, 1162–1166. <https://doi.org/10.1021/ie00004a027>.
- Molina-Sabio, M., Gonzalez, M.T., Rodriguez-Reinoso, F., Sepúlveda-Escribano, A., 1996. Effect of steam and carbon dioxide activation in the micropore size distribution of activated carbon. *Carbon N. Y.* 34, 505–509. [https://doi.org/10.1016/0008-6223\(96\)00006-1](https://doi.org/10.1016/0008-6223(96)00006-1).
- Montgomery, D.C., 2005. *Design and Analysis of Experiments*, 6th editio. ed. Hoboken.
- Mullen, C.A., Boateng, A.A., 2011. Characterization of water insoluble solids isolated from various biomass fast pyrolysis oils. *J. Anal. Appl. Pyrolysis* 90, 197–203. <https://doi.org/10.1016/j.jaap.2010.12.004>.
- Myers, A.L., Prausnitz, J.M., 1965. Thermodynamics of Mixed-Gas Adsorption. *AIChE J.* 11, 121–127. <https://doi.org/10.1002/aic.690110125>.
- Mythili, R., Venkatachalam, P., Subramanian, P., Uma, D., 2013. Characterization of bioresidues for bio-oil production through pyrolysis. *Bioresour. Technol.* 138, 71–78. <https://doi.org/10.1016/j.biortech.2013.03.161>.
- Nakagawa, S., Schielzeth, H., 2010. Repeatability for Gaussian and non-Gaussian data: A practical guide for biologists. *Biol. Rev.* 85, 935–956. <https://doi.org/10.1111/j.1469-185X.2010.00141.x>.
- Nelder, J.A., Mead, R., 1964. A Simplex Method for Function Minimization. *Comput. J.* 7. <https://doi.org/10.1093/comjnl/7.4.308>.
- Nelson, K.M., Mahurin, S.M., Mayes, R.T., Williamson, B., Teague, C.M., Binder, A.J., Baggetto, L., Veith, G.M., Dai, S., 2016. Preparation and CO₂ adsorption properties of soft-templated mesoporous carbons derived from chestnut tannin precursors. *Microporous Mesoporous Mater.* 222, 94–103. <https://doi.org/10.1016/j.micromeso.2015.09.050>.
- Netpradit, S., Thiravetyan, P., Towprayoon, S., 2003. Application of ‘waste’ metal hydroxide sludge for adsorption of azo reactive dyes. *Water Res.* 37, 763–772. [https://doi.org/10.1016/S0043-1354\(02\)00375-5](https://doi.org/10.1016/S0043-1354(02)00375-5).
- Nguyen, B.T., Lehmann, J., Kinyangi, J., Smernik, R.J., Riha, S., Engelhard, M.H., 2009. Long-term black carbon dynamics in cultivated soil. *Biogeochemistry* 92, 163–176. <https://doi.org/10.1007/s10533-008-9220-9>.

- Nieto, A., Gascó, G., Paz-Ferreiro, J., Fernández, J.M., Plaza, C., Méndez, A., 2016. The effect of pruning waste and biochar addition on brown peat based growing media properties. *Sci. Hortic. (Amsterdam)*. 199, 142–148. <https://doi.org/10.1016/j.scienta.2015.12.012>.
- NOAA Climate.gov [WWW Document], 2021. URL <https://www.climate.gov/news-features/understanding-climate/climate-change-atmospheric-carbon-dioxide>.
- Noumi, E.S., Blin, J., Valette, J., Rousset, P., 2015. Combined Effect of Pyrolysis Pressure and Temperature on the Yield and CO₂ Gasification Reactivity of Acacia Wood in macro-TG. *Energy & Fuels* 29, 7301–7308. <https://doi.org/10.1021/acs.energyfuels.5b01454>.
- Nunoura, T., Wade, S.R., Bourke, J., Antal, M.J., 2006. Studies of the flash carbonization process. 1. Propagation of the flaming pyrolysis reaction and performance of a catalytic afterburner. *Ind. Eng. Chem. Res.* 45, 585–599. <https://doi.org/10.1021/ie050854y>.
- Parshetti, G.K., Chowdhury, S., Balasubramanian, R., 2015. Biomass derived low-cost microporous adsorbents for efficient CO₂ capture. *Fuel* 148, 246–254. <https://doi.org/10.1016/j.fuel.2015.01.032>.
- Paz-Ferreiro, J., Gascó, G., Gutiérrez, B., Méndez, A., 2012. Soil biochemical activities and the geometric mean of enzyme activities after application of sewage sludge and sewage sludge biochar to soil. *Biol. Fertil. Soils* 48, 511–517. <https://doi.org/10.1007/s00374-011-0644-3>.
- Paz-Ferreiro, J., Lu, H., Fu, S., Méndez, A., Gascó, G., 2014. Use of phytoremediation and biochar to remediate heavy metal polluted soils: a review. *Solid Earth* 5, 65–75. <https://doi.org/10.5194/se-5-65-2014>.
- Peiris, C., Gunatilake, S.R., Mlsna, T.E., Mohan, D., Vithanage, M., 2017. Biochar based removal of antibiotic sulfonamides and tetracyclines in aquatic environments: A critical review. *Bioresour. Technol.* 246, 150–159. <https://doi.org/10.1016/j.biortech.2017.07.150>.
- Peredo-Mancilla, D., Ghimbeu, C.M., Ho, B.-N., Jeguirim, M., Hort, C., Bessieres, D., 2019. Comparative study of the CH₄/CO₂ adsorption selectivity of activated carbons for biogas upgrading. *J. Environ. Chem. Eng.* 7, 103368. <https://doi.org/10.1016/j.jece.2019.103368>.
- Perry, R.H., Green, D.W., 1998. *Perry's chemical engineers handbook*, 7th Editio. ed. McGraw Hill, Australia.
- Plaza, M.G., González, A.S., Pis, J.J., Rubiera, F., Pevida, C., 2014. Production of microporous biochars by single-step oxidation: Effect of activation conditions on CO₂ capture. *Appl. Energy* 114, 551–562. <https://doi.org/10.1016/J.APENERGY.2013.09.058>.

- Premarathna, K.S.D., Rajapaksha, A.U., Sarkar, B., Kwon, E.E., Bhatnagar, A., Ok, Y.S., Vithanage, M., 2019. Biochar-based engineered composites for sorptive decontamination of water: A review. *Chem. Eng. J.* 372, 536–550. <https://doi.org/10.1016/j.cej.2019.04.097>.
- Prins, M.J., Ptasiński, K.J., 2005. Energy and exergy analyses of the oxidation and gasification of carbon. *Energy* 30, 982–1002. <https://doi.org/10.1016/J.ENERGY.2004.08.010>.
- Przepiórski, J., Skrodzewicz, M., Morawski, A.W., 2004. High temperature ammonia treatment of activated carbon for enhancement of CO₂ adsorption. *Appl. Surf. Sci.* 225, 235–242. <https://doi.org/10.1016/j.apsusc.2003.10.006>.
- Qian, K., Kumar, A., Zhang, H., Bellmer, D., Huhnke, R., 2015. Recent advances in utilization of biochar. *Renew. Sustain. Energy Rev.* 42, 1055–1064. <https://doi.org/10.1016/j.rser.2014.10.074>.
- Qian, Y., Zhang, J., Wang, J., 2014. Pressurized pyrolysis of rice husk in an inert gas sweeping fixed-bed reactor with a focus on bio-oil deoxygenation. *Bioresour. Technol.* 174, 95–102. <https://doi.org/10.1016/j.biortech.2014.10.012>.
- Rackley, S.A., 2010. Carbon capture and storage. Joe Hayton. <https://doi.org/10.1016/j.enpol.2008.09.058>.
- Raveendran, K., Ganesh, A., Khilar, K.C., 1995. Influence of mineral matter on biomass pyrolysis characteristics. *Fuel* 74, 1812–1822. [https://doi.org/10.1016/0016-2361\(95\)80013-8](https://doi.org/10.1016/0016-2361(95)80013-8).
- Recari, J., Berrueco, C., Abellò, S., Montané, D., Farriol, X., 2014. Effect of temperature and pressure on characteristics and reactivity of biomass-derived chars. *Bioresour. Technol.* 170, 204–210. <https://doi.org/10.1016/j.biortech.2014.07.080>.
- Rengaraj, S., Yeon, K.-H., Moon, S.-H., 2001. Removal of chromium from water and wastewater by ion exchange resins. *J. Hazard. Mater.* 87, 273–287. [https://doi.org/10.1016/S0304-3894\(01\)00291-6](https://doi.org/10.1016/S0304-3894(01)00291-6).
- Resende, F.L.P., 2016. Recent advances on fast hydrolysis of biomass. *Catal. Today* 269, 148–155. <https://doi.org/10.1016/j.cattod.2016.01.004>.
- Rissanen, T., Hyötyläinen, T., Kallio, M., Kronholm, J., Kulmala, M., Riekkola, M.-L., 2006. Characterization of organic compounds in aerosol particles from a coniferous forest by GC–MS. *Chemosphere* 64, 1185–1195. <https://doi.org/10.1016/j.chemosphere.2005.11.079>.

- Robinson, T., McMullan, G., Marchant, R., Nigam, P., 2001. Remediation of dyes in textile effluent: a critical review on current treatment technologies with a proposed alternative. *Bioresour. Technol.* 77, 247–255. [https://doi.org/10.1016/S0960-8524\(00\)00080-8](https://doi.org/10.1016/S0960-8524(00)00080-8).
- Rodríguez-Mirasol, J., Bedia, J., Cordero, T., Rodríguez, J.J., 2005. Influence of Water Vapor on the Adsorption of VOCs on Lignin-Based Activated Carbons. *Sep. Sci. Technol.* 40, 3113–3135. <https://doi.org/10.1080/01496390500385277>.
- Rogovska, N., Laird, D., Cruse, R.M., Trabue, S., Heaton, E., 2012. Germination Tests for Assessing Biochar Quality. *J. Environ. Qual.* 41, 1014–1022. <https://doi.org/10.2134/jeq2011.0103>.
- Ronsse, F., van Hecke, S., Dickinson, D., Prins, W., 2013. Production and characterization of slow pyrolysis biochar: influence of feedstock type and pyrolysis conditions. *GCB Bioenergy* 5, 104–115. <https://doi.org/10.1111/gcbb.12018>.
- Rousset, P., Figueiredo, C., De Souza, M., Quirino, W., 2011. Pressure effect on the quality of eucalyptus wood charcoal for the steel industry: A statistical analysis approach. *Fuel Process. Technol.* 92, 1890–1897. <https://doi.org/10.1016/j.fuproc.2011.05.005>.
- Sadaka, S., Negi, S., 2009. Improvements of biomass physical and thermochemical characteristics via torrefaction process. *Environ. Prog. Sustain. Energy* 28, 427–434. <https://doi.org/https://doi.org/10.1002/ep.10392>.
- Saidur, R., BoroumandJazi, G., Mekhilef, S., Mohammed, H.A., 2012. A review on exergy analysis of biomass based fuels. *Renew. Sustain. Energy Rev.* 16, 1217–1222. <https://doi.org/https://doi.org/10.1016/j.rser.2011.07.076>.
- Scala, F., Chirone, R., Salatino, P., 2006. Combustion and attrition of biomass chars in a fluidized bed. *Energy & Fuels* 20, 91–102. <https://doi.org/10.1021/ef050102g>.
- Scheirs, J., Camino, G., Tumiatti, W., 2001. Overview of water evolution during the thermal degradation of cellulose. *Eur. Polym. J.* 37, 933–942. [https://doi.org/10.1016/S0014-3057\(00\)00211-1](https://doi.org/10.1016/S0014-3057(00)00211-1).
- Schmidt, H.P., Hilber, I., Bucheli, T.D., 2015. Polycyclic aromatic hydrocarbons and polychlorinated aromatic compounds in biochar, in: *Biochar for Environmental Management*. Routledge, London, p. 30.
- Schmidt, M.W.I., Noak, A.G., 2000. Black carbon in soils and sediments: analysis, distribution, implications, and current challenges. *Global Biogeochem. Cycles* 14, 777–793. <https://doi.org/10.1029/1999GB001208>.

- Şensöz, S., Angin, D., Yorgun, S., 2000. Influence of particle size on the pyrolysis of rapeseed (*Brassica napus* L.): fuel properties of bio-oil. *Biomass and Bioenergy* 19, 271–279. [https://doi.org/10.1016/S0961-9534\(00\)00041-6](https://doi.org/10.1016/S0961-9534(00)00041-6).
- Şensöz, S., Kaynar, I., 2006. Bio-oil production from soybean (*Glycine max* L.): fuel properties of bio-oil. *Ind. Crops Prod.* 23, 99–105. <https://doi.org/10.1016/j.indcrop.2005.04.005>.
- Serafin, J., Narkiewicz, U., Morawski, A.W., Wróbel, R.J., Michalkiewicz, B., 2017. Highly microporous activated carbons from biomass for CO₂ capture and effective micropores at different conditions. *J. CO₂ Util.* 18, 73–79. <https://doi.org/10.1016/j.jcou.2017.01.006>.
- Shafeeyan, M.S., Daud, W.M.A.W., Houshmand, A., Arami-Niya, A., 2011. Ammonia modification of activated carbon to enhance carbon dioxide adsorption: Effect of pre-oxidation. *Appl. Surf. Sci.* 257, 3936–3942. <https://doi.org/10.1016/j.apsusc.2010.11.127>.
- Shen, Y., Fu, Y., 2018. KOH-activated rice husk char via CO₂ pyrolysis for phenol adsorption. *Mater. Today Energy* 9, 397–405. <https://doi.org/10.1016/j.mtener.2018.07.005>.
- Shen, Y., Zhao, P., Shao, Q., 2014. Porous silica and carbon derived materials from rice husk pyrolysis char. *Microporous Mesoporous Mater.* 188, 46–76. <https://doi.org/10.1016/j.micromeso.2014.01.005>.
- Shuba, E.S., Kifle, D., 2018. Microalgae to biofuels: ‘Promising’ alternative and renewable energy, review. *Renew. Sustain. Energy Rev.* 81, 743–755. <https://doi.org/10.1016/j.rser.2017.08.042>.
- Simoneit, B.R.T., 1998. Biomarker PAHs in the Environment., in: *PAHs and Related Compounds. The Handbook of Environmental Chemistry (Anthropogenic Compounds)*. Springer, Berlin, Heidelberg. https://doi.org/10.1007/978-3-540-49697-7_5.
- Singh, R., Krishna, B.B., Mishra, G., Kumar, J., Bhaskar, T., 2016. Strategies for selection of thermo-chemical processes for the valorisation of biomass. *Renew. Energy* 98, 226–237. <https://doi.org/10.1016/j.renene.2016.03.023>.
- Sohi, S., Lopez-Capel, S., Krull, E., Bol, R., 2009. Biochar, Climate Change and Soil: A Review to Guide Future Research. <https://doi.org/10.4225/08/58597219a199a>.
- Sopeña, F., Semple, K., Sohi, S., Bending, G., 2012. Assessing the chemical and biological accessibility of the herbicide isoproturon in soil amended with biochar. *Chemosphere* 88, 77–83. <https://doi.org/10.1016/j.chemosphere.2012.02.066>.
- Srinivas, T., Gupta, A.V.S.S.K.S., Reddy, B. V., 2009. Thermodynamic equilibrium model and exergy analysis of a Biomass gasifier. *J. Energy Resour. Technol. Trans. ASME* 131, 318011–318017. <https://doi.org/10.1115/1.3185354>.

- Steiner, C., Harttung, T., 2014. Biochar as a growing media additive and peat substitute. *Solid Earth* 5, 995–999. <https://doi.org/10.5194/se-5-995-2014>.
- Stenseng, M., Jensen, A., Dam-Johansen, K., 2001. Investigation of biomass pyrolysis by thermogravimetric analysis and differential scanning calorimetry. *J. Anal. Appl. Pyrolysis* 58, 765–780. [https://doi.org/10.1016/S0165-2370\(00\)00200-X](https://doi.org/10.1016/S0165-2370(00)00200-X).
- Strack, M., 2008. *Peatlands and Climate Change*. Jyväskylä, Finland.
- Sun, H., Hockaday, W.C., Masiello, C.A., Zygourakis, K., 2012. Multiple Controls on the Chemical and Physical Structure of Biochars. *Ind. Eng. Chem. Res.* 51, 3587–3597. <https://doi.org/10.1021/ie201309r>.
- Swift, R.S., 2001. Sequestration of carbon by soil. *Soil Sci.* 166, 858–871. <https://doi.org/10.1097/00010694-200111000-00010>.
- Szargut, J., 2005. *Exergy method: technical and ecological applications*. WIT, outhampton, UK.
- Thangalazhy-Gopakumar, S., Adhikari, S., Gupta, R.B., 2012. Catalytic Pyrolysis of Biomass over H+ZSM-5 under Hydrogen Pressure. *Energy Fuels* 26, 5300–5306. <https://doi.org/10.1021/ef3008213>.
- Tian, Y., Sun, X., Li, S., Wang, H., Wang, L., Cao, J., Zhang, L., 2012. Biochar made from green waste as peat substitute in growth media for *Calathea rotundifolia* cv. *Fasciata*. *Sci. Hortic. (Amsterdam)*. 143, 15–18. <https://doi.org/10.1016/j.scienta.2012.05.018>.
- Tiessen, H., Cuevas, E., Chacon, P., 1994. The role of soil organic matter in sustaining soil fertility. *Nature* 371, 783–785. <https://doi.org/10.1038/371783a0>.
- Titirici, M.-M., White, R.J., Falco, C., Sevilla, M., 2012. Black perspectives for a green future: hydrothermal carbons for environment protection and energy storage. *Energy Environ. Sci.* 5, 6796–6822. <https://doi.org/10.1039/C2EE21166A>.
- Tong, Y., McNamara, P.J., Mayer, B.K., 2019. Adsorption of organic micropollutants onto biochar: a review of relevant kinetics, mechanisms and equilibrium. *Environ. Sci. Water Res. Technol.* 5, 821–838. <https://doi.org/10.1039/C8EW00938D>.
- Tripathi, M., Sahu, J.N., Ganesan, P., 2016. Effect of process parameters on production of biochar from biomass waste through pyrolysis: A review. *Renew. Sustain. Energy Rev.* 55, 467–481. <https://doi.org/10.1016/j.rser.2015.10.122>.
- Tsai, W.T., Chang, C.Y., Lee, S.L., 1997. Preparation and characterization of activated carbons from corn cob. *Carbon N. Y.* 35, 1198–1200. [https://doi.org/10.1016/S0008-6223\(97\)84654-4](https://doi.org/10.1016/S0008-6223(97)84654-4).
- Tyndall, J., 1859. Note on the Transmission of Radiant Heat through Gaseous Bodies.

- United Nations, Framework Convention on Climate Change [WWW Document], 2008. URL http://unfccc.int/kyoto_protocol/items/2830.php.
- Varhegyi, G., Szabo, P., Mok, W.S., Antal, M.J., 1993. Kinetics of the thermal decomposition of cellulose in sealed vessels at elevated pressures. Effects of the presence of water on the reaction mechanism. *J. Anal. Appl. Pyrolysis* 26, 159–174. [https://doi.org/10.1016/0165-2370\(93\)80064-7](https://doi.org/10.1016/0165-2370(93)80064-7).
- Varhegyi, G., Szabo, P., Till, F., Zelei, B., Antal, M.J., Dai, X., 1998. TG, TG-MS, and FTIR characterization of high-yield biomass charcoals. *Energy Fuels* 12, 969–974. <https://doi.org/10.1021/ef9800359>.
- Varma, A.K., Mondal, P., 2017. Pyrolysis of sugarcane bagasse in semi batch reactor: effects of process parameters on product yields and characterization of products. *Ind. Crops Prod.* 95, 704–717. <https://doi.org/10.1016/j.indcrop.2016.11.039>.
- Vochozka, M., Maroušková, A., Váchal, J., Straková, J., 2016. Biochar pricing hampers biochar farming. *Clean Technol. Environ. Policy* 18, 1225–1231. <https://doi.org/10.1007/s10098-016-1113-3>.
- Wade, S.R., Nunoura, T., Antal, M.J., 2006. Studies of the flash carbonization process. 2. Violent ignition behavior of pressurized packed beds of biomass: A factorial study. *Ind. Eng. Chem. Res.* 45, 3512–3519. <https://doi.org/10.1021/ie051374+>.
- Wang, C., Wang, Y., Herath, H.M.S.K., 2017. Polycyclic aromatic hydrocarbons (PAHs) in biochar – Their formation, occurrence and analysis: A review. *Org. Geochem.* 114, 1–11. <https://doi.org/10.1016/j.orggeochem.2017.09.001>.
- Wang, D., Xiao, R., Zhang, H., He, G., 2010. Comparison of catalytic pyrolysis of biomass with MCM-41 and CaO catalysts by using TGA–FTIR analysis. *J. Anal. Appl. Pyrolysis* 89, 171–177. <https://doi.org/10.1016/j.jaap.2010.07.008>.
- Wang, X., Lv, W., Guo, L., Zhai, M., Dong, P., Qi, G., 2016. Energy and exergy analysis of rice husk high-temperature pyrolysis. *Int. J. Hydrogen Energy* 41, 21121–21130. <https://doi.org/10.1016/J.IJHYDENE.2016.09.155>.
- Wang, Z., Wang, F., Cao, J., Wang, J., 2010. Pyrolysis of pine wood in a slowly heating fixed-bed reactor: Potassium carbonate versus calcium hydroxide as a catalyst. *Fuel Process. Technol.* 91, 942–950. <https://doi.org/10.1016/j.fuproc.2009.09.015>.
- Wartel, M., Pauwels, J.-F., Desgroux, P., Mercier, X., 2010. Quantitative measurement of naphthalene in low-pressure flames by jet-cooled laser-induced fluorescence. *Appl. Phys. B* 100, 933–943. <https://doi.org/10.1007/s00340-010-4135-2>.

- Wei, H., Deng, S., Hu, B., Chen, Z., Wang, B., Huang, J., Yu, G., 2012. Granular Bamboo-Derived Activated Carbon for High CO₂ Adsorption: The Dominant Role of Narrow Micropores. *ChemSusChem* 5, 2354–2360. <https://doi.org/10.1002/cssc.201200570>.
- Woolf, D., Amonette, J.E., Street-Perrott, F.A., Lehmann, J., Joseph, S., 2010. Sustainable biochar to mitigate global climate change. *Nat. Commun.* 1, 56. <https://doi.org/10.1038/ncomms1053>.
- Wu, W., Yang, M., Feng, Q., McGrouther, K., Wang, H., Lu, H., Chen, Y., 2012. Chemical characterization of rice straw-derived biochar for soil amendment. *Biomass and Bioenergy* 47, 268–276. <https://doi.org/10.1016/j.biombioe.2012.09.034>.
- Yaashikaa, P.R., Kumar, P.S., Varjani, S., Saravanan, A., 2020. A critical review on the biochar production techniques, characterization, stability and applications for circular bioeconomy. *Biotechnol. Reports* 28, e00570. <https://doi.org/10.1016/j.btre.2020.e00570>.
- Yan, Q., Wan, C., Liu, J., Gao, J., Yu, F., Zhang, J., Cai, Z., 2013. Iron nanoparticles in situ encapsulated in biochar-based carbon as an effective catalyst for the conversion of biomass-derived syngas to liquid hydrocarbons. *Green Chem.* 15, 1631–1640. <https://doi.org/10.1039/C3GC37107G>.
- Yang, H., Yan, R., Chen, H., Lee, D.H., Zheng, C., 2007. Characteristics of hemicellulose, cellulose and lignin pyrolysis. *Fuel* 86, 1781–1788. <https://doi.org/10.1016/j.fuel.2006.12.013>.
- Yang, J., Yue, L., Hu, X., Wang, L., Zhao, Y., Lin, Y., Sun, Y., DaCosta, H., Guo, L., 2017. Efficient CO₂ Capture by Porous Carbons Derived from Coconut Shell. *Energy & Fuels* 31, 4287–4293. <https://doi.org/10.1021/acs.energyfuels.7b00633>.
- Yang, K., Peng, J., Xia, H., Zhang, L., Srinivasakannan, C., Guo, S., 2010. Textural characteristics of activated carbon by single step CO₂ activation from coconut shells. *J. Taiwan Inst. Chem. Eng.* 41, 367–372. <https://doi.org/10.1016/j.jtice.2009.09.004>.
- Yang, Y., Brammer, J.G., Mahmood, A.S.N., Hornung, A., 2014. Intermediate pyrolysis of biomass energy pellets for producing sustainable liquid, gaseous and solid fuels. *Bioresour. Technol.* 169, 794–799. <https://doi.org/10.1016/j.biortech.2014.07.044>.
- Yang, Y., Brammer, J.G., Ouadi, M., Samanya, J., Hornung, A., Xu, H.M., Li, Y., 2013. Characterisation of waste derived intermediate pyrolysis oils for use as diesel engine fuels. *Fuel* 103, 247–257. <https://doi.org/10.1016/J.FUEL.2012.07.014>.
- Yanik, J., Kornmayer, C., Saglam, M., Yüksel, M., 2007. Fast pyrolysis of agricultural wastes: characterization of pyrolysis products. *Fuel Process. Technol.* 88, 942–947. <https://doi.org/10.1016/j.fuproc.2007.05.002>.

- Yu, A., Chabot, V., Zhang, J., 2013. Applications of Electrochemical Supercapacitors, in: *Electrochemical Supercapacitors for Energy Storage and Delivery*. p. 383. <https://doi.org/10.1201/b14671>.
- Zazycki, M.A., Godinho, M., Perondi, D., Foletto, E.L., Collazzo, G.C., Dotto, G.L., 2018. New biochar from pecan nutshells as an alternative adsorbent for removing reactive red 141 from aqueous solutions. *J. Clean. Prod.* 171, 57–65. <https://doi.org/10.1016/j.jclepro.2017.10.007>.
- Zech, W., Senesi, N., Guggenberger, G., Kaiser, K., Lehmann, J., Miano, T.M., Miltner, A., Schroth, G., 1997. Factors controlling humification and mineralization of soil organic matter in the tropics. *Geoderma* 79, 117–161. [https://doi.org/10.1016/S0016-7061\(97\)00040-2](https://doi.org/10.1016/S0016-7061(97)00040-2).
- Zhang, L., Chunbao, X., Champagne, P., 2010. Overview of recent advances in thermochemical conversion of biomass. *Energy Convers. Manag.* 51, 969–982. <https://doi.org/10.1016/j.enconman.2009.11.038>.
- Zhao, L., Cao, X., Mašek, O., Zimmerman, A., 2013. Heterogeneity of biochar properties as a function of feedstock sources and production temperatures. *J. Hazard. Mater.* 256–257, 1–9. <https://doi.org/10.1016/j.jhazmat.2013.04.015>.
- Zhao, Y., Liu, X., Han, Y., 2015. Microporous carbonaceous adsorbents for CO₂ separation via selective adsorption. *RSC Adv.* 5, 30310–30330. <https://doi.org/10.1039/C5RA00569H>.
- Zheng, Y., Li, Q., Yuan, C., Tao, Q., Zhao, Y., Zhang, G., Liu, J., 2019. Influence of temperature on adsorption selectivity: Coal-based activated carbon for CH₄ enrichment from coal mine methane. *Powder Technol.* 347, 42–49. <https://doi.org/10.1016/j.powtec.2019.02.042>.